E\PCOS 2025

MARSEILLE, FRANCE
23-26 SEPTEMBER 2025

EUROPEAN PHASE CHANGE OVONIC SIMPOSIUM

Proceedings

Institut Matériaux Microélectronique Nanosciences de Provence
Aix Marseille Université
VILLE DE MARSEILLE
OFFICE DE TOURISME LOISIRS & CONGRÈS MARSEILLE
SOLNIL Nanoimprint your world

Welcome to E \ PCOS 2025 !

E \ PCOS 2025
MARSEILLE, FRANCE
23-26 SEPTEMBER 2025

On behalf of the Program Committee, it is our great pleasure to welcome you to the 2025 European Symposium on Phase change and Ovonic Science (E\PCOS 2025). This year, our symposium is held in Marseille, France.

When the first E\PCOS took place in Switzerland, its primary focus was fundamental science of phase change materials and their application to rewritable optical disks, which ultimately led to the successful commercialization of DVD-RAM, DVD-RW, and Blu-ray technologies. The symposium itself grew out of the Phase-Change Optics Symposium (PCOS), first organized in Japan in 1990 under the leadership of Professor Masahiro Okuda, who served as an advisor to E\PCOS from its inception. Building on the pioneering work of both Stanford Ovshinsky and Masahiro Okuda, research in this field has since expanded into a wide range of exciting domains, including phase change memories, topological insulators, spintronics, neuromorphic computing, photonics, and plasmonics.

We hope you will not only enjoy the rich technical program, but take this opportunity to engage in stimulating discussions and strengthen the bonds within our community.

Welcome to Marseille !

Prof. Matthias WUTTIG (Conference Chair)
RWTH Aachen University of Technology, Germany

Prof. Junji TOMINAGA (Advisory committee members)
National Institute of Advanced Industrial Science and Technology, AIST, Japan

Prof. Bart KOOI (Programme Committee Chairman)
University of Groningen, Netherlands

Prof. Magali PUTERO (Chair of Organizing Committee)
Aix-Marseille Université and CNRS, IM2NP, France

E \ PCOS 2025 Committees

Chairman

Prof. Dr. Matthias Wuttig (RWTH-Aachen, Germany)

Advisory committee member

Prof. Junji Tominaga (AIST, Japan)

Program Committee Chairman

Prof. Bart Kooi (University of Groningen, Netherlands)

Programm Committee Members

Dr. Dong-ho Ahn (Samsung Electronics, Korea)
Prof. Harish Bhaskaran (University of Oxford, UK)
Dr. Raffaella Calarco (CNR-IMM, Roma, Italy)
Dr. Huai-Yu (Michelle) Cheng (Macronix International, Taiwan)
Dr. Giuseppe D'Arrigo (CNR-IMM, Catania, Italy)
Prof. Stephen R. Elliott (Cambridge University, UK)
Prof. Daniele Ielmini (Milano Polytechnical University, Italy)
Dr. Derchang Kau (Intel, Santa Clara, USA)
Prof. Suyoun Lee (Korea Institute of Science and Technology, Korea)
Dr. Massimo Longo (University of Rome Tor Vergata, Rome, Italy)
Dr. Andriy Lotnyk (IOM, Leipzig, Germany)
Prof. Anbarau Manivannan (Indian Institute of Technology Madras, India)
Dr. Pierre Noé (CEA Leti, France)
Dr. Elisa Petroni (STMicroelectronics, Italy)
Prof. Magali Putero (Aix-Marseille University, France)
Dr. Abu Sebastian (IBM Research – Zurich, Switzerland)
Prof. Robert Simpson (University of Birmingham, UK)
Prof. Yuji Sutou (Tohoku University, Sendai, Japan)
Prof. Ding Ping Tsai (Taiwan University, Taiwan)
Prof. David Wright (University of Exeter, UK)
Prof. Ming Xu (Huazhong University of Science and Technology, China)
Prof. Wei Zhang (Xi'an Jiaotong University, China)

Organizing Committee

Prof. Magali Putero (IM2NP, amU, CNRS, Marseille, France)
Dr. Jacopo Remondina (IM2NP, CNRS, Marseille, France)
Prof. David Grosso (CINaM, amU & SOLNIL, Marseille, France)

Dr. Alain Portavoce (IM2NP, CNRS, Marseille, France)
Leslie Scala (IM2NP, Marseille, France)
Yves Klein (IM2NP, Marseille, France)
Maxime Bertoglio (IM2NP, Marseille, France)
Oumaima Meskini (IM2NP, Marseille, France)
Hamid Neggaz (IM2NP, Marseille, France)
Anthony Gourdin (SOLNIL, Marseille, France)
Chaimae El Mokaddem (SOLNIL , Marseille, France)

SPONSORS

We would like to thank our sponsors for their generosity:

General information for E \ PCOS 2025

CONFERENCE LOCATION

Aix-Marseille University - Pharo
Jardin du Pharo,
58 Boulevard Charles Livon, 13007 Marseille, France

Metro: Line n°1 exit "**Vieux Port**" at 1.4 km.

Bus : n° **82**, **83** and **82S** stop at station « **le Pharo** ».

TAXI and PUBLIC TRANSPORT

Metro: from 5h30 am to 21h30 pm from Monday to Thursday, to 00h30 pm from Friday to Sunday.
Tramway: from 5h10 am to 01h00 am
Bus: from 6h00 am to 21h00 pm
Taxi : 00 33 (0)4 91 02 20 20 (Taxi central reservation)

USEFUL AND EMERGENCY TELEPHONE NUMBERS

Police : 17
Emergency/ambulance : 15 or 18 (also fire brigade)
European emergency phone number: 112
Prof. Magali Putero: 00 33 (0) 6 16 90 38 81

Gala Dinner

Gala diner will take place at restaurant:

"**Fort Ganteaume** »
2 Bd Charles Livon
13007 Marseille

Insurance and Responsibility

Liability insurance is the responsibility of each individual delegate. Delegates should have their own medical coverage.

The organizers are not responsible for accidents, looses, damages or any changes in the program arising from unforeseen circumstances.

Program

Note: 🔗 Click on a speaker's name to go directly to their abstract.

Tuesday, Septembre 23

15:00-17:00 **Social Activity (optional)**
Guided tour of Marseille – Notre Dame de La Garde
Meeting time: no later than 14:45
Meeting point: 174 Quai du port, 13002 Marseille

18:00-20:00 **Registration and Welcome Reception**
Espace Villeneuve Bargemon, Marseille City Hall
13002 Marseille

19:30-22:00 **Committee meeting & dinner (restricted)**

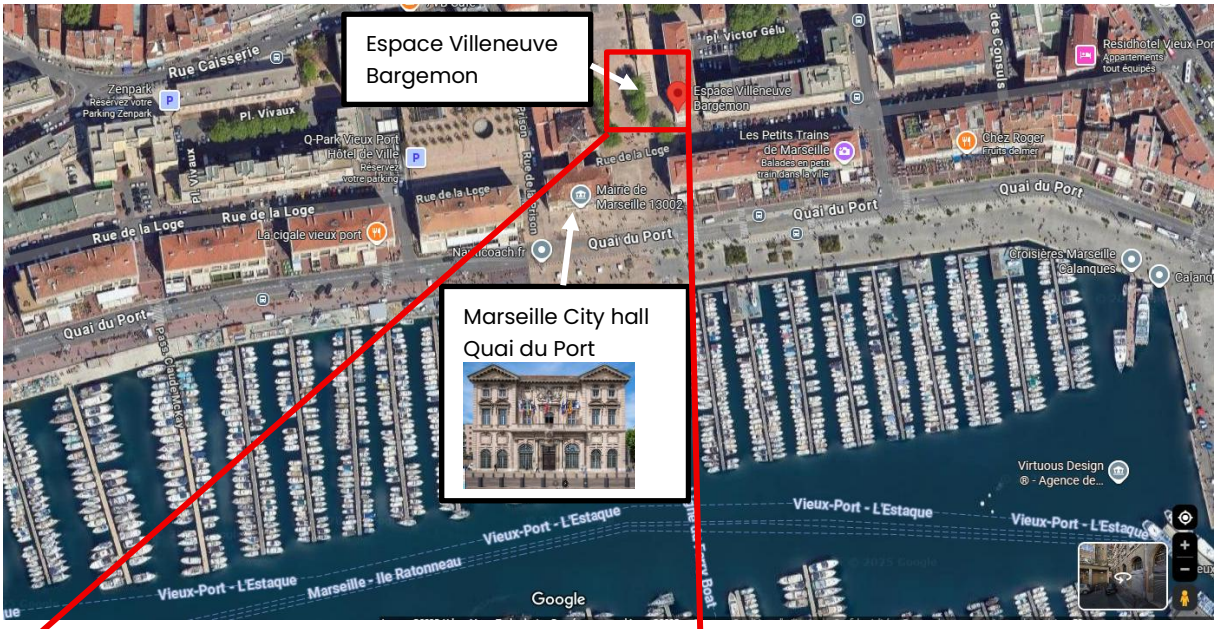

Wednesday, Septembre 24

8:00-9:00 **REGISTRATION & Coffee**

9:00-9:15 **Opening remarks**

SESSION-1 High Resolution *(Session chair: Matthias Wuttig)*

9:15-9:50 **Ovshinsky Lecture Award**
Der Chang Kau, Intel & **Fabio Pellizzer**, Micron

9:50-10:15 Invited: **Ritesh Agarwal**- University of Pennsylvania, USA
Unconventional amorphization in layered materials from multimodal coupling of fields to competing orders

10:15-10:30 **Andriy Lotnyk**- IOM Leipzig, Germany
In situ atomic-scale investigation of structural transitions in $Ge_2Sb_2Te_5$ thin films

10:30-11:05 **COFFEE BREAK**

SESSION-2 Theory - atomistics *(Session chair: Ming Xu & Raffaella Calarco)*

11:05-11:30 Invited: **Matthias Wuttig** – RWTH Aachen University, Germany
Tailoring Phase Change Materials for different Applications: The Role of Metavalent Bonding

10:30-11:45 **Wei Zhang** - Xi'an Jiaotong University, China
High-throughput screening for layered phase-change memory materials

11:45-12:00 **Omar Abou El Kheir** - University of Milano-Bicocca, Italy
(STMicroelectronics Luca Laurin's prize)
Million-atom simulation of the set process in phase change memories at the real device scale

12:00-12:25 Invited: **Martin Salinga** - University of Münster, Germany
State dynamics in amorphous PCMs — a closer look.

12:25-12:40 **Nils Holle** - University of Münster, Germany
Effect of Peierls-like distortions on transport in amorphous phase change devices

12:40-12:50 **GROUP PHOTO**

12:50-14:40 **Lunch & Posters Session 1**

12:50 – 14:40 POSTER SESSION 1: all odd-numbered posters

SESSION-3 **Alternative materials & properties** ***(Session chair: Massimo Longo & Bart Kooi)***

14:40-15:05 Invited: **Pierre Noé** – CEA-LETI, France

Large-Scale Deposition of Thin Films Based on Chalcogenide Phase-Change Materials: From GeTe/Sb_2Te_3 Superlattices for Phase-Change Memory Toward Spin-Orbitronic and Reconfigurable Photonic Devices

15:05-15:20 **Jules Lagrave** – CEA-LETI, France

Van der Waals Epitaxy of Self-Poled α-GeTe(111) Ferroelectric Thin Films for Spin-Orbitronic Devices

15:20-15:45 Invited: **Joao M. J. Lopes** – Paul Drude Institut für Festkörperelektronik, Germany

Above room temperature ferromagnetism in epitaxial thin films of the layered ternary chalcogenides Fe_5GeTe_2 and Fe_3GaTe_2

15:45-16:00 **Shih-Yuan Li** – Tohoku University, Japan

The volatile and non-volatile resistance switching behavior in $MnTe_2$-based device

16:00-16:15 **Shuhei Orihara** - Tohoku University, Japan

Characterization of Phase-Change Behaviors and Memory Operation Properties in V-Te Thin Film

16:15-16:45 **COFFEE BREAK**

SESSION-4 **GaSb, GST & Ge-rich GST** ***(Session chair: Pierre Noé & Elisa Petroni)***

16:45-17:00 **Jacopo Remondina** - Aix-Marseille Univ. & CNRS – IM2NP, France

Tuning the properties of GaSb with C-doping

17:00-17:25 Invited: **Sabrina Calvi** – University of Rome Tor Vergata & CNR-IMM – Italy

Storage class memories for flexible edge electronics

17:25-17:40 **Sijia Ran** – CEMES-CNRS Toulouse, France

Partial RESET and partial SET states in Ge-rich GeSbTe-based phase change memory cells

17:40-18:05 Invited: **Enrico Piccinini** - Applied Materials, Italy

Evolution of Ge-rich GST from post deposition to programming operations: a simulative approach

Thursday, Septembre 25

8:30-9:00 **REGISTRATION & Coffee**

SESSION-5 Photonics & Metasurfaces 1 *(Session chair: Wei Zhang & Robert Simpson)*

9:00-9:25 Invited: **David Wright** - University of Exeter, UK
Reconfigurable phase-change metasurfaces for optical mode conversion and optical angular momentum control

9:25-9:40 **Anbarasu Manivannan** - Indian Institute of Technology Madras, India
Optical Phase Change Materials for hyperspectral sensing

9:40-9:55 **Konstantinos Iliopoulos** – Aix-Marseille Univ. & CNRS - Fresnel, France
Tunable colour coatings using phase change materials

9:55-10:10 **Shaojie Yuan** - Huazhong University, China
Dynamically Tunable Asymmetric Bragg-Enhanced Fabry–Pérot Cavity for Near-Perfect Mid-Infrared Absorption

10:10-10:35 Invited: **Juejun Hu** - Massachusetts Institute of Technology (MIT) – USA
Mid-infrared PCM spatial light modulator

10:35-11:10 **COFFEE BREAK**

SESSION-6 Photonics & Metasurfaces 2 *(Session chair: A. Manivannan & Magali Putero)*

11:10-11:25 **Yoann Brûlé** – CEA-LETI, France
Low-Energy and High Endurance All-Optical Reconfigurable Silicon Photonic Devices based on Phase-Change Materials

11:25-11:40 **Peter Kepic** - Brno University of Technology, Czech Republic
Inverse-designed Si-Sb_2S_3 tunable integrated meta-switch

11:40-11:55 **Robert E. Simpson** - School of Engineering, University of Birmingham, UK
The metastable phase of Bi_2Te_3

11:55-12:10 **Nicolas Bottin** – STMicroelectronics & CNRS-IM2NP, France
PCM cycling endurance Monitored in situ by engineered multi-beam Laser irradiations

12:10-12:35 Invited: **Thomas Taubner** - RWTH Aachen University, Germany
Programmable Nanophotonics with Phase-Change Materials: From Metasurfaces to Polaritons

12:35-12:50 **David Grosso** – SOLNIL & CINaM - Aix-Marseille Univ. & CNRS, France
Passive and active metasurfaces elaborated by nanoimprint and derived methods

12:50-14:45 **Lunch & Posters Session 2**

12:50 – 14:45 POSTER SESSION 2: all <u>even-numbered</u> posters

SESSION-7 **Non-digital computing** ***(Session chair: Suyoun Lee)***

14:45-15:10 Invited: **Wen Zhou** - Xi'an Jiaotong University, China
Neuromorphic photonic computing devices based on phase-change memory

15:10-15:35 Invited: **Xilin Zhou** – Shanghai Inst. of Microsystem&Information Techno., China
A Verification-Free Multi-Level Phase Change Memory for On-Chip Activation Compressed Training

15:35-16:00 Invited: **Hongsik Jeong** - UNIST, Republic of Korea
Deep-Cryogenic Phase Change Memory

16:00-16:30 **COFFEE BREAK**

SESSION-8 **OTS & Applications** ***(Session chair: Yuji Sutou)***

16:30-16:45 **Suyoun Lee** - Korea Institute of Science and Technology, Korea
True random number generator (TRNG) based on Ovonic Threshold Switch (OTS) and its applications for Restricted Boltzmann Machine (RBM)

16:45-17:00 **Yoshimasa Matsushita** - Nippon Electric Glass Co., Ltd., Japan
High-Selectivity Ge-Te-Based Ovonic Threshold Switching Material for Selectors

17:00-17:25 Invited: **Daniele Garbin** - IMEC, Belgium
Innovations in OTS Selectors and Memory Materials: Theoretical Insights and Experimental Validations

19:00 - ... **GALA DINNER at Fort Ganteaume**

Friday, Septembre 26

8:30-9:00 **Coffee**

SESSION-9 OTS & SOM *(Session chair: Dongho Ahn)*

9:00-9:25 Invited: **Min Zhu** - Shanghai Jiao Tong University, China
Volatile to Non-Volatile Switching Transition in Chalcogenides

9:25-9:40 **Rivka-Galya Nir-Harwood** - Israel Institute of Technology, Israel
Exploring Sub-Nanosecond Programming of Selector-Only Memory

9:40-10:05 Invited: **Massimo Borghi** - STMicroelectronics, Italy
Programmable OTS. An interesting option for the embedded PCM scaling roadmap?

10:05-10:20 **Renzo Antonelli** – CEA-LETI & CNRS-LTM , France
OTS+PCM Material Exploration and Thermal Analysis for Crossbar Arrays

10:20-10:55 **COFFEE BREAK**

SESSION-10 Growth, Heterostructures *(Session chair: Andriy Lotnyk)*

10:55-11:10 **Mark Clark** – Intermolecular, USA
Efficient Screening of Chalcogenides and Down-Selection to Promising Compositions for ALD Process Development

11:10-11:25 **Stefano Cecchi** - University of Milano Bicocca - Italy
Van der Waals epitaxy and characterization of two-dimensional tellurium on silicon

11:25-11:40 **Seppe van Dyck** – Ghent University, Belgium
Taming Thermal Transport: TMD Superlattices are the Key to Controlling Heat in Phase Change Memory

11:40-12:05 Invited: **Simone Prili** - University of Rome Tor Vergata & CNR-IMM – Italy
Growth, Epitaxy and Thermal Stability of Phase Change Heterostructures

12:05-12:25 **BREAK (Processing Votes for Awards)**

12:25 – 12:40 Closing + AWARD CEREMONY (3 prizes for oral & 3 prizes for posters)

12:40-13:30 **Lunch (Take away / Packed lunches)**

Poster List for POSTER SESSION 1

(all odd-numbered posters)

Wednesday, Sept. 24, 12:50 – 14:40

P-01 **Hur Namwook** - Ulsan NIST, Republic of Korea
Multi-Threshold Voltage Selector-Only Memory Based on Non-Toxic amorphous Bi-Chalcogenides

P-03 **Hengyi Hu** - Huazhong University of Science & Technology, China
Investigation of the Electrical Performance and Crystallization Behavior of Carbon-Doped $Ge_1Sb_4Te_7$

P-05 **Xue-Peng Wang** - Shenzhen University, China
Ultrathin antimony for ultralow-drift phase-change memory applications

P-07 **Stuart Kendall** - University of Exeter, UK
Mid-Infrared Reconfigurable Spatial Filtering via an Extraordinary Optical Transmission Phase-Change Metasurface

P-09 **Oumaima Meskini** – IM2NP, Aix-Marseille univ., CNRS & Solnil, France
Phase change materials combined with soft-NIL-prepared metasurfaces for large scale tunable photonic applications

P-11 **Mouad Mraouni** – INL, CNRS & STMicroelectronics, France
Nanostructures with low-loss phase-change materials: Towards large-scale reconfigurable nanophotonics

P-13 **Yudha Ramanda** – CINaM, Aix-Marseille univ. & CNRS, France
Sol-gel-based Vanadium Dioxide Thin Film and Conformal Metasurface

P-15 **Filip Ligmajer** – Brno University of Technology, Czechia
VO_2 nanostructures with controlled hysteresis for multilevel nanoscale switchable devices

P-17 **Junchao Song** - University of Exeter, UK
Fabrication-friendly Plasmonically-enhanced All-optical Integrated Photonic Phase-change Memory

P-19 **Kostiantyn Shportko** - Lashkaryov Instit. of Semicond. Physics of NAS, Ukraine
Optical characterization of GeTe-Sb_2Te_3 heterostructures prepared by pulsed laser deposition

P-21 **Joseph Pady** – University of Exeter, UK
Optimisation of Device Readout Efficiency for Phase-Change Integrated Photonic Computing

P-23 **Pierre Meilleur** – Univ. Grenoble Alpes, CEA-LETI & STMicroelectronics, France
Pushing the limits of embedded phase-change memories with innovative Se-rich alloys

P-25 **Mohamad Kanaan** - LTM, CEA-LETI & STMicroelectronics, France
Innovative Threshold-Changeable Memory (TCM) Based on Amorphous GeSbSeN

P-27 **Tushar Chakrabarty**– IEMN, Univ. Lille, CNRS & STMicroelectronics, France
Thermal metrology for phase change materials

P-29 **Victor Bogenschutz** – CEA-LETI & STMicroelectronics, France
Driving the Segregation and Crystallization in Ge-rich GeSbTe by Dopant Introduction

P-31 **Thomas Fernadez** - IM2NP, Aix-Marseille univ., CNRS, France
Time-resolved X-Ray Diffraction from laser-irradiated Ge-rich GST thin films

P-33 **Wei-Chiao Chang** - Tohoku University, Japan
The effects of V doping in CrN based ultra-low energy consumption phase change material

P-35 **Florent Mignerot** – IM2NP, Aix-Marseille univ. & CNRS, France
Crystallization investigations of Ge-rich GST cells using in situ thermal pulses coupled with STEM-EDX and HR-TEM analyses

P-37 **Jiangjing Wang** - Xi'an Jiaotong University, China
High-quality synthesis of $Ge_2Sb_2Te_5$/$TiTe_2$ thin films

P-39 **Shan Song** - Chemnitz University of Technology & Fraunhofer Institute for Electronic Nano Systems, Germany
Influence of Sputtering Parameters on the Stoichiometry and Crystallization Behavior of Germanium Telluride (GeTe) Films Grown by Confocal Magnetron Sputtering

P-18 **Chaymaa Boujrouf** – IM2NP, Aix-Marseille univ., CNRS, France
Nanoscale investigation of electrically-induced transformations in Ge-rich GST for advanced phase change memory applications

Poster List for POSTER SESSION 2

(all even-numbered posters)

Thursday, Sept. 25, 12:50 – 14:45

P-02 **Kim Seunghwan** - Ulsan NIST, Republic of Korea
Threshold Switching in Solid-State Amorphous Tellurium Accessed via On-Device Electrothermal Melt-Quenching

P-04 **Simone Marcorini** - University of Milano-Bicocca, Italy
Viscosity and the breakdown of Stokes-Einstein relation in supercooled liquid $Ge_2Sb_2Te_5$ from simulations with a neural network potential

P-06 **Piotr Popek** - University of Groningen, The Netherlands
Towards cryogenic phase change materials for neuromorphic image recognition

P-08 **Dario Baratella** - University of Milano-Bicocca, Italy
Ab-initio study of electromigration in liquid GeAsSe alloys for selector device

P-10 **Beomsung Park** - Ulsan NIST, Republic of Korea
Self-aligned Atomically Thin Thermal Barrier for Highly Energy-Efficient Phase-Change Memory

P-12 **Sara De Simone** – CNR-IMM, Italy
Phase-change heterostructures based on $MoSe_2$ intercalated with $Ge_2Sb_2Te_5$

P-14 **Christian Petrucci** – CNR-IMM & Univ. Tor Vergata, Italy
Structural and electronic characterization of Ti-doped GST films: preliminary results

P-16 **Hamid Neggaz** - IM2NP, Aix-Marseille univ. & CNRS, France
Exploring ZnSb Phase Change Material Alloys for Nonvolatile Embedded-Memory Applications

P-20 **Nian-Ke Chen** - Jilin University, China
Thermal melting induced band-gap closing and electronic delocalization in Ovonic threshold switching material GeSe

P-22 **Yuxing Zhou** - University of Oxford, UK
Atomistic simulations of Ge–Sb–Te devices for memory applications and neuromorphic computing tasks

P-24 **Qundao Xu** – Huazhong University of Science and Technology, China
Multiscale Design of Doped Antimony-Based Phase-Change Materials

P-26 **Wen-Xiong Song**- Shanghai Instit. of Microsystem and Information Techno., China
Structural ordering of amorphous motifs under electric field in threshold switching chalcogenides

P-28 **Yu-Ting Huang**- State Key Laboratory of Integrated Optoelectronics, Jilin University, China
Complex charge density waves and phases transitions in two-dimensional III_2–VI_3 materials for low-power consumption memory

P-30 **Minh-Anh Luong** – CEMES-CNRS & Univ. Toulouse, France
On the origin and growth of voids in N-doped Ge-rich GeSbTe alloys subjected to thermal annealing

P-32 **Adrien Delpoux**- LPCNO, Univ. Toulouse, France
Impedance Spectroscopy of intermediate states in Ge-rich GeSbTe PCM cells

P-34 **Anbarasu Manivannan** – Indian Institute of Technology Madras, India
Design of All-dielectric Ge-rich Ge-Sb-Te based optical modulator with high modulation efficiency

P-36 **Aastik Agnihotri** - Indian Institute of Technology Madras, India
Improving Insertion Loss and Isolation in GeTe-based RF Switch using Coplanar Waveguide Layout Optimization

P-38 **Frédéric Leroy** - CINaM, Aix-Marseille univ. & CNRS, France
Ferroelectric domain structure and growth of GeTe thin films on silicon substrates: the key role of atomic steps

P-40 **Konstantinos Konstantinou**- University of Turku, Finlan
Evolution of structural disorder and energy landscape in amorphous $Ge_2Sb_2Te_5$ under non-equilibrium conditions

Ovshinsky Lectureship Award

The Ovshinsky Lectureship Award was established in 2014 in memory of American Inventor and pioneer in the field of Ovonics, **Stanford Ovshinsky**. The award enjoys the patronage of members of his family, Rosa Ovshinsky, Robin Dibner and Steve Dibner who have asked Dr Alex Kolobov to chair the selection process. The award rules are that (i) the Award can be given only once and (ii) the International Selection Committee is formed from the winners of the previously existing Ovshinsky Award for Excellence in Amorphous Chalcogenides who themselves cannot be nominated for the Lectureship Award. The award is announced prior to the annual E\PCOS conference, and the awardees give the inaugural lecture at this conference.

This year, **Derchang Kau** and **Fabio Pellizzer** are the winners.

Congratulations to the winners!

Ovshinsky Lectureship Award 2025

Switches in Chalcogenide Glass

Ovshinsky Lecture, September 24, 2025

By
DerChang Kau – Intel Fellow, Ret'd. Adjunct Professor, National Taiwan University
Fabio Pellizzer – Fellow at Micron Technology

The quest for a universal memory that combines the speed of volatile memory with the permanence of storage has been a decades-long endeavor, a journey marked by significant advancements in chalcogenide-based cross-point technologies. Early explorations into Ovonic materials in the 1970s, including concepts like the read-mostly memory, laid the foundational understanding for storing information using phase-change properties. Renewed interest at the turn of the millennium, spurred by breakthroughs in optical storage materials, reignited the field. This period saw the emergence of Ovonic Unified Memory (OUM) at the 180nm technology node, demonstrating capabilities such as direct overwrite, exceptionally swift reset and set operations, and an extraordinary endurance extending well beyond a trillion cycles, positioning it as a compelling alternative to Flash memory.

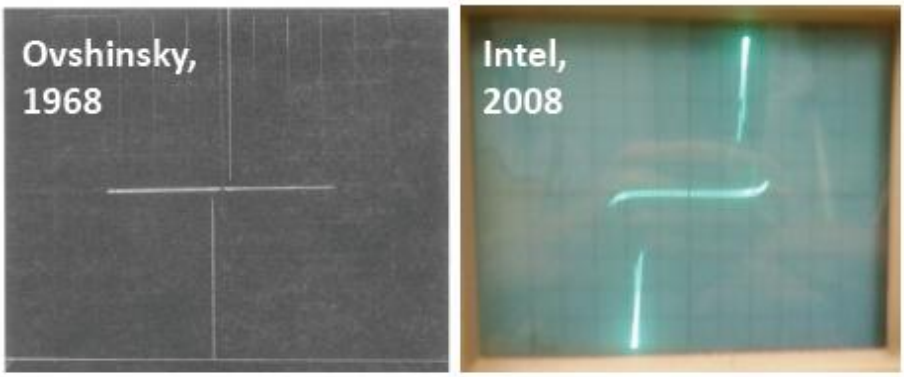

The evolution continued with phase-change memory (PCM) products, such as a 90nm technology featuring a vertical pnp-BJT selector and various heater architectures. This generation achieved very low programming currents and robust reliability, also showcasing multi-level cell storage capability, which allowed the storage of multiple bits per cell by precisely controlling intermediate resistance states. Further scaling led to a 45nm generation PCM with a very small cell area, affirming PCM's maturity for mainstream applications.

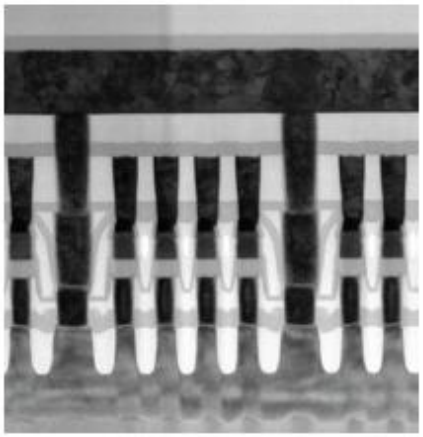

Technology node	45 nm
Cell size	0.0108 μm^2
Bit-Line/Word-Line pitch	104/104 nm
Effective cell size*	0.015 μm^2 (5.5 F^2)
Array selector	Vertical pnp-BJT
Periphery CMOS	Dual gate oxide 8/3 nm
Interconnection	3 Cu + 1 AlCu
Supply voltage	1.8 V

45nm1T1R in 1Gb PCM array

A pivotal development was the PCMS prototype, which integrated a phase-change storage element with an Ovonic Threshold Switch (OTS) selector in a true cross-point array. This innovative, stackable backend technology achieved very rapid reset speeds and substantial endurance, while enabling a highly area-efficient layout by stacking over CMOS circuitry. This progression culminated in the 3D XPoint™ product, which entered volume production in 2015. With multiple stacked arrays at fine dimensions, 3D XPoint combined a phase-change material with a chalcogenide selector, offering a compelling balance of high capacity, low latency, direct write, and non-volatility. It demonstrated superior performance in terms of average and tail latency when compared to 3D-NAND, aiming to fill the performance-cost gap between DRAM and 3D-NAND. 3D XPoint proved that a robust, byte-addressable, high-endurance NVM can create real system-level wins but faced significant ecosystem economics and tough market challenges between two juggernauts (DRAM and NAND). Despite its launch and initial success, 3D XPoint eventually ceased production, a testament to the long and often challenging path of disruptive memory technologies.

PCM

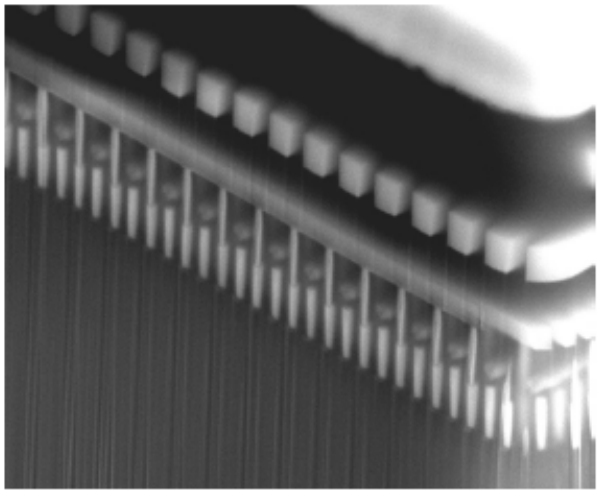

8λ² BiPCM array with a CMOS based circuits for bitline/wordline select/decode functions, not shown, are implemented at the edge of array.

PCMS

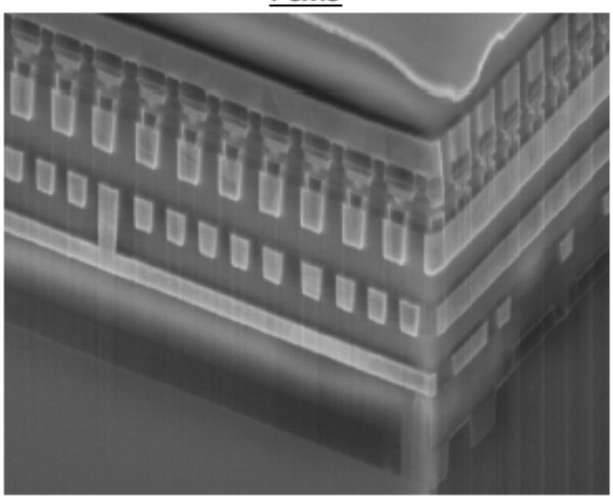

One layer of 4λ² PCMS array stacks on the top of 2-level metal CMOS circuits for bitline and wordline select/decode functions.

The perseverance in chalcogenide research led to the **S**ingle-chalcogenide **X**Point **M**emory (SXM) concept, a significant simplification that eliminates the separate phase-change storage element entirely. SXM innovatively leverages the ability to modulate the threshold voltage of the chalcogenide-based selector itself through programming conditions to store information. This streamlined structure results in a more cost-effective process, enhanced production yield, and improved scaling prospects, crucially eliminating the thermal disturb issue inherent in 3D XPoint. SXM offers symmetric read and write low latency, approaching the speeds of dynamic random-access memory, and has demonstrated significantly higher write endurance and lower programming current compared to its predecessor. Its inherent simplicity also makes it exceptionally well-suited for three-dimensional vertical integration, akin to 3D-NAND technology, offering a robust path for future scalability.

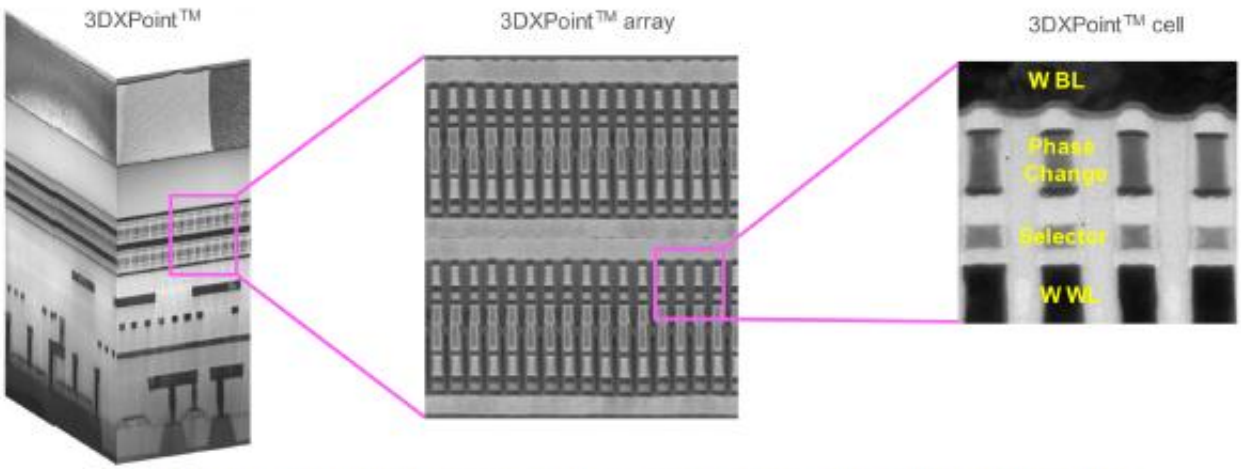

Second generation 3DXPoint™ component 20nm half-pitch 256Gb with 4 decks.

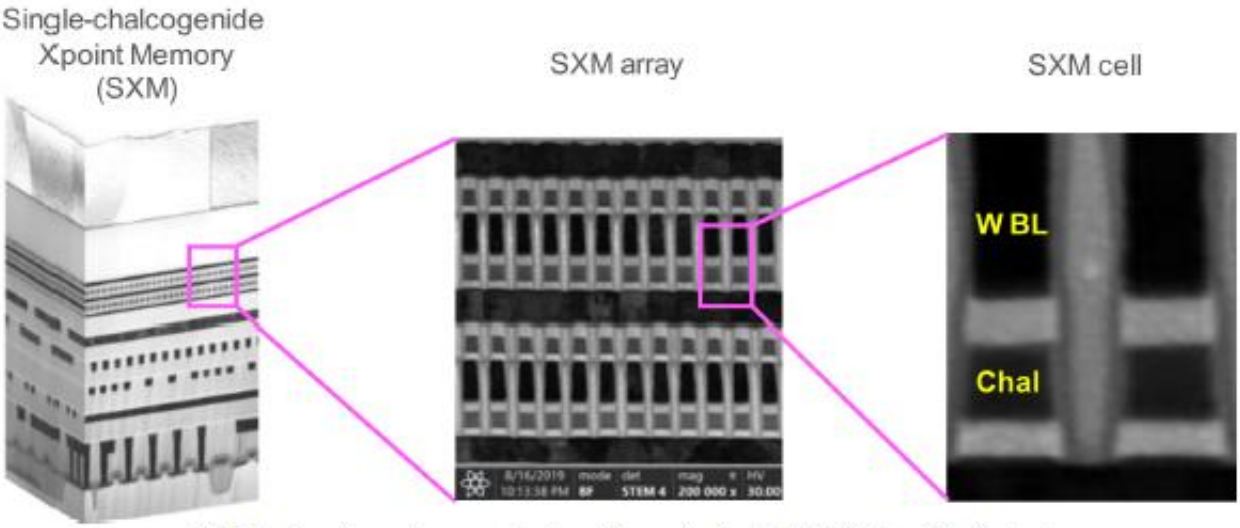

SXM technology demonstrator: 20nm half-pitch 256Gb with 4 decks

The journey of chalcogenide-based memories exemplifies the typically long gestation period for disruptive memory technologies. While establishing mainstream adoption remains a formidable challenge, these solutions have proven their technological viability and continue to hold substantial potential for future market opportunities.

Unconventional amorphization in layered materials from multimodal coupling of fields to competing orders

[Invited]

Ritesh Agarwal[1]*

[1] Department of Materials Science and Engineering, University of Pennsylvania
Philadelphia, PA 19104-6272

*corresponding author: riteshag@seas.upenn.edu

ABSTRACT

We report unconventional long-range solid-state amorphization in ferroic In_2Se_3 nanowires via direct current biasing. The interplay of the electric-field, current, heat and piezoelectric stress results in the formation of interlayer sliding defects, polarization rotation induced disorder followed by a sudden collapse to the amorphous phase. We will compare our work from earlier studies on melt-quench free amorphization in Ge-Sb-Te nanowires.

Key words: Ferroic, polar domain, solid-state amorphization, memory

1. INTRODUCTION

Our group while working on Ge-Sb-Te phase change nanowires has extensively reported that conventional understanding of melt-quench based amorphization process needed to be revisited. Nanowires, due to their long lengths do not typically reach high temperatures required for conventional melting of the material. Our earlier results on Ge-Sb-Te systems with high carrier densities showed that crystal-amorphous transformation can be achieved through a defect-based pathway. This pathway involves creation of extended defects such as anti-phase boundaries (APBs) in GeTe and dislocations in Ge-Sb-Te, rotation of polar domains, migration and accumulation of defects at a region of local inhomogeneity followed by collapse of order. However, in polar materials, the external electric field does not couple to polar domains due to carrier screening. Thus, in Ge-Sb-Te nanowires, carrier-wind force interaction with defects and polar domains was utilized to construct a low power solid-state amorphization pathway. Conventional ferroelectrics are electrically insulating, which allows the order parameter to couple with the electric field. Utilizing field-controlled frustration and disorder in ferroic systems to design low-energy amorphization pathway is an unexplored territory and requires finding materials with a right balance of ferroic nature and electrical conductivity to enable a multimode coupling to electric field and current. Polymorphs of In_2Se_3 provide rare materials platforms which can be both ferroic and semiconducting. Here, we report the unusual coupling between the electric field/current, ensuing piezoelectric stress and structural order in a new ferroelectric phase of In_2Se_3 nanowires and illustrate how it leads to an unconventional crystal-amorphous transformation. Our experiments shed light on the mechanisms behind a fundamentally different order-disorder transition via a multimodal coupling between ferroic and crystalline order with external field, current and piezoelectric stress and opens up new pathways for exploring low energy amorphization.

2. EXPERIMENTAL

We synthesized In2Se3 nanowires in a new ferroelectric variant of the β″-In_2Se_3 by a catalyst-assisted vapor-liquid-solid growth mechanism. To understand the evolution of microstructure and its relationship to its peculiar ferroelectric order upon applying external electric fields, we fabricated nanowire devices on TEM grids and probed their structural evolution with applied electrical bias.

3. RESULTS & DISCUSSION

The nanowires are single-crystalline with a $<11\bar{2}0>$ growth direction. In addition to the primary SAED reflections for a rhombohedral crystal, three superlattice reflections along $<1\bar{1}00>$ were observed, suggesting a superstructure formation. HAADF-STEM imaging shows the bright-dark

contrast modulation due to superstructure formation with ~1.35 nm ($4d_{1\bar{1}00}$) periodicity along $< 1\bar{1}00 >$. Contrast from the lattice sites in HRSTEM images suggests a stacking variant of type 1T. Atomic displacement map shows that, on average, the in-plane Se displacement is ~15 pm and along <11$\bar{0}$0> showing a ferroelectric order.

Based on *in situ* TEM measurements of nanowire devices under d.c. bias, we propose a model for amorphization: electric field and carrier-wind force provide driving force for polarization rotation (domain boundary motion) and sliding fault formation, initially in a local nanoscale region. The ensuing piezoelectric stress due to polarization rotation creates similar defects over a longer range, dictated by the lengthscale of the mechanical stress. As more sliding faults are created, they interact and cause strain-field fluctuations, which further create more sliding faults, leading to much smaller domains (and more domain boundaries). Interaction of many sliding faults and domain boundaries locally causes loss of long-range order at the nanometer scale, "nucleating" a solid state amorphized region. These regions are replicated spatially over micrometer lengthscales via long-range strain fields, leading to multiple nucleation events of the amorphous phase. These amorphous nuclei locally grow as acoustic jerks further disrupt the local crystalline order. Electrically, a collapse of current occurs once the percolative crystalline pathways are cut off completely by the growing amorphous nuclei. Such long-range electrically induced amorphization highlights the interplay of unique structure, piezo/ferroelectricity in β'' -In2Se3 and the multimodal coupling of the order parameter to external fields.

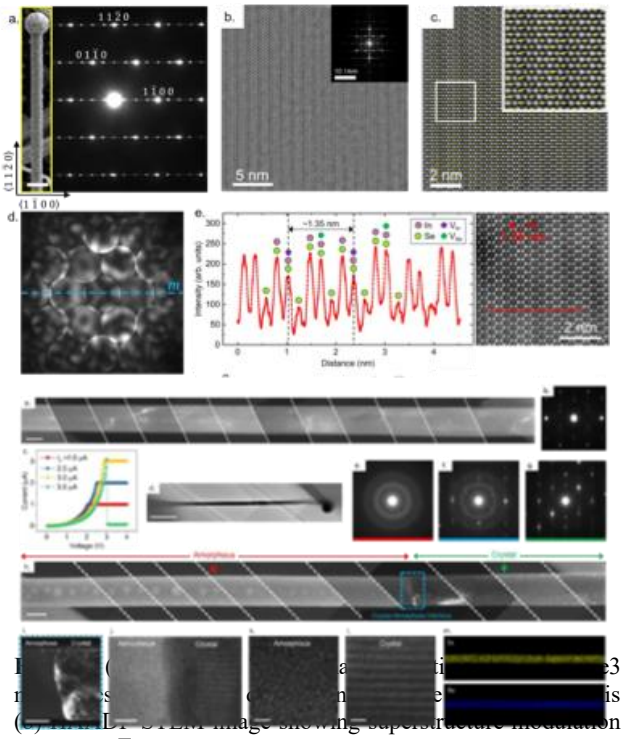

I (a ti e3
r s c n e is
(c) HAADF-STEM image showing superstructure modulation along <11$\bar{0}$0>. (c) Se atom displacement map (d) CBED showing the presence of a {112$\bar{0}$} mirror plane. (e) Line intensity profile mapping along <11$\bar{0}$0> from the region indicated by red line in the HAADF-STEM image t reveals a 1T stacking variant and the periodic dark regions are due to the presence of ordered In vacancies. (**bottom panel**) D.C. voltage induced amorphization in a β″-In2Se3 nanowire device. (a) DF-TEM image and (b) SAED of the pristine nanowire device. (c) A series of 0-4 V d.c. I-V sweeps applied on the nanowires where the compliance current was gradually increased. A sudden drop in current indicating amorphization. (d) TEM image of the nanowire confirming amorphization. (e-g) SAED of the nanowire from different regions as indicated in the DF-TEM image. (h) DF-TEM image of the nanowire where the crystal-amorphous interface is indicated by the blue dashed box. The crystal-amorphous interface is further shown in (i) DF-TEM image and (j) HR-TEM image. (k-l) HR-TEM image from the amorphous and crystalline regions of the nanowire, respectively. (m) EDX mapping of the nanowires. *From Ref. 1.*

4. CONCLUSIONS

In conclusion, we uncovered a unique long-range solid-state amorphization process in ferroelectric In2Se3 nanowires upon applying a d.c. bias, facilitated by a complex interplay of electric field, current, piezoelectric stress, acoustic jerks and Joule heating. In2Se3 is a model material system in which the synergistic confluence of various material properties (layered, semiconducting, ferro- and piezoelectric) results in an unconventional amorphization process. We believe that similar studies on other semiconducting ferroic materials can unlock other metastable phase transformations, which holds the potential for designing new materials and devices for low-energy consuming devices.

REFERENCES

1. G. Modi, et al, *Nature*, 635, 847 (2024).

In situ atomic-scale investigation of structural transitions in $Ge_2Sb_2Te_5$ thin films

A. Lotnyk[1,*], T. Dankwort[2,3], M. Behrens[1], L. Voß[2], S. Cremer[1], L. Kienle[2]

[1]Leibniz Institute of Surface Engineering (IOM), Permoserstr. 15, 04318, Leipzig, Germany

[2]Institute for Materials Science, Faculty of Engineering, University of Kiel, Kaiserstr. 2, 24143, Kiel, Germany

[3]Fraunhofer Institute for Silicon Technology ISIT, Fraunhoferstrasse 1, 25524 Itzehoe, Germany

*corresponding author: andriy.lotnyk@iom-leipzig.de

ABSTRACT

Using *in situ* heating atomic-scale transmission electron microscopy (TEM), the transformations from vacancy-disordered to vacancy-ordered (vo) and van der Waals (vdW)-like bonded trigonal structures in $Ge_2Sb_2Te_5$ (GST225) thin films are studied. Detailed characterization of vo-grains reveals transient structures that indicate a shear-driven transformation mechanism, along with the presence of various defects and associated chemical changes during the transitions.

Key words: *in situ* TEM, structural transition, thin film, vacancy layer

1. INTRODUCTION

Ge-Sb-Te materials are a remarkable class of functional materials, widely used in non-volatile memory, thermoelectric devices, and as topological insulators. These alloys exhibit significant structural distortion and contain a high concentration of vacancies, which critically influences their structural and electronic transitions. Therefore, controlling disorder and understanding structural transformations in GST materials are essential for optimizing memory device design and reliability [1]. In this study, structural transformations in GST225 thin films prepared as membranes on carbon-coated TEM Ni grids are investigated using *in situ* heating TEM, focusing on structural changes within <110>-oriented fcc-GST225 grains. Complementary *in situ* XRD heating was also performed on epitaxial GST225 thin films to monitor structural evolution [2].

2. EXPERIMENTAL

18-nm-thick amorphous GST225 (a-GST225) thin films were deposited by pulsed laser deposition onto carbon-coated TEM Ni grids and subsequently coated with a thin protective layer of amorphous $LaAl_2O_{3-x}$. *In situ* heating TEM experiments were conducted using a probe Cs-corrected Titan^3 G2 60–300 microscope operated at 300 kV. A Gatan double-tilt heating holder was used for the experiments. Complementary *in situ* XRD heating measurements were carried out using a Rigaku SmartLab diffractometer.

3. RESULTS & DISCUSSION

At TEM holder temperatures between 135°C and 150°C, crystallization of a-GST225 led to the formation of fcc-GST225 grains with randomly distributed vacancies. Beginning at 160°C, vacancies gradually accumulated into distinct vacancy layers (Fig. 1(a)-(c)). Further heating to 220°C and 240°C induced the formation of vo-GST225 grains and trigonal GST225 domains with vdW-like gaps within the vo-GST grains, alongside the growth of large <001>-oriented trigonal GST225 grains. These observations align well with in situ XRD heating results of epitaxial vo-ordered GST255 thin films. Additionally, vo- and fcc-GST structures can coexist with trigonal GST225 phases within a single grain. Complete transformation to <11-20>-oriented trigonal GST225 grains occurs at 280°C. Unlike other grains, the <001>-oriented trigonal grains exhibit abnormal grain growth, which is further accelerated by electron beam irradiation. Detailed characterization of vo-GST225 grains reveals transient structures indicative of a shear transformation mechanism, various defects, and chemical changes during the transition (Fig. 1(d))

[2]. Particularly, layered defects were identified in both vo- and trigonal-GST225 structures, along with dislocations emerging in the layered regions after *in situ* TEM heating. Based on these observations, a shear-driven transformation mechanism from the vo- to-trigonal phase is proposed. It initiates in domains with highly ordered vacancy layers within vo-grains and involves short-range motion of Te and GeSb planes within GST225 building units. This leds to shearing of GST building blocks. The transformation proceeds with a continuous reduction of Te-Te distances, ultimately resulting in the formation of vdW-like gaps from the original vacancy layers.

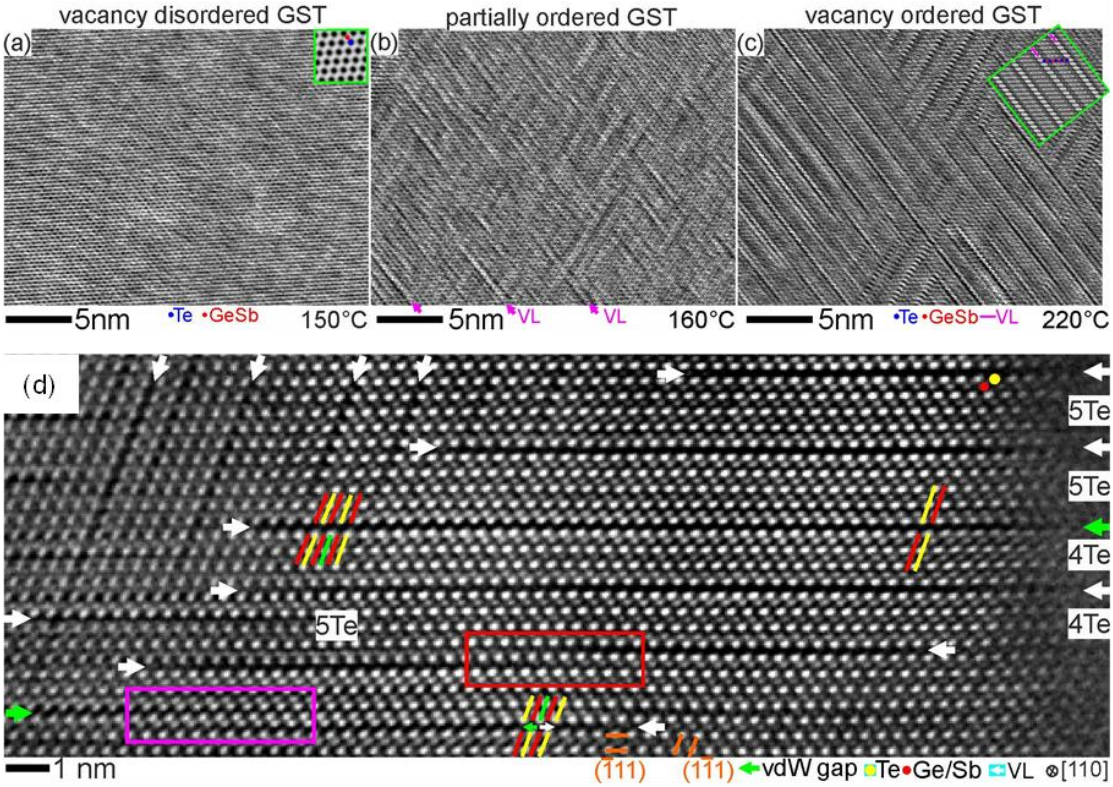

Fig. 1. (a), (b) and (c) HRTEM micrographs acquired at TEM holder temperatures of 150°C, 160°C and 220°C, respectively. Insets in (a) and (c) show simulated HRTEM images. VL shows a vacancy layer. (d) HAADF-HRSTEM image acquired after thermal heating of GST225 thin film in TEM to a holder temperature of 240°C. Yellow and red strokes depict Te and GeSb layers, respectively. Green stroke marks the core of transition area and extra Te plane. The rectangles depict layered defects.

4. CONCLUSIONS

Overall, this study offers new insights into the phase transition mechanisms in thin GST-based layers and provides a foundation for microstructure optimization through disorder control in these systems [2].

REFERENCES

1. A. Lotnyk, M. Behrens, B. Rauschenbach, *Nanoscale Adv.* 1 (2019) 3836-3857

2. A. Lotnyk, T. Dankwort, M. Behrens, L. Voß, S. Cremer, L. Kienle, *Acta Mater.* 266 (2024) 119670

The authors thank A. Mill (IOM) for FIB lamellae preparation. German Research Foundation (DFG, project number 445693080) is acknowledged for financial support.

Tailoring Phase Change Materials for different Applications

The Role of Metavalent Bonding

[Invited]

Matthias Wuttig[1,2]

[1] I. Institute of Physics, Physics of Novel Materials, RWTH Aachen University, 52056 Aachen, Germany

[2] PGI 10 (Green IT), Forschungszentrum Jülich GmbH, 52428 Jülich, Germany

*corresponding author: wuttig@physik.rwth-aachen.de

ABSTRACT

Controlling a state of material between its crystalline and glassy phase has fostered many real-world applications. Switching between these two different states is particularly interesting if it is accompanied by a significant change of material properties. Phase change materials provide the interesting property combination of fast switching between these two states which is accompanied by a pronounced property change. Crystallization can be accomplished in these phase change materials by changes of up to 6 orders in the electrical conductivity. For neuromorphic applications it is crucial to tailor the crystallization kinetics, the relevant length scale of the switching processes as well as the electrical contrast between both states. In this presentation, we will devise design rules for crystallization and vitrification kinetics, control of the nanostructure as well as the contrast of the corresponding optical properties. In the past, for all three aspects only basic stoichiometry trends had been established. Here, we identify systematic stoichiometry trends for these processes in phase change materials, i.e. along the GeTe-GeSe, GeTe-SnTe, and GeTe-Sb_2Te_3 pseudo-binary lines employing a pump-probe laser setup and calorimetry. We present a clear stoichiometry dependence of electrical properties and crystallization speed along a line connecting regions characterized by two fundamental bonding types, metallic and covalent bonding. Increasing covalency slows down crystallization by six orders of magnitude and promotes vitrification. The stoichiometry dependence is correlated with material properties, such as the electrical properties of the crystalline phase and a bond indicator, the number of electrons shared between adjacent atoms. A quantum-chemical map explains these trends and provides a blueprint to design crystallization kinetics, nanostructure control and property contrast.

Key words: phase change materials, metavalent bonding

High-throughput screening for layered phase-change memory materials

Wei Zhang[1,*]
[1]Center for Alloy Innovation and Design (CAID), State Key Laboratory for Mechanical Behavior of Materials, Xi'an Jiaotong University, Xi'an 710049, China.
*corresponding author: wzhang0@mail.xjtu.edu.cn

Chalcogenide phase-change materials (PCMs) are showing versatile possibilities in cutting-edge applications, including non-volatile memory, neuromorphic computing, and nano-photonics. However, for embedded phase-change memory applications, conventional PCMs suffer from insufficient thermal stability because of their relatively low crystallization temperatures (T_x). Although doping with additional alloying elements could improve the amorphous stability, it also increases the tendency towards compositional partitioning and phase separation. Recently, a two-dimensional (2D) layered compound $CrGeTe_3$ (CrGT) was developed as a PCM, showing a high T_x ~ 276 °C with an inverse change in resistive-switching character upon phase transition [1]. Here, we report a high-throughput materials screening for 2D layered phase-change chalcogenides [2, 3]. We aim to clarify whether the high Tx and the inverse electrical resistance contrast are intrinsic features of 2D PCMs. In total, twenty-five 2D chalcogenides with CrGT trilayer structures have been identified from a large database. We then focused on selected layered tellurides by performing thorough ab initio simulations and experimental investigations and confirming that their amorphous phase indeed has a much higher T_x than conventional PCMs. We attribute this enhanced amorphous stability to the structurally complex nuclei required to render crystallization possible. Overall, we regard $InGeTe_3$ as a balanced 2D PCM with both high thermal stability and large electrical contrast for embedded memory applications.

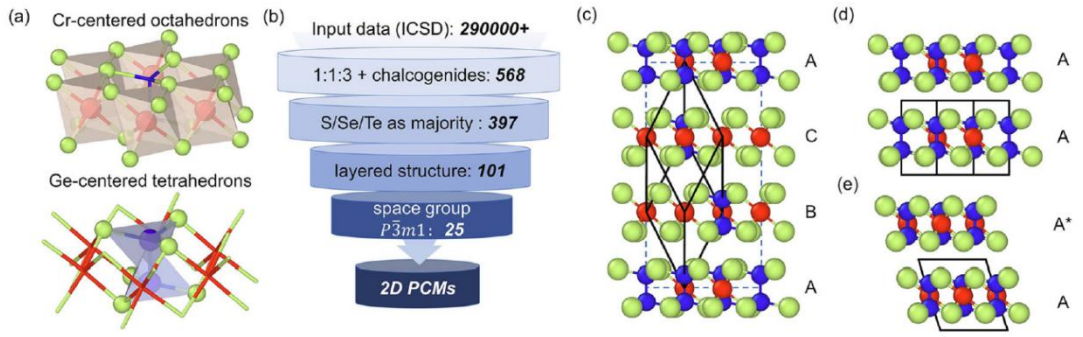

Figure 1. The computational screening procedure of layered phase-change materials.

REFERENCES

1. S. Hatayama, *et al. ACS Appl. Mater. Interfaces* (2018) 10, 2725-2734.
2. S. Sun, *et al. npj Comput. Mater.* (2024) 10, 189.
3. Y. Jiang, *et al.* Nanoscale (2025) 17, 4372-4380.

Million-atom simulation of the set process in phase change memories at the real device scale

[STMicroelectronics Luca Laurin's prize]

O. Abou El Kheir[1] and M. Bernasconi[1]*
[1]Department of Materials Science, University of Milano-Bicocca, Milan, Italy
*corresponding author: marco.bernasconi@unimib.it

ABSTRACT

Phase change materials are exploited in several enabling technologies such as storage class memories, neuromorphic devices and memories embedded in microcontrollers. A key functional property for these applications is the fast crystal nucleation and growth in the supercool liquid phase. Over the last decade, atomistic simulations based on density functional theory (DFT) have provided crucial insights on the early stage of this process. These simulations are, however, restricted to a few hundred atoms for at most a few ns. More recently, the scope of the DFT simulations has been greatly extended by leveraging on machine learning techniques. In this paper, we show that the exploitation of a recently devised neural network potential for the prototypical phase change compound $Ge_2Sb_2Te_5$ (GST) [1,2] allows simulating the crystallization process in a multimillion atom model at the length and time scales of real memory devices [3]. The simulations provide a vivid atomistic picture of the subtle interplay between crystal nucleation and crystal growth from the crystal/amorphous rim in a model mimicking the operation of memories in the Wall geometry (see Figure 1). The evolution in time of the recrystallized atoms belonging to the initially amorphous dome is shown by the snapshots in Figure 2. At the end of the simulations lasting 1.55 ns, 80 % of the atoms are recrystallized mainly from crystal growth at the amorphous-crystalline interface (88 % of the recrystallized atoms). A minor fraction of recrystallized atoms belongs to new crystallites nucleated inside the dome (see Figure 2). At the conditions of the set operation of the memory in the Wall architecture the crystallization is thus dominated by growth at the crystal-amorphous interface. Moreover, the simulations have allowed quantifying the distribution of point defects that control electronic transport, in a very large crystallite grown at the real conditions of the set process of the device.

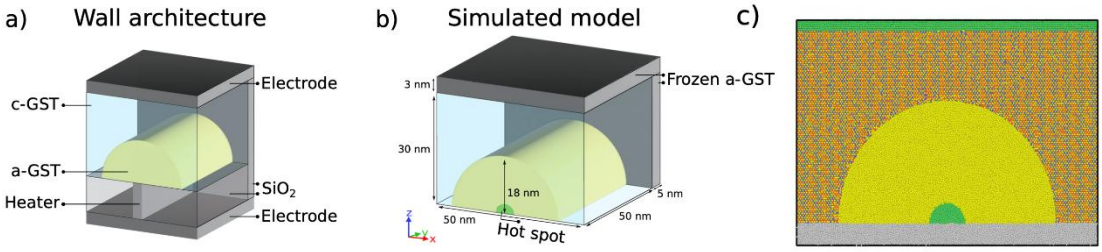

Figure 1: a) Sketch of the active region of a phase change memory (PCM) in the Wall architecture. A semi-cylindrical region of amorphous GST (a-GST) is embedded in a crystalline matrix (c-GST, not shown) and confined by dielectrics (SiO_2) in the *y* direction and by the top and bottom electrodes in the *z* direction. The heater in contact with a-GST and embedded in SiO_2 is also shown. b) Atomistic model of the PCM cell with 3D periodic boundary conditions. The gray regions correspond to the confining materials that consists of frozen GST, the yellow region is the active amorphous semi-cylindrical dome, embedded in a crystalline matrix (not shown). The smaller semi-cylindrical green region highlights the atoms inside the dome that are thermostatted at 880 K to mimic the hot spot generated by the heater underneath in the real device. c) A front view of the model with atomic resolution with the semi-cylindrical green region corresponding to the hot spot thermostatted at 880 K and the other green region in the upper part of the model that indicates atoms thermostatted at 300 K to mimic heat dissipation via the top electrode. The model contains 2.323 million mobile atoms and 0.472 million atoms in the frozen layers. The semi-cylindrical amorphous dome contains 786,412 atoms.

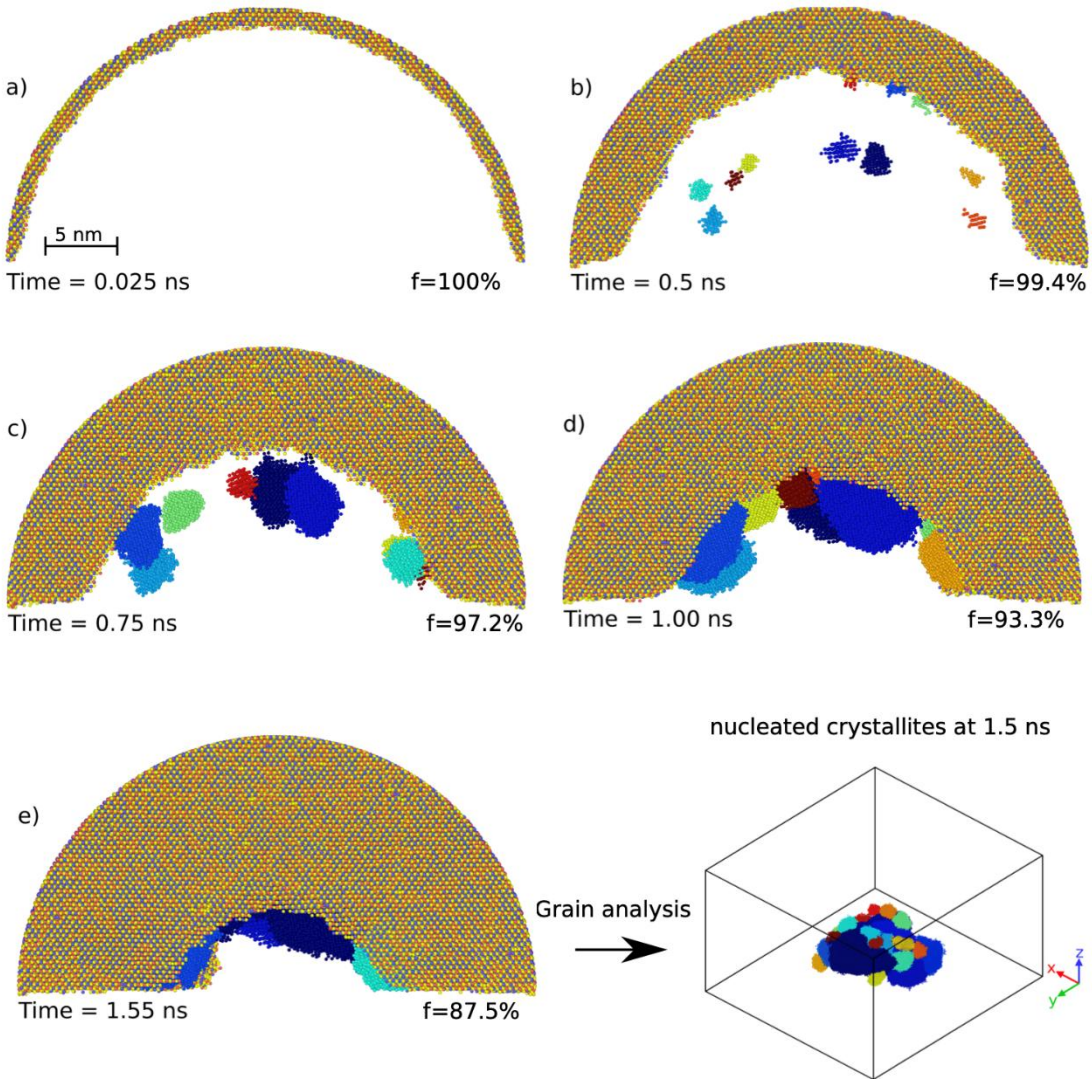

Figure 2: a-e) Snapshots of the recrystallization of the amorphous dome at different times (in ns) with a thermostat in contact with the upper electrode and the hot spot inside the dome (see Figure 1). Only recrystallized atoms that were originally present in the amorphous semi-cylindrical dome are shown. Atoms belonging to the largest crystallite growing form the outer amorphous-crystal interface are shown with the same colors of Figure 1c. The largest crystallite contains 554,752 atoms. The smaller crystallites nucleated inside the dome are shown each one with a different color. The fraction of recrystallized atoms (number f) belonging to the outer crystallite growing from the rim is given in each panel. A side view of the smaller crystallites (grains) embedded in the largest one is shown on bottom right. The crystallites nucleated far from the confining walls (see Figure 1) lead to the formation of a polycrystalline region at the center of the model.

REFERENCES

1. O. Abou El Kheir, L. Bonati, M. Parrinello, and M. Bernasconi, *npj Comput. Mater.* **10** (2024) 33.
2. D. Acharya, O. Abou El Kheir, S. Marcorini, and M. Bernasconi, *Nanoscale*, in press (2025); arXiv: 2501.18370v1 (2025).
3. O. Abou El Kheir and M. Bernasconi, *arXiv*, arXiv:2501.07384v1 (2025).

State dynamics in amorphous PCMs — a closer look

[Invited]

Sebastian Walfort[1], Xuan Thang Vu[2], Jakob Ballmaier[1], Nils Holle[1], Niklas Vollmar[1], and Martin Salinga[1]*
[1]Institute of Materials Physics, University of Münster, Germany
[2]Institute of Materials in Electrical Engineering, RWTH Aachen University, Germany
*corresponding author: martin.salinga@uni-muenster.de

ABSTRACT

In this invited talk, we describe an approach we developed to experimentally probe the potential energy landscape of a phase change material in its melt-quenched glass state.

1. INTRODUCTION

Building on decades of research, the peculiar structural dynamics of supercooled liquids and glasses remain an important problem in condensed matter. A major difficulty in understanding these disordered systems arises from a considerable separation between the microscopic (atomistic) theories on the one hand and the macroscopic observables in experiments on the other. Here, we establish a direct connection between a fluctuating observable and a theory based on potential energy landscapes. The central prediction of the theory is a separation of timescales, where the system rapidly explores the landscape basins surrounding local minima and only occasionally manages to escape. Quite naturally, these energy landscapes have been studied in molecular dynamics simulations, which afford access to all atomic positions at each time step, but are limited to dynamics on short timescales and struggle to resolve entropic contributions. In experiments, the transitions between basins, and as such any details about the landscape, are usually obscured by the vast number of other transitions simultaneously taking place in the probed volume.

2. EXPERIMENTAL

We succeed in resolving individual interbasin transitions by developing an experimental platform that allows us to probe the resistance of a tunable nanoscopic glass volume and, equally important, by applying a statistical model that takes the time series nature of the observation into account. With this approach we move beyond the explanation of experimental results in terms of broad distribution functions, and can infer about the microscopic details of an underlying (free) energy landscape.

3. RESULTS & DISCUSSION

Our results reveal a picture of a diverse landscape, with both energetic and entropic contributions to basins and barriers determining the structural dynamics. As a material system, we investigate germanium telluride, a phase change material, because of the high sensitivity of its electrical resistance to smallest reconfigurations at the atomic scale. It is precisely this property that makes phase change materials and other material systems (e.g. valence change materials) attractive as memristive memory elements in neuromorphic hardware applications. In addition to contributing to the fundamental understanding of glasses, our method may therefore provide new insights into the state dynamics inside all kinds of memristive materials, especially since continued device scaling will inevitably evolve their noise dynamics from the currently characteristic 1/f type towards the resistance fluctuations observed in this study.

4. CONCLUSIONS

We hope that people from very different scientific communities could be inspired by how much one can learn about a system from listening to the noise it emits.

Effect of Peierls-like distortions on transport in amorphous phase change devices

N. Holle[1]*, S. Walfort[1], R. Mazzarello[2], and M. Salinga[1]
[1]University of Münster, Institute of Materials Physics, Germany
[2]Sapienza Università di Roma, Department of Physics
*corresponding author: nils.holle@uni-muenster.de

ABSTRACT

Phase change materials (PCMs) show promise for applications in neuromorphic computing. However, resistance drift in amorphous PCMs, which limits the number of states in multi-level cells, is not fully understood. Using *ab-initio* transport simulations, we demonstrate a direct link between these distortions and local current densities in nanoscale antimony devices. We highlight nanoconfinement effects and the importance of interface design.

Key words: phase change materials, neuromorphic computing, electronic transport, Peierls-like distortions, non-equilibrium Green's functions

1. INTRODUCTION

Memristive devices based on phase change materials (PCMs) offer very desirable properties to act as the basis of analog devices for in-memory computing and are increasingly explored for neuromorphic computing architectures in general [1, 2]. An important characteristic of amorphous PCMs is resistance drift, the increase in electrical resistance over time due to structural relaxation. This phenomenon, sometimes linked to the evolution of Peierls-like distortions within the material's atomic structure [3, 4], presents challenges for multi-level cell stability. However, a complete understanding of electronic transport mechanisms in amorphous PCMs, particularly the direct influence of these local atomic distortions, remains elusive. Current models often rely on phenomenological descriptions or ground-state electronic properties, lacking a direct atomistic picture of non-equilibrium transport.

In a recent work [5], we aim to bridge this gap by investigating pure antimony (Sb), a compositionally simple PCM, allowing for an isolated study of Peierls-like distortions without complexities from multi-component alloys [6]. We employ first-principles calculations, combining density functional theory (DFT) with non-equilibrium Green's functions (NEGF), to directly simulate electron transport through nanoscale amorphous Sb devices. Our objectives are to establish a quantitative link between local Peierls-like distortions and current densities, and to explore the impact of nanoconfinement and electrode interfaces on these phenomena.

2. METHODS

Our study combines *ab-initio* molecular dynamics (MD) simulations with electronic structure and quantum transport calculations. Amorphous Sb structures were generated by melt-quenching using the CP2k package (Quickstep code, 2nd generation Car-Parrinello MD). Bulk amorphous Sb models contained 728 atoms, while device structures consisted of approximately 528 Sb atoms interfaced with tungsten (W) electrodes (total ~1100 atoms). The PBE exchange-correlation functional was used.

Peierls-like distortions were quantified using the angular-limited bond length ratio and the r_2/r_1 ratio (average of three longer vs. three shorter nearest-neighbor bond distances). The spatial correlation of these distortions was also analyzed. Electronic structure properties, including the density of states (DOS) and inverse participation ratio (IPR), were calculated using QuantumATK with an LCAO DFT approach (again using the PBE functional).

Non-equilibrium electron transport was simulated using the NEGF method as implemented in QuantumATK. This allowed for calculations of transmission spectra and local current densities through the Sb/W device structures under an applied bias voltage, providing a direct link between atomic configuration and transport characteristics.

3. RESULTS & DISCUSSION

Peierls-like distortions increase continuously during cooling into the supercooled liquid and glassy states. Our simulations reveal a heterogeneous distribution of Peierls-like distortions in amorphous Sb. The distortions are thus not uniformly distributed, but form structurally correlated regions with sizes of approximately 1 nm at 500 K, an intrinsic feature of the supercooled liquid. Analysis of the electronic structure shows that states near the Fermi level tend to localize in regions characterized by lower amounts of Peierls-like distortion.

Transport calculations on nanoscale Sb/W device models using NEGF demonstrate that current flow through the amorphous Sb channel is also heterogeneous. A clear correlation emerges: regions within the amorphous Sb exhibiting lower Peierls-like distortions sustain significantly higher local current densities. This finding directly links the atomic-scale structural order to the material's conductive properties. Furthermore, the simulations highlight profound effects of nanoconfinement by the tungsten electrodes. These include oscillations in the mass density of Sb near the interfaces and the formation of a distinct antimony wetting layer on the tungsten surface. Such interfacial phenomena significantly alter the local electronic structure and the electrostatic potential profile across the device, which emphasizes the important role of interfaces in nanoscale PCM devices.

The observed relationship between reduced Peierls-like distortions and enhanced local conductivity provides a microscopic basis for understanding resistance drift. As amorphous PCMs age, an increase in the overall Peierls-like distortion [3] would lead to a reduction in conductive pathways, thereby increasing the device resistance. The factor of two variation in local current density observed in our simulations due to distortion differences is consistent with the magnitude of resistance drift reported experimentally over timescales of tens of seconds.

4. CONCLUSIONS

This study provides direct evidence from first-principles simulations that local Peierls-like distortions significantly influence electronic current density in amorphous antimony. We demonstrate that atomic environments with a lower degree of such distortions facilitate higher current flow. This finding supports the hypothesis that the progressive increase of Peierls-like distortions during the structural relaxation (aging) of amorphous PCMs is an important contributing factor to the phenomenon of resistance drift.

Furthermore, our simulations underscore the importance of nanoconfinement and interfacial effects in determining the atomic structure, electronic properties, and ultimately, the transport behavior of PCM devices scaled to a few nanometers. The observed density oscillations and wetting layer formation at PCM-electrode interfaces necessitate their inclusion in realistic device models. These insights pave the way for improved understanding and atomistic-level design of next-generation phase change memory and neuromorphic computing devices.

REFERENCES

1. M. Wuttig, N. Yamada, *Nat. Mater.* **6** (2007) 824.
2. D.V. Christensen *et al.*, *Neuromorphic Comput. Eng.* **2** (2022) 022501.
3. J.-Y. Raty *et al.*, *Nat. Commun.* **6** (2015) 7467.
4. B. Chen *et al.*, *Adv. Sci.* **10** (2023) 2301043.
5. N. Holle *et al., Nat. Commun. Mater.* **6** (2025) 56.
6. M. Salinga *et al.*, *Nat. Mater.* **17** (2018) 681.

Large-Scale Deposition of Thin Films Based on Chalcogenide Phase-Change Materials: From GeTe/Sb_2Te_3 Superlattices for Phase-Change Memory Toward Spin-Orbitronic and Reconfigurable Photonic Devices

[Invited]

P. Noé[1*], D. Térébenec[1], O. Mouawad[1], J. Lagrave[1], P. Meilleur[1], Y. Brûlé[1], A. Albanese[1], R. Sawant[2], C. Pourny[2], A. Rogemond[2], A. Coillet[2], N. Bernier[1], J.-B. Dory[1], S. Malhouitre[1], B. Charbonnier[1], T. Frottier[3], M. Culot[3], L. Vila[3,4], J.-P. Attané[3,4], J.-B. Jager[5], B. Cluzel[2], F. Hippert[6]

[1]Univ. Grenoble Alpes, CEA, LETI, F-38054, Grenoble, France.
[2]ICB, UMR CNRS 6303, Université Bourgogne Europe, F-21078 Dijon cedex, France.
[3]Univ. Grenoble Alpes, CEA, IRIG, SPINTEC, F-38054, Grenoble, France.
[4]Nellow, F-38054, Grenoble, France.
[5]Univ. Grenoble Alpes, CEA, IRIG, F-38054, Grenoble, France.
[6]Univ. Grenoble Alpes, CNRS, Grenoble INP, LMGP, F-38000 Grenoble, France.
*Email: pierre.noe@cea.fr

ABSTRACT

Phase-change memories (PCMs) are a key component of modern memory technology, offering advantages such as multi-level data storage, fast read/write speeds, and non-volatility. They effectively bridge the gap between volatile DRAM and non-volatile Flash memory. PCM devices operate based on the reversible transition between amorphous and crystalline states in phase-change materials like GeTe or $Ge_2Sb_2Te_5$ [1].

Despite their potential, PCM devices face limitations, particularly high-power consumption during the RESET operation. To address this, current research is focused on optimizing device architecture and investigating alternative materials, including GeTe/Sb_2Te_3 superlattices (SLs). SLs have demonstrated lower programming power compared to conventional PCMs. GeTe/ Sb_2Te_3 SLs fabricated via sputtering have been successfully integrated into PCM devices using a "wall structure" design [2]. The high structural quality of these SLs, whether deposited on TiN (serving as the metallic bottom heater) or SiN_x (the dielectric bottom layer), has been confirmed by X-ray diffraction both in the as-grown state and after annealing under thermal conditions representative of the maximum budget during device integration. Scanning transmission electron microscopy (STEM) imaging of SLs embedded within PCM cells further confirms that the SL architecture remains intact throughout the integration process. A comprehensive statistical analysis conducted on a large number of devices clearly shows that SL-based devices exhibit lower RESET currents than reference devices based on GeTe alone. Moreover, the RESET current decreases systematically as the Sb_2Te_3 layer thickness within the SL increases from 2 to 8 nm. STEM analysis of a PCM cell containing a SL reveals that the transition from the low-resistance to the high-resistance state occurs via a melting–quenching mechanism. This finding contradicts the widely accepted view in the literature on interfacial phase-change memories (iPCMs), which attributes switching to crystal–crystal transitions or defect reorganization. More recently, we went a step forward this theory. Indeed, we demonstrated that the RESET current of $(GeTe)_2/(Sb_2Te_3)_2$ SL devices can be substantially reduced by annealing the SL into an out-of-plane oriented $Ge_1Sb_2Te_4$ layer [3]. These findings demonstrate that such a reduction does not depend on any specific structural feature of the SL—often cited in the literature—but can be achieved simply by incorporating an out-of-plane oriented $Ge_1Sb_2Te_4$ layer into the device. This insight holds significant promise for the industrial integration of these films. The interest in GeTe/Sb_2Te_3 SLs has largely stemmed from their observed reduction in RESET current compared to devices based on $Ge_2Sb_2Te_5$ alloys. However, this conclusion was drawn from experiments on test structures—like those in the present work—that underwent only moderate thermal processing. A key open question concerns whether this benefit in RESET current would persist after full back-end-of-line (BEOL) integration in industrial microelectronics. Our present results provide encouraging evidence: thermal treatment of a

$(GeTe)_2/(Sb_2Te_3)_2$ SL is not only non-detrimental but actually further lowers the RESET current, reinforcing the viability of these materials for large-scale application.

Despite all these improvements in performance, PCM technology faces a technological limitation related to the energy requirement for melting or recrystallization of the phase-change material. Nevertheless, GeTe has garnered growing interest in the field of spintronics, particularly within the emerging domain of spin-orbitronics. GeTe serves as a prototype for a new class of materials known as Ferroelectric Rashba Semiconductors (FERSCs), which uniquely integrate semiconducting behavior, strong spin-orbit coupling, and non-volatility arising from intrinsic ferroelectricity [4]. Notably, it has been shown that switching the ferroelectric polarization direction in GeTe induces a change in the spin chirality of its electronic band structure [5,6]. This effect has enabled room-temperature demonstrations of spin–charge interconversion [7], paving the way for the concept of the Ferro-Electric Spin Orbit (FESO) device, based on FERSC materials [8]. To date, molecular beam epitaxy (MBE) has been the preferred method for growing high-crystalline-quality GeTe films for fundamental studies. However, its limited scalability poses a significant barrier to widespread device integration. A major challenge remains the lack of an industry-compatible technique to grow oriented, functional GeTe(111) thin films that retain ferroelectric properties. In that context, we introduced the van der Waals epitaxial growth of ferroelectric α-GeTe thin films using industrial magnetron sputtering tools on 200/300 mm wafers. This approach demonstrates a scalable and CMOS-compatible route for integrating GeTe into microelectronic platforms, marking a critical step toward the development of next-generation, low-power FESO devices.

Last but not least, Phase-Change Materials are also a key player for the field of reconfigurable and nonlinear photonics [9]. In this context, we demonstrate CMOS-compatible, all-optical programming of $Ge_2Sb_2Te_5$ and $GeSe_{1-x}Te_x$ phase-change materials integrated on silicon waveguides [10]. This approach enables energy-efficient, non-volatile modulation of both optical amplitude and phase, with ultra-low switching thresholds. The devices exhibit exceptional endurance, surpassing 10^8 switching cycles, making them suitable for long-term operation. Our results highlight phase-change photonics as a promising technology for next-generation photonic computing platforms. We identify chemical segregation caused by steep temperature gradients as the main degradation mechanism, providing guidance for improving device reliability. These advances support scalable integration into programmable photonic circuits for neuromorphic and reconfigurable computing applications.

REFERENCES

1. P. Noé, et al., *Phase-change materials for non-volatile memory devices: from technological challenges to materials science issues,* Semicond. Sci. Technol. 33, 013002 (2018). https://doi.org/10.1088/1361-6641/aa7c25
2. D. Térébénec, et al., *Improvement of Phase-Change Memory Performance by Means of GeTe/Sb2Te3 Superlattices,* physica status solidi (RRL) – Rapid Research Letters 15, 2000538 (2021). https://doi.org/10.1002/pssr.202000538
3. D. Térébénec, et al., *GeTe/Sb2Te3 Super-Lattices: Impact of Atomic Structure on the RESET Current of Phase-Change Memory Devices,* Advanced Electronic Materials 11, 2400290 (2025). https://doi.org/10.1002/aelm.202400290
4. D. Di Sante et al., Advanced Materials 25, 509–513 (2013).
5. C. Rinaldi et al., Nano Lett. 18, 2751–2758 (2018).
6. J. Krempaský et al., Phys. Rev. X 8, 021067 (2018).
7. S. Varotto et al., Nat Electron 4, 740–747 (2021).
8. P. Noël et al., Nature 580, 483–486 (2020).
9. F. Pavanello, B. Charbonnier, P. Noe, *Phase-change materials for photonic applications.* Photoniques 45–49 (2024). https://doi.org/10.1051/photon/202412545
10. R. Sawant, et al., *High-endurance and energy-efficient all-optical programming of scalable silicon waveguides with integrated phase-change material patches*, accepted in Advanced Optical Materials (2025).

Van der Waals Epitaxy of Self-Poled α-GeTe(111) Ferroelectric Thin Films for Spin-Orbitronic Devices

J. Lagrave[1*], N. Bernier[1], J.-B. Dory[1], Y. Brûlé[1], P. Meilleur[1], O. Mouawad[1], D. Térébenec[1], T. Frottier[2], M. Culot[2], P. Pappas[2], L. Vila[2,3], J.-P. Attané[2,3], F. Hippert[4] and P. Noé[1*]

[1] Univ. Grenoble Alpes, CEA, LETI, F-38000 Grenoble, France.
[2] Univ. Grenoble Alpes, CEA, IRIG, SPINTEC, F-38000 Grenoble, France.
[3] Nellow, F-38000 Grenoble, France.
[4] Univ. Grenoble Alpes, CNRS, Grenoble INP, LMGP, F-38000 Grenoble, France.
*Email: jules.lagrave@cea.fr ; pierre.noe@cea.fr

ABSTRACT

Thanks to their strong spin-orbit coupling, chalcogenide materials open exciting prospects for ultra-low-power spin-based electronics. Among them, α-GeTe stands out as a prime candidate for next-generation Ferro-Electric Spin-Orbit (FESO) devices. In our upcoming study, we demonstrate the van der Waals epitaxy of high-quality, self-poled α-GeTe(111) ferroelectric thin films using industrial magnetron sputtering on 200/300 mm wafers. A nucleation layer and unconventional growth conditions are key parameters, paving the way to FESO technology to align with standard CMOS electronics.

Key words: GeTe, phase-change materials, van der Waals epitaxy, ferroelectric, spin-orbitronics

Chalcogenide materials exhibit a wide array of properties that make them highly attractive for various technological applications. Among these, Ge–Sb–Te alloys are particularly notable due to their distinctive characteristics, which have led to their extensive use in non-volatile phase-change memory devices [1,2]. GeTe alloys also show promise in RF switches, thermoelectrics, photonics, and optical technologies. More recently, GeTe has attracted significant interest in spintronics, especially in the emerging field of spin-orbitronics. GeTe is considered a prototype for a new class of materials known as Ferroelectric Rashba Semiconductors (FERSC), which uniquely combine semiconducting properties, strong spin-orbit coupling, and non-volatility due to intrinsic ferroelectricity [3]. It has been observed that switching the ferroelectric polarization induces a change in the spin chirality of GeTe electronic band structure [4,5]. This phenomenon has enabled the demonstration of spin-charge interconversion at room temperature [6], leading to the introduction of the FERSC-based Ferro-Electric Spin Orbit (FESO) device concept [7]. Although molecular beam epitaxy (MBE) has been used to grow high-crystal-quality GeTe films for fundamental research, its scalability is limited, hindering broader device integration. The absence of a industry-compatible method for growing functional GeTe(111) films with controlled orientation and preserved ferroelectricity remains a significant challenge. We present here in details the van der Waals epitaxial growth method using the industrial magnetron sputtering technique in 200/300 mm tools of ferroelectric α-GeTe thin films demonstrating the feasibility of industrial integration of these alloys for the future realization of innovative low-power FESO devices compatible with the CMOS technology of microelectronics.

REFERENCES

[1] P. Noé et al., Semicond. Sci. Technol. **33**, 013002 (2018)
[2] P. Noé and F. Hippert, Structure and Properties of Chalcogenide Materials for PCM, in: Redaelli, A. Phase Change Memory. Springer, Cham. (2018)
[3] D. Di Sante et al., Advanced Materials **25**, 509–513 (2013)
[4] C. Rinaldi et al., Nano Lett. **18**, 2751–2758 (2018)
[5] J. Krempaský et al., Phys. Rev. X **8**, 021067 (2018)
[6] S. Varotto et al., Nat Electron **4**, 740–747 (2021)
[7] P. Noël et al., Nature **580**, 483–486 (2020)

Above room temperature ferromagnetism in epitaxial thin films of the layered ternary chalcogenides Fe_5GeTe_2 and Fe_3GaTe_2

[Invited]

Joao Marcelo J. Lopes
Paul-Drude-Institut für Festkörperelektronik, Leibniz-Institut im Forschungsverbund Berlin e.V., Berlin, Germany,
E-mail: lopes@pdi-berlin.de

Layered magnetic materials are promising building blocks for the realization of ultra-compact devices for spintronics and quantum technologies with low-power consumption. Moreover, combining them with other layered crystals to form the so-called van der Waals (vdW) heterostructures is a very attractive route to realize hybrid systems exhibiting integrated electronic, optical, and magnetic functionalities. So far, most of the experimental research on layered magnets and related vdW heterostructures has been conducted utilizing micrometer-sized flakes exfoliated from bulk single crystals. However, the implementation of these materials in various technologies depends strongly on the development of bottom-up, scalable synthesis approaches allowing to realize highly uniform films with well-defined interfaces. It also requires that each material component of the heterostructure remains functional, which ideally includes magnetic order above room temperature for the magnetic materials. Among different candidates, the ternary transition metal chalcogenides Fe_5-$xGeTe_2$ (FGeT, $x \sim 0$) and Fe_3GaTe_2 (FGaT) show a great potential due to their relatively high Curie temperature and highly tunable properties. Both materials possess a layered vdW structure with each single layer being formed of Fe and Ge (Ga) slabs encapsulated by layers of Te.

In this talk, I will report on our results on epitaxial growth of FGeT and FGaT thin films on substrates such as single crystalline graphene (on SiC) and WSe_2 (on Al_2O_3) via molecular beam epitaxy. Structural characterization using different methods reveals the formation of high-quality crystalline films with sharp interfaces to the underlying templates. Importantly, magneto-transport and magnetometry measurements reveal ferromagnetic order persisting above 350 K with a predominant out-of-plane anisotropy for both FGeT and FGaT films. I will discuss the correlation between structure and magnetism, in particular the effect of compositional tuning (including Ni doping) on the magneto-transport properties. These results represent an important advance beyond non-scalable flake exfoliation from bulk crystals, thus marking a crucial step towards the implementation of ferromagnetic chalcogenides in practical applications.

The volatile and non-volatile resistance switching behavior in $MnTe_2$-based device

Shih-yuan Li[1], Yi Shuang[1,2], Daisuke Ando[1] & Yuji Sutou[1,2]
[1]Department of Materials Science and Engineering, Tohoku University, 6-6-11 Aoba-yama, Aoba-ku, Sendai 980-8579, Japan
[2]WPI-Advanced Institute for Materials Research, Tohoku University
E-mail: li.shih-yuan.r1@dc.tohoku.ac.jp

ABSTRACT

In this study, we fabricated a $MnTe_2$-based device and investigated its resistance-switching behavior under electric field. The device exhibited volatile resistance switching under unipolar voltage sweep, and non-volatile resistance switching under bipolar voltage sweep. This behavior is considered to be governed by a mechanism involving thermally assisted ion migration.

Key words: transition metal dichalcogenide, volatile resistance change, non-volatile resistance change

1. INTRODUCTION

Transition metal dichalcogenides (TMDs) are compounds composed of transition metals and chalcogen elements. In recent years, they have attracted considerable attention and have been widely studied for their unique electrical properties. Their resistance-switching behavior has enabled the development of various electronic devices. For example, electric field–induced structural changes in $MoTe_2$ have been employed in resistive random-access memory (RRAM) applications[1], while the threshold-type current–voltage characteristics of $SiTe_2$ have been utilized in ovonic threshold switch (OTS) devices[2]. The key difference between these two types of resistance change lies in whether the altered state is retained after power is removed. If the device returns to its initial state when power is turned off, it is referred to as volatile switching. In contrast, if the device retains the changed state, it is considered non-volatile. TMDs are known to exhibit both volatile and non-volatile resistance-switching behaviors, owing to their distinctive bonding characteristics and electronic structures. In this study, we present a $MnTe_2$-based device that uniquely exhibits both volatile and non-volatile switching behaviors simultaneously.

2. EXPERIMENTAL

The $MnTe_2$ films were made by RF magnetron co-sputtering of pure Mn (99.99%) and Te (99.99%) targets at room temperature with the rotating of the substrate during deposition. The base pressure of the sputtering chamber was under 5.0×10^{-5}Pa and the Ar gas was supplied at 10 sccm for film deposition. The working pressure was set to be 1Pa. The film thickness was confirmed using atomic force microscopy (KEYENCE, VN-8000). The temperature versus resistance curve of $MnTe_2$ films was measured using the two-point probe method in the temperature range from 25 °C to 400 °C under an Ar atmosphere with a heating rate of about 13 °C min^{-1}. The as-depo and annealed $MnTe_2$ films were then measured by XRD (Ultima IV, Rigaku) with the diffraction angle 2θ between 20° and 60°. The $MnTe_2$ device is fabricated using the conventional photolithography process with the addition of a focus ion beam (FIB) drilling method. First, the 50nm tungsten bottom electrode was deposited on a Si (725 μm)/SiO_2 (100 nm) substrate using photolithography. Next, a 100nm thick SiO_2 was deposited on the bottom electrode with another photolithography pattern. Then, a hole was produced by using the FIB drilling method. Finally, the 150nm thick $MnTe_2$ was deposited into the hole followed by the deposition of the 200nm thick tungsten top electrode. The $MnTe_2$ device was evaluated by the semiconductor parameter analyzer (Keysight, B1500A). The cross section of the device was observed by STEM (JEM-2100F).

3. RESULTS & DISCUSSION

The as-deposited $MnTe_2$ film was in a crystalline state with a pyrite structure. Annealing up to 400 °C resulted in a slight increase in resistance, with no observable change in crystal structure, as confirmed by X-ray diffraction (XRD). The $MnTe_2$-based device was then successfully fabricated using a photolithography process, with no unwanted reactions occurring during fabrication. The structure of the device is shown in the right figure.

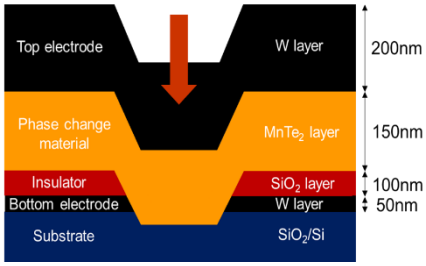

The device was initially tested using a positive voltage sweep, where the positive direction is indicated by the arrow in the figure. It exhibited an initial resistance of approximately 2000 Ω. As the voltage increased to around 0.8 V, the resistance dropped to about half of its initial value. This ultra-low resistance state persisted as the voltage continued to increase. When removing the voltage, the device returned to its original resistance at approximately 0.6 V, indicating a volatile resistance switching behavior. While such behavior is commonly observed in amorphous chalcogenides, it is rarely seen in crystalline chalcogenides.

Next, a negative voltage sweep was applied. This caused the device to switch into a high-resistance state, which did not revert to the initial state after the voltage was removed, indicating non-volatile resistance switching. The resistance in this high-resistance state was over two orders of magnitude higher than the initial state. This state could be turned back to the low-resistance state by applying a positive voltage sweep. This type of bipolar switching behavior is commonly observed in oxide materials and is widely used in resistive switching memory applications.

The resistance switching behavior observed in the $MnTe_2$ device is believed to be driven by a thermally induced ion migration mechanism. Transmission electron microscopy (TEM) analysis of the device in its high-resistance state revealed void formation near the electrode, leading to a reduced contact area and result in increased resistance. Additionally, EDX mapping confirmed the migration of Te anions, which were found to accumulate near the bottom electrode which is consistent with predictions.

4. CONCLUSIONS

The coexistence of volatile and non-volatile resistance switching behaviors was first observed in the $MnTe_2$-based device. In current memory architectures, a separate selector is typically required to suppress sneak currents, often implemented in a 1S1R (one selector–one resistor) structure. $MnTe_2$-based device presents a promising opportunity to eliminate the need for an external selector, potentially avoiding many of the complex issues that arise at the memory–selector interface and from their differing operating conditions. Future work will focus on enhancing device performance through structural design and material optimization.

REFERENCES

1. F. Zhang *et al.*, Electric-field induced structural transition in vertical $MoTe_2$- and $Mo_{1-x}W_xTe_2$-based resistive memories. *Nature Materials* **18**, 55-61 (2019).

2. S. Hatayama et al., Origins of midgap states in Te-based Ovonic threshold switch materials. Acta Materialia 258, 119209 (2023).

Acknowledgments: This work was supported by the KAKENHI (21H05009, 21K18805) and by the National Institute of Information and Communications Technology (NICT), Japan (No. JPJ012368C03701).

Characterization of Phase-Change Behaviors and Memory Operation Properties in V-Te Thin Film

Shuhei Orihara[1]*, Yi Shuang[1,2], Daisuke Ando[1] and Yuji Sutou[1,2]
[1]Dept. of Materials Science, Grad. Sch. of Eng., Tohoku University, Sendai, Japan
[2]WPI Advanced Institute for Materials Research, Tohoku University, Sendai, Japan
*Orihara.shuhei.p4@dc.tohoku.ac.jp

ABSTRACT

Phase-change memory (PCRAM) relies on the phase change between amorphous and crystalline states, but suffers from high energy consumption, limited operating speed, and reliability issues. To address these challenges, this study investigated the crystalline polymorphic phase-change behavior of Vanadium-tellurium (V-Te) binary system as an alternative. We deposited V-Te thin films and characterized the phase change properties and memory operation behavior.

Key words: Vanadium telluride, Phase-change material, thin film, chalcogenide

1. INTRODUCTION

PCRAM has emerged as a promising candidate to bridge the performance gap between DRAM and NAND flash memory. PCRAM is based on the reversible phase transition between crystalline and amorphous states of phase-change materials (PCM). However, conventional PCMs, such as $Ge_2Sb_2Te_5$ (GST) face significant challenges associated with amorphous phases, which leads to high energy consumption and limited operating speed due to the use of amorphization process. Recently, manganese telluride (MnTe) has demonstrated reversible resistance switching between different crystalline phases, representing a new class of crystalline-polymorphic phase-change materials. MnTe is considered a promising candidate for next-generation PCMs with ultra-low energy consumption and high operating speed, as it avoids the amorphous state [1]. Thus, in this study, we focus on V-Te thin films to explore the potential of other crystalline-polymorphic phase-change materials. The V-Te binary system exhibits several polymorphic phases near the 1:1 composition. Notably, the difference between the crystal structures of the V_3Te_4 and V_5Te_8 phases is primarily the vacancy occupation (50% - 25%) within the van der Waals layers of the 2D layered VTe_2 structure, suggesting the possibility of crystalline polymorphic phase transitions [2]. Therefore, we investigated the phase-change behavior and memory operation characteristics of V–Te thin films with a composition of approximately V: Te = 4:6.

2. EXPERIMENTAL

V-Te thin films were deposited by RF-magnetron co-sputtering of a V target (99.9%), and a Te target (99.99%). The composition was determined by scanning electron microscope (SEM) with energy-dispersive X-ray spectroscopy (EDX, JEOL, JSM-6500F). Crystal structures of as-deposited and annealed films were measured using XRD (Rigaku, Ultima IV). The temperature dependence of electrical resistance was measured with a two-point probe in a annealing furnace. Electrical properties were investigated using Hall-effect measurement (Toyo Corp., ResiTest 8400), while optical properties were measured by a spectrophotometer (JASCO Corp., V-770). Phase-change behavior was further evaluated by differential scanning calorimetry (DSC; TA instruments, Q20). Cross-sectional microstructures were observed using TEM (JEOL, JEM-2100F) at 200 kV. Contact-hole memory devices were fabricated, and their electrical characteristics were evaluated using a semiconductor device analyzer (Keysight, B1500A).

3. RESULTS & DISCUSSION

Figure 1a shows the XRD patterns of the as-deposited and annealed V-Te thin films. The as-deposited film was identified as an amorphous phase. Upon annealing up to 400ºC, the film exhibited a phase change from the amorphous to the V_3Te_4 phase, which was characterized by its

distinct diffraction patterns. By further annealing to 500ºC, the V_5Te_8 phase appeared, which indicates a sequential crystalline polymorphic phase change from V_3Te_4 phase to V_5TeFigure 1b presents the temperature-dependent electrical resistance of V-Te thin films. The as-deposited film exhibited an initial resistance of approximately 150 Ω at room temperature. The resistance decreased upon annealing to 400ºC, corresponding to the phase change from the amorphous phase to V_3Te_4 phase. Subsequent annealing up to 500ºC resulted in further resistance reduction, which is attributed to the formation of V_5Te_8 phase. As shown in Figure 2, DSC revealed two distinct exothermic peaks; the first peak observed around 400ºC, corresponding to crystallization into V_3Te_4 phase, while the second peak observed around 440ºC, indicating a phase change to V_5Te_8 phase. Figure 3 displays the resistance – voltage characteristics of the memory device. Reversible resistance switching between a low-resistance crystalline phases and a high-resistance amorphous phase was observed upon application of voltage pulses.

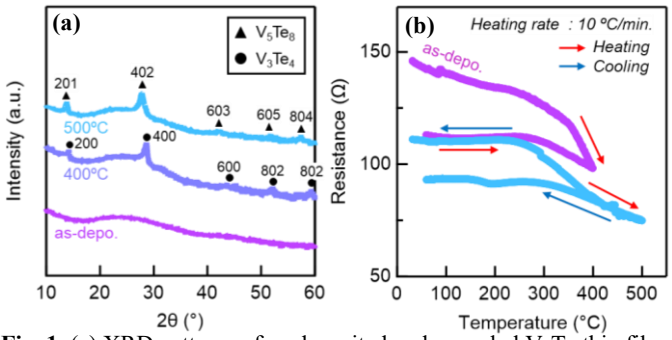

Fig. 1. (a) XRD patterns of as-deposited and annealed V-Te thin film; (b) temperature dependent resistance of V-Te thin film
Color modifications from Ref. [3].

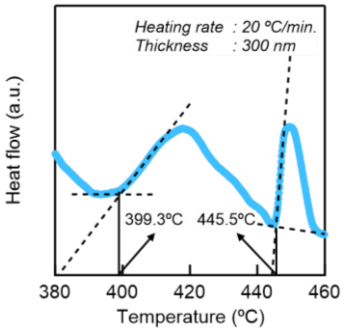

Fig. 2. DSC heating curve of V-Te thin film
Color modifications from Ref. [3].

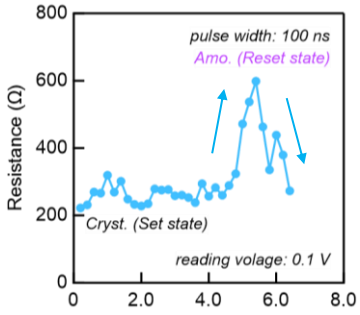

Fig. 3. Resistance-voltage (R-V) characteristics of V-Te based memory device
Color modifications from Ref. [3].

4. CONCLUSIONS

We investigated the phase-change behaviors of V-Te thin films with a V: Te composition of ~ 0.4:0.6. XRD and DSC results revealed a phase change from an amorphous phase to a stable V_5Te_8 phase via the V_3Te_4 phase through the annealing process. However, the resistance contrast during the phase change in the V-Te thin films was much smaller than that of the other phase-change materials for PCRAM, which makes it difficult to apply the V-Te binary system to PCRAM devices. Therefore, future studies should focus on optimizing the memory device structure and the composition of V-Te thin films to enhance the difference of electrical properties during the phase changes.

REFERENCES

[1] S. Mori, S. Hatayama, Y. Shuang, D. Ando, Y. Sutou, *Nat. Commun.* (2020), 11, 85
[2] R. Guzman, S. Ning, R. Zhang, H. Liu, Y. Ma, Y.Y. Zhang, L. Bao, H. Yang, S. Du, M. Bosman, S.J. Pennycook, H.J. Gao, W. Zhou, *ACS Nano* (2023), *17*, 2450.
[3] S. Orihara, T. Shuang, D. Ando, Y. Sutou, *Phys. Status Solidi RRL* (2025), early access, doi: 10.1002/pssr.202400430.

ACKNOWLEDGMENT

This work was supported by KAKENHI (Grant No. 21H05009 and 24K21668). This work was supported in part by the Commissioned Research (JPJ012368C03701) of the National Institute of Information and Communications Technology (NICT), JAPAN. The authors acknowledge the financial support from the JST FOREST Program, Grant No. J240002622, and the Nippon Sheet Glass Foundation for Materials Science and Engineering (NSG Foundation).

Tuning the properties of GaSb with C-doping

J. Remondina[1]*, G. Navarro[2], and M. Putero[1]
[1] Aix-Marseille Univ, CNRS, IM2NP, Marseille, France
[2]CEA-LETI, Grenoble, France
*corresponding author: jacopo.remondina@im2np.fr

ABSTRACT

We investigated the effect of carbon doping in GaSb alloys for Phase-Change Memory (PCM), using a combination of *in situ* and *ex situ* characterization techniques. Key parameters such as crystallization temperature, activation energy of crystallization, amorphous/crystalline sheet resistance (Rs) ratio, and density/thickness changes upon crystallization were evaluated. Our results demonstrate that by tuning the carbon concentration, it is possible to significantly enhance the amorphous phase stability – evidenced by a +40°C increase in crystallization temperature and a +0.6 eV rise in activation energy – while preserving the low density variation of GaSb during the crystallization process. These findings highlight the potential of carbon-doped GaSb as a promising candidate for PCM devices featuring high endurance and data retention at high temperature.

Key words: GaSb, carbon doping, data retention, PCRAM, material optimization

1. INTRODUCTION

In the field of Phase-Change Memory (PCM), certain alloys are widely considered as benchmarks -most notably the $Ge_xSb_yTe_z$ system and its various binary and ternary compounds- which have been the primary focus of both academic and industrial research. However, alternative phase-change alloys also exist, among which gallium antimonide (GaSb) stands out due to its unique and promising properties.
One of the features that makes this alloy particularly interesting is that it is among the few phase-change materials that can exhibit no change in density, volume, or thickness between the amorphous and crystalline phases under specific conditions [1,2]. However, its relatively low crystallization temperature – around 250°C for the 40:60 stoichiometry [3] – and its more difficult deposition/integration (with respect to other alloys) has likely limited its diffusion in PCM applications.
In this work, we propose the use of carbon doping in GaSb to improve the amorphous phase stability, while preserving the advantage of zero density/thickness change of GaSb during the crystallization process.

2. EXPERIMENTAL

Three carbon-doping level were investigated, all based on GaSb with a 40:60 %at stoichiometry and deposited as 50 nm-thick films capped with SiN to prevent oxidation. The composition was selected after comparing several other stoichiometries (not shown), based on its favorable properties. We compared the undoped (0C) sample considered as a reference, with two doping concentrations [x_C] and [y_C] such as [x_C] < [y_C], both in the range of a few atomic percent. A combination of *ex situ*, *in situ*, and coupled X-Ray Diffraction (XRD), X-Ray Reflectometry (XRR) and sheet resistance (Rs) measurements was used to investigate the samples during and after various annealing condition, including isochronal ramping and isothermal treatments.

3. RESULTS & DISCUSSION

Our XRR results (Figure 1) show that the carbon incorporation has almost no effect on the magnitude of density and thickness changes upon crystallization process. However, significant improvements are observed in the crystallization temperature (Tx), which increases by approximately +40°C (Figure 2 left), and the activation energy rises by about +0.6 eV for the highest

C-doping level. The extrapolations suggest that the 10-years retention temperature increases from approximately 140°C to around 190°C (Figure 2 right), making this material a highly promising candidate for PCM applications.
Other key properties, such as crystallites size (and their homogeneity), the amorphous/crystalline resistivity ratio (relevant for two- or multi-state programming PCM performance) and the sheet resistance of the crystalline phase exhibit only minor changes upon C-doping.

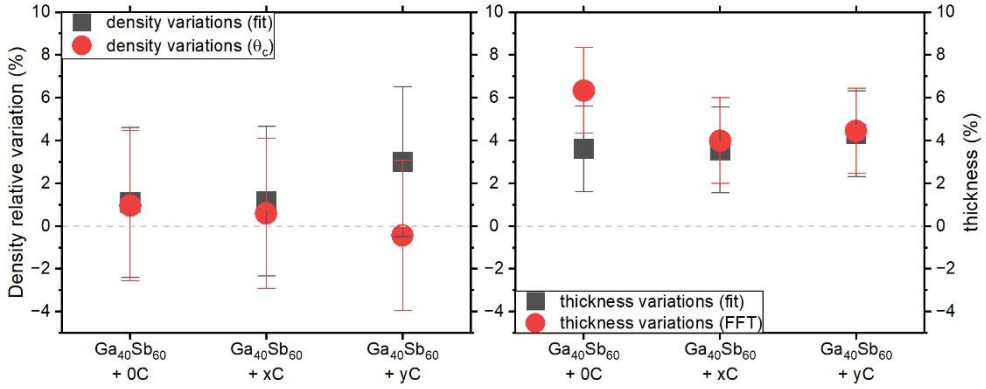

Figure 1: Relative variations between the amorphous and the crystalline phases for the density (left) and film thicknesses (right) obtained from XRR data. Black squares are the results from the simulation and fitting of the full XRR curves, while red circles are extracted from the position of the critical angle (density) and the FFT peaks (thickness).

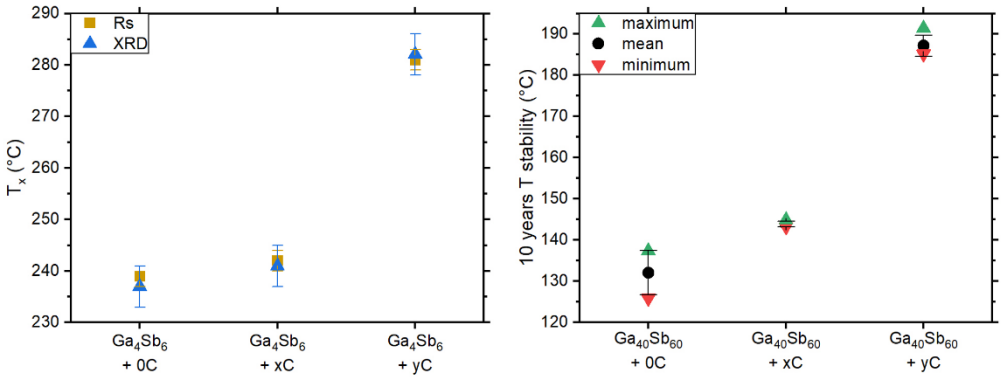

Figure 2: Left: the crystallization temperatures obtained for the 3 samples extracted starting from the sheet resistance (Rs) and for in-situ XRD (XRD). Right: the 10-year crystallization temperature obtained from extrapolating the Arrhenius equation linking the incubation time and the temperature of several isotherms. The graph shows the shortest (minimum), the average + standard deviation (mean) and the longest (maximum) extrapolated time.

4. CONCLUSIONS

In this work, we investigated the effect of carbon doping in GaSb alloys, and analyzed how it modulates various structural and functional properties. Our results demonstrate overall improvements in several key parameters relevant to PCM applications, particularly with respect to data retention capability, while exhibiting minimal adverse side effects. A combined approach involving carbon-doping and Ga/Sb ratio optimization could represent a major breakthrough in the field by enabling high-temperature, stress-free phase-change materials.

ACKNOWLEDGEMENTS

This work was partially funded by European commission through ECSEL-IA 101007321 project StorAIge.

REFERENCES

1. M. Putero, *Appl. Phys. Lett.* **103** (2013) 231912
2. M. Putero, *Appl. Phys. Lett.* **108** (2016) 101909.
3. Q. Yin, *Nanotechnology*, **31** (2020), 215709.

Storage class memories for flexible edge electronics

[Invited]

S. Calvi[1,2,*], S. Prili[1,2], A. Valletta[2], E. Piccinini[3], S. De Simone[2], F. De Matteis[4], A. Foglietti[2,5], A. Diaz Fattorini[1,2], C. Petrucci[1,2], M. Longo[5,2], R. Calarco[2] and F. Arciprete[1,2]

[1] Department of Physics University of Rome Tor Vergata, Via della Ricerca Scientifica 1, 00133 Rome, Italy
[2] Institute for Microelectronics and Microsystems (CNR-IMM), Via del Fosso del Cavaliere 100, 00133 Rome, Italy
[3] Applied Materials, Reggio Emilia, Italy
[4] Department of Industrial Engineering University of Rome Tor Vergata, Via del Politecnico 1, 00133 Rome, Italy
[5] Department of Chemistry University of Rome Tor Vergata, Via della Ricerca Scientifica 1, 00133 Rome, Italy
* sabrina.calvi@roma2.infn.it

ABSTRACT

Lately, edge computing solutions are spreading, exploiting purposely designed embedded systems to process data near the sensors. This approach reduces the power consumption, shortens the delay time in data processing and ensures data protection [1]. Consequently, such devices are expected to conform to large curved surfaces, to be cost-effective, lightweight and thin. In fact, the request for flexible edge electronics is strongly emerging from the automotive, aerospace and biomedical fields, requiring robust, fast and safe data processing with a limited power budget. The operative center of the embedded device is the processor with the memory and, ideally, the best computational approach would be to overcome the Von Neumann architecture processing the data directly in the memory [2]. At present, edge devices are mainly composed of hybrid electronics, which is a compromise due to the poor performances of the devices directly developed on flexible substrates. Besides, the reduction of the cost per device is a mandatory step to reach the overwhelming compelling value for a potential new technology to be considered for introduction in the market.

In this framework, the target of our research is to develop a device capable to comply with the requirements of this emerging field. Recently, our research group has investigated alloys based on phase change materials (PCM) with excellent thermal stability and mechanical toughness [3]. This work was intended to lay the groundwork for the development of low-cost and large-area compatible processes for high performance flexible memories. We have demonstrated the compatibility of these alloys with large-area scalability and their processability on flexible substrates. The integration of such PCM alloys as active material in flexible memories is discussed and the prospects of PCMs for flexible edge electronics are presented. The electrical properties of the cells and the compliance of the performance to the target requirements are assessed with specific figures of merit, such as the write speed, energy consumption, programming window and endurance. A numerical model is presented to simulate the dynamics of the memories during set and reset operations. This model aims to reproduce the device behavior using an approach that mimics the possible accountable microscopic physical mechanisms. Overall, the obtained research results prove that the cell features and performances are well in line with the current industrial targets for flexible edge electronics.

Keywords: Ge-Sb-Te (GST), edge electronics, green electronics

REFERENCES

1. Greco, L., et al. *Pattern Recognition Letters* **135**, 346–353 (2020).
2. Boniardi, M., et al. *Adv Elect Materials* **10**, 2400599 (2024).
3. Calvi, S. et al. *Adv Elect Materials* 2400184 (2024).

Partial RESET and partial SET states in Ge-rich GeSbTe-based phase change memory cells

S. Ran[1]*, M. A. Luong[1], A. Delpoux[2], E. Petroni[3], D. Benoit[4], J. Grisolia[2], A. Claverie[1], and N. Cherkashin[1]

[1]CEMES-CNRS, 29 Rue Jeanne Marvig, 31055 Toulouse, France

[2]Laboratoire de Physique et Chimie des Nano Objets (LPCNO), INSA, Toulouse, France

[3]STMicroelectronics, Via Olivetti 2, 20864 Agrate Brianza, Italy

[4]STMicroelectronics, 850 Rue Jean Monnet, 38920 Crolles, France

*corresponding author: sijia.ran@cemes.fr

ABSTRACT

Combining electrical and TEM experiments, we reveal the microstructural evolution in Ge-rich GeSbTe-based phase-change memory cells during partial RESET and partial SET. We show that the same intermediate resistance can be accessed either by partial amorphization or by partial crystallization of the dome. The precision and accuracy of these programming methods are evaluated and explained by its material origin.

Key words: Ge-rich GeSbTe, phase change memory, intermediate resistance states, TEM

1. INTRODUCTION

Phase-change memory (PCM) shows great potential for in-memory computing applications, where a device is required to store and process information simultaneously[1]. This is facilitated by the analog feature of PCM, within which various intermediate resistance states (IRS) can be achieved by tuning the amorphous-to-crystalline ratio of the active material. Ge-rich GeSbTe (G-GST) alloys have been developed by the industry to address the high-temperature data retention capabilities required by embedded applications[2]. Beyond the binary applications, there are also various interests in utilizing G-GST PCM for multilevel storage[3]. Due to the off-stoichiometric nature of G-GST alloys, they undergo complex material evolution upon electrical programming, involving chemical phase separation and formation of multiple crystalline phases[4]. A thorough understanding of the material origins behind IRSs is thus critical when selecting proper programming algorithms for multilevel computation. In this work, we have performed a comprehensive microstructural analysis based on (S)TEM to reveal the physics behind different electrical properties of IRSs accessed by different programming methods.

2. EXPERIMENTAL

The studied PCM consists of single 1R analytical cells. The cells have a “wall” architecture, where a nanometer scale G-GST layer is deposited on top of a thin heater and capped by a metallic top electrode. Electrical tests were conducted to program PCM cells to various IRSs and to evaluate the precision and accuracy of the programming methods. Extremely thin (< 30 nm) TEM lamellas were prepared using FIB. Multiple (S)TEM-based methods were applied to study the G-GST alloy, including dark-field (DF) and high-resolution (HR) imaging for crystallographic analyses.

3. RESULTS & DISCUSSION

Fig. 1a shows the amorphous size evolution when applying a partial RESET (“pRESET”) pulse to a crystallized dome. The amorphous volume enlarges with the pulse amplitude, following melting and quenching of the active layer, resulting in a progressive increase in resistance. This method offers a high programming precision and repeatability upon cycling thanks to a direct correlation between the amorphous size and the temperature profile generated by a specific pulse amplitude.

Fig. 1b shows the crystallization process when applying partial SET (“pSET”) pulses to an amorphous dome. Before pSET, the dome has a polycrystalline surrounding made by two Ge

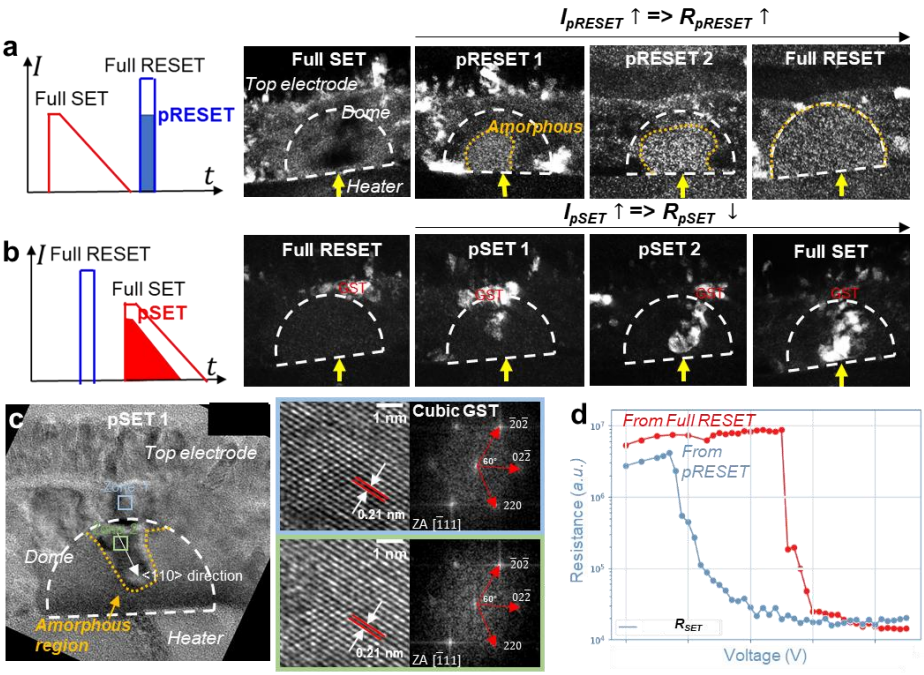

Fig. 1: Pulse squences (on the left) and TEM DF images (on the right) of IRSs in G-GST cells accessed by (a) partial amorphization of the dome intially in the crystallized Full SET state, and (b) partial crystallization of the dome initially in the amorphous Full RESET state. (c) TEM HR images of a partially crystallized dome created by pSET. (d) Resistance as a function of pSET voltage when starting from the Full RESET or from the pRESET state.

accumulated "walls" and a "roof" occupied by cubic GST grains[4]. During pSET, the dome partially (re-)crystallizes through a downward columnar-like growth of cubic GST grain(s) initiated from the top of the dome. The crystallographic analysis (see Fig. 1c) reveals that such a process is likely to be triggered by a preferential orientation of the GST "template" grains formed underneath a metallic electrode and above the dome by electrical operation. The heterogeneous epitaxy of GST crystals predominately occurs on their bottom {110} facets. The resistance rapidly decreases with a shrink of the distance between the heater and the (re-)crystallized region, as the GST growth rate is high along the <110> direction. Consequently, the programmed resistance is less controllable by the pSET method in comparison to the pRESET one and results in a higher cycle-to-cycle variabilities.

By starting with a pRESET instead of Full RESET before crystallization, a better resistance continuity can be obtained (Fig. 1d). As grains surrounding a smaller amorphous dome are randomly orientated, GST crystallization can be initiated over facets providing a smaller growth rate. As a result, the resistance can be reduced more slowly. This method bring benefit to limit the accuracy degradation (caused by the resistance drift) compared to the "fresh" amorphous material created by pRESET, providing a trade-off between programming precision and reliability.

4. CONCLUSIONS

We demonstrate the possibility to reach the same IRS level in G-GST cells either by partial amorphization of the crystallized dome (pRESET), or by partial crystallization of the amorphous dome (pSET). During pSET, the growth of GST grain(s) from above the dome is the dominating mechanism. The stochasticity brought by the anisotropic growth process can be overcome by tuning the RESET conditions before crystallization, which render the shape and GST-to-amorphous interfaces more appropriate. These observations in the real device environment provide critical information to define the dedicated algorithm to reach a desired IRS level for specific applications.

REFERENCES

1. A. Sebastian *et al. Nat. Nanotechnol.* (2020) 529-544.
2. F. Arnaud, *et al. 2020 IEDM* (2020) 24.2.1-24.2.4.
3. M. Boniardi, *et al. Adv. Electron. Mater.* (2024) 24.2.1-24.2.4.
4. S. Ran and E. Petroni, *et al. Sci. Rep.* (2025) 11357.

Evolution of Ge-rich GST from post deposition to programming operations: a simulative approach

[Invited]

E. Piccinini[1], N. Giuliani[1], M. Baldo[2], E. Petroni[2], S. Calvi[3], L. Laurin[2], F. Nardi[1], A .Redaelli[1], R. Annunziata[2] , L. Larcher[1]

[1] Applied Materials, Italy
[2] STMicroelectronics, Italy
[3] Department of Physics, University of Rome Tor Vergata, Italy

ABSTRACT

This study introduces a simulation-based methodology to trace the transformations occurring to Ge-rich GST alloys from the initial thermal treatment post-deposition to active memory cycling. The simulations capture elemental migration and phase separation. These insights contribute to a deeper understanding of material behavior and support the optimization of embedded PCM memories.

Keywords: Ge rich-GST, programming operations, phase segregation, elemental migration

1. INTRODUCTION

To meet the rigorous demands of automotive applications, conventional GST alloys must be tailored through Ge enrichment to enhance data retention and thermal stability[1]. Historically, the development of such materials has relied heavily on empirical approaches involving iterative fabrication and characterization. This work proposes a simulation strategy that leverages the Ginestra™ platform[2], which incorporates advanced models for phase transitions and ion migration in chalcogenide systems. By correlating simulation outputs with experimental data, the study aims to establish a reliable framework for guiding material and process optimization in ePCM development.

2. THERMAL EVOLUTION IN THE BEOL

The transition from the as-deposited amorphous state to a crystalline configuration with distinct phase separation is modeled through an isothermal annealing process: the initially homogeneous amorphous film evolves into a microstructure comprising segregated Ge and GST crystalline grains.

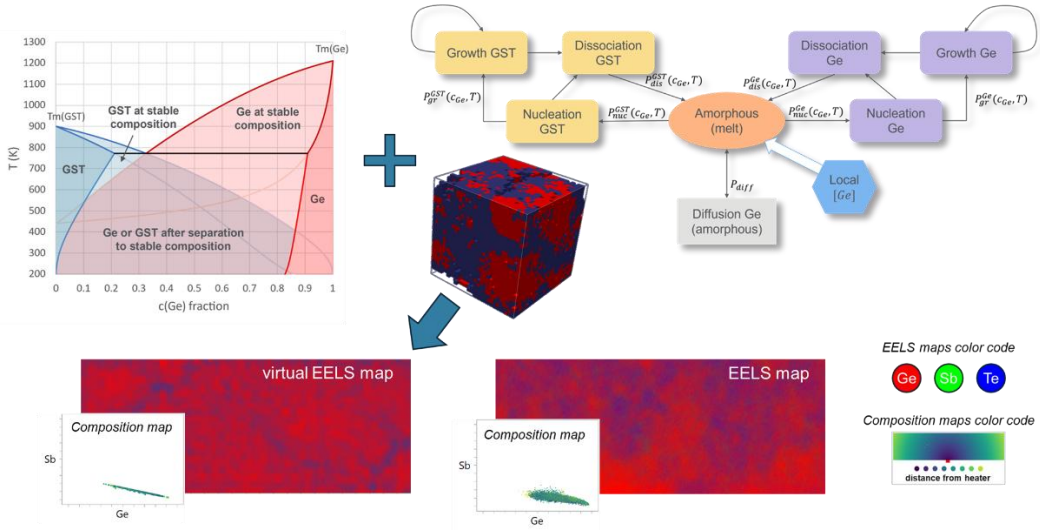

Figure 1 – The framework for simulating the BEOL anneal relies on the eutectic decomposition of Ge and GST domains and on a KMC algorithm derived from a stochastic model of crystallization. (Bottom) Virtual EELS and composition maps obtained with simulations compared to experimental outcomes.

At first, a pseudo-binary eutectic phase diagram using the free energy densities of Ge and GST as functions of temperature and Ge content is calculated. The decomposition of the amorphous alloy into its crystalline constituents is then modeled using a Kinetic Monte Carlo algorithm [3], which incorporates nucleation, growth, and dissociation events (Fig. 1). These events are governed by local thermodynamic conditions and material properties interpolated between the pure phases.
The simulation results, including EELS maps and scatter plots of elemental distributions, show strong agreement with experimental data.

3. ELEMENTAL MIGRATION DURING PROGRAMMING

The electrical conduction in the amorphous phase is modeled using an energy-activated transport mechanism, whereas the crystalline and the molten phase are treated as having a constant resistivity. The overall resistivity and the thermal conductivity are computed as a temperature-dependent weighted averages, using a logistic function centered around the melting point [4].
During programming operations, electrical pulses induce both phase transitions and elemental migration. The simulation relies on a modified Fickian diffusion model, where the concentration flux is complemented by the electric field and gradients in temperature, and phase [5].
Trapezoidal pulses initiate melting and diffusion. As the temperature rises, a Ge-deficient molten region forms above the heater, surrounded by a Ge-rich shell. Upon cooling, Sb accumulates near the heater due to electromigration, forming a core, while a Ge-Te intermediate shell develops between the core and the outer Ge layer. The presence of dielectric materials near the bitlines alters the thermal profile, promoting Ge accumulation at the cell edges; higher programming currents expand the molten dome but preserve the same compositional layering.
During reset operations, a high-temperature pulse followed by rapid quenching produces a nearly homogeneous amorphous dome. The elevated temperature promotes mixing of previously segregated elements, while the fast cooling prevents further redistribution.
These simulated distributions align well with experimental EELS maps (Fig. 2).

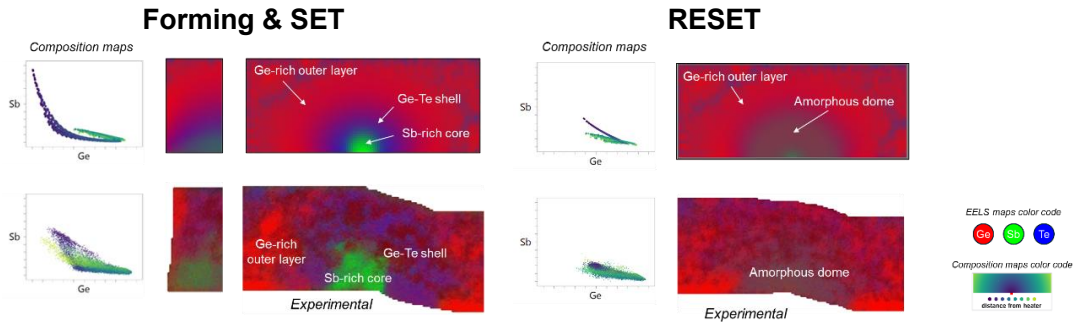

Figure 2 – EELS and composition maps for forming/SET pulses and for RESET pulses, obtained with simulations (top) and experimental data (bottom). All the main regions are correctly identified by the simulation.

4. CONCLUSIONS

This study presents a comprehensive simulation framework for modeling the material evolution of Ge-rich ePCM devices from post-deposition annealing and memory operations. By exploiting phase change dynamics, eutectic decomposition, and field-assisted diffusion, the framework successfully reproduces experimental observations, including EELS maps and electrical characteristics.
The results underscore the importance of understanding elemental migration and phase behavior in optimizing the performance and reliability of ePCM technologies, particularly for demanding applications such as those in the automotive market.

REFERENCES

1. Zuliani et al., *IEEE Trans Electron Dev*, **60** (2013) 4020.
2. www.appliedmaterials.com (Ginestra™ software).
3. Y. Wang et al., *npj Computat Mater*, **7** (2021) 183.
4. Baldo et al., IMW (2021).
5. G. Novielli et al., IEDM (2013).

Reconfigurable phase-change metasurfaces for optical mode conversion and optical angular momentum control

[Invited]

Joe Shields[1], Carlota Ruiz de Galerreta[1,2], Stuart Kendall[1], Jacopo Bertolotti[1], A. Alù[3], Guoce Yang[4], Mengyun Wang[4], Nikolaos Farmakidis[4], Harish Bhaskaran[4], C. David Wright[1*]

[1]Centre for Metamaterials Research and Innovation, University of Exeter, Exeter, EX4 4QJ, UK
[2]Institute of Materials Science of Barcelona (ICMAB-CSIC), Bellaterra, 08193, Spain
[3]Photonics Initiative, Advanced Science Research Center, CUNY, New York, NY 10031, USA
[4]Department of Materials, University of Oxford, Parks Road, OX1 3PH, UK
*corresponding author: david.wright@exeter.ac.uk

Optical mode conversion and optical orbital angular momentum control find a variety of important applications ranging across information processing, communication and quantum optics [1]. Phase-change material (PCM) metasurfaces have the potential to deliver such conversion and control capabilities, in a switchable, non-volatile, compact and low power form factor. In this work we showcase two PCM metasurface device configurations that use appropriately designed arrays of Sb_2Se_3 cylindrical resonators to deliver (i) switchable optical mode conversion, here specifically TEM_{00} to HG_{10} conversion, and (ii) a switchable spiral PCM optical phase plate for the control of optical orbital angular momentum, here specifically by inducing a helical phase onto a TEM_{00} mode with zero topological charge to produce a LG_{01} mode with a topological charge of 1. The two device concepts are illustrated in Figure 1. For the mode conversion application, the metasurface comprises Sb_2Se_3 cylinders of two different sizes (on an SiO_2 substate), see Figure 1(a). With the resonators in the amorphous phase, a high transmission pass-through functionality (mode conversion OFF) is achieved. On crystallisation of the resonators, an optical phase shift of π radians is imparted to half of the beam (mode conversion ON), and conversion from the TEM_{00} to HG_{10} mode is accomplished. The PCM spiral phase plate for optical angular momentum control is shown in Figure 1(b). This uses the same type of Sb_2Se_3 meta-atoms as the former design, but with resonators of different sizes now occupying eight segments of a circle. By careful design of resonator size, we provide a full 2π optical phase shift as one rotates around the segments when the Sb_2Se_3 is in its crystalline phase (orbital angular moment control ON), while switching the Sb_2Se_3 to the amorphous state allows the beam to propagate unaltered (momentum control OFF). In this paper we describe the design, fabrication, experimental characterisation and potential applications of these PCM metasurface-based mode conversion and momentum control devices.

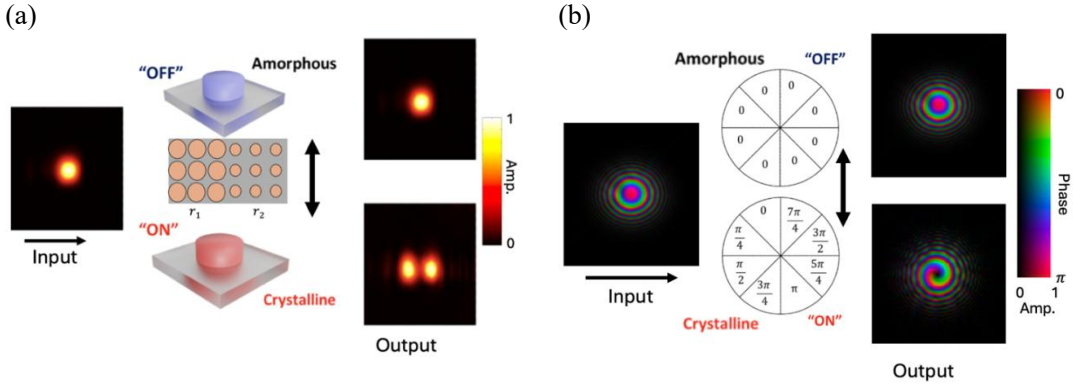

Figure 1: (a) Schematic and experimental results of a switchable phase-change metasurface performing ON/OFF TEM_{00} to HG_{10} mode conversion. (b) Schematic and simulated performance of a switchable metasurface for ON/OFF optical orbital angular momentum control.

Funding is acknowledged from the UK EPSRC (EP/W003341/1, and EP/W022931/1) and Marie Sklodowska-Curie Postdoctoral Fellowship 101068089 (METASCALE).

REFERENCES

[1] Yao, A. M., & Padgett, M. J. (2011). Orbital angular momentum: origins, behaviour and applications. Advances in Optics and Photonics, 3(2), 161.

Optical Phase Change Materials for hyperspectral sensing

Sourav Mondal[1,2,3], Kanikrishnan Sethupathi[1], A. Manivannan[2,3*]

[1]Low Temperature Physics Laboratory, Department of Physics, Indian Institute of Technology Madras, Chennai 600036, India

[2]Phase Change Memory Laboratory, Department of Electrical Engineering, Indian Institute of Technology Madras, Chennai 600036, India

[3]Advanced Memory and Computing Group, Department of Electrical Engineering, Indian Institute of Technology Madras, Chennai 600036, India

Email: anbarasu@ee.iitm.ac.in

ABSTRACT

Optical Phase Change Materials (O-PCMs) have attracted significant interest for their ultra-low absorption across the infrared spectrum, enabling high-performance, low-loss photonic devices. By leveraging these properties and integrating them into carefully engineered structures, we proposed an efficient light control for the development of tunable optical filters (TOFs) tailored for hyperspectral sensing applications.

Key words: O-PCMs, TOFs, Hyperspectral Sensing

1. INTRODUCTION

Optical Phase Change Materials (O-PCMs), a subclass of phase change materials, exhibit fundamentally distinct optical properties across different phases. Unlike conventional materials, where the refractive index (n) and extinction coefficient (k) are coupled via the Kramers–Kronig relation, O-PCMs exhibit an effective decoupling of these parameters, enabling independent control over n and k. Upon phase transition, they exhibit a significant change in refractive index (Δn) while minimizing the change in extinction coefficient (Δk), resulting in a high figure of merit (FOM = $\Delta n/\Delta k$). Moreover, their consistently low absorption in both phases makes them ideal for low-loss, reconfigurable photonic devices such as RF switches, photonic memory, hyperspectral sensors, and beam-steering systems [1,2].

Additionally, depending on the active volume involved, O-PCMs can support multi-level intermediate states, allowing continuous tunability—an essential feature for tunable optical filters (TOFs) in hyperspectral sensing. To exploit this, we adopted a Fabry–Pérot resonator design, where the active O-PCM layer is sandwiched between two distributed Bragg reflectors (DBRs). This configuration enables narrowband filtering based on constructive interference. The filter can be dynamically tuned by switching the phase of the PCM layer, either electrically or optically. Device performance was modelled using the Transfer Matrix Method (TMM) in MATLAB and further validated with finite element method (FEM) simulations in COMSOL Multiphysics.

2. EXPERIMENTAL

Tunable Optical Filters (TOFs) were designed for the long-wave infrared (LWIR, 8–12 µm) region using $Ge_2Sb_2Se_4Te_1$ (GSST41), which exhibits a high figure of merit (FOM) in this range [1]. Thin films of GSST41 were deposited via DC magnetron sputtering and annealed at 330 °C. Resistivity vs. temperature measurements revealed a crystallization temperature of ~290 °C. Structural analysis using XRD and GIXRD confirmed the hexagonal crystalline phase. Spectroscopic ellipsometry data, fitted with the Tauc–Lorentz oscillator model, highlighted distinct optical property differences between amorphous and crystalline phases. SEM imaging revealed the characteristic needle-like morphology of crystalline GSST41.

3. RESULTS & DISCUSSION

The filter design consists of two distributed Bragg reflectors (DBRs) made of Ge/CaF_2 multilayers, with a GSST41 layer sandwiched in between. These materials were selected for their minimal absorption in the LWIR range. The individual layer thicknesses are 500 nm (Ge), 1500 nm (CaF_2), and 1300 nm (GSST41). By transitioning the GSST41 layer between amorphous, intermediate, and crystalline phases—having refractive indices of 3.2, 3.8, and 4.6 respectively—the optical path length changes, shifting the constructive interference condition and thus tuning the transmission window.

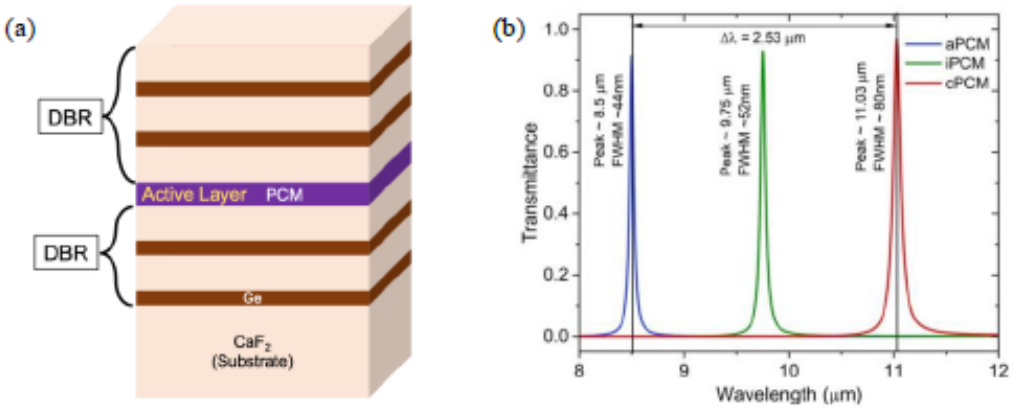

Fig-1 : (a) Design of Fabry-Perot filter on CaF2 substrate. (b) Simulated transmittance spectra for amorphous, intermediate, and crystalline phases of GSST41.

This design demonstrates a spectral tunability of ~2.5 μm with narrow full-width at half-maximum (FWHM) transmission peaks. Increasing the number of DBR periods can further enhance peak sharpness. Additionally, the DBR-based structure offers fabrication tolerance of ±10–15% in layer thickness, with less than 3% variation in transmission peak position, providing robust performance under practical fabrication conditions.

4. CONCLUSIONS

In this work, we have designed and simulated a Fabry–Pérot-based tunable optical filter using an Optical Phase Change Material (O-PCM) as the active tuning layer. Thin films of GSST41 were deposited, exhibiting low absorption in the LWIR range. While multi-level phase exploration and complete device fabrication and testing are ongoing, the proposed concept is readily extendable to other wavelength ranges such as SWIR and MWIR. Owing to its planar layered architecture, the device can be easily fabricated and integrated with existing photonic platforms. This approach offers a fast and reliable alternative to traditional physical gratings, overcoming their inherent limitations.

REFERENCES:

1. Zhang, Yifei, et al. "Broadband transparent optical phase change materials for high-performance nonvolatile photonics." *Nature communications* 10.1 (2019): 4279.
2. Wuttig, Matthias, Harish Bhaskaran, and Thomas Taubner. "Phase-change materials for non-volatile photonic applications." *Nature photonics* 11.8 (2017): 465-476.

Tunable colour coatings using phase change materials

J. Martinez, R. Shurvinton, A. Karimbana-Kandy, P. Dominic, A. Moreau, O. Hector, K. Iliopoulos, F. Lemarchand, J. Lumeau

Aix Marseille Univ, CNRS, Centrale Med, Institut Fresnel, Marseille, France

*corresponding author: Julien.lumeau@fresnel.fr

ABSTRACT

Colours created by thin-film coatings can be rendered tunable by introducing phase-change materials (PCMs), whose optical response changes due to an external signal. However, commonly-used PCMs are limited in their applications for colour coatings, due to high absorption of visible light. In this work the Sb_2S_3 PCM is used and we demonstrate a novel coating design which incorporates this layer into an asymmetric Fabry-Perot cavity with Ag, SiO_2 and Ti layers. The phase change of the Sb_2S_3 layer is demonstrated using direct heating using a hotplate, and also using laser annealing.

Key words: thin films, colour coatings, phase-shift materials, active colour, Sb_2S_3

1. INTRODUCTION

Thin-film stacks are a powerful and well-controlled option for generating colour. By using thin layers of materials (typically tens to hundreds of nanometers thick), interference effects occur to create a reflectance (or transmittance) spectrum that depends on the thickness and refractive index of each layer. With proper material choice, this stack can be used to create highly saturated colour in a wide variety of hues, making it a versatile option for precise colour control [1]. Another advantage of thin-film coatings is that they may be made active and tunable by the inclusion of a phase-change material (PCM). An external signal, such as a laser or heater, causes the PCM to switch between its phases, which changes the refractive index of the PCM. When incorporated into a thin-film stack, this phase change can be exploited to yield tunable colour, where the colour of the coating depends on the phase of the PCM layer.

Antimony trisulfide (Sb_2S_3), has seen significant interest for visible photonics in recent years, due to its lower absorption and large optical contrast [2, 3]. In this work we propose a coating design based on a Fabry-Perot cavity with a layer of Sb_2S_3 between the opaque lower mirror and the cavity material. This design allows a wide gamut of colours to be generated by tuning the thickness of the cavity layer, but also maximises the optical contrast between the amorphous and crystalline phases of Sb_2S_3.

2. EXPERIMENTAL

The thin-film layers in this work were deposited using electron beam evaporation in one of two Buhler-Leybold SyrusPRO 710 vacuum deposition machines. In order to prevent contamination of the material layers, one machine was used to deposit Sb_2S_3, and the other was used to deposit the remaining materials (Cr, Ag, SiO_2 and Ti). Deposition was carried out under a vacuum of approximately $5x10^{-7}$ mbars. Coatings were deposited on rough (unpolished) surfaces in order to aid adhesion and improve the visual appearance of the resulting colour. The layer thickness was monitored using a quartz balance.

3. RESULTS & DISCUSSION

An electric hotplate was used to anneal samples containing layers of phase-change materials. The hot-plate was heated to a steady temperature of 300◦C, and samples were placed directly on its surface to anneal. The annealing was performed in air. Annealing time was judged by eye via

observing when the colour change appeared to be stable, which took about 2 minutes for both Sb_2S_3. Representative results are shown in Figure 1.

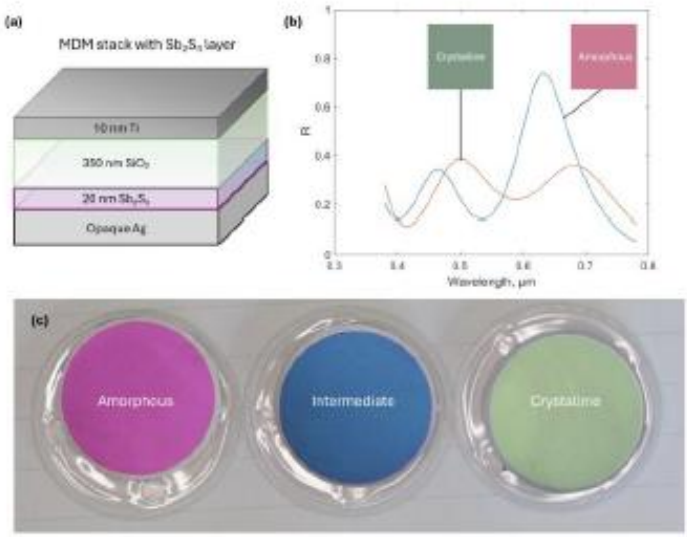

Figure 1: (a) Deposited thin-film stack (b) Simulated reflectance of the stack in the amorphous and crystalline phases (c) Left: As-deposited coating Middle: Coating after 30 seconds hotplate annealing Right: Coating after full crystallization

The laser annealing was performed using a 1030 nm wavelength, 400 fs pulse duration laser, 2.7 μJ energy per pulse with a repetition rate of 200 kHz and a 1 ms exposure time. A 40 cm converging lens was used to focus the laser then laser scanning was performed by mounting the sample on a motion stage at the focal plane of the lens. An example of the colour change obtained by laser can be seen in the inscribed image of Figure 2.

Figure 2: Ultrafast laser inscription employing the colour-change principle presented in this work.

4. CONCLUSIONS

An active colour-shift coating design incorporating Ag, SiO_2 and Ti, as well as the phase-change material Sb_2S_3, has been demonstrated. The coating uses a layer of Sb_2S_3 to modify the lower mirror of a Fabry-Perot cavity, enabling a wide gamut of colours to be obtained with high chroma and brightness. Colour switching by both hotplate and laser annealing has been demonstrated.

REFERENCES

[1] R. Shurvinton, F. Lemarchand, A. Moreau, J. Lumeau, Advanced Photonics Research 2022, 2200102.

[2] W. Dong, H. Liu, J. K. Behera, L. Lu, R. J. H. Ng, K. V. Sreekanth, X. Zhou, J. K. W. Yang, R. E. Simpson, Advanced Functional Materials 2019, 29.

[3] M. Delaney, I. Zeimpekis, D. Lawson, D. W. Hewak, O. L. Muskens, ADVANCED FUNCTIONAL MATERIALS 2020, 30, 36.

Dynamically Tunable Asymmetric Bragg-Enhanced Fabry–Pérot Cavity for Near-Perfect Mid-Infrared Absorption

Qingshan Tan[1], Shaojie Yuan[1], Binhao Wang[1], Ming Xu[1], and Hao Tong[1]*
[1] Huazhong University of Science and Technology, China
*Corresponding author: tonghao@hust.edu.cn (H.T.)

ABSTRACT

This work proposes a novel dynamically tunable broadband mid-infrared absorber integrating a high-loss asymmetric Fabry-Pérot cavity, a periodic asymmetric distributed phase-change Bragg reflector and a top anti-reflection coating. It achieves ~96.5% average absorptance and a relative bandwidth of 143.75% over 1.8–11 μm with ~55% tunability and wide-angle tolerance, all via planar fabrication. This design enables scalable, efficient solutions for infrared stealth, thermal control, and adaptive sensing.

Key words: periodic asymmetric Bragg reflector, ultra-broadband absorption, dynamically tunable, perfect absorption, phase change materials

1. INTRODUCTION

The 1.8–11 μm mid-infrared (MIR) range is vital for molecular sensing and thermal management, yet achieving efficient, broadband, and tunable absorption remains difficult[1,2]. The metal-insulator-metal (MIM) Fabry-Pérot (F-P) cavities offer strong absorption but suffer from narrow bandwidths and static response, limiting adaptive applications[3]. Strategies like high-loss metals, plasmonic coupling, or cascaded resonances improve bandwidth but reduce efficiency or demand complex nanostructures[4]. Phase-change materials (PCMs, e.g., VO_2, GST) offer dynamic tuning but face optical contrast or bandwidth limitations. Here, we propose a lithography-free planar thin-film absorber combining an asymmetric distributed Bragg reflector (DBR) with a high-loss F-P cavity. Through synergistic optimization of multi-resonant coupling, broadband impedance matching, and reflection suppression, this architecture achieves near-perfect absorption performance, achieving ultra-broadband, high-efficiency, tunable absorption with wide-angle stability. This scalable design overcomes key trade-offs, advancing MIR stealth, thermal control, and sensing applications.

2. EXPERIMENTAL

First-principles calculations (VASP) modeled amorphous/crystalline AIST using AIMD and DFT with PBE/PBE0 functionals (500 eV cutoff, 2×2×2 k-grid). Experimentally, a seven-layer thin-film stack (Cr/Ge/AIST/TiO_2/MgF_2) was sputter-deposited (base pressure: 8×10^{-5} Pa, 100°C) and annealed (290°C, 5 min) for phase transition. Optical properties were characterized via FT-IR (Nicolet iS50R) and ellipsometry (IR-VASE Mark II). Numerical simulations (Lumerical FDTD, Macleod) used ellipsometry-derived optical constants to validate the design.

3. RESULTS & DISCUSSION

As shown in Fig. 1(a), the absorber consists of three key components. At the bottom, an asymmetric high-loss F–P cavity (Cr/Ge/TiO_2/Cr) serves as the main absorption unit. In the middle, an asymmetric distributed Bragg reflector (A-DBR) made of alternating AIST and TiO_2 layers enables phase-change optical modulation. The top MgF_2 antireflection (AR) coating reduces interfacial reflection and improves impedance matching. The entire structure is fabricated using planar thin-film deposition techniques without nanolithography, offering excellent scalability, ease of fabrication, and compatibility with standard semiconductor processes.

As illustrated in Fig. 1(b), the device achieves a simulated average absorption of ~96.5% (~83% experimentally) over 1.8–11 μm, a record-high relative bandwidth of 143.7%, angle insensitivity up

to 70°, and dynamic modulation depth of ~55% through the phase transition of AIST. The absorption can also be tuned by modifying the cavity or A-DBR parameters.

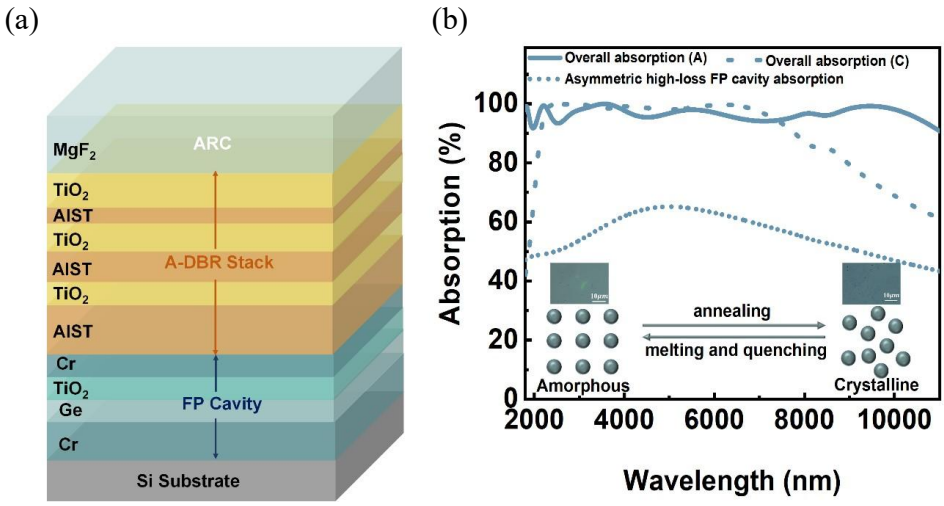

Figure 1. Schematic and optical response of the proposed absorber. (a) Schematic illustration of the ultrabroadband absorber architecture. (b) Simulated absorption spectra of the integrated structure before and after phase transition, along with the optical response of the Fabry–Pérot cavity. The insets depict the experimentally observed phase transition behavior.

4. CONCLUSIONS

This work demonstrates a lithography-free, planar mid-infrared absorber combining a high-loss asymmetric Fabry–Pérot cavity with a TiO_2/AIST Bragg reflector and MgF_2 coating. It achieves broadband, angle-insensitive absorption (~96.5% simulated, ~83% experimental) from 1.8 to 11 µm, with a 143.75% fractional bandwidth and ~40% improvement over traditional MDIM structures. The reversible phase transition of AIST enables dynamic tunability (~55% simulated, ~30% experimental) without geometry change. First-principles analysis links broadband absorption to phase-driven electronic and permittivity changes. Compatible with thin-film fabrication, the absorber is scalable for infrared camouflage, thermal control, and tunable MIR sensing.

REFERENCES

1. K. Li, *Microsyst Nanoeng*, 2025, **11**, 2.
2. R. Wei, *ACS Photonics*, 2025, **12**, 628-635.
3. M. Aghaeipour, *Nanophotonics*, 2018, **7**, 819-825.
4. Y. Song, *J. Mater. Sci.: Mater. Electron.*, 2020, **31**, 4696-4701.

Mid-infrared PCM spatial light modulator

[Invited]

Cosmin-Constantin Popescu[1], Zhiyun Xu[1], Rui Chen[1], Khoi Dao[1], Brian Mills[1], Luigi Ranno[1], Tian Gu[1], Hyun Jung Kim[2], Oleg Maksimov[3], Harish Bhandari[3], and Juejun Hu[1]

[1]Department of Materials Science and Engineering, Massachusetts Institute of Technology, Cambridge, MA, USA

[2]Department of Aerospace Engineering, Korea Advanced Institute of Science and Technology, Daejeon, South Korea

[3]Radiation Monitoring Devices Inc., Watertown, MA, USA

*corresponding author: hujuejun@mit.edu

ABSTRACT

We report what we believe to be the first experimental demonstration of a chalcogenide phase-change material (PCM)-based spatial light modulator employing a scalable two-dimensional (2D) array architecture. Our approach integrates a free-space transmissive metasurface[1] with a silicon platform, leveraging a monolithic backend-of-the-line (BEOL) process fully compatible with industry-standard foundry fabrication. This integration was enabled by atomic layer deposition (ALD) of high-quality, low-loss chalcogenide PCMs, along with a ZnS/ZnTe wetting layer to ensure film conformity and interface control. Each metasurface pixel is independently controlled via electrothermal actuation using a 2D doped-silicon microheater array. Crucially, every microheater is co-integrated with a silicon junction selector, which effectively suppresses sneak path currents—a critical requirement for scaling to large arrays. The combination of sneak path suppression and pixel-level electrical addressing through multi-layer CMOS BEOL metal routing underpins the scalability of our architecture for practical, high-density spatial light modulation.

Key words: phase change materials, photonics, optics, modulator, atomic layer deposition

1. INTRODUCTION

Spatial light modulators (SLMs) are indispensable components in a wide range of optical systems, enabling dynamic beam shaping, wavefront control, and adaptive optics. While numerous technologies exist for visible and near-infrared applications, viable options for mid-infrared (mid-IR) SLMs remain limited. Liquid crystal-based modulators suffer from strong optical absorption and slow response times in the mid-IR regime, while digital micromirror devices (DMDs) offer only binary amplitude modulation without any phase control—severely limiting their functionality for coherent wavefront engineering.

Nanophotonic approaches, particularly those based on metasurfaces[2], offer a promising path forward. Their subwavelength-scale structures allow precise control over light phase, amplitude, and polarization, and their planar form factor is inherently compatible with dense integration. However, realizing a practical nanophotonic two-dimensional SLM presents two major challenges. First, achieving individual electrical addressing of each pixel in a dense array requires intricate routing solutions that are difficult to scale. Second, in conventional cross-bar architectures, the absence of isolation elements leads to significant sneak path currents, which not only waste power but also prevent reliable operation as array size increases.

In this work, we present what we believe to be the first demonstration of a mid-IR spatial light modulator based on chalcogenide PCMs that overcomes both of these challenges. Our device features a CMOS backend-compatible, monolithically integrated 2D Sb_2S_3-based metasurface array on a silicon platform. Each pixel is individually controlled using electrothermal microheaters integrated with silicon junction selectors that suppress sneak path currents. Combined with multilayer CMOS BEOL metal routing, this architecture enables scalable, energy-efficient, pixel-level control—marking a critical step toward practical, high-resolution mid-IR SLMs.

2. EXPERIMENTAL

The micro-heater array, interconnected in a cross-bar manner, was fabricated leveraging the standard active silicon photonics fabrication process at AIM Photonics. Using a cross-bar array architecture reduces the number of electrical leads to $2n$ for n^2 pixels, with $n = 6$ in our design. The metal level M1 and doped Si level were used for the signal lines while the M2 and top aluminum metal line were leveraged for the ground lines, with vias connecting them for added robustness. The fabrication and BEOL integration process is shown in Fig. 1a. Fig. 1b shows the pixel structure including the integrated Si diode selector. A circuit diagram of the pixel array is shown in Fig. 2.

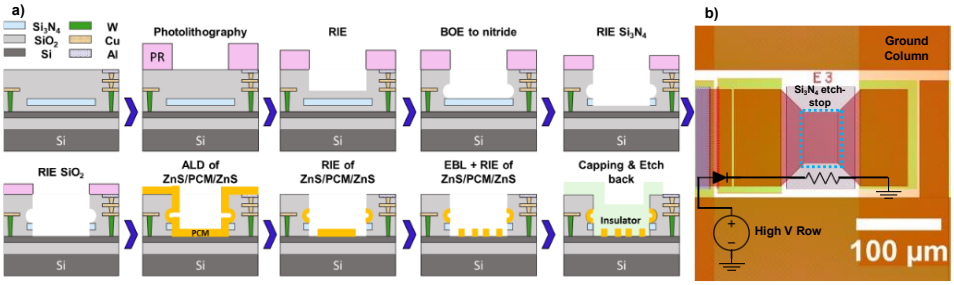

Figure 1. (a) Fabrication flowchart for BEOL integration of ALD PCM on the foundry-processed chips. Most of the photolithography steps are implied. (b) Layout of a 300 µm square pixel with heavily doped tapers, and a 40 µm × 60 µm medium doped region (cyan dashed rectangle) for the PCM metasurface and optical element. The diode selector and presumed off-chip ground and voltage source are also depicted for reference.

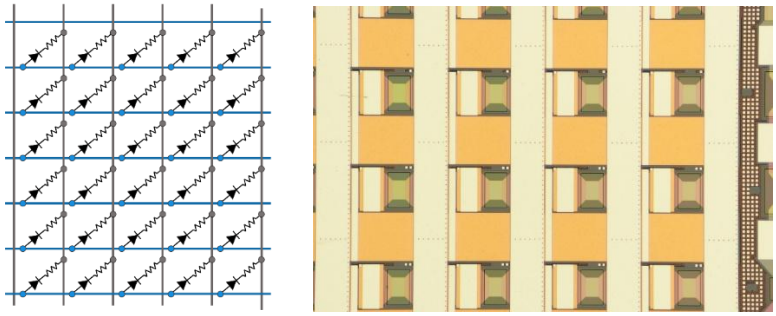

Figure 2. (Left) Circuit diagram of the cross-bar matrix heater array with selector for preventing sneak path current. (Right) Top-view optical micrograph of the 2-D micro-heater array.

3. RESULTS & DISCUSSION

We experimentally verified that the pixel can be reversibly switched for thousands of cycles. The optical contrast stabilizes after the first few hundred cycles and no sign of failure or degradation was observed up to 6,000 cycles[3].

4. CONCLUSIONS

In summary, we report BEOL integration of PCMs with doped Si micro-heater arrays fabricated leveraging standard photonic foundry service. We realized PCM integration with an individually addressed 2-D cross-bar micro-heater arrays with integrated selectors for the first time. This scalable PCM array technology can empower future applications in imaging, LiDAR, sensing, artificial neural networks, and beyond.

REFERENCES

1. Popescu, C. C. *et al.* Electrically Reconfigurable Phase-Change Transmissive Metasurface. *Advanced Materials* **36**, 2400627 (2024).
2. Gu, T., Kim, H. J., Rivero-Baleine, C. & Hu, J. Reconfigurable metasurfaces towards commercial success. *Nat Photonics* **17**, 48–58 (2023).
3. Popescu, C.-C. *et al.* Heterogeneous integration of nonvolatile phase-change photonics. in *Proc. SPIE* (eds. Notomi, M. & Zhou, T.) vol. 13375 133750D (SPIE, 2025)

Low-Energy and High Endurance All-Optical Reconfigurable Silicon Photonic Devices based on Phase-Change Materials

Y. Brûlé[1,*], A. Albanese[1], L. Karam[1], J. Lagrave[1], P. Meilleur[1], O. Mouawad[1], R. Sawant[2], C. Pourny[2], A. Rogemond[2], G. Gonzalez-Cortes[2], J.-B. Jager[3], S. Malhouitre[1], B. Charbonnier[1], A. Coillet[2], B. Cluzel[2] and P. Noé[1,*]

[1]Univ. Grenoble Alpes, CEA, LETI, F-38054, Grenoble, France.
[2]ICB, UMR CNRS 6303, Université Bourgogne Europe, F-21078 Dijon cedex, France.
[3]Univ. Grenoble Alpes, CEA, IRIG, F-38054, Grenoble, France.
*corresponding authors: yoann.brule@cea.fr , pierre.noe@cea.fr

ABSTRACT

We present CMOS-compatible, all-optical programming of $Ge_2Sb_2Te_5$ and $GeSe_{1-x}Te_x$ phase-change patches integrated on silicon waveguides, achieving energy-efficient and high-endurance modulation of both optical amplitude and phase. Our approach demonstrates ultra-low optical switching thresholds, markedly below those reported in previous studies, and robust non-volatile operation exceeding 10^8 switching cycles. These results position phase-change photonics as a strong candidate for next-generation non-volatile photonic computing platforms. Finally, we identify chemical segregation induced by the huge temperature-gradient in patches as the primary degradation pathway, offering critical insights for extending device endurance.

Keywords: Phase-Change Materials, Reconfigurable Silicon Photonics, Neuromorphic computing.

1. INTRODUCTION

Phase-Change Materials (PCMs), particularly those belonging to chalcogenide family, have emerged as key enablers for next-generation non-volatile photonic computing and neuromorphic systems [1]. Their unique ability to reversibly switch between amorphous and crystalline states—coupled with high contrast in optical properties arising from their bonding characteristics [2]—makes them attractive for programmable photonic integrated circuits (PICs). Here, we present a fully CMOS-compatible platform integrating $Ge_2Sb_2Te_5$ (GST) and $GeSe_{1-x}Te_x$ [3] patches on silicon waveguides, achieving record-low switching energies, cycling endurance, and dynamic control of complex optical transmission [4].

2. EXPERIMENTAL

Devices were fabricated on 200 mm silicon-on-insulator wafers using industrial-grade processes. 20 nm PCM films were deposited atop planarized silicon waveguides and encapsulated with GeN_x and SiO_2 capping layers. All-optical programming was performed using pulsed lasers in a heterodyne interferometer setup [4], enabling simultaneous measurement of amplitude and phase changes at telecom wavelength. Programming involved nanosecond pulses for crystallization and sub-nanosecond pulses for amorphization, with precise tuning of pulse energy and timing.

3. RESULTS & DISCUSSION

GST patches showed significant transmission modulation (~60%) and optical phase shift (~55°) as shown in Fig.1(a). The programming thresholds were remarkably low: ~100 pJ for amorphization and ~7.4 nJ for crystallization. Device response was fully reversible and non-volatile. Stable operation beyond 10^8 cycles was achieved without degradation in optical contrast, outperforming prior state-of-the-art endurance records by several orders of magnitude [5] (Fig. 1(b)). Multi-level

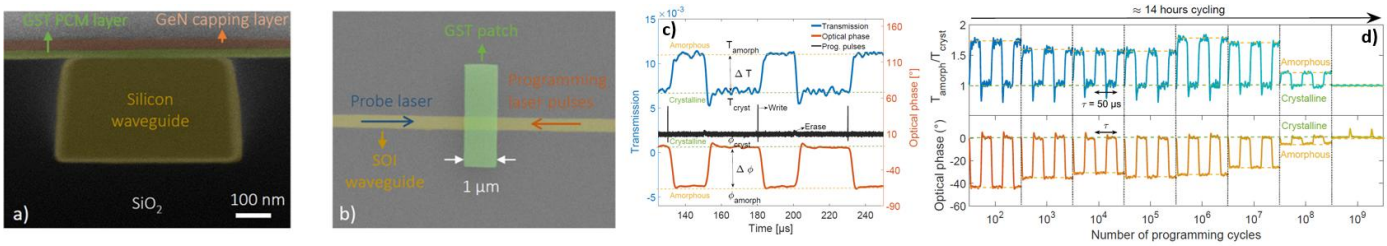

programming was also demonstrated using repeated amorphization pulses, accessing intermediate levels for analog data encoding.

Figure 3: a) SEM image of SOI waveguide cross section covered by GST PCM and GeN capping layers. b) Typical top SEM image of the final device with the GST patch and the buried silicon waveguide. A schematic of the optical experiments further conducted to program and read the PCM state is superimposed. (c) Change of transmission and optical phase recorded at output of Si waveguides after exposure to a sequence of programming laser pulses i.e. amorphization (write) and crystallization (erase) pulses for devices with a GST patch of 1.5 µm length, (d) Plot of changes of the transmitted amplitude and optical phase through silicon waveguides decorated with PCM patches recorded each 10^N programming sequences (write/erase), with N ranging from 1 to 9, reaching up to 1 billion cycles.

Material degradation after extreme cycling was investigated via Scanning Electron Microscopy (SEM) associated to Energy-dispersive X-ray spectroscopy (EDX). Evidence of phase segregation (Ge accumulation and Sb/Te depletion) confirmed thermal-gradient-induced migration (known as "Soret effect" [7]) as the primary aging mechanism (Fig.2).

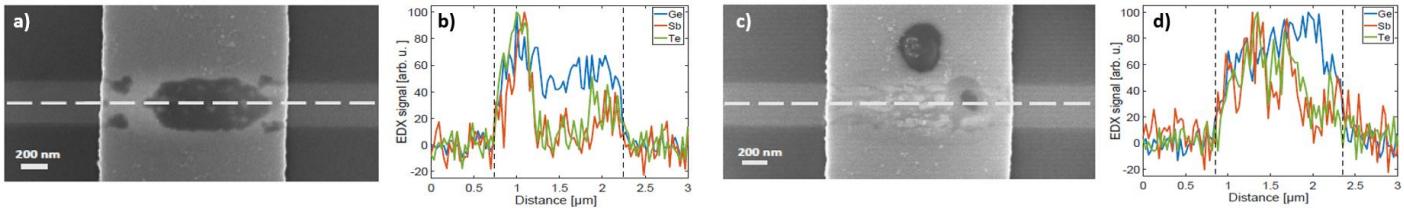

Figure 4: SEM images of GST patches surmounting Si waveguides programmed in amorphous state after (a) a few tens of cycles and (c) after failure at one billion cycles. In (b) and (d) are plotted the Ge, Sb and Te relative concentration profiles obtained by EDX line scans acquired along the white dashed lines shown in (a) and (c) SEM images, respectively.

In comparison, $GeSe_{1-x}Te_x$ patches exhibited similar programming behavior and endurance, but with significantly reduced optical losses. However, their limited transmission modulation (~6%) renders them far more suitable as reconfigurable phase shifters than optical signal amplitude modulators.

3. CONCLUSIONS

We report the demonstration of high-endurance, energy-efficient, all-optical PCM programming in silicon photonic waveguides, enabling both binary and multi-level modulation of transmission and phase. The scalable fabrication and record cycling endurance support immediate integration into programmable PICs, particularly for neuromorphic and reconfigurable photonic computing. These results mark a significant step toward novel non-von Neumann optical architectures as those offered by in-memory computing.

REFERENCES

[1] F. Brückerhoff-Plückelmann, et al., *J. Appl. Phys.,* vol. 129, no. 15, p. 151103 (2021)
[2] J.-Y. Raty, et al., *J. Phys. D: Appl. Phys.*, vol. 53, no. 23, p. 234002 (2020)
[3] A. Albanese, et al., *Phys. Status Solidi RRL*, vol. 18, no. 10, p. 2400129 (2024)
[4] M. Ibnoussina, et al., *Opt. Lett.*, vol. 45, no. 18, p. 5053 (2020)
[5] R. Sawant, et al., submitted to *Adv. Optical Mater.*, under revision (2025)
[6] J. Meng, et al., *Light Sci. Appl.,* vol. 12, no. 1, p. 189 (2023)
[7] L. Martin-Monier, et al., *Opt. Mater. Express,* vol. 12 no. 11, p. 4235 (2022)

Inverse-designed Si-Sb_2S_3 tunable integrated meta-switch

P. Kepič[1]*, C. Li[2], H. Yu[2], S. Maier[2], T. Šikola[1,3], H. Ren[2] and F. Ligmajer[1,3]

[1] Central European Institute of Technology, Brno University of Technology, Purkyňova 123, Brno, 612 00, Czech Republic

[2] School of Physics and Astronomy, Monash University, Melbourne, VIC, 3800, Australia

[3] Institute of Physical Engineering, Faculty of Mechanical Engineering, Brno University of Technology, Technická 2, Brno, 616 69, Czech Republic

*corresponding author: peter.kepic@ceitec.vutbr.cz

ABSTRACT

While GST-based phase-change materials dominate photonic integrated circuits, their crystalline-state absorption limits device functionality. We present an inverse-designed, phase-only tunable metasurface switch based on a hybrid Si–Sb_2S_3 nanostructure. Exploiting large index contrast and low losses of Sb_2S_3, our single-pulse reconfigurable device enables compact, efficient, and purely refractive modulation—offering a promising path toward scalable, high-performance tunable photonic integrated platforms.

Key words: photonic integrated circuits, antimony trisulfide, metasurface, inverse design

1. INTRODUCTION

Emerging technologies such as artificial intelligence and quantum computing require faster and more energy-efficient data processing and storage. Photonic integrated circuits (PICs) — chips that use light instead of electricity — thus represent a natural evolution of the current electronic paradigm. Metasurfaces have become a powerful platform for manipulating light at subwavelength scales, offering compact and highly efficient solutions for PICs [1]. Inverse design, an algorithmic optimization approach, enables the automated discovery of even more compact and non-intuitive photonic metasurfaces tailored for specific optical functionalities [2]. However, these functionalities are typically fixed post-fabrication when using conventional photonic materials like silicon (Si). To overcome this limitation, we integrate the phase-change material antimony trisulfide (Sb_2S_3) into an inverse-designed metasurface waveguide switch (meta-switch) based on a silicon-on-insulator platform. While Sb_2S_3 has been previously employed in this domain due to its large refractive index contrast ($\Delta n>1$) and broadband transparency in the near-infrared (NIR) [3], prior switching relied on speed-limited laser-writing of discrete amorphous/crystalline pixels [4]. We propose an inverse-designed hybrid Si–Sb_2S_3 nanostructured metasurface that enables switching via a spatially extended single pulse, offering a faster, more compact, and more energy-efficient alternative to prior designs, while establishing a promising direction for tunable PIC platforms.

2. EXPERIMENTAL

First, amorphous Sb_2S_3 film was deposited at room temperature by pulsed laser deposition (10 Hz, 0.5 J/cm^2, Ar 100 mTorr, Sb_2S_3 target) on top of commercial epitaxially grown 300 nm Si on r-cut sapphire. The 30 nm planned thickness ended up as 37 nm (see Figure 1a). The film was coated by a 256 nm SiO_2 protective coating by electron beam evaporation (6 kV, 30 mA, 1 Å/s). The refractive indices and absorption coefficients of amorphous and crystalline Sb_2S_3 (see Figure 1b) were obtained by ellipsometry. The inverse-designed metasurface was calculated using the adjusted open-source Python script ‘spins-B’ [2]. The device was fabricated by two-step electron beam lithography. In the first step, Sb_2S_3 square patches were deposited into a positive electron beam resist mask. In the second step, the whole device (see Figure 1c) was etched by argon ions through a negative resist mask. The device functionality and efficiency were measured by mapping intensity

at the outputs (and dividing them by those of the reference waveguide) while illuminating the input by a 1550 nm confocal laser source.

3. RESULTS & DISCUSSION

As the refractive indices of amorphous and crystalline phases of Sb_2S_3 vary with thickness [3], we aimed for 30 nm, which should be possible to amorphize but sufficient for modulation in the metasurface. With an acceptable thickness of 37 nm (see Figure 1a), we obtained a 2.38 refractive index in amorphous and 2.85 in crystalline phases at the device's operational 1550 nm wavelength (see Figure 1b). Besides obtaining refractive indices, the multilayer film in Figure 1a was used to verify and obtain parameters for amorphization.

The device comprised one input coupler, two output couplers, 150 nm Si rib-waveguides, and a 150 nm Si – 30 nm Sb_2S_3 metasurface square patch. The patch was optimized by inverse design to maximize (minimize) output 1 (output 2) in the amorphous phase and to reverse its functionality upon phase change to the crystalline phase. After the metasurface was optimized by inverse design, the device was fabricated and measured following the steps in the experimental part.

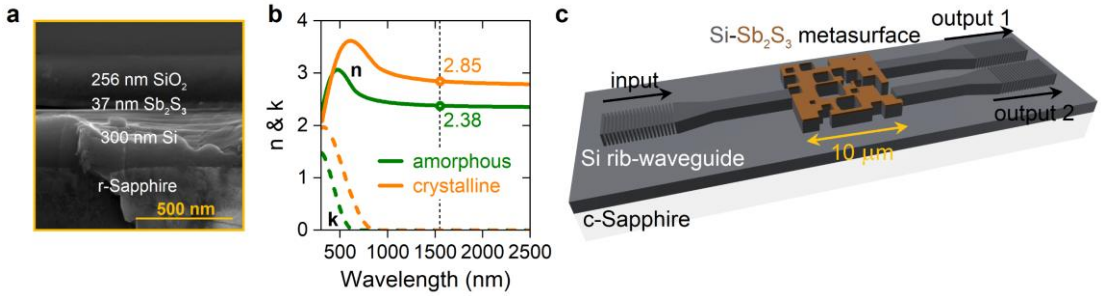

Figure 1 a) SEM micrograph of r-Sapphire-Si-Sb_2S_3-SiO_2 multilayer cross-section with listed thicknesses. b) Measured refractive index and absorption coefficient of 37 nm Sb_2S_3 film from (a) in amorphous (green) and crystalline (orange) phases. The dashed line highlights the 1550 nm wavelength of interest. c) Scheme of the inverse-designed Si- Sb_2S_3 tunable integrated meta-switch.

4. CONCLUSIONS

This extended abstract presents a new photonic integrated switchable component based on a hybrid Si–Sb_2S_3 metasurface. We combine inverse-designed metasurface with almost lossless phase-change material that changes purely refractive index during the transition. Despite being still in the preliminary stages, we believe this type of device offers a faster (possibly switchable by single shot), more compact, and more energy-efficient alternative to prior designs and establishes a promising direction for tunable PIC platforms.

REFERENCES

1. Y. Yang et al., *Light Sci. Appl.* **12** (2023) 152.
2. S. Molesky et al., *Nature Photon.* **12** (2018) 659–670.
3. P. Kepič et al., *New J. Phys.* **26** (2024) 013005.
4. M. Delaney et al., *Sci. Adv.* **7** (2021) eabg3500.

The metastable phase of Bi_2Te_3

S. Wredh[1], V. Nasrollahi[2], N. Q. Adanan, N.W.L. Munn[3], P. Chong[3], S. Dimov[2], D. Chambers-Sims[2], E.J. Gaggs[2], J.K.W. Yang[1], R. E. Simpson[2*]

[1]Singapore University of Technology and Design, Singapore
[2]School of Engineering, University of Birmingham, UK
3Institute of Materials Research and Engineering, Agency for Science Technology and Research (A*STAR), Singapore
*corresponding author: r.e.simpson.1@bham.ac.uk

ABSTRACT

We study the potential of Bi_2Te_3 for programmable photonics applications. Femtosecond laser pulses were used to induce a metastable structure in Bi_2Te_3 for the first time. The structure and optical properties of this state are measured and understood via atomistic modeling.

Key words: Bi_2Te_3, Phase Change Material, Photonics, mid-infrared red

1. INTRODUCTION

Bismuth telluride (Bi_2Te_3) has excellent thermoelectric properties and is a topological insulator[1-3]. Recently, we have also used this material for photodetection across the visible and infrared spectrum[4-6]. However, to our knowledge, structural phase transitions and the resultant properties of Bi_2Te_3 have not been widely studied. Herein, we report how femtoseconds laser pulses can be used to induce a metastable state. Reversible switching is possible between the trigonal and metastable states. We report the optical properties of the metastable state in the visible and infrared spectrum.

2. EXPERIMENTAL

Bi_2Te_3 thin films were deposited on Si substrates using RF sputtering. The base pressure of the sputtering system was better than 1.6×10^{-5} Pa, the deposition pressure was 0.5 Pa, and deposition power was 20 W applied to a 50 mm Bi_2Te_3 target. We annealed the films in a microscope furnace whilst flowing Ar over the film and simultaneously monitoring reflectance in-situ with an Ocean Optics Flame spectrometer. The XRD patterns were measured using a Bruker D8 Discover Micro-XRD and validated against the JCPDF 15-0863 reference pattern for Bi_2Te_3 powder.

The films were switched into a metastable state using a Yb-doped femtosecond laser from Amplitude Systems S.A.. The laser system wavelength was 1030 nm with 310 fs pulse duration. Experiments were conducted at a 10 kHz repetition rate with pulse energies from 0.44 to 7.4 µJ. We adjusted the incident beam diameter (35-140 µm) by defocusing along the optical axis, tuning laser fluence between 5.7-1540 mJ/cm².

We measured the metastable state's optical properties using an Accurion EP4 micro-ellipsometer for visible spectrum and a J.A. Woollam IR-VASE ellipsometer for the mid-infrared spectrum. The dispersion model included Tauc-Lorentz and Drude terms, fitting visible and mid-infrared measurements simultaneously.

The laser switched state was modelled using MatterSim by instantly heating the trigonal structure to different temperatures using a Maxwell-Boltzmann distribution to provide the ions with kinetic energy. The structure evolution was then analyzed whilst it evolved into the metastable phase. The electronic band structure of the metastable phase was studied using VASP.

3. RESULTS & DISCUSSION

Femtosecond laser pulses can induce the metastable state. The laser switched areas are visible due to their substantially lower reflectance of the metastable state. Adjusting the pulse energy and beam diameter enabled the laser-switched mark diameter to be varied between 8-90 µm. Larger areas of the metastable structure were produced by raster scanning the laser spot over the film. Heating the films to 200 °C induced recrystallization resulting in a higher reflectance than the initial crystalline state.

X-ray diffraction (XRD) measurements revealed that the as-deposited Bi_2Te_3 film was partially crystalline. Annealing enhanced the crystallinity and the diffraction pattern matched that of Bi_2Te_3 powder references. Laser processing induced a crystal-to-crystal transition into a metastable phase.

4. CONCLUSIONS

Femtosecond laser switching can induce a Bi_2Te_3 metastable phase. This structure has significant optical contrast compared to the equilibrium phase. This optical contrast, which exists across the visible and infrared spectrum could be useful for tunable thermoelectric photodetectors and reconfigurable photonic devices.

REFERENCES

1. H. J. Goldsmid, *Materials*, (2014) ,4, a7042577.
2. H. J. Goldsmid and R. W. Douglas,. J. Appl. Phys. (*1954*), 5, 11, p. 386
3. J. P. Heremans et al., Nat Rev Mater, (2017) 2, 10, pp. 1–21,
4. S. Wredh et al. *Adv. Optical Mater* (2024), 12, 2401450
5. G. Zamiri et al, *Nanophotonics* (2025), 14(9): 1365–1373
6. S. Zhang et al, *Adv. Sci.* (2025), 12, 2413858

PCM cycling endurance Monitored in situ by engineered multi-beam Laser irradiations

N. Bottin[1, 2, 3],*, M. Abel[3], K. Meepron[3], M. Majumder[2], M. Koudia[3], E. Petroni[4], Y. Le-Friec[1], I. Berbezier[3], D. Grojo[2].

[1] STMicroelectronics - Crolles (France),
[2] LP3 - Marseille (France),
[3] IM2NP - Marseille (France),
[4] STMicroelectronics - Agrate Brianza (Italy)
*corresponding author: nicolas.bottin@st.com

ABSTRACT

We present an all-optical, multi-beam laser method to cycle and monitor phase transformations in GeSbTe thin films/multilayers in real time. Tailored pulses drive crystallization/amorphization, while IR measurements track resulting structural changes. Our work provides new insights into phase transformation mechanisms, including the effect of doping and layer stacking.

Key words: Phase-change materials, Laser annealing, Optical characterization, Switching studies

1. INTRODUCTION

Phase-change memory (PCM) materials like Ge2Sb2Te5 (GST) are key for embedded non-volatile memory (e-NVM) due to their high speed, scalability and endurance. GST stores data by switching between amorphous (high resistivity) and crystalline (low resistivity) states. Despite outperforming EEPROM and FLASH, GST's low crystallization temperature (~150°C) limits high-temperature use. Doping and germanium enrichment raise transition temperatures, but it has been demonstrated that both GGST and N-doped GGST alloys undergo a significantly more intricate, multistep crystallization process (1). Here, we develop a multi-beam laser annealing setup that leverages GST's optical contrast for reliable, reproductible phase transitions at tunable timescales and real-time monitoring. This method offers new insights into crystallization and amorphization mechanisms, including the impact of doping and thin film design (composition and stacking). We show laser beam engineering enables both single and repeated transitions, supporting endurance and degradation studies based on initial composition and GGST-GST multilayer stacking. Meeting industrial needs for better cycling endurance and speed, this technique efficiently optimizes material performance, with electronic switching reserved for production tracking.

2. EXPERIMENTAL

GST thin films are deposited on 300 mm Si(001) substrates using physical vapor deposition (PVD) with varying concentrations of germanium (Ge) and dopants (mainly nitrogen). The samples consist of stacked layers of different thicknesses and positions (GGST on top or bottom), all capped with 20 nm TiN to prevent oxidation. The presentation will cover results for single GGST layer and GST/GGST stacks with various doping levels. Our multi-beam setup enables irradiation from 220 fs to 50 ms at ~1.05 µm, ensuring uniform heating via high cap layer absorption. Real-time microscopy (1200 nm transmission, 680 nm reflection) provides quantitative data enabling precise phase identification via distinct optical responses of amorphous and crystalline phases (Ge, $G_2Sb_2Te_5$), using silicon's near-IR transparency. Phase states are confirmed by STEM/EDX of FIB cross-sections, correlating each transition stage to its optical signature. Experiments were repeated for reproducibility.

3. RESULTS & DISCUSSION

By varying laser pulse duration, we selectively induce crystallization, amorphization, or segregation. While the broader study covers various layer configurations, here we focus on a GST (undoped)/GGST (highly N-doped) single stack. For femtosecond pulses, amorphization occurs via

grain dissolution and lattice disorder, driven by either thermal melting and rapid quenching or non-thermal bond destabilization via electronic excitation. These effects, confirmed by STEM, SAED, and EDX, fully suppress crystallization regardless of fluence (2). With micro- and millisecond pulses at low temperatures, the GST layer crystallizes into 225 elongated crystals on the substrate while GGSTN remains amorphous. At higher temperatures, microseconds pulses cause Ge crystallization by melting-driven phase separation and rapid quenching, forming large Ge crystals while GGSTN stays amorphous. Millisecond pulses replace the 225 crystals with large, elongated Ge crystals, still leaving GGSTN amorphous. Only at a much higher temperature does the entire GST-GGSTN stack crystallizes, with GST and Ge crystals coexisting throughout, consistent furnace annealing studies of similar material (3). Nitrogen doping directly affects germanium segregation and crystallization temperature and kinetics.

These findings, combined with IR monitoring, enable effective tracking and analysis of cycling studies. Infrared transmission measurements reveal distinct crystallization signatures ($\Delta T/T \sim +5\%$ expected for germanium-only crystallization; $\Delta T/T \sim -20\%$ for full crystallization). In blanket-film experiments, nucleation-dominated crystallization of GGSTN from the amorphous state shows limited endurance (13 cycles). Pre-crystallization by targeted pulse activation is required to form the "formal stage" and the resulting "forming" state directly influences subsequent switching behavior. Research has also shown that this step is essential for device applications (4).

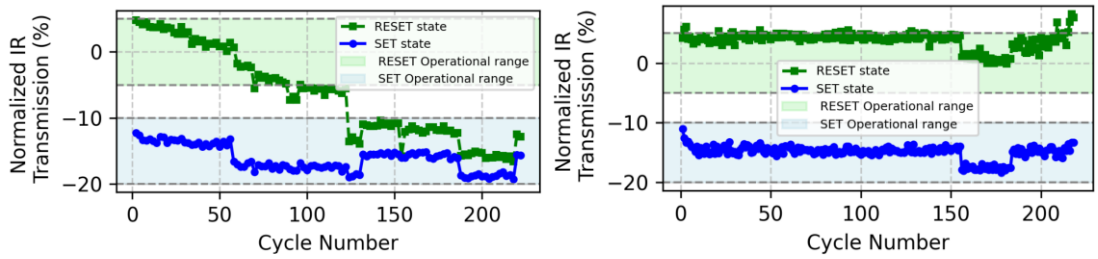

Figure 1. Infrared transmission response of a GST/GGSTN stack under repeated irradiation with milliseconds pulses for crystallization and microsecond pulse for amorphization.

Figure 1 shows two graphs of infrared transmission during SET (crystallization) and RESET (amorphization) cycles after the initial "forming" step (single-pulse laser activation). Shaded bands define arbitrarily operational thresholds. In the left graph, SET maintains stable IR values, indicating consistent crystallization, while RESET transmission declines, leading to incomplete transitions and eventual drift after ~125 cycles. In the right graph, multiple laser activation pulses address this drift, increasing stable switching cycles to 216 before capping layer ablation. STEM monitoring after increasing cycles until full degradation reveals the structural and chemical evolution of the layers, providing new understandings of the mechanisms that cause degradation.

4. CONCLUSIONS

In summary, our multi-beam laser-based study demonstrates that the engineering of laser pulses, enables precise control of amorphous and crystalline states in GST-based materials. The GST/GGSTN stack, offers enhanced thermal stability and facilitates germanium segregation and crystallization, improving reversible switching and cycling endurance. Infrared microscopy proves to be a simple yet powerful tool for real-time monitoring of phase-change dynamics. STEM monitoring allows a precise correlation of infrared transmittance responses with microstructural states. It also shed light on the mechanisms of structural transformation and helps understanding the degradation mechanisms.

REFERENCES

[1] J. Remondina et al., Sci. Rep. 14, 14677 (2024).
[2] K. Meeporn et all., in submission
[3] M. Luong et all., pss RRL. 18 (10), 2300421, (2024)
[4] S. Ran et all., Scientific Reports, 15, 11357 (2025).

Programmable Nanophotonics with Phase-Change Materials: From Metasurfaces to Polaritons

[Invited]

L. Conrads[1], M. Wuttig[1], and T. Taubner[1]*
[1] I. Institute of Physics (IA), RWTH Aachen University, Germany

*corresponding author: taubner@physik.rwth-aachen.de

ABSTRACT

We exploit the non-volatile insulator-to-metal transition of the plasmonic phase-change material In_3SbTe_2 for optical programming of metasurfaces for infrared beam-shaping and for optical programming surface polariton resonators on polar crystals and doped semiconductors. Our approach enables rapid-prototyping of customized infrared meta-optics, ranging from beam steering, lensing, optical vortex beams and holography towards reconfigurable polariton resonators even with anisotropic 2D-materials.

Key words: Phase-Change Materials, Metasurfaces, Polaritons, Infrared

1. INTRODUCTION

Conventional optical elements are bulky and limited to specific functionalities, contradicting the increasing demand of miniaturization and multi-functionalities. Nanophotonic concepts like optical metasurfaces, which usually consist of metallic or dielectric nanoantennas, enable tailoring light-matter interaction at will, especially important for the infrared spectral range which lacks commercially available beam-shaping elements. Tailoring light-matter interaction is essential to realize such nanophotonic components and can also be achieved with polaritons. These excitations of photons coupled with the collective (plasmon) oscillation of charge carriers in metals and semiconductors or with phonons in polar crystals and 2D-materials can lead to Surface Plasmon Polaritons (SPPs) and Surface Phonon Polaritons, (SPhPs), respectively. [1] Based on a reversible change in their refractive indices [2], Phase-Change Materials (PCMs) enabled the modification of SPhPs propagation [3] and the on/off switching of SPhP resonators [4]. While ultraconfined resonances are in principle possible by restricting these polaritons to cavities, the direct laser writing of such launching and resonator structures in PCMs has been so far elusive.

Recently, the plasmonic PCM In_3SbTe_2 (IST) was introduced for programmable nanophotonics due to the ability of reversibly switching from an amorphous dielectric to a crystalline metallic state in the infrared [5]. This material has been previously exploited for resonance tuning by reconfiguring the antenna shapes themselves [6] and tailoring thermal emission of metasurfaces [7,8]. However, rapid-prototyping of complex IST metasurfaces for real-world applications has not been shown yet. Tailored phase-modulated metasurfaces with the plasmonic PCM IST promise arbitrary beam-shaping in the infrared spectral range, which inherently lacks commercially available devices.

2. EXPERIMENTAL RESULTS

In the first part of this presentation, we exploit direct laser writing for programming large-area IST metasurfaces and investigate their respective functionalities. We use the concept of geometric phase metasurface to locally modify the phase of circularly polarized light by optically written crystalline IST nanoantennas in an amorphous IST film [9]. By using a commercial large-area direct laser writing system, we demonstrate beam steering metasurfaces for infrared light with varied supercell periods to obtain different beam deflection angles. We also design and investigate a metalens with a focal length of 11.5 cm and even perform more advanced beam shaping. For example, we can tailor the orbital angular momentum of infrared light and verify the mediated topological charges by revealing the spiral intensity pattern. Then, the phase profile of a metasurface hologram is

designed with the Gerchberg-Saxton algorithm and combined with the phase profile of a magnifying lens, highlighting an easy way for combining multiple functionalities within a single metasurface. Finally, we use a diffractive neural network for designing a single hologram metasurface featuring two different hologram patterns at certain distances behind the metasurface.

In the second part of this talk, we apply IST for the creation and modification of polaritonic cavities. We investigate surface phonon polariton resonators optically programmed via laser irradiation in the plasmonic PCM IST on top of the phonon polariton hosting polar crystal silicon carbide with scanning near-field optical microscopy (s-SNOM) [10]. Circular resonators are reconfigured in their diameters to shift the resonance modes accordingly. In addition, smaller resonator diameters facilitate stronger field confinements up to a value of $\lambda/35$. The vast flexibility of direct programming resonators is highlighted by investigating square and triangular resonators featuring complex field distributions according to their unusual shape. Moreover, we apply the same principle to study infrared SPPs on doped semiconductors CdO and InAs covered with thin layers of PCMs [11]. Conventionally, the small polariton confinement and the dispersion close to the light line aggravate real-space observation of SPPs in bulk materials in the infrared. Increasing the SPP confinement with thin dielectric layers modifies the SPP dispersion and allows for direct fabrication of resonators by locally switching the PCM.

3. DISCUSSION & CONCLUSIONS

The concept of directly programming metasurfaces with IST antennas is much simpler, more cost-effective and faster compared to cumbersome fabrication techniques such as conventional lithography involving multiple costly and complex patterning and etching steps. The operation wavelength of the metasurfaces is only given by the length of the rotated antennas and can be easily scaled to target the entire infrared range. Currently, the infrared spectral range displays a significant lack of commercially available beam shaping elements. Hence, our demonstrated concept paves the way towards fabrication of large-area metasurfaces within hours, enabling rapid-prototyping of customized infrared meta-optics for sensing, imaging and quantum information.

In a similar way, directly programming polariton resonators with PCMs without cumbersome fabrication techniques facilitates sub-wavelength polaritonic devices such as biosensors or optical data storage systems. The combination of PCMs with polariton-hosting materials can be easily extended to 2d hyperbolic and anisotropic crystals featuring lower losses and higher polariton propagation lengths, enabling reconfigurable light-matter control on the nanoscale.

Acknowledgements: The authors acknowledge support by the Deutsche Forschungsgemeinschaft (DFG No. 518913417 & SFB 917 "Nanoswitches").

REFERENCES

1. D.N. Basov et al., *Nanophotonics* **10** (2021) 549.
2. M.Wuttig et al., *Nat. Photonics* **11** (2017) 465.
3. K. Chaudhary et al., *Nat. Commun.* **10** (2019) 4478.
4. H. Sumikura et al., *Nano. Lett.* **19** (2019) 2549.
5. A. Heßler et al., *Nat. Commun.* **12** (2021) 924.
6. A. Heßler, L. Conrads et al., *ACS Photonics* **9** (2022) 1821.
7. L. Conrads et al., *Adv. Opt. Mat.* **11** (2023) 2202696.
8. M. Giteau, L. Conrads et al., *Laser Phot. Rev.* **19** (2024) 2401438.
9. L. Conrads et al., *Nat. Commun.* **16** (2025) 3698.
10. L. Conrads et al., *Nat. Commun.* **15** (2024) 3472.
11. L. Conrads et al., *Sci. Adv.* **11** (2025) eadr6844.

Passive and active metasurfaces elaborated by nanoimprint and derived methods.

D. Grosso[1,2*], B. Kerzabi,[1] M. Abbarchi,[1] M. Putero,[3] J. Remondina,[3] B. Sciacca,[2] A. Gourdin,[1] M. Bouabdellaoui,[1] E. Daher, and L. Weber[1]

[1] Solnil SAS, 95 rue de la république, 13002, Marseille, France (badre.kerzabi@solnil.com)
[2] Center for Interdisciplinary for Nanoscience of Marseille, CINaM, UMR 7325, Campus de Luminy – Case 913, 13288 Marseille, France
[3] Institut of Materials Microelectronics and Nanosciences of Provence, IM2NP, Avenue escadrille Normandie Niemen 13 397, UMR 7334, Marseille, France

*corresponding author: david.grosso@univ-amu.fr

Conventional top-down fabrication methods for metasurfaces are often cumbersome and expensive (both CapEx and production costs). Here, we showcase the use of Soft-Nano-Imprint-Lithography (soft-NIL) as a scalable, cost-effective, and CMOS-compatible method, to elaborate metasurfaces (see Figure 1)[1] as final passive or active optical systems, or as etching masks to transfer the motifs into targeted material. Meta-atoms can be prepared with transversal dimension down to 20nm and vertical aspect up to 7, on diverse substrates such as glass, fused silica, sapphire, and silicon wafers. A precise adjustment of the chemical and nano-imprint conditions ensure faithful replicas over large areas: the method is scalable up to 200 mm wafers, limited only by the plate-to-plate machinery employed

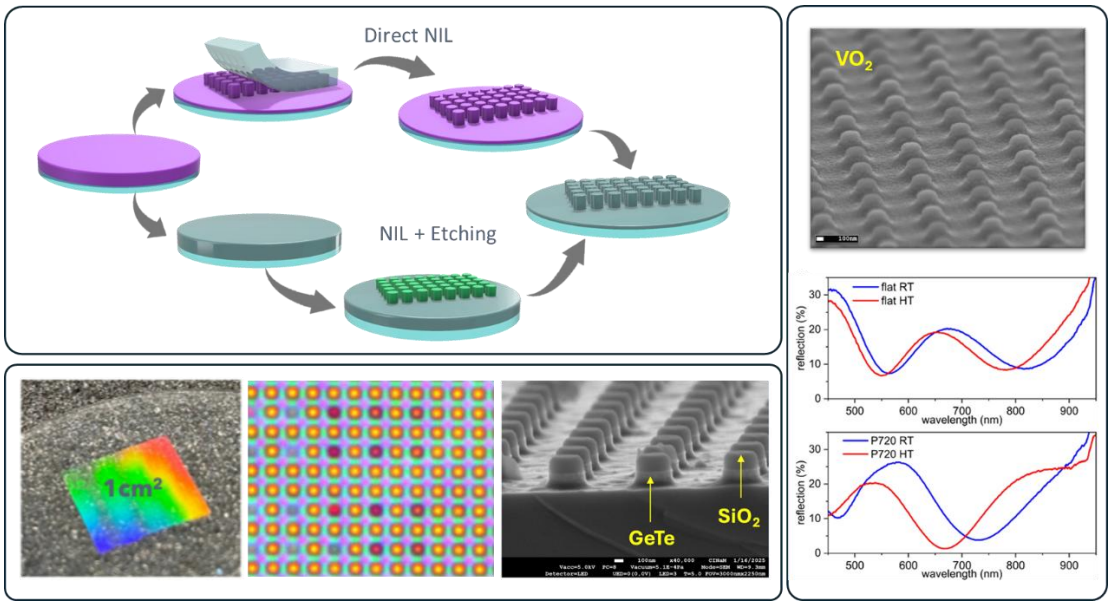

Figure 1. Schemes of the NIL method and examples of GeTe and VO_2 metasurfaces with optical switching capability.

The resulting materials offer controlled, on-demand, refractive indices ranging from 1.12 to 2.7@520 nm with zero extinction, and extremely low haze, for passive photonic devices (*e.g.* SiO_2, TiO_2). Various metasurface designs addressing diverse functionalities have already been demonstrated.[1-6] including controlled-wetting, optical and chemical sensors, diffraction gratings for light in-and-out-coupling, multispectral filters, light emitting surfaces, structural colour, anti-reflection coatings, and flow cells for DNA sequencing.

The next step was to apply this method to the fabrication of PCM materials since they are ideal candidates to couple with dielectrics metasurfaces with the aim to develop tunable photonic devices. In this presentation, we demonstrate that non-volatile GeTe and volatile VO_2

metasurfaces can be elaborated on cm^2 scales and that the switching can be performed all over the active surface or over a single meta-atom (laser) (see Figure 1). In situ spectroscopic measurements in reflection mode revealed a spectral shift over 100nm in the visible range between both PCM states, which is accompanied by an intensity variation of one order of magnitude at specific wavelengths with a standard, non-optimized, design.[7] This work highlights the potential of soft-NIL in advancing the field of optical metasurfaces and paves the way for their widespread applications in next-generation devices.

REFERENCES

1. Modaresialam, M.; Chehadi, Z.; Bottein, T.; Abbarchi, M.; Grosso, D. *Nanoimprint Lithography Processing of Inorganic-Based Materials*. **Chemistry of materials 2021**, *33*, 5464–5482. https://doi.org/https://doi.org/10.1021/acs.chemmater.1c00693.
2. Chehadi, Z.; Montanari, M.; Granchi, N.; Modaresialam, M.; Koudia, M.; Abel, M.; Putero, M.; Grosso, D.; Intonti, F.; Abbarchi, M. *Soft Nano-Imprint Lithography of Rare-Earth-Doped Light-Emitting Photonic Metasurface*. **Adv Opt Mater 2022**, 2201618. https://doi.org/10.1002/adom.202201618.
3. Modaresialam, M.; Bordelet, G.; Chehadi, Z.; Byrne, M. O.; Favre, L.; Putero, M.; Abbarchi, M.; Grosso, D. Enhanced *Refractive Index Sensitivity through Combining a Sol − Gel Adsorbate with a TiO_2 Nanoimprinted Metasurface for Gas Sensing*. **ACS Appl Mater Interfaces 2021**, *13* (44), 53021–53029. https://doi.org/10.1021/acsami.1c13248.
4. Bochet-Modaresialam, M.; Claude, J. B.; Grosso, D.; Abbarchi, M. *Methylated Silica Surfaces Having Tapered Nipple-Dimple Nanopillar Morphologies as Robust Broad-Angle and Broadband Antireflection Coatings*. **ACS Appl Nano Mater 2020**, *3* (6), 5231–5239. https://doi.org/10.1021/acsanm.0c00646.
5. Checcucci, S.; Bottein, T.; Gurioli, M.; Favre, L.; Grosso, D.; Abbarchi, M. *Multifunctional Metasurfaces Based on Direct Nanoimprint of Titania Sol–Gel Coatings*. **Adv Opt Mater 2019**, *7* (10), 1801406. https://doi.org/10.1002/adom.201801406.
6. Faustini, M.; Cattoni, A.; Peron, J.; Boissière, C.; Ebrard, P.; Malchère, A.; Steyer, P.; Grosso, D. *Dynamic Shaping of Femtoliter Dew Droplets*. **ACS Nano 2018**, *12* (4), 3243–3252. https://doi.org/10.1021/acsnano.7b07699.
7. Ramanda, Y., Remondina, J., Putero, M. Soppera, O., Abbarchi, M. Malgras, V. and Grosso D., *Tailoring the Visible Spectral Response of Phase-Change VO_2 Sol-Gel Coatings with Large Resistivity Contrast using Nanoimprinted Metasurfaces* - Submitted to **ACS Applied Materials & Interfaces**, 2025.

Neuromorphic photonic computing devices based on phase-change memory

[Invited]

Wen Zhou[1,*]

[1]Center for Alloy Innovation and Design (CAID), State Key Laboratory for Mechanical Behavior of Materials, Xi'an Jiaotong University, Xi'an 710049, China.

*corresponding author: wen.zhou@xjtu.edu.cn

Neuromorphic computing hardware aims to mimic biological neural networks and has emerged as a viable path in overcoming limitations of the von Neumann architecture. By eliminating the latency and energy losses associated with transferring data between the memory and central processing unit, these systems promise to improve on both speed and energy. Phase-change materials with a huge optical contrast upon phase transition is a promising candidate to develop photonic waveguide memory. Heterogeneous integration of silicon photonic chips with phase-change materials enables non-volatile photonic memory and in-memory photonic computing architectures, combining the advantages of high speed, high throughput, and low-energy consumption. Here, we report photonic implementation using on-chip, nonvolatile waveguide memories to deliver energy-efficient processing within the photonic memory. We developed waveguide biphasic synapses based on the growth-dominated $Ag_3In_4Sb_{76}Te_{17}$ and photonic memories based on Sb_2Te with a large switching contrast and a high-bit programming precision. For system-level application, a compact photonic-electronic dot-product engine based on the electrically reconfigurable photonic memory cells for in-memory computing was demonstrated with a high contrast-to-noise ratio (≥87.36) and a high computational accuracy (standard deviation $\sigma \leq 0.007$) for convolutional image processing and classification. This optoelectronic platform offers advantages of high scalability, in-situ training, and CMOS-compatible manufacturing.

REFERENCES

4. W. Zhou, *et al. Phys. Status Solidi RRL* (2022) 16, 2100487.
5. X. Wang, *et al. npj Comput. Mater.* (2023) 9, 136.
6. W. Zhou, *et al. Nat. Commun.* (2023) 14, 2887.

A Verification-Free Multi-Level Phase Change Memory for On-Chip Activation Compressed Training

[Invited]

Jia Zheng[1,2], Ruobing Wang[1], Xi Li[1], Sannian Song[1], Zhitang Song[1*], and Xilin Zhou[1*]
[1]State Key Laboratory of Materials for Integrated Circuits, Shanghai Institute of Microsystem and Information Technology, Chinese Academy of Sciences, Shanghai 200050 China.
[2]University of Chinese Academy of Sciences, Beijing 100049, China.
[*]Email: ztsong@mail.sim.ac.cn, xilinzhou@mail.sim.ac.cn

ABSTRACT

A 2-bit/cell multi-level phase change memory (MLPCM) using a bit-wise verification-free programming scheme (BVFPS) is demonstrated is this work. A sub-100 ns latency and 6×10^7 endurance cycles at up to 125 °C is achieved in the MLPCM device. The on-chip CIFAR-10 and CIFAR-100 inference with ActNN validate the stable device operation, showing substantial improvement in memory usage, write energy, and data latency with negligible accuracy loss. This work offers a scalable path toward efficient multilevel PCM technology.

Key words: multilevel programming, verification free, thermal stability, on-chip inference.

1. INTRODUCTION

The increasing demand for in-memory compute and high-density data storage presents a significant challenge for PCM, particularly in increasing bit density. While cross-point architecture demonstrates up to four stacked decks to increase storage density, the required complex patterning and etching process is a big challenge [1, 2]. An alternative strategy focuses on material engineering, leveraging phase change materials with multilevel storage capability that shows excellent compatibility with standard fabrication process.

Multilevel PCM (MLPCM) stores multiple bits in one memory cell by co-optimizing material properties and programming schemes. However, the exist approaches such as gradient-descent-based tuning [3], closed-loop adjustment [4], and iterative programming with verification [5] rely heavily on pulse iteration, which result in long write latency and is therefore unsuitable for on-chip training tasks. Furthermore, the resistance drift of PCM device puts additional challenge on the accuracy of multilevel bits over time.

In this study, we demonstrate a verification-free MLPCM with 2-bit/cell storage using GeSbTeIn phase change material, in which a sub-100 ns write latency and switching endurance beyond 6×10^7 cycles at up to 125 °C is achieved. The on-chip integration with ResNet-18 and ActNN yields classification accuracies of 93.17% and 70.32% on CIFAR-10 and CIFAR-100, respectively, using a 2-bit activation. The benchmark comparison reveals significant reductions in memory usage, energy consumption, and write latency, suggesting the scheme a viable solution for energy-efficient and scalable multilevel PCM.

2. EXPERIMENTAL

The mushroom type PCM device is fabricated based on 40 nm CMOS process using GeSbTeIn phase change material. Each MLPCM cell is addressed through a dedicated selection path and programmed via nanosecond pulses that applied to a TiN heater. The memory cell is integrated with a configurable write circuit. The switching current is highly dependent on the composition of phase change material, which requires design-technology co-optimization to receive reliable intermediate resistance states in MLPCM.

3. RESULTS & DISCUSSION

The multilevel resistance states of PCM with BVFPS is investigated at the chip level using 8 Kb PCM cells. The cumulative distribution function (CDF) of cell resistance demonstrates a resistance window with a minimum read margin of 15 μA in the four resistance states, as shown in Fig. 1(a). Figure 1(b) shows the CDF of the multilevel resistance measured 5 days after the 10^7 switching cycles with BVFPS, in which the multilevel resistance states remain well-distinguished. The validity of the 2-bit/cell data storage were examined for over 60 hours at 85 ℃ and 1 hour at 125 ℃, respectively, as shown in Fig. 1(c) and Fig. 1(d).

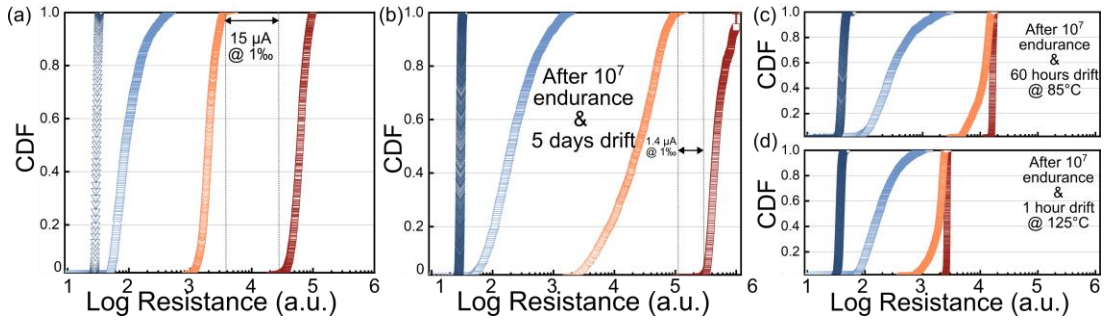

Figure 1 CDFs of the four resistance states of MLPCM cells: (a) fresh device, (b) five days after 10^7 switching cycles, (c) after 10^7 switching cycles followed by 60 hours at 85 °C, and (d) after 10^7 switching cycles followed by 1 hour at 125 °C.

The MLPCM-based ActNN achieves an accuracy equivalent to 32-bit software on CIFAR-10 and CIFAR-100 right after the on-chip activation compressed training. The accuracy on both dataset decreases substantially when considering the resistance drift effect of memory device. The proposed model maintains 1% accuracy loss at a time scale of 10^5, 4×10^3, and 10 s at 25, 85, and 125 ℃, respectively, on the CIFAR-10 dataset, as shown in Fig. 2(a). While for the CIFAR-100 dataset in Fig. 2(b), less than 2% accuracy loss is achieved at 25, 85, and 125 ℃, respectively.

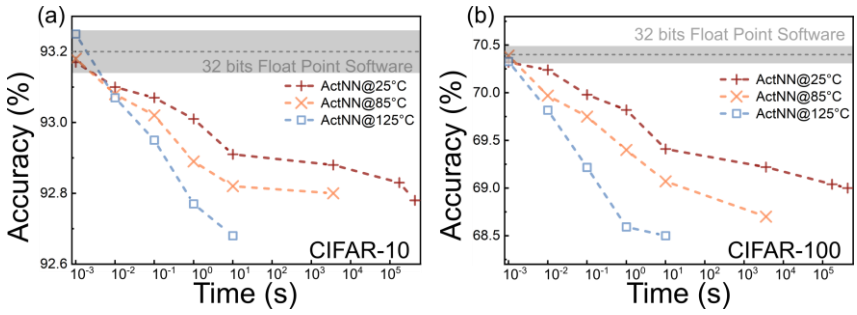

Figure 2 The effect of time and temperature on the inference accuracy of ActNN with (a) CIFAR-10 and (b) CIFAR-100 datasets based on the performance of MLPCM.

4. CONCLUSIONS

This work demonstrates a verification-free 2-bit/cell MLPCM with sub-100 ns write latency and high thermal stability, which provides a scalable and energy-efficient solution for in-memory compute using phase change memory.

REFERENCES

1. A. Fazio, IEDM Tech. Dig., 2020, pp.24.1.1-24.1.4.
2. J. Zheng et al., Nature Communications, 2025, accepted.
3. J. Büchel et al., IEDM Tech. Dig., 2022, pp.33.1.1-33.1.4.
4. P. Narayanan et al., IEEE Trans. Electron Devices, 2021, pp. 6629-6636.
5. L.H Yan et al., IEDM Tech. Dig., 2021, pp.28.2.1-28.2.4.

Deep-Cryogenic Phase Change Memory

[Invited]

S. Yoon[1,†], N. Hur[1], B. Park[1], D. Lim[2,†], J. Suh[1,3,★] and H. Jeong[1,3,★]

[1]Department of Materials Science and Engineering, UNIST, Republic of Korea
[2]Division of AI Semiconductor, Yonsei University, Republic of Korea
[3]Graduate School of Semiconductor Materials and Devices Engineering, UNIST, Republic of Korea
Correspondence and requests should be addressed to H.Jeong. (jeonghs1@unist.ac.kr) or S.Y. (shyoon49@unist.ac.kr)

ABSTRACT

Cryogenic electronic devices are gaining increasing attention for applications in quantum computing and space exploration, driving active research in this field. Phase-change memory (PCM), a promising non-volatile memory with reversibly tunable resistivity, holds significant potential for cryogenic data storage. In this work, we assess the cryogenic compatibility of the prototypical chalcogenide $Ge_2Sb_2Te_5$ by demonstrating reliable performance down to 4 K. Time-resolved electrical measurements reveal the inherent trade-offs between speed and power, governed by the unique distribution of gap states. By utilizing static ambient temperature and dynamic electric fields as key parameters, we propose a strategy for energy-efficient cryogenic write operations, enabling PCM functionality based on the Ovonic threshold switching mechanism.

Key words: phase change memory, cryogenic, hopping, switching energy

1. INTRODUCTION

In the realm of cryogenic memory devices, paramount considerations include speed, power consumption, and scalability, each vital for practical implementation under 4 K circumstance.[1, 2] Remarkably, the latest advances in chalcogenide PCM have achieved power consumption rates as low as a few pJ/bit by favor of material design[3], proposing research on cryogenic chalcogenide PCM can be rationalized as ongoing fundamental achievement in the PCM technology. The quest for cryogenic solutions involves exploring the power efficiency of chalcogenide PCM, underscoring a pioneering effort to comprehensively analyze the speed-power characteristics of chalcogenide PCM for operation below 4 K. The unique electronic excitation behavior of $Ge_2Sb_2Te_5$, rooted in its distinct gap states, suggests the insights into the temperature, energy, and temporal aspects to a more comprehensive understanding of $Ge_2Sb_2Te_5$'s fundamentals and performance in cryogenic environments.

2. EXPERIMENTAL

$Ge_2Sb_2Te_5$-based mushroom-type PCM devices were fabricated on a silicon wafer with a 300-nm thermal oxide layer. Via holes were patterned using standard electron-beam lithography techniques. Electrical characterization was performed using a switching box connected to a Keithley 4200A-SCS parameter analyzer. All measurements were conducted in a vacuum chamber (<100 mTorr) over a temperature range from 300 K to 4.0 K, utilizing a Montana Instruments S50 cryogenic system.

3. RESULTS & DISCUSSION

PCM has categorized physics interacting across electrical, thermal, and structural subsystems[4] as illustrated in **figure 1a**. The overall system is directly influenced by the ambient temperature (T_{amb}) and is composed of tightly coupled interactions across a broad range of timescales (t). Given that most electronic devices are voltage-driven, time-dependent voltage input (V/t) can be an effective probe for investigating the dynamic responses in the cryocooled phase change memory system. The applied voltage driving the electrical subsystem delivers energy to the thermal subsystem in the form of power (IV), resulting in a temperature rise due to Joule heating (T_{jh}). In the structural system, we can observe phase transitions of diverse crystallographic states and then their structurally relaxed state (Σ), which is promoted by device temperature and electrical field. Therefore, we introduced T_{amb} and V/t as additional controllable parameters to understand the role of each subsystem. To clearly see the effect of ambient temperature on the switching process of the PCM, we investigated the switching behaviour of the device

by controlling the ambient temperature from 300 K to 4 K, as described in **figure 1b-1d**. Threshold voltage (V_{th}), which indicates the transition from amorphous to crystalline, notably increases as Tamb decreases at a rate of 12 mV/K, indicating a change in the threshold switching condition. Therefore, we introduced the subthreshold slope (STS), extracted by V_{th}/t_{delay}, which allows the same electric field to be applied at the same time under different T_{amb}. By controlling the STS with the same step resolution, we can trace the relationship between the ambient temperature (Tamb) and the switching time (defined as tdelay = trise), as shown in Figure 1e. It was observed that as Tamb decreases, the tendency of thermally induced Vth lowering weakens and eventually becomes uncorrelated with STS. This indicates that higher STS reduces the dependency on Tamb and enables an ideal minimum switching condition without excessive energy consumption. We interpret this STS-induced convergence of Vth towards the threshold energy (Eth) as representing the minimum thermal energy required within the device. The transition energy as a function of STS in PCM, shown in Figure 1f, reveals that as STS increases, the phase transition becomes more field-dominant, with a smaller ΔQloss(T) from cryogenic temperatures (Tcryo) to room temperature (Troom), and Eth decreases asymptotically to its minimum value (Eth,min ≈ 33 pJ). In contrast, in the region where STS starts to decrease gradually (around 13.3), thermal excitation becomes an important factor that distinguishes the Tamb-dependent dynamics of PCM. At Tcryo, Qloss(t) increases much more sharply as STS decreases compared to Qloss(t) at Troom, which is consistent with the lack of thermal excitation at cryogenic temperatures. We conclude that a fully field-driven transition corresponds to the minimum Eth achievable through the highest possible STS across a wide Tamb range from 300 K to 4 K. This strategy is expected to be readily applicable to most other PCM devices.

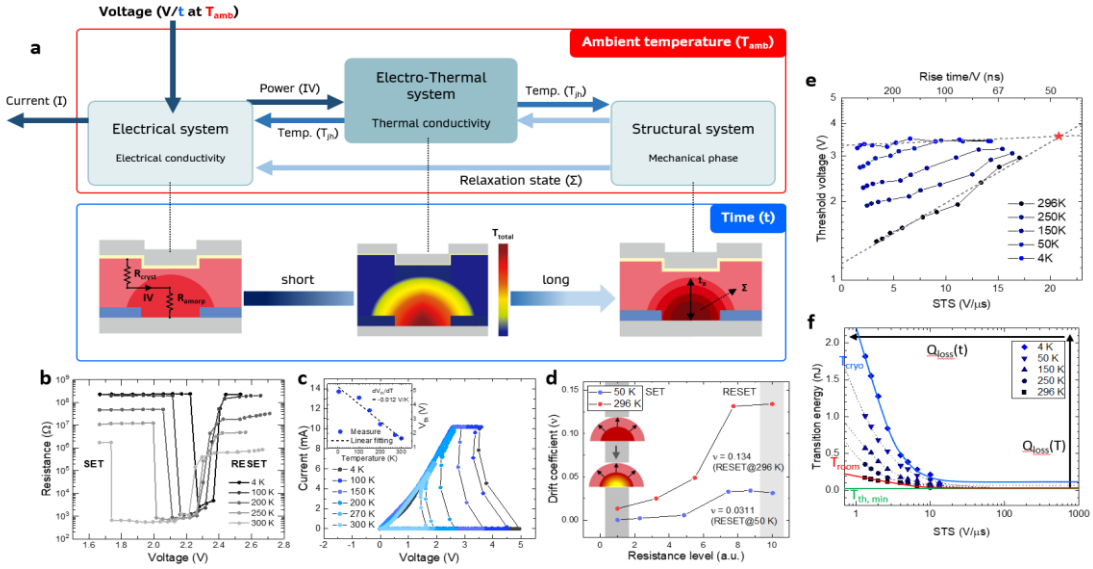

Figure 5. Subsystems in GST-based PCM and T_{amb}-dependent typical characterization

4. CONCLUSIONS

This study provides evidence of the reliable switching functionality of PCM, elucidating its crucial switching characteristics at cryogenic temperatures down to 4K. By flexibly controlling voltage, time, and temperature, we present an analysis of the threshold switching mechanism, a topic of debate for decades, and describe the effect of each parameter on this process. Moreover, PCM represents the potential to enhance reliability and expand applications as an option worth exploring for cryogenic memory components that could be operated in the 4K range.

REFERENCES

1. J. Hur, D. Kang, D. Moon, J. Yu, Y. Choi, and S. Yu, Adv. Electron. Mater. 9, 6 (2023)
2. S. Alam, M.S. Hossain, S.R. Srinivasa, and A. Aziz, Nat. Electron. 6, 3, 185–198 (2023)
3. S.-O. Park, S. Hong, S.-J. Sung, D. Kim, S. Seo, H. Jeong, T. Park, W.J. Cho, J. Kim, and S. Choi, Nature, 628, 8007, 293–298 (2024)
4. M.L. Gallo, and A. Sebastian, J. Phys. D: Appl. Phys. 53, 21, 213002 (2020)

True random number generator (TRNG) based on Ovonic Threshold Switch (OTS) and its applications for Restricted Boltzmann Machine (RBM)

JinGyeong Hwang[1], Seongil Im[2], Hyunsu Ju[2], and Suyoun Lee[1]*
[1]Center for Semiconductor Technology, Korea Institute of Science and Technology, Seoul 02792, Korea
[2]Center for Quantum Technology, Korea Institute of Science and Technology, Seoul 02792, Korea
*corresponding author: slee_eels@kist.re.kr

ABSTRACT

To improve energy efficiency in machine learning, a stochastic neuron device using an ovonic threshold switch (OTS) and resistor is proposed. Governed by the Boltzmann distribution, it functions as a true random number generator and supports RBM and DBN applications. Simulation results confirm its effectiveness in digit recognition and reconstruction tasks.

Key words: Ovonic threshold switch (OTS), true random number generator (TRNG), restricted Boltzmann machine (RBM).

1. INTRODUCTION

Recent advancements in artificial intelligence (AI) systems have been largely driven by progress in machine learning (ML) techniques, such as deep neural networks (DNNs) and spiking neural networks (SNNs). However, these software and CMOS-based approaches face challenges in energy efficiency and scalability, prompting significant efforts to develop novel energy-efficient ML methodologies. Among these, the restricted Boltzmann machine (RBM) has gained increasing attention as a generative stochastic artificial neural network (ANN) due to its exceptional energy efficiency, which is attributed to its simple structure and effective learning process. The RBM operates as a generative stochastic ANN that models a probability distribution over input data. Its nodes function probabilistically, with each node having a certain likelihood of adopting a value of 1, reflecting the network's inherent stochasticity. This configuration facilitates efficient data representation and feature extraction through unsupervised learning. By leveraging a local learning algorithm known as Contrastive Divergence [2], the RBM eliminates the energy-intensive backpropagation process typically required in conventional ANNs. Furthermore, the RBM serves as a foundational unit for more advanced models, such as deep belief networks (DBNs) [3].

In this study, we introduce a simple stochastic neuron device designed for ease of fabrication, scalability, and tunable switching probability—characteristics that make it highly suitable for RBM hardware implementation. The proposed OTS-TRNG device comprises an Ovonic threshold switch (OTS) and a resistor (R_{load}) connected in series (1OTS+1R), as depicted in Fig. 1(a). Relying on the randomness of the switching delay time, it plays as a TRNG device with the probability distribution function (PDF) modulated by electrical means.

2. EXPERIMENTAL

To demonstrate the randomness of the OTS-TRNG, we have performed the randomness test using the NIST 800.22 test suite. In addition, we have examined the change in the probability distribution function (PDF) of the OTS-TRNG by systematically varying the pulse width and the pulse period. Furthermore, we have applied our OTS-TRNG device to RBM and DBN to conduct a few machine-learning tasks (image generation and image classification).

3. RESULTS & DISCUSSION

Figure 1(a) shows a basic RBM structure composed of OTS-TRNG devices, which is composed of 1OTS. Figure 1(b) shows the input bias pulse train and the concomitant output waveforms of the OTS-TRNG device, demonstrating an irregular pattern. Figure 1(c) shows the expanded figure of the region in the red box in Figure 1(b). It also shows a bit stream obtained by setting a threshold (V_{ref}, green dashed line). Figure 1(d) shows a structure of the deep-belief network (DBN) composed of OTS-TRNG devices. Figure 1(e) shows the process of image recovery by using the RBM structure shown in Figure 1(a).

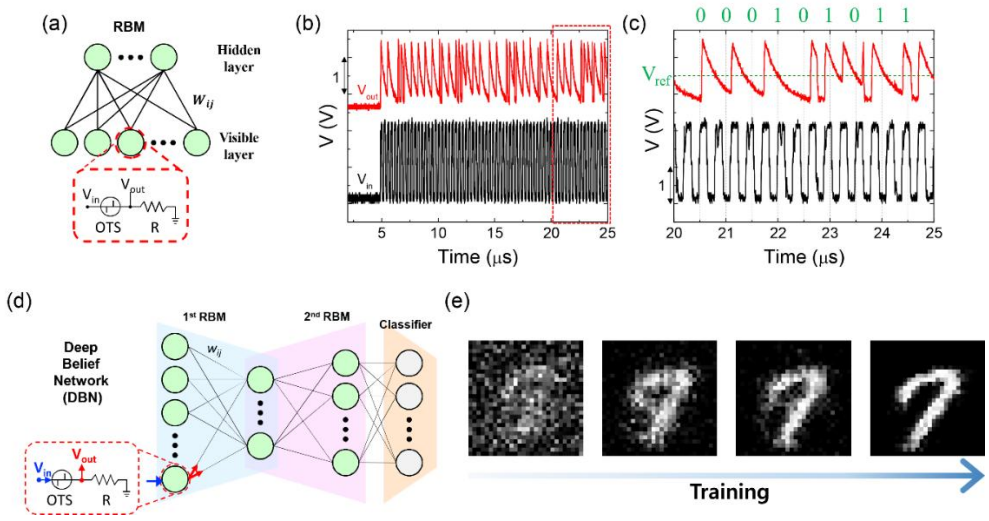

Figure 1. Ovonic threshold switch (OTS) – based random number generator and its application in Deep Belief Network. (a) Concept of the restricted Boltzmann machine (RBM) and the structure of a stochastic artificial neuron based on the OTS. (b) The output waveform of the OTS neuron (red) responding to the periodic input pulse (black). (c) Expanded waveforms in the red-dotted box in (b) and the readout scheme for generating random bits. (d) Structure of the Deep Belief Network (DBN) based on the OTS neuron. (e) Reconstruction process of images from the 1st RBM unit of DBN.

4. CONCLUSIONS

The device's simple structure, combined with its high scalability and controllable switching probability, positions it as a strong candidate for hardware-based neural networks. The characteristics of the device, notably the controllable Boltzmann distribution, were rigorously analyzed, revealing tunability based on the amplitude, width, and interval of the input pulses. A simulated DBN, built upon the 1OTS+1R device, showed promising results when trained on the MNIST dataset, achieving classification accuracy consistently above 95%. These findings highlight the potential of the 1OTS+1R device for future energy-efficient hardware implementations of neural networks

REFERENCES

1. D. H. Ackley, G. E. Hinton and T. J. Sejnowski, Cognitive Science **9** (1), 147-169 (1985).

2. Y. Bengio and O. Delalleau, Neural computation **21** (6), 1601-1621 (2009).

G. E. Hinton, Scholarpedia **4** (5), 5947 (2009).

High-Selectivity Ge-Te-Based Ovonic Threshold Switching Material for Selectors

Y. Matsushita[1]*, Y. Shuang[2], K. Karakida[1], F. Sato[1], K. Choju[1] and Y. Sutou[2]
[1]Nippon Electric Glass Co., Ltd., Japan
[2] Tohoku University, Japan
*Corresponding author: ymatsushita@neg.co.jp

ABSTRACT

Threshold-switching devices are key to emerging memory with 3D crossbar array structure. We demonstrated the threshold-switching behavior of an Ag-Ga-Ge-Te (AGGT) amorphous film. Our findings revealed that the co-addition of Ag and Ga to the Ge-Te system modified the conduction mechanism, enhancing both the ON/OFF current ratio and endurance.

Key words: ovonic threshold switching, selector, chalcogenide, memory.

1. INTRODUCTION

Chalcogenide-based amorphous thin films exhibiting ovonic threshold switching (OTS) are anticipated as promising selector materials for next-generation semiconductor memory devices [1]. For selectors, OTS materials with high ON/OFF current ratios and amorphous stability are essential. Additionally, it is desirable to eliminate the use of highly toxic elements such as arsenic. We demonstrate that an Ag-Ga-Ge-Te (AGGT) amorphous film exhibits desirable OTS properties due to its high ionicity and amorphous stability, offering a new paradigm for OTS material design.

2. EXPERIMENTAL

To investigate compositional effects on resistive switching, we fabricated test devices using AGGT, Ge-Te (GT), Ag-Ge-Te (AGT), and Ga-Ge-Te (GGT) amorphous films as active layers. A schematic representation of the test device is shown in Fig. 1. In this study, the transient current was measured during a 1 μs voltage pulse.

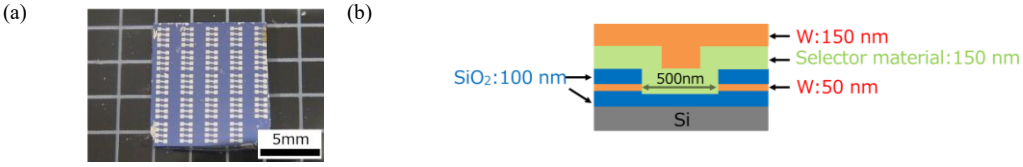

Fig. 1 *Selector device samples for evaluation. (a) Image of the selector device. (b) Cross-section of one cell, W corresponds to the electrode, and SiO_2 corresponds to the insulating layer.*

3. RESULTS & DISCUSSION

As shown in Fig. 2(a), the current in AGGT increased sharply at an applied voltage of 1.5 V, indicating threshold-switching behavior with a threshold voltage (V_{th}) of 1.5 V. The ON current reached approximately 3.7×10^{-3} A. Reducing the voltage to 0 V returned the device to its high-resistance state. The OFF current, measured using a post-pulse voltage of 0.6 V (~ V_{th} / 3), was 1.7×10^{-9} A, resulting in an ON/OFF current ratio of ~ 2.2×10^{6}. Endurance was tested using a pulse voltage of V_{th} to switch to the ON state and 0.6 V pulses to read the OFF current, and it was defined as the number of switching cycles after which the ON/OFF current ratio degraded by more than an order of magnitude. In the AGGT, the ON/OFF current ratio was maintained for up to 10^5 switching cycles. A summary of the initial ON /OFF current ratios and endurances for each composition is shown in Fig. 2(b).

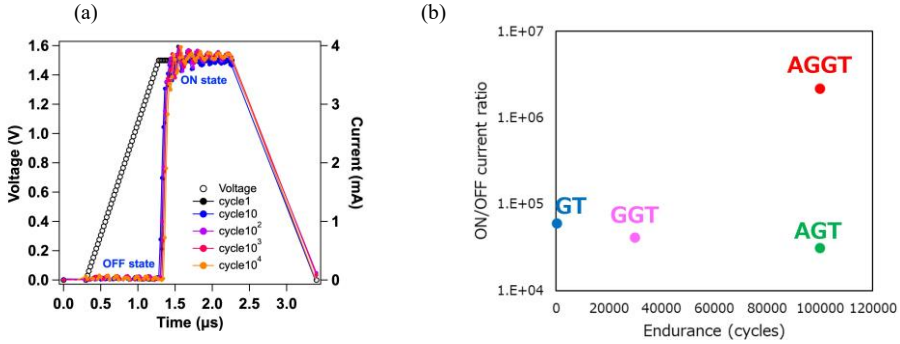

Fig. 2 *(a) Dynamic transient current measurement in the AGGT device. (b) Summary of the ON/OFF current ratios and endurance. The OFF current was 1.5 × 10^{-7} A, 3.7 × 10^{-7} A, and 8.6 × 10^{-8} A for the GT, AGT, and GGT devices, respectively.*

Among the tested devices, AGGT exhibited the highest ON/OFF current ratio and longest endurance. The reduced leakage current in the OFF state was identified as the primary reason for the superior ON/OFF current ratio in AGGT. X-ray photoelectron spectroscopy results suggested that the co-addition of Ag and Ga increased the system's ionicity, significantly lowering carrier mobility of amorphous Ge-Te and thus reducing leakage current in the OFF state. Additionally, the evaluation of the activation energy for crystallization indicated that incorporating Ag or Ga into Ge-Te enhanced the thermal stability of the amorphous phase, thereby improving the endurance of the OTS effect.

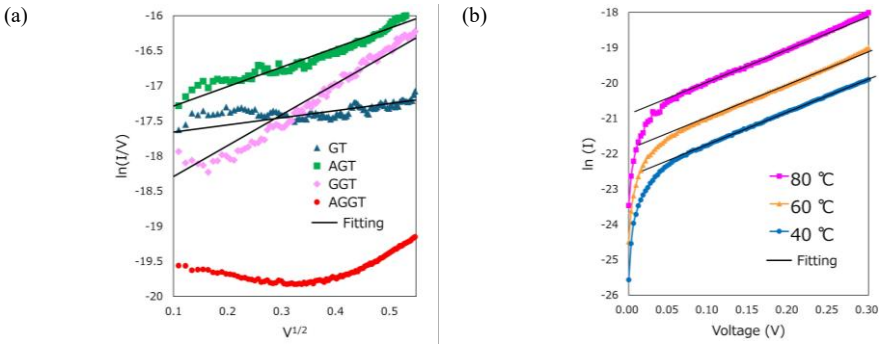

Fig. 3 (a) The ln(I/V) as a function of $V^{1/2}$ for verifying the Poole–Frenkel conduction. (b) The ln(I) as a function of V for verifying the Schottky conduction in the AGGT device.

Fig. 3(a) presents ln(I/V) plots as a function of $V^{1/2}$ to assess whether the conduction follows the Poole–Frenkel mechanism [2]. For the GT, AGT, and GGT devices, a linear relationship was observed within the $V^{1/2}$ range of 0.2 to 0.6, indicating good agreement with this model. In contrast, the AGGT device deviated significantly from linearity, suggesting a different conduction mechanism from those of the other three devices. To investigate further, ln(I) was plotted against V for the AGGT device to verify the Schottky conduction model [3]. As shown in Fig. 3(b), a clear linear relationship was observed, indicating a strong agreement with Schottky conduction.

4. CONCLUSIONS

We demonstrated that co-addition of Ag and Ga to a binary Ge-Te film significantly enhances the ON/OFF current ratio and threshold-switching endurance. Furthermore, this co-addition causes the conduction mechanism to deviate significantly from the Poole–Frenkel model. These findings suggest that engineering the ionicity and amorphous stability of a material to achieve interface-dominated conduction is a promising strategy for developing advanced OTS selectors.

REFERENCES

1. M. Anbarasu et al., *Appl. Phys. Lett.* **100** (2012) 143505.
2. M. Nardone et al., *J. Appl. Phys.* **112** (2012) 071101.
3. I. Jyothi et al., *Materials Transactions* **54**(2013) 1655.

Innovations in OTS Selectors and Memory Materials: Theoretical Insights and Experimental Validations

[Invited]

D. Garbin*, T. Ravsher, W. Devulder, S. Clima, R. Degraeve, and A. Belmonte

imec, Kapeldreef 75, 3001 Leuven, Belgium
*corresponding author: daniele.garbin@imec.be

ABSTRACT

Recent progress in ovonic threshold switching (OTS) materials has underscored the importance of identifying sustainable alternatives to toxic-element-based compounds, such as those containing arsenic. A systematic computational screening framework, based on ab initio calculations and multi-parameter filtering, recently identified several ternary alloys as promising selector candidates [1-3]. Among these, material systems based on SnS_2 and GeS_2 have been selected for experimental validation due to their favorable predicted electronic structure, thermodynamic stability, and OTS-specific performance indicators.
This work reports on the electrical characterization of devices based on Sn–S and Ge–S ternary alloys, integrated in nanoscale mushroom-type devices on 300 mm wafers. SnS_2-based alloys, doped with N and Si, exhibit functional OTS behavior, with tunable threshold voltage and amorphous phase stability. However, limitations in OFF-state leakage indicate that further improvement is needed for compatibility with high-density memory arrays [4].
To address this, a family of GeS_2-based materials with Si incorporation was developed and assessed. The optimized compositions achieve higher thermal stability (T_x > 500 °C) and significantly lower I_{OFF}, approaching the level of reference state-of-art materials such as SiGeAsSe [5], while avoiding the use of toxic precursors.
A benchmark comparison against literature-reported OTS materials [5-7] highlights the progress of these novel chalcogenide systems in terms of key metrics such as OFF-state leakage and threshold voltage. These results provide a proof-of-concept for the predictive design of sustainable OTS materials, offering a validated pathway for future integration into selector and selector-only memory applications.

Key words: OTS, ovonic threshold switch, selector, SOM, selector-only memory

REFERENCES

1. D. Matsubayashi et al., “OTS physics-based screening for environment friendly selector materials,” in IEDM Tech. Dig., San Francisco, CA, USA, Dec. 2022, pp. 1–4, doi: 10.1109/IEDM45625.2022.10019445.
2. S. Clima et al., “In silico screening for As/Se-free ovonic threshold switching materials,” npj Comput. Mater., vol. 9, no. 1, p. 96, Jun. 2023, doi: 10.1038/s41524-023-01043-2.
3. D. Matsubayashi et al., Computational screening towards eco-friendly ovonic threshold switching materials, E\PCOS 2023.
4. D. Garbin et al., "Electrical Demonstration of Sn–S-Based OTS Materials From Theoretical Design for Sustainable Innovation," IEEE Transactions on Electron Devices, vol. 71, no. 9, pp. 5339-5344, Sept. 2024, doi: 10.1109/TED.2024.3423772.
5. H. Y. Cheng et al., “Si incorporation into AsSeGe chalcogenides for high thermal stability, high endurance and extremely low Vth drift 3D stackable cross-point memory,” in Proc. IEEE Symp. VLSI Technol., Jun. 2020, pp. 1–2, doi: 10.1109/VLSITechnology18217.2020.9265039.
6. S. Jia et al., “Ultrahigh drive current and large selectivity in GeS selector,” Nature Commun., vol. 11, no. 1, p. 4636, Sep. 2020, doi: 10.1038/s41467-020-18382-z.
7. S. Jia et al., “Scalability of sulfur-based ovonic threshold selectors for 3D stackable memory applications,” Phys. status solidi (RRL), vol. 15, no. 6, Jun. 2021, Art. no. 2100084, doi:10.1002/pssr.202100084

Volatile to Non-Volatile Switching Transition in Chalcogenides

[Invited]

Min Zhu[1, 2]

[1] School of Integrated Circuits, Shanghai Jiao Tong University, Shanghai 200240, China.
[2] Shanghai Institute of Micro-System and Information Technology, 200050 Shanghai, China
*Corresponding author: mzhu2@sjtu.edu.cn

ABSTRACT

Over the past 60 years, three distinct electrical switching behaviors have been discovered in chalcogenides: ovonic threshold switch (OTS), ovonic memory switch (OMS), and phase-change switch (PCS) [1]. The first two have been successfully utilized in commercialized 3D Xpoint chips, serving as selector and memory cells, respectively. However, the relationships among these three behaviors remain unclear. Here, we demonstrate that the Ge-Te binary system exhibits these three transition mechanisms (Figure 1). Specifically, the switching behavior transforms from PCS-like to OTS-like within the composition range from $GeTe_8$ to $GeTe_6$, while the shift from volatile (OTS) to non-volatile switching behavior (OMS) occurs between the compositions $GeTe_2$ and GeTe. The PCS-to-OTS transition is primarily driven by enhancements in glass-forming ability, with the Turnbull parameter increasing from 0.58 to 0.6, and the crystallization temperature exceeding 145 °C (Figure 1), while the shift from OTS to OMS behavior is largely due to the significantly accelerated crystallization speed, from microseconds to nanoseconds [2].

Key words: Ovonic Threshold Switch, Phase Change Memory, Phase Change Switch, Ge-Te

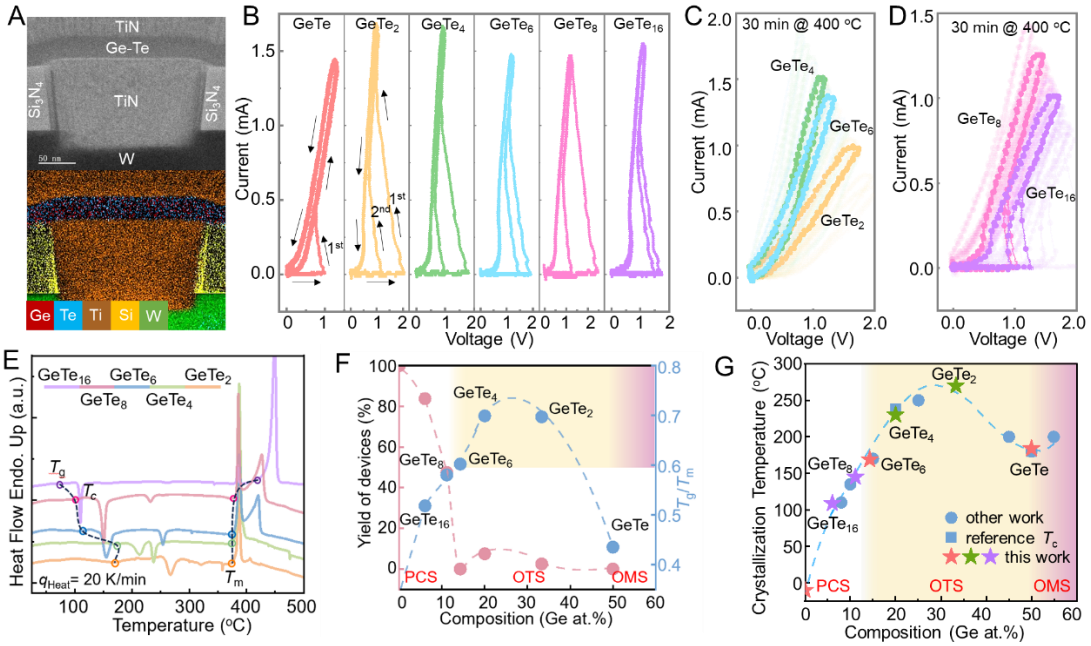

Figure 1. The evolutionary history of three threshold switching behaviors in Ge-Te devices. A) Cross sectional TEM image of a Ge-Te cell with a ≈200 nm TiN plug and corresponding stacked EDS mapping of the device. B) I–V curves of Ge-Te devices. C) Electrical performance of $GeTe_2$, $GeTe_4$, and $GeTe_6$ devices annealed at 400 °C for 30 min. D) Volatile I–V behaviors of $GeTe_8$ and $GeTe_{16}$ devices annealed at 400 °C. E) Differential scanning calorimeter curves of Ge-Te samples. F) Comparison of device yield after annealing and T_g/T_m values of Ge-Te alloys. G) Crystallization temperature versus Ge concentration in Ge-Te alloys.

REFERENCES

1. J. Shen, S. Jia, N. Shi, Q. Ge, T. Gotoh, S. Lv, Q. Liu, R. Dronskowski, S. R. Elliott, Z. Song*, M. Zhu*, *Science*, 2021, 374, 1390.
2. Y.Sun, B. Li, T. Yang, Q. Yang, H. Yu, T. Gotoh, C. Shi, J. Shen, P. Zhou, S. R. Elliott, H. Li*, Z. Song*, and M. Zhu*, *Advanced Functional Materials*, 2025, 2423940.

Exploring Sub-Nanosecond Programming of Selector-Only Memory

Rivka-Galya Nir-Harwood[1], Taras Ravsher[2], Daniele Garbin[2], Attilio Belmonte[2], Eilam Yalon[1,*], and Gouri Sankar Kar[2]

[1]Electrical and Computer Engineering, Technion - Israel Institute of Technology, Haifa, 32000, Israel

[2]IMEC, Kapeldreef 75, 3001 Leuven, Belgium

*Contact: eilamy@technion.ac.il

ABSTRACT

Selector-only memory (SOM) based on ovonic threshold switches (OTS) holds strong potential for high-density, high-performance self-selecting memory applications. In this work, we investigate the ultimate programming speed limits of SiGeAsSe-based SOM devices. Using a high-speed measurement setup, we demonstrate programming with write pulses as short as 300 ps, while maintaining a distinct memory window.

Key words: Ovonic threshold switches, Selector-only memory, sub-nanosecond programming

1. INTRODUCTION

Chalcogenide-based ovonic threshold switches (OTS) exhibit abrupt, volatile switching with low leakage and high endurance—features that have made them indispensable as selectors in high-density phase change memory [1]. Recent developments have shown that OTS devices can also retain memory-like behavior without an additional element, giving rise to the selector-only memory (SOM) concept [2], [3]. By removing the conventional memory layer, SOM offers a simplified and highly scalable approach to nonvolatile storage. However, its dynamic switching limits remain underexplored. To date, the fastest reported SOM programming speed is ~10 ns [4]. In this work, we investigate the intrinsic speed limits of SiGeAsSe-based SOM devices, demonstrating sub-nanosecond operation.

2. EXPERIMENTAL

We employ a high-speed measurement setup to characterize 10-nm-thick pillar-type SiGeAsSe-based OTS devices, with a 70-nm cell dimension (CD) (**Figure 1a**). The write operation is performed using a fast pulse generator (PG) with a 70 ps rise/fall time and pulse widths (PW) down to 300 ps. The read operation is executed with an arbitrary waveform generator (WGFMU), applying a triangular voltage pulse of 5 V with a 10 ns rise/fall time. The OTS device and a high-speed oscilloscope are connected in-line, and a switching matrix (SM) is used to alternate between write and read operations, as illustrated in **Figure 1b**. To ensure signal integrity, all connections utilize ground-signal (GS) transmission lines with a characteristic impedance of Z_0=50 Ω. This configuration minimizes pulse broadening, signal reflections, and ringing caused by parasitic capacitances. Both the output impedance of the waveform generator and the input impedance of the oscilloscope are matched to Z_0=50 Ω, allowing for the generation and accurate measurement of sub-nanosecond pulses. The applied voltage of the WGFMU during the read pulse is monitored and captured on a separate oscilloscope channel. The current through the OTS during both write and read operations is extracted as $I(t)=\frac{V_{scope}(t)}{50\ \Omega}$.

3. RESULTS & DISCUSSION

We applied approximately 30 programming pulses for each of the four polarity combinations ($\pm V_{pulse}, \pm V_{read}$). For a programming pulse of 7.5 V and a pulse width of 300 ps (**Figure 1a**), the current–voltage (I–V) characteristics during the read operation are shown in **Figure 2b**. As expected, the threshold voltage is slightly higher when the read voltage polarity is opposite to that of the programming pulse, compared to when they share the same polarity. This asymmetry enables a measurable memory window (MW), as illustrated in **Figure 2c**, of 50 mV and 20 mV for positive

and negative reads, respectively. Although this MW is relatively small, its clear presence serves as a proof of concept that OTS-based SOM devices can be programmed within the sub-nanosecond regime. Increasing the amplitude of the programming pulse is likely to further enhance the MW. A detailed understanding of the time- and voltage-dependence of the MW will provide deeper insight into the underlying switching physics of SOM devices.

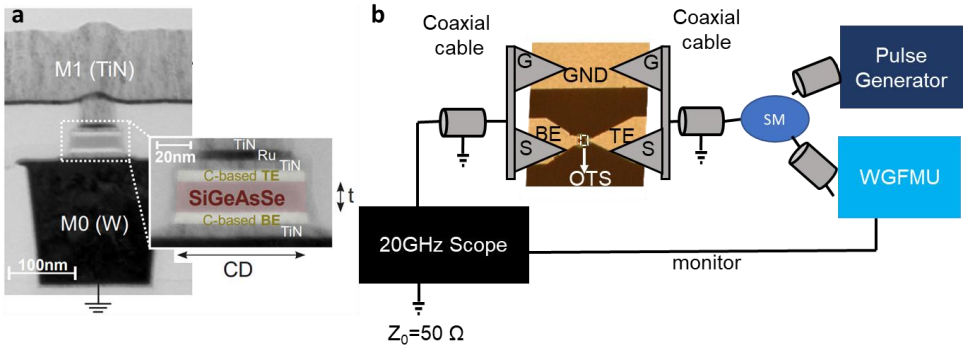

Fig. 1: Device structure & high-speed measurement setup. (a) Cross-section TEM image of the investigated SiGeAsSe-based SOM device. **(b)** Schematic of the high-speed measurement setup. The pulse generator (PG) or arbitrary waveform generator (WGFMU) is connected via coaxial cables to RF probes. The signal (S) is routed to the top electrode (TE) pad of the OTS device, while the ground (G) connects to a local ground plane. A high-speed oscilloscope is connected to the bottom electrode (BE) using a second RF probe. A switching matrix (SM) alternates between write (PG) and read (WGFMU) operations. During read, the applied voltage is also monitored on a separate oscilloscope channel.

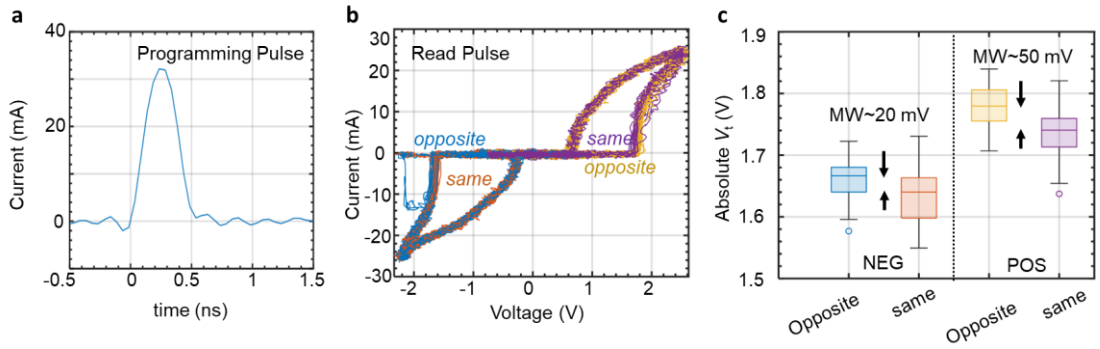

Fig. 2: Electrical characterization of sub-nanosecond programming. (a) Oscilloscope capture of a typical programming pulse with a 300 ps pulse width, 70 ps rise/fall time, and 7.5 V amplitude. **(b)** Current-voltage *(I-V)* characteristics measured after ~120 programming pulses. **(c)** Extracted threshold voltages for positive and negative read operations. Results confirm that the SOM device exhibits a measurable memory window under sub-nanosecond programming conditions.

4. CONCLUSIONS

We have demonstrated distinct sub-ns programming of selector-only memory (SOM) devices based on SiGeAsSe ovonic threshold switches (OTS). Using write pulses as short as 300 ps, we achieved clear memory windows of 50 mV and 20 mV for positive and negative reads, respectively. These results confirm that OTS-based SOM can operate well below the previously reported 10 ns programming limit, establishing a new benchmark for switching speed. This work underscores the promise of SOM as a simplified, high-speed, and scalable memory concept for future high-density electronics.

REFERENCES

[1] S. Ban *et al.*, *Adv Elect Materials*, **11** (2025) 2400665 [2] T. Ravsher *et al.*, *IEEE Trans. Electron Devices* **70** (2023) 2276–2281 [3] T. Ravsher *et al.*, *IEDM* (2021) 28.4.1-28.4.4 [4] J. Lee *et al.*, *IEDM* (2023) 1–4.

Programmable OTS. An interesting option for the embedded PCM scaling roadmap?

[Invited]

Massimo Borghi*

STMicroelectronics, Italy
*corresponding author: massimo.borghi@st.com

ABSTRACT

Amongst the diversified BEOL Non-Volatile-Memories portfolio, PCM has demonstrated to be able to play a primary role thanks to valuable features like scalability, small cell footprint, high programming speed, high endurance, low read latency and magnetic field immunity. Furthermore, with the introduction of Ge-rich GST it has been demonstrated that PCM can meet automotive requirements and can sustain soldering reflow thermal treatment. Today, solutions based on Ge-rich GST are available for the automotive and MCU market segments at 28nm technology node with 18nm ramping up. PCM scaling roadmap started relying on bitcell area reduction adopting more compact solutions for the selector element (e.g. from planar CMOS to vertical BJT) coupled with the shrink of the memory element to reduce the required programming current. In this scenario, OTS materials have gathered interest as selector in a crossbar architecture enabling a more compact NVM array fully integrated in the BEOL. But, in the last years, several OTS alloys have been studied and it has been shown their capability to modify the switching threshold voltage thanks to the programming pulse polarity. This solution is already under evaluation from pure memory players for an all-in-one memory with crossbar architecture (SOM, SSM) and now they have attracted interest inside the embedded market too. In this work a preliminary check about 3DXpoint, SOM or embedded OTS (OTS with selector) as the next embedded memory is presented. First electrical results on GeSeSbN, appealing features like low programming currents, low operating voltages and the ease of integration together with main challenges to be addressed by the eOTS are reported.

Key words: PCM, programmable OTS, embedded memory

OTS+PCM Material Exploration and Thermal Analysis for Crossbar Arrays

R. Antonelli[1,2], O. Cueto[1], C. de Camaret[1], G. Bourgeois[1], A. Salvi[1], S. Gout[1], M. Bernard[1], L. Fellouh[1], J. Rottner[1], N. Castellani[1], F. Andrieu[1], A. Souifi[2] and G. Navarro[1,*]

[1] CEA-Leti, Univ. Grenoble Alpes, F-38000 Grenoble, France

[2] Univ. Grenoble Alpes, CNRS, LTM, 38054 Grenoble, France

* Email: gabriele.navarro@cea.fr

ABSTRACT

This study demonstrates the suitability of $Ge_1Sb_4Te_4$-based Phase-Change Memory (PCM) for co-integration with a GeSbSeN-based Ovonic Threshold Switching (OTS) selector. This optimized composition exhibits larger voltage window, lower programming current, and reduced SET state variability versus standard $Ge_2Sb_2Te_5$, validated in a 1S1R Crossbar array. Finally, TCAD thermal simulations reveal the impact of lateral confinement.

Keywords: PCM, OTS, Crossbar, $Ge_1Sb_4Te_4$, Sb/Te ratio

1. INTRODUCTION

The expanding memristor market demands solutions for both standalone and embedded non-volatile memory (NVM) applications [1]. Phase-Change Memory (PCM) is a well-established technology, and its co-integration with an Ovonic Threshold Switching (OTS) selector holds promise for scaling to smaller technology nodes [1-3]. Sb-rich GeSbTe compositions are particularly attractive due to their rapid crystallization kinetics and stable crystalline phase [2, 3]. For the first time to our knowledge, we demonstrate the performance improvement in $Ge_1Sb_4Te_4$ (GST144) PCM over standard $Ge_2Sb_2Te_5$ (GST225) co-integrated with an OTS selector in a Crossbar array. The OTS selector is based on a GeSbSeN (GSSN) alloy. We co-integrated the PCM and the OTS through a Double-Patterned Self-Aligned (DPSA) scheme (**Fig. 1**) [4]. The resulting devices have a critical dimension of 100 nm and are integrated in 16 kb-sized arrays (1T1S1R). Electrical characterization was performed to program and measure the threshold voltage (V_{th}) in both SET and RESET states. The programming current (I_{prog}) is compared among the two compositions and the programming distributions are evaluated in 1 kb 1S1R Crossbar arrays. Additionally, TCAD thermal simulations were conducted to investigate the modified thermal behavior of the OTS+PCM (1S1R) system over the PCM (1R) alone.

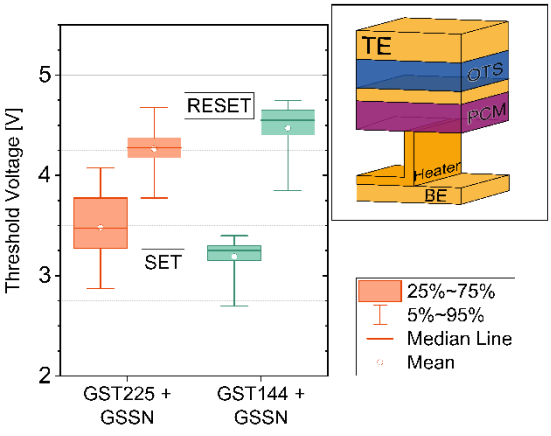

***Fig. 1**: SET/RESET Threshold Voltage (V_{th}) of 1T1S1R devices integrating either GST225 or GST144. The inset shows the device architecture, from top to bottom: Top Electrode (TE), OTS, Intermediate Metal, PCM, Heater element, and Bottom Electrode (BE).*

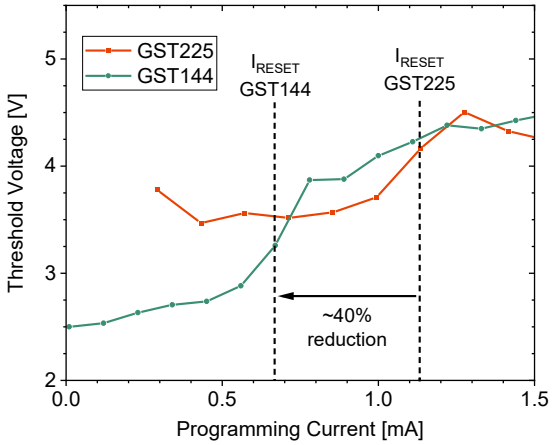

***Fig. 2**: Median Threshold Voltage (V_{th}) vs programming current (I_{prog}) of OTS+PCM for both GST225 and GST144 alloys in a 1T1S1R matrix. The device size is 100×100 nm. GST144 shows a SET/RESET transition at lower programming current.*

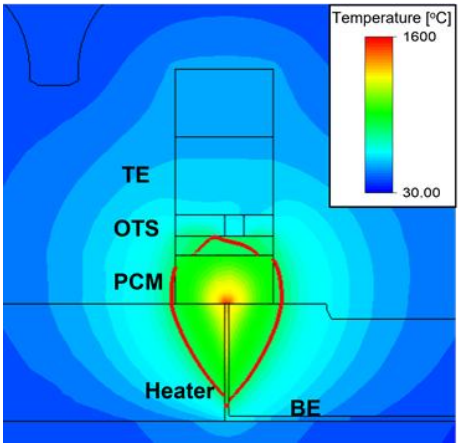

Fig. 3: TCAD thermal simulation of the OTS+PCM during a programming pulse. The red contour line corresponds to the melting temperature. Simulations were performed using the Synopsis® Sentaurus suite.

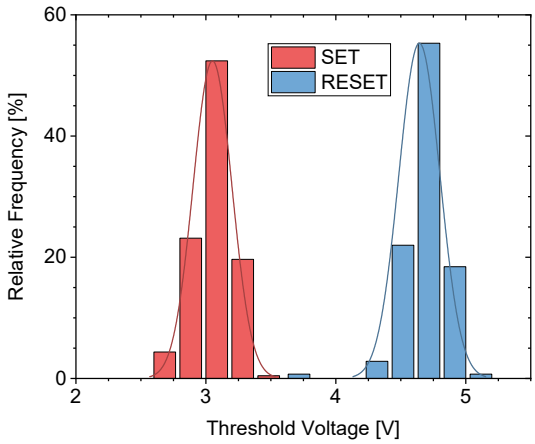

Fig. 4: SET and RESET V_{th} distributions measured from a 1 kb 1S1R OTS+PCM Crossbar array. PCM device is based on GST144 alloy.

2. RESULTS AND DISCUSSION

The increase of the Sb/Te ratio from 0.4 (GST225) to 1 (GST144) enhances the voltage window and reduces the SET variability (**Fig. 1**). The SET state exhibits a lower V_{th} in GST144 wrt GST225. GST144 demonstrates a RESET current (I_{RESET}) approximately 40% lower than standard GST225 for the same device lateral dimension (**Fig. 2**). The faster crystallization kinetics of congruent GST144 phase (compatibly with what observed for Sb-rich systems [3]) with respect to GST225, gives rise to a more reliable SET operation, responsible for the observed SET V_{th} reduction.
To investigate the SET programming speed, we carried out TCAD simulations on the OTS+PCM device (**Fig. 3**), comparing them with the ones on PCM device alone (w/o OTS). The maximum temperature reached in the OTS+PCM cell is higher than in the PCM for an equivalent programming current. Moreover, the melting temperature is achieved uniformly across the whole cell volume. Therefore, a longer fall time is required to fully SET a GST225 OTS+PCM cell [4], while in GST144 the SET is achieved with a shorter pulse duration confirming its high growth speed.
Finally, we provide the demonstration of GST144-based Crossbar arrays (1S1R) featuring well separated SET and RESET V_{th} distributions, with a wide voltage window margin of more than 1.5 V (**Fig. 4**).

3. CONCLUSIONS

In this study we investigate $Ge_1Sb_4Te_4$-based PCM co-integrated with a GeSbSeN OTS selector. This optimized composition allows an OTS+PCM device featuring a larger voltage window margin, reduced SET variability, and lower programming currents compared to standard $Ge_2Sb_2Te_5$. The co-integration of OTS with PCM results in higher temperatures during programming, hindering crystallization and reducing the SET speed, outlining the key knobs in material design for optimized thermal management. We evaluate the potential of GST144 PCM in a 1 kb 1S1R Crossbar array, showing well separated SET and RESET distributions and a voltage window of more than 1.5 V.
These findings highlight the potential of Sb/Te ratio optimization in enhancing the performance and reliability of OTS+PCM devices, and offer paths for further research.

ACKNOWLEDGMENTS

This work has been partially supported by Univ. Grenoble Alpes through LabEx Minos ANR-10-LABX-55-0 and partially supported by the French Public Authorities within the frame of France 2030 as part of the IPCEI Microelectronics and Connectivity.

REFERENCES

[1] M. Lanza et al., Nature, vol. 640, no. 8059, pp. 613–622, Apr. 2025, doi: 10.1038/s41586-025-08733-5.
[2] J. Shen et al., Adv. Mater., vol. 35, no. 11, p. 2208065, Mar. 2023, doi: 10.1002/adma.202208065.
[3] G. Navarro et al., IEEE IMW, 2019, pp. 1-4, doi: 10.1109/IMW.2019.8739656.
[4] R. Antonelli et al., Phys. Status Solidi RRL, p. 2300429, Feb. 2024, doi: 10/gtkc9q.

Efficient Screening of Chalcogenides and Down-Selection to Promising Compositions for ALD Process Development

M. M. Miller and M. H. Clark*,
Intermolecular, USA
*corresponding author: mark.clark@emdgroup.com

ABSTRACT

Chalcogenide-based devices play a crucial role in various technologies, including nonvolatile memory, which is a promising approach for in-memory computing and advanced computing architectures. The demand for these technologies is rapidly increasing due to the rise of AI applications. In this study, we present a systematic methodology for developing and validating new multinary compositions tailored for specific device functionalities. This process begins with physical vapor deposition (PVD) screening, followed by the development of atomic layer deposition (ALD) processes.

Key words: PVD, ALD, Chalcogenide, GeAsSeTe, composition screening

1. INTRODUCTION

Chalcogenides, particularly those based on germanium (Ge), arsenic (As), selenium (Se), and tellurium (Te), are notable for their unique properties that can be finely tuned through compositional adjustments. These materials have found applications in a wide range of technologies, including: **Infrared Optics:** Utilized in detectors, lenses, fibers, optical sensors, and mid-infrared sources. **Nonlinear Photonics:** Chalcogenide glasses exhibit ultrahigh third-order optical nonlinearity, making them ideal for applications such as supercontinuum generation and all-optical integrated circuits. **Memory Devices:** Employed in phase-change memory technologies, such as CD-RW, DVD-RAM, and phase-change random access memory (PRAM), as well as selectors in 3D memory arrays and resistive switches, contributing to neuromorphic hardware. **Other Applications:** These include chemical sensors, solar cells, optoelectronic devices, and graded-index lenses.

To optimize the performance of these materials, it is essential to leverage theoretical models and machine learning techniques to predict the most promising compositions. Experimental data must be collected from a diverse range of compositions to identify combinations that exhibit desirable properties. This screening process is more efficiently conducted using physical vapor deposition (PVD) compared to atomic layer deposition (ALD) or chemical vapor deposition (CVD), where the specific requirements of each precursor can complicate processing and limit the range of compositions that can be effectively screened. Our study aims to address these challenges by presenting a systematic methodology that integrates PVD screening with subsequent ALD process development, enabling the efficient identification of optimal compositions for targeted device functionalities.

2. EXPERIMENTAL

To optimize the performance of chalcogenide materials, theoretical models delineated regions of compositional space that exhibit desirable thermal and electrical properties. This approach facilitated the identification of promising compositions for further exploration. The feasibility of achieving these compositions was assessed using a defined set of sputtering targets, which were optimized to cover the entire desired compositional range. Once the target compositions were established, corresponding PVD targets were fabricated and prepared for deposition. Each target underwent qualification at three different power levels to determine the deposition rate, allowing conversion of power settings into atomic arrival rates on the wafer. This step is crucial for ensuring accurate thickness and composition during the qualification deposition for each data point in the composition space. The composition of the deposited films was analyzed using X-ray photoelectron spectroscopy (XPS) or X-ray fluorescence (XRF), depending on the elements involved. In cases where the measured composition deviated from the target, precise adjustments to the power settings

were made to align the compositions for subsequent qualification rounds. Once the compositions matched their targeted values within acceptable error margins, devices were fabricated from each composition and evaluated for electrical functionality. The final qualification samples were also tested for their physical properties. To enhance predictive capabilities, the machine learning model was updated with the new electrical and physical data, incorporating any significant differences observed. This iterative process refined predictions and identified new optimal compositions for further testing. Compositions that demonstrated the best performance were selected for ALD deposition. Precursors were carefully chosen based on effectiveness in ligand exchange reactions for binary films and suitability for single atomic depositions, ensuring compatibility with the selected compositions. Subsequently, ALD processes were developed, employing a supercycle approach to achieve the targeted compositions identified during PVD screening. The films were constructed through a series of layered depositions of the constituent materials, as illustrated in figure 1[1], allowing for a variety of compositions to be synthesized using different cycle ratios and stoichiometries. The newly developed compositions were integrated into devices for comprehensive testing of electrical and physical properties. This data was incorporated into an ALD-specific version of the machine learning model, which was periodically assessed for new optimal compositions that could be further explored.

3. RESULTS & DISCUSSION

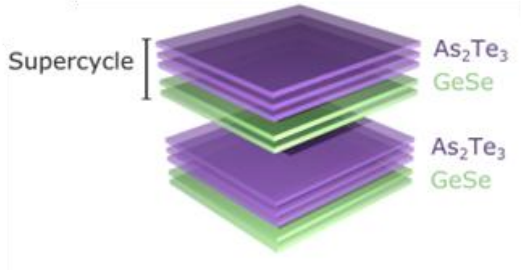

Figure 1: Schematic of the supercycle approach - alternating GeSe to As_2Te_3 cycles to produce GAST films

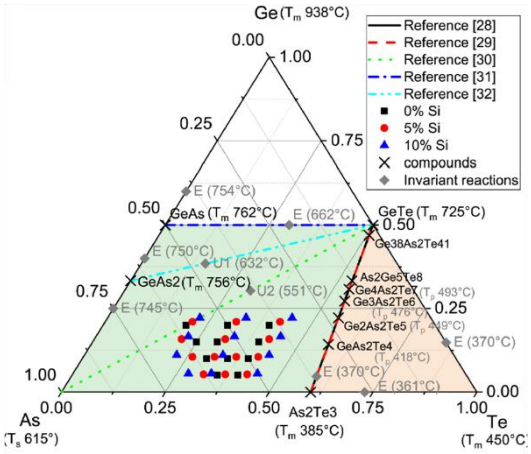

Figure 2: Ternary Ge-As-Te composition space, indicating the intermetallic binary and ternary compounds with their melting temperature (Tm) or temperature where they are formed peritectically (Tp). The reported ternary cross sections are also indicated, together with the invariant reactions deduced from these diagrams. The compositions that are studied in this work are projected in the Ge-As-Te composition diagram.

Experimental PVD compositions projected down to the As-Ge-Te plane (as if As+Ge+Te = 1) in Figure 2[2] for a previous set of experiments. Because target compositions and those around them have already been qualified, if there are any interesting electrical or physical results of the new compositions, additional near-neighbor compositions or any in between compositions can be deposited to check the performance across the ALD composition space. In this way the process can be adjusted to improve the device performance further.

4. CONCLUSIONS

While the development of ALD processes that cover a large four-dimensional composition manifold can be a daunting amount of work, we have demonstrated a method to only have to target a compositional subspace or subspaces within the larger manifold by ALD, allowing efficient and precise targeting of chemical composition and mapping of film and device properties near the optimum performance.

REFERENCES

1. ALD heterojunction Ovonic Threshold Switches P.C. Material, *Appl. Phys. Lett.* **X** (2009) 12345.

2. A combinatorial study of SiGeAsTe thin films for application as an Ovonic threshold switch selector, Thin Solid Films 753 (2022) 139278, https://doi.org/10.1016/j.tsf.2022.139278.

Van der Waals epitaxy and characterization of two-dimensional tellurium on silicon

S. Isceri[1,2], M. Hanke[2], G. Gandini[1], M. C. Paolozzi[3], D Kriegner[4], O. Abou El Kheir[5], A. M. Mio[6], F. Fagiani[1], I. Martinelli[3], S. Macis[3], M. Ramsteiner[2], S. Lupi[3], C. Rinaldi[1] and S. Cecchi[2,5*]

[1] Department of Physics, Politecnico di Milano, Piazza L. Da Vinci 32, Milan, 20133, Italy.
[2] Paul-Drude-Institut für Festkörperelektronik, Leibniz-Institut im Forschungsverbund Berlin e.V., Hausvogteiplatz 5-7, Berlin, 10117, Germany.
[3] Department of Physics, Sapienza University, Piazzale Aldo Moro 5, Rome, 00185, Italy.
[4] Institute of Physics, Czech Academy of Sciences, Cukrovarnická 10/112, Praha 6, 162 00, Czech Republic.
[5] Department of Materials Science, University of Milano-Bicocca, via R. Cozzi 55, Milan, I-20125, Italy.
[6] Institute for Microelectronics and Microsystems–IMM, National Research Council (CNR), Zona Industriale Ottava Strada 5, Catania, 95121, Italy.
*corresponding author: stefano.cecchi@unimib.it

ABSTRACT

The fabrication by molecular beam epitaxy of high-quality thin films of tellurium integrated on Si(111) is presented. After identifying the optimal growth conditions, we investigated the structural and electrical properties of the epilayers. We record a high hole mobility and thickness-dependent structural and vibrational properties. This work paves the way for the design of novel heterostructures of layered tellurides.

Key words: Two-dimensional tellurium, high-mobility, van der Waals, molecular beam epitaxy.

1. INTRODUCTION

Single-element phase-change materials are gathering the attention of our community in the recent years. For instance, nanoscale-confined layers of Sb showed thickness-dependent phase-change properties,[1] whereas Te has been proposed as active material in volatile ovonic threshold switch devices.[2] Also, a memristor design based on nanoscaled tellurium was demonstrated.[3]

Tellurene, the two-dimensional (2D) form of tellurium, has emerged as a novel monoelemental van der Waals (vdW) material. It is a narrow band-gap semiconductor featuring a pseudo-one-dimensional chiral crystalline structure, granting it with intriguing properties for next-generation electronic, optoelectronic, and piezoelectric applications.[4,5] The possibility to integrate 2D tellurium on silicon is appealing in view of its application in electronics. In this context, the Si(111)−(√3×√3)R30°−Sb surface was successfully used by our group for the vdW epitaxy of Sb_2Te_3, $Sb_{2+x}Te_3$ and $(GeTe)_m(Sb_2Te_3)_n$ layered alloys.[6–8]

2. EXPERIMENTAL

We fabricated high-quality thin films of tellurium on Sb-passivated Si(111) surfaces by molecular beam epitaxy (MBE). We first optimized the growth parameters, targeting the formation of smooth and continuous films of Te. The structural properties of the deposited material were characterized by reflection high-energy electron diffraction (RHEED), atomic force microscopy (AFM), X-ray diffraction (XRD) and scanning transmission electron microscopy (STEM). Then, we analyzed the electrical and infrared optical properties of a ≈20 nm thick Te epilayer at room temperature (RT). Finally, we investigated Te films as thin as 4 nm by AFM, XRD and Raman spectroscopy.

3. RESULTS & DISCUSSION

The influence of growth temperature on the synthesis of Te films on Si(111)−(√3×√3)R30°−Sb surfaces was studied by combining *in situ* RHEED with *ex situ* AFM and XRD. The optimal temperature for the 2D growth of tellurium films on Sb-passivated Si(111) was found to be 130°C (see panels (a) and (b) of Figure 1), corresponding to a preferential $10\bar{1}0$ out-of-plane orientation with Te chains parallel to the Si surface. The high structural quality of the epitaxial Te films was confirmed by STEM measurements, as shown in Figure 1(c). The vdW epitaxy occurs with the formation of a Sb_2Te_3 interlayer at the interface with silicon and peculiar rotational domains. Still, the MBE-grown material displays a high hole mobility above 250 cm^2/Vs at RT. Also, by reducing the epilayer thickness, Raman features characteristic of few-layer tellurium were observed.

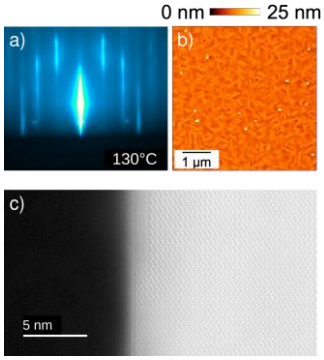

Fig. 1 Structural characterization of the epitaxial Te film deposited on Si(111)−(√3×√3)R30°−Sb surface at 130°C. (a) RHEED image along a Si$\langle 11\bar{2} \rangle$ azimuth. (b) AFM topography image. (c) High-angle annular dark-field STEM micrograph along the $[11\bar{2}0]$ zone axis of Te.

4. CONCLUSIONS

We presented the vdW epitaxy and characterization of 2D tellurium on Sb-passivated Si(111). High-quality Te films with thicknesses down to 4 nm were fabricated by MBE, exhibiting thickness-dependent properties. We report the high hole mobility of epitaxial Te at RT, unveiling an unprecedented value for thin films above 250 cm^2/Vs. These results open the way for the engineering of novel vdW heterostructures for memory applications integrated on silicon.

REFERENCES

1. Salinga, M. *et al.* Monatomic phase change memory. *Nature Mater* **17**, 681–685 (2018).
2. Shen, J. *et al.* Elemental electrical switch enabling phase segregation–free operation. *Science* **374**, 1390–1394 (2021).
3. Ghomi, S. *et al.* Non-Volatile Resistive Switching in Nanoscaled Elemental Tellurium by Vapor Transport Deposition on Gold. *Advanced Science* **12**, 2406703 (2025).
4. Qiu, G. *et al.* The resurrection of tellurium as an elemental two-dimensional semiconductor. *npj 2D Mater Appl* **6**, 1–10 (2022).
5. Deckoff-Jones, S. *et al.* Tellurene: A Multifunctional Material for Midinfrared Optoelectronics. *ACS Photonics* **6**, 1632–1638 (2019).
6. Boschker, J. E. *et al.* Surface reconstruction-induced coincidence lattice formation between two-dimensionally bonded materials and a three-dimensionally bonded substrate. *Nano Letters* **14**, 3534–3538 (2014).
7. Cecchi, S. *et al.* Interplay between Structural and Thermoelectric Properties in Epitaxial $Sb_{2+x}Te_3$ Alloys. *Adv. Funct. Mater.* **29**, 1805184 (2019).
8. Cecchi, S. *et al.* Thick Does the Trick: Genesis of Ferroelectricity in 2D GeTe-Rich $(GeTe)_m(Sb_2Te_3)_n$ Lamellae. *Advanced Science* **11**, 2304785 (2024).

Taming Thermal Transport: TMD Superlattices are the Key to Controlling Heat in Phase Change Memory

Seppe Van Dyck[1]*, W. Riffe[2], E. A. Scott[2], R. Coleman[3, 4], E. Seabron[3, 4], P. E. Hopkins[2], C. Detavernier[1]

[1]Dept. of Solid-state Science, Ghent University, Gent , 9000, Belgium
[2]Dept. of Aerospace Engineering, Univ. of Virginia, Charlottesville, VA 22904-4746, USA
[3]Dept. of Electrical Eng. and Computer Sci., Howard University, Washington, D.C., 20001, USA
[4]IBM-HBCU Quantum Center, Howard University, Washington, D.C., 20001, USA
*corresponding author: Seppe.VanDyck@UGent.be

ABSTRACT

Combining the phase change material Sb_2Te_3 with a transition metal-ditelluride (TMD) in a superlattice is presented as a strategy to control the heat flow in phase change memory devices. While the added interfaces of the superlattice already lower the thermal conductivity at room temperature, the choice of TMD also heavily influences the high temperature behavior.

Key words: 2D Materials, Superlattices, Sb_2Te_3, TDTR, Thermal Conductivity

1. INTRODUCTION

The switching of a phase change memory device relies on very local heating. This heat is meant to either crystallize or melt-quench the phase change material. Heat that is lost to the surroundings, however, is wasted and does not contribute to the phase change. Heat dissipation is governed by the thermal conductivity of the materials involved and most phase change materials suffer from a high contrast in thermal conductivity between their phases. With the crystalline phase often having the highest value, this is detrimental, as the change away from this phase requires the most energy. Creating a superlattice of Sb_2Te_3 and $TiTe_2$ can lower this thermal conductivity contrast, with $TiTe_2$ acting as a thermal barrier. In this work, we compare $TiTe_2$ to two other transition metal-ditellurides (TMD), VTe_2 and $ZrTe_2$, to evaluate the impact of this material choice.

2. EXPERIMENTAL

Deposition and Structure

All materials are deposited through room temperature magnetron sputtering from elementary pure targets. The wanted stoichiometry is reached by tuning the sputtering power, as the substrate periodically passes underneath each target. Film growth rates for the chalcogenides lie between 5 and 10 nm/min. When necessary, capping layers are deposited without breaking the vacuum. For structural characterization, X-Ray Diffraction (XRD) is used. In *ex-situ* XRD, a 1D detector with an opening of 15° is used in the typical Bragg-Brentano configuration. To study the thermal stability of the deposited superlattices during anneal, *in-situ* XRD is performed with source and detector kept at a fixed position.

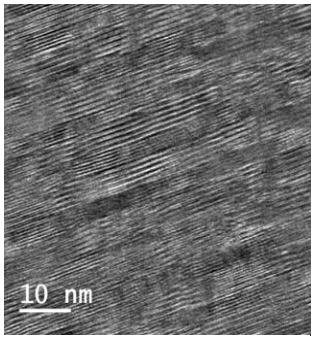

Figure 1 Cross-sectional TEM image of a sputtered superlattice with a period of 5 nm Sb_2Te_3 and 3 nm $TiTe_2$.

Time-domain Thermoreflectance (TDTR)

To study the thermal conductivity, TDTR is performed. This is a pump-probe technique that uses femtosecond laser pulses to directly probe the thermal response of a material. Samples are coated with a thick metal transducer layer (e.g. 80 nm Ru). The pump beam will periodically heat up this surface, causing heat to diffuse into the underlying layers. The probe beam is then used to measure the reflectance of the transducer layer after a delay, as this is proportional to the local temperature. Following the evolution of the temperature with picosecond resolution, allows us to model the thermal transport and extract values for the thermal conductivity.

3. RESULTS & DISCUSSION

Structural Characterization

The sputtered Sb_2Te_3 is amorphous, while the TMDs typically possess some (poly)crystallinity upon deposition. After a ramp anneal to 300°C, all materials crystallize into a high quality crystalline phase. All three TMDs crystallize into the CdI_2 structure, containing 2D sheets, parallel to the substrate, as XRD shows only 00L peaks in the diffraction pattern. This can be seen in figure 2. Rocking curve measurements confirm that these samples contain a fiber texture. Superlattices containing Sb_2Te_3 and one of these TMDs follow the trend of the individual materials and minimal intermixing is evident from our XRD analysis. A cross-sectional TEM image, shown in figure 1 confirms this highly oriented nature for a superlattice with a period of 5nm Sb_2Te_3 and 3nm $TiTe_2$, after an anneal at 300°C. The period boundaries are clearly visible, as well as the 2D sheets that make up the individual materials.

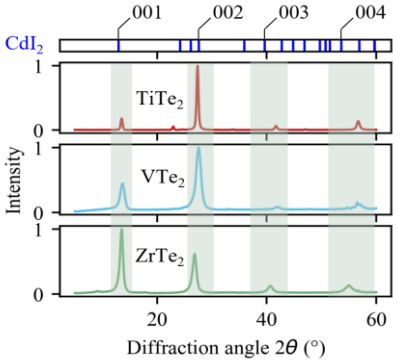

Figure 2 Ex-situ XRD after a 400°C anneal shows that all three materials form the CdI_2 structure with 00L planes parallel to the substrate.

Thermal Conductivity

TDTR is performed, both at room temperature and in an *in-situ* fashion at high temperatures. This allows us to directly study the effect of the crystallization on the thermal transport. The phase change material Sb_2Te_3, demonstrates a very high contrast in thermal conductivity, with the crystalline value being more than double the amorphous value (figure 3). This high contrast almost completely disappears when studying the superlattices. Regardless of the TMD used, the superlattices show little to no contrast at room temperature. The real impact of the choice of TMD can be seen in figure 4, where they are compared at higher temperatures. The $ZrTe_2$ superlattice outperforms the other two, with a low thermal conductivity across the entire temperature range.

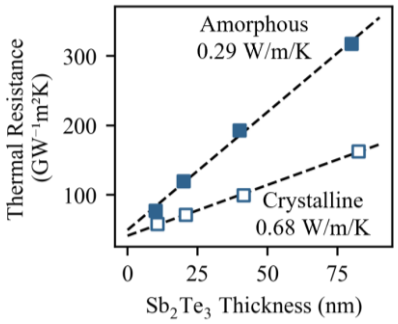

Figure 3 Sb_2Te_3 by itself shows a high contrast in thermal conductivity between its amorphous and

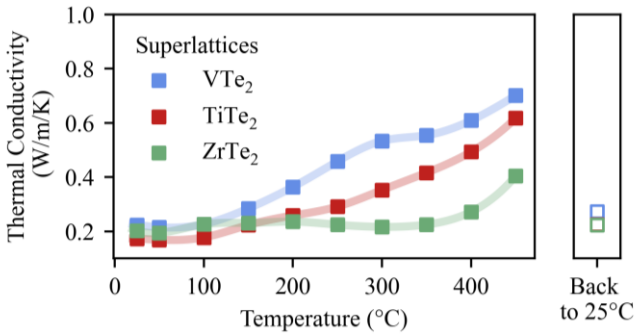

Figure 4 Comparing the different superlattices, it is clear that the choice of TMD has a large effect on the thermal conductivity, especially at high-temperatures.

Laser-based Optothermal Switching

To evaluate the switching characteristics, a novel, laser-based switching technique is currently being developed. The laser of a confocal microscope is used to expose the surface of a sample to a precise amount of energy. Reducing the laser intensity then allows to measure the change in reflectance as a result of the exposure. By adjusting the laser output power, threshold energies for crystallization and amorphization can be identified, allowing for repeatable, optothermal cycling.

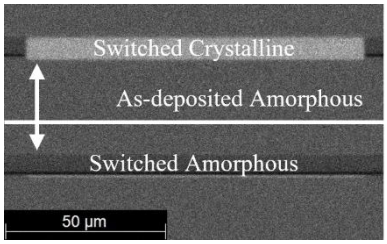

Figure 5 Repeatable switching, demonstrated on a sample of

4. CONCLUSIONS

Sb_2Te_3 by itself demonstrates a high contrast in thermal conductivity between its two states. All superlattices are successful in lowering that contrast significantly when studied at room temperature. The superlattice with $ZrTe_2$ is best at maintaining these low values over the studied temperature range.

Growth, Epitaxy and Thermal Stability of Phase Change Heterostructures

[Invited]

S. Prili[1,2,3*], C. Petrucci[1,3], V. Bragaglia[2], V.P. Jonnalagadda[2], A. M. Mio[4], J. Luchtenveld[2,5], S. Calvi[1,3], F. Righi Riva[1], S. De Simone[3], A. Diaz Fattorini[1,3], M. Longo[3,6], B. J. Kooi[4], R. Calarco[3] A. Sebastian[2], G.S. Syed[2] and F. Arciprete[1,3]

[1] Department of Physics, University of Rome "Tor Vergata" Via della Ricerca Scientifica 1, Rome 00133, Italy
[2] IBM Research – Europe, Saumerstrasse 4, 8803 Rueschlikon, Switzerland
[3] Institute for Microelectronics and Microsystems (CNR–IMM) Via del Fosso del Cavaliere 100, Rome 00133, Italy
[4] Institute for Microelectronics and Microsystems (CNR-IMM) Strada VIII n. 5, 95121 Catania, Italy
[5] Zernike Institute for Advanced Materials and Center for Cognitive Systems and Materials, University of Groningen, 9747 AG Groningen, Netherlands
[6] Department of Chemical Science and Technologies, University of Rome "Tor Vergata" Via della Ricerca Scientifica 1, 00133 Rome, Italy
*prili@roma2.infn.it

ABSTRACT

In recent years, phase-change memories (PCM) have emerged as one of the most promising technologies for analog in-memory computing, an innovative approach that performs computations directly within memory, thereby overcoming the Von Neumann bottleneck[1]. Despite their potential, two major PCM limitations still need to be addressed: high reset current and resistance drift. In fact, both these issues critically affect the scalability and computational precision of this technology, making their resolution essential for its systematic implementation. In this context, the introduction of phase-change superlattices and heterostructures as active layers of PCM device offers an elegant, material-based solution to both these issues[2]. The presence of numerous van der Waals (vdW) gaps within these alloys significantly reduces cross-plane thermal conductivity, enabling a more energy-efficient memory switch[3]. Furthermore, innovative heterostructures based on $TiTe_2$ intercalated into standard phase change alloys have demonstrated notably lower resistance drift, likely due to reduced structural relaxation[4].

In this presentation I will discuss the sputter growth of $Ge_2Sb_2Te_5/Sb_2Te_3$ phase-change superlattices, exploring the influence of the deposition parameters on the growth of both the individual layers and the overall stack[5]. This understanding is essential for the industrial scaling of these alloys, where deposition using industry-compatible tools must ensure high structural quality, particularly regarding the formation of vdW gaps. I will also address the growth process on technologically relevant substrates, as well as the use of Sb_2Te_3 seed layers deposited under varying temperature. Next, I will explore the thermal stability of $TiTe_2$-based heterostructures, illustrating how, despite starting from epitaxial films with atomically sharp interfaces, thermal annealing inevitably compromises the structural integrity of the stack. In particular, I will present the effects of thermal treatments performed at different temperatures and durations, offering valuable data that help bridge the gap between theoretical predictions of stability[4] and recent experimental results from actual PCM devices[6].

Keywords: superlattices, heterostructures, vdW gaps, epitaxy, interfaces

REFERENCES

1. Le Gallo, M. *et al. Nat. Electron.* **6**, 680–693 (2023).
2. Simpson, R. E. *et al. Nat. Nanotechnol.* **6**, 501–505 (2011).
3. Kwon, H. *et al. Nano Lett.* **21**, 5984–5990 (2021).
4. Ding, K. *et al. Science* **366**, 210–215 (2019).
5. Prili, S. *et al. Adv. Mater. Interfaces*, 2500058 (2025).
6. Cohen, G. M. *et al. Phys. Status Solidi RRL – Rapid Res. Lett.* **18**, 2300426 (2024).

Wednesday, Septembre 24

12:50 – 14:40 POSTER SESSION 1: all odd-numbered posters

--

Thursday, Septembre 25

12:35 – 14:30 POSTER SESSION 2: all even-numbered posters

P-01

Multi-Threshold Voltage Selector-Only Memory Based on Non-Toxic Amorphous Bi-Chalcogenides

Namwook Hur[1], Seunghwan Kim[2], Youngseok Cho[2], Seonguk Yang[1], and Joonki Suh[1,2,*]

[1]Department of Materials Science and Engineering, Ulsan National Institute of Science and Technology, Ulsan 44919, Republic of Korea

[2]Graduate School of Semiconductor Materials and Devices Engineering, Ulsan National Institute of Science and Technology, Ulsan 44919, Republic of Korea

*Corresponding author: jsuh@unist.ac.kr

ABSTRACT

Selector-only memory (SOM) has been highlighted as one of promising storage class memory; still, challenges remain toward its non-toxic material design and multi-level cell strategy (MLC). Here, we demonstrate a ternary $Ge_xSe_yTe_z$-based SOM device, exhibiting a 2.0 V memory window at a 0.012 MA/cm^2 current density and reliable 2-bit MLC performance. This work provides potentials in SOM technology for high-density, low-power storage.

Key words: *Selector-only memory (SOM), Ovonic threshold switching (OTS), amorphous chalcogenide, multi-level cell (MLC)*

1. INTRODUCTION

Dual-functional memory, which enables the integration of memory and selector functionalities in a single unit, has been of intense interest for parallel computing components[1]. From this perspective, technologically mature amorphous chalcogenides have emerged as promising materials for dual-functional selector-only memory (SOM), leveraging the polarity-dependent threshold voltage (V_{th}) shift phenomenon[2]. In parallel, toxic elements such as arsenic (As) have traditionally been adopted into selector materials to enhance device reliability. However, their usage poses challenges for industry-compatible film deposition technology. Furthermore, a comprehensive understanding of beyond polarity-dependent binary memory operation is required to enable precise multi-V_{th} modulation for high-density multi-level cell strategies. For this purpose, we proposed an amorphous Ge-Se-Te (a-GST) as the active memory layer. Through systematic electrical measurement, the device exhibited a sufficient memory window (MW) and multi-level cell (MLC) strategy, which will be discussed in the Results and Discussion section.

2. EXPERIMENTAL

For the device fabrication, the W (25 nm)/Si_3N_4 (200 nm) layers were sequentially deposited on the bare substrate. Nanoscale holes were then patterned via dry etching. Next, an amorphous alloy and a capping layer were deposited inside a via-hole. Lastly, W metallization was done for both bottom and top electrodes. Electrical measurements were performed using a Keithley 4200A-SCS semiconductor analyzer. The dark-field scanning transmission electron microscope (HAADF-STEM) with corresponding energy dispersive spectrometry (EDS) images were analyzed using a high-resolution TEM (JEOL, JEM-ARM300F) operating at 160 kV.

3. RESULTS & DISCUSSION

The fabricated non-toxic ternary a-GST incorporated SOM device utilized a via-hole architecture (**Fig. 1a**). The two-terminal device is composed of the top electrode contact (TEC) and the bottom electrode contact (BEC), whereas the active memory layer of a-GST is located between them. Specifically, the serial connection of external resistance (R_{Ext}) to the TEC enables the on-current adjustment above the V_{th} region when applying the identical bias injection. Initially, the devices were evaluated using R_{Ext}=3.3 kΩ. **Fig. 1b** displays an operational method for the binary memory operation for achieving a high V_{th} state (HVS) and a low V_{th} state (LVS). The difference between

HVS and LVS defines MW. Following this procedure, we achieved reliable >1.0 V of MW with low device variations (**Fig. 1c**). After that, a 15 kΩ resistor was adopted to reduce the operational current. **Fig. 1d** represents the gradual increment in MW as a function of HVS programming current density (J_{PRG}). The applied pulse amplitude varied from 3.5 V to 6.0 V. Interestingly, the MW was gradually increased and finally saturated, achieving ~2.0 V within the J_{PRG} of ~0.012 MA/cm^2, evident in the possibility of the MLC strategy. The compositional effect of bi-chalcogens was then investigated. We prepared four specimens of Se0-Se3, which indicate zero to the highest Se concentration in the ternary a-GST layer. **Fig. 1e** shows the thermal stability of the a-GST films integrated into the devices. In a range of 25-400 °C, Se1-Se3 reverted to their initial resistance states with minimal thermal degradation, whereas Se0 transited to an irreversible crystallization at 240 °C. In terms of V_{th} shift, Se0 exhibited negligible MW, whereas it gradually enlarged with increasing Se concentration, saturating at Se2-Se3 (**Fig. 1f**). Simultaneously, Se3 exhibited severe variation than the case of Se2. Based on these comparisons, we selected Se2 as the optimal a-GST composition for integration into SOM devices. Finally, the 2-bit MLC was successfully implemented in a single SOM device (**Fig. 1g**). The four memory states, denoted as (11), (10), (01), and (00) from low-to-high V_{th} values, were demonstrated via controlling pulse amplitude. Within the 40 individual SOM devices, each memory state was successfully separated by a ~0.5 V difference. Furthermore, sequential 2-bit MLC operations of more than 500 cycles indicated a reliable MLC demonstration as shown in **Fig. 1h**.

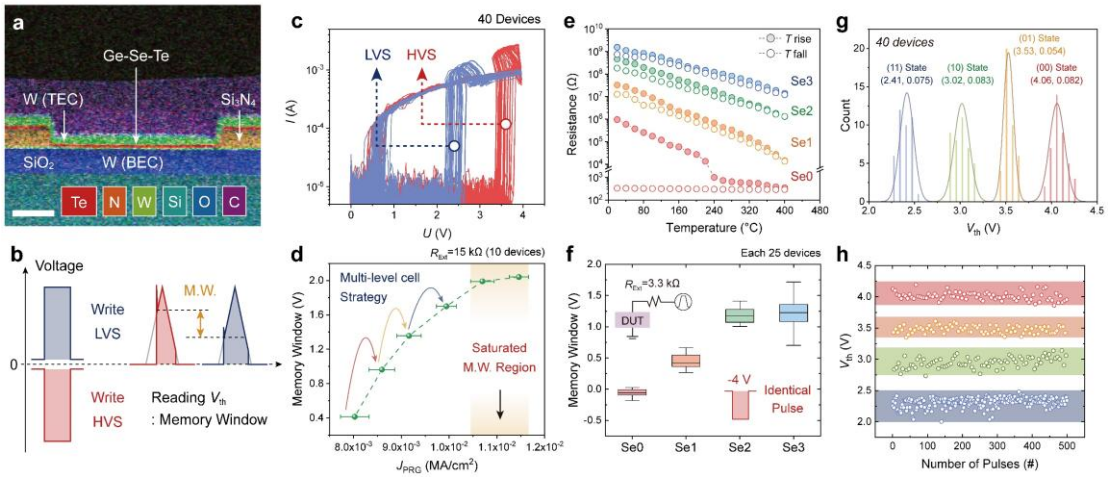

Fig. 1. (**a**) Integrated energy dispersive X-ray spectroscopy (EDS) elemental mapping of cross-sectional SOM device. The scale bar is 500 nm. (**b**) Illustration of the programming and reading pulses for achieving the binary SOM performance. (**c**) *I-V* plots of LVS and HVS across 40 individual SOM devices. (**d**) Relationship between memory window and programming current density (J_{PRG}) using R_{Ext}=15 kΩ. (**e**) Thermal degradation of Se0-Se3 devices. (**f**) Memory window of Se0-Se3 devices under identical programming using R_{Ext}=3.3 kΩ. (**g**) Device variation of 2-bit MLC states. (**i**) Sequential reproducibility of 2-bit MLC operations.

4. CONCLUSIONS

In conclusion, we presented a binary chalcogenide alloy-incorporated SOM device, achieving reliable large MW, low programming current density, and robust thermal stability with low device variations. The optimized chalcogen ratios of the active memory layer compromised the MW and device reliability. Additionally, the proposed device demonstrated the high-density memory applications of 2-bit MLC by regulating programming voltage. Consequently, our work provides a robust foundation for SOM materials and operational methods, paving the way for developing next-generation non-volatile memory technologies that support parallel computing applications, including logic-in-memory and edge computing devices.

REFERENCES

1. Ielmini, D. & Wong, H. S. P. *Nat. Electron.* **1** (2018) 333-343.
2. Zhao, Z. *et al.* *Nano-Micro Lett.* **16** (2024) 81.

P-03

Investigation of the Electrical Performance and Crystallization Behavior of Carbon-Doped $Ge_1Sb_4Te_7$

Hengyi Hu, Shaojie Yuan, Xiangshui Miao, and Ming Xu*
School of Integrated Circuits, Huazhong University of Science and Technology, Wuhan
*corresponding author: mxu@hust.edu.cn (M.X.)

ABSTRACT

$Ge_1Sb_4Te_7$ (GST), as a typical stoichiometric phase-change chalcogenide, is limited in its neuromorphic applications due to fast crystallization and high resistance drift. This study investigates the effects of C doping on the thermal stability and crystallization dynamics, as well as its relations to the microstructures. The results demonstrate that phase-change memory (PCM) devices based on C doped GST material exhibit excellent thermal stability, electrical configuration stability and multivalued reliability, highlighting their potential as neuromorphic computing device.

Key words: PCM, carbon dopant, high thermal stability, low resistance drift, Multilevel resistance

1. INTRODUCTION

Neuromorphic computing addresses the von Neumann bottleneck by emulating the brain's energy-efficient architecture.[1] PCM materials are attractive candidates due to their tunable resistance and unipolar switching characteristics.[2] However, limited data retention and resistance drift hinder their broader application. Carbon doping in GST effectively enhances thermal stability and suppresses drift, making it a promising material for neuromorphic devices. In this study, $Ge_1Sb_4Te_7$ films and devices with different C contents (GST-C) were fabricated via co-sputtering, and the effects of dopants on the thermodynamic properties, electrical properties, and microstructure of GST were investigated through both experimental analysis and DFT calculations. With increasing carbon concentration, GST-C exhibits enhanced amorphous stability and a suppressed crystallization kinetics. PCM cells based on this material exhibit excellent reliable multilevel resistance and reduced drift, demonstrating its potential for advanced memory and neuromorphic computing applications.

2. EXPERIMENTAL

The 100 nm thick phase-change material films were deposited onto SiO_2/Si (100) substrates by co-sputtering carbon and GST targets at room temperature, in an argon atmosphere with a background pressure of 0.6 Pa. A series of GST-C films with varying carbon concentrations were prepared by adjusting the sputtering power of the carbon target. The films were characterized using R–T measurements, X-ray diffraction, X-ray photoelectron spectroscopy. Via-hole structured PCM devices were fabricated, and their electrical performance was evaluated using a Keysight B1530A semiconductor parameter analyzer. The *ab initio* molecular dynamics (AIMD) simulations were conducted using the melt-quench-relaxation approach to construct amorphous $C_{24}Ge_{25}Sb_{100}Te_{175}$ and $Ge_{27}Sb_{108}Te_{189}$ models. The time step was set to 3 fs, and the energy cutoff was 500 eV. The models were fully melted at 2000 K, followed by rapid cooling of the liquid phase to 300 K at a rate of 30 K/ps. Structural analysis was conducted after eliminating residual stress by adjusting the cell size. AIMD simulations of crystallization were performed at 600 K to accelerate the phase transition.

3. RESULTS & DISCUSSION

we fabricated PCM cells with a via-hole structure. The R-V electrical test of the PCM cell based on GST-C is shown in **Fig. 1(a)**. The PCM cell based on the GST-C can be programmed at lower switching voltages and maintain an order of magnitude of switching range with programming pulses as short as 70 ns. by controlling the voltage of the pulses, an array of finely tunable resistance states can be achieved. We performed resistance drift measurements on the intermediate states of GST-C, as shown in **Fig. 1(b)**. The results indicate that the intermediate states of the GST-C PCM cell maintain good distinguishability, with a maximum drift coefficient of 0.032, lower than the drift

coefficient of conventional $Ge_2Sb_2Te_5$ (ν=0.11)[3]. AIMD simulations were used to study the crystallization behavior of GST and C-doped GST (GST-C). Both models were melted at 2000 K for 6 ps, then quenched to 300 K to form amorphous structures, followed by crystallization at 600 K. Crystallinity was analyzed using the Polyhedral Template Matching (PTM)[4] method. At 30 ps, GST began forming ordered cubic regions, while GST-C remained amorphous. By 60 ps, GST showed significant crystallization, whereas GST-C only developed early 4-fold ring precursors, mainly away from carbon-rich regions. Carbon atoms in GST-C formed chains and tetrahedral clusters, which hindered nearby crystal growth and slowed crystallization.

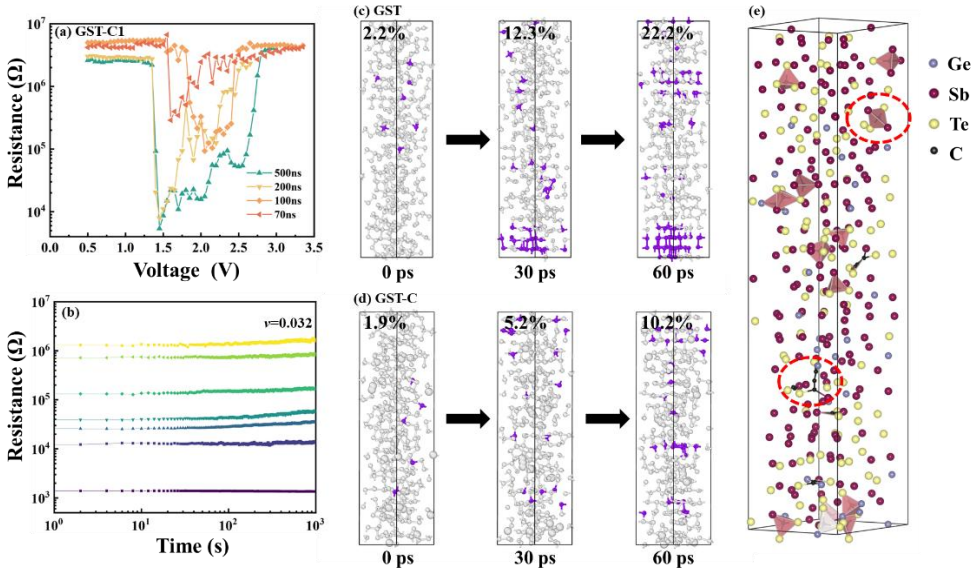

Fig. 1 (a) The R-V electrical test of the PCM cell using GST-C. (b) The resistance drift coefficient ν of the GST-C phase-change cell obtained by fitting with the equation. The evolution of the crystallinity of the GST(c) and GST-C(d) models during the first 60 ps of the crystallization process. The ordered cubic local motifs are highlighted in purple. (e) the snapshot of the GST-C system at 60 ps. The primary forms of carbon atom presence are marked with red circles.

4. CONCLUSIONS

This study was conducted on carbon-doped $Ge_1Sb_4Te_7$ phase-change material, systematically examining the effect of carbon doping on the thermal stability of material, microstructure, and crystallization behavior, as well as the overall device performance. The results demonstrate that carbon doping significantly enhances the thermal stability of amorphous $Ge_1Sb_4Te_7$. Crystallization simulation analysis shows that the stable presence of carbon chains and carbon tetrahedra creates carbon-rich regions, which notably inhibit the growth of nearby $Ge_1Sb_4Te_7$ crystals, thereby reducing the crystallization driving force and slowing the long-range movement of other atoms in the system. Devices based on $Ge_1Sb_4Te_7$ phase-change material exhibit high thermal stability, fast switching, and reliable multivalued storage performance, with a drift coefficient as low as 0.032. These results suggest that carbon-doped $Ge_1Sb_4Te_7$ holds significant potential for neuromorphic device applications.

REFERENCES

1 M. Lanza, A. Sebastian, W. D. Lu, M. Le Gallo, M. F. Chang, D. Akinwande, F. M. Puglisi, H. N. Alshareef, M. Liu, and J. B. Roldan, Science **376** (6597), eabj9979 (2022).
2 Meng Xu, Ming Xu, and Xiangshui Miao, InfoMat **4** (6) (2022).
3 R. S. Khan, F. Dirisaglik, A. Gokirmak, and H. Silva, Applied Physics Letters **116** (25) (2020).
4 Peter Mahler Larsen, Søren Schmidt, and Jakob Schiøtz, Modelling and Simulation in Materials Science and Engineering **24** (5) (2016).

P-05

Ultrathin antimony for ultralow-drift phase-change memory applications

Xin Chen[1], Junzhao Yang[1], Bin Chen[1],Xue-Peng Wang[1,*]

[1]College of Materials Science and Engineering, Shenzhen Key Laboratory of New Information Display and Storage Materials, Shenzhen University, Shenzhen 518060, China.

xpwang@szu.edu.cn

ABSTRACT

Phase-change random-access memory (PCRAM) devices suffer from pronounced resistance drift originating from considerable structural relaxation of phase-change materials (PCMs), which hinders current developments of high-capacity memory and high-parallelism computing that both need reliable multibit programming. Compositional simplification and geometrical miniaturization of traditional GeSbTe-like PCMs are feasible routes to suppress relaxation. While to date, the aging mechanisms of the simplest PCM, Sb, at nanoscale, have not yet been unveiled. Here we demonstrate that in an optimal thickness of only 4 nm, the thin Sb film can enable a precise multilevel programming with ultralow resistance drift coefficients, in a regime of ~10^{-4}-10^{-3}. This advancement is mainly owed to the slightly changed Peierls distortion in Sb across the Sb/SiO_2 interfaces. Our work highlights a new indispensable approach, interfacial regulation of nanoscale PCMs, for pursuing ultimately reliable resistance control in aggressively-miniaturized PCRAM devices, to boost the storage and computing efficiencies substantially.

Key words: phase-change memory, interfacial regulation, resistance drift, antimony

1. INTRODUCTION

Aging of amorphous PCMs leads to resistance drift phenomenon that will blur the data resolution, resulting in unavoidable decoding errors. The widely used GeSbTe-like PCMs and GeTe exhibit pronounced resistance drift in the amorphous state. Reducing homopolar Ge-Ge bonds and tetrahedral Ge motifs, as well as reinforced Peierls distortion, together form the driving forces of the noticeable structural relaxation of the vitreous phases.[1] In addition, the abundant lone-pair electrons on Te atomic chains promote the creation of valence alternation pairs (VAPs).[2] Either generation or recombination of the charged VAP defects can modify electronic band structure sensitively. Therefore, removing Ge and Te element would probably relieve the relevant disturbance in conductance upon aging for the simplest PCM, i.e., Sb, in its amorphous phases. Another feasible way to decrease resistance drift is miniaturing the PCM geometry. Because the much-enlarged surface-to-volume ratio benefits a more efficient stress release in structural relaxation. In addition, bulk Sb film has no glassy phases due to its spontaneous crystallization nature. Geometrical miniaturization will be beneficial for stabilizing amorphous phase of Sb. To date, whether a low resistance drift can be accomplished by the Sb-based PCRAM devices is still elusive, yet the aging mechanism of nanoscale Sb has not been touched in previous studies.

2. EXPERIMENTAL

Device fabrication. The PCRAM device shown in Fig. 1a was fabricated on a silicon substrate. On top of the TiN bottom electrode layer, the cell structure was developed using electron beam lithography (EBL) patterning, following the ~20 nm-thick SiO_2 deposition in PVD. Then a via hole with the dimension of 150 × 150 × 20 nm^3 was formed. Another EBL patterning process was required for the Sb film and top TiN electrode. ~1.5 nm-thick SiO_2, ~4 nm-thick Sb, and ~1.5 nm-thick SiO_2 layers were then sequentially deposited.

DFT calculations. Our *ab initio* molecular dynamic (MD) simulations were performed in the VASP code. We used ~10 Å-thick amorphous SiO_2 layers sandwiching the 4 nm-thick Sb. The amorphous Sb/SiO_2 interface was obtained by melting at 3,000 K for 6 ps, followed by another melting at 1,000 K for 6 ps with amorphous SiO_2 part locked. The amorphous less-equilibrium (LE) model was

created by directly placing the 1,000 K-melted Sb at 300 K, while the more-equilibrium (ME) model was obtained by continuously quenching the 1000-K melted Sb to 300 K with a cooling rate of 29 K ps^{-1}. Both the LE and ME (Fig. 1c) Sb models were further relaxed at 300 K for 90 ps.

3. RESULTS & DISCUSSION

Figure 1b shows the 12 resistance levels with ultralow drift coefficient (ν) ranging from 10^{-4} to 10^{-3} in RESET programming of our PCRAM devices. We generated the LE and MD Sb models signifying the unrelaxed high-energy and relaxed low-energy phases before and after aging, respectively. Nearby the interfaces, electrons on homopolar Sb-Sb bonds turn to be more localized, as the average electron localization function (ELF) values are noticeably larger than those for the internal Sb parts (Fig. 1d). Due to the interface-proximity effect, the interface regions constitute stronger covalent bonds, that stabilize a disordered network on two-dimensional scale. We then examined Peierls distortion for Sb-Sb bonds by angular-limited three-body correlation (ALTBC) analysis (Fig. 1e-h). In the LE model, the central distribution for the bond length-splitting ratio (r_2 / r_1) between ~1.00 and ~1.07 decreases dramatically upon relaxation from 40 to 87 ps. On the contrary, the ME model has a rather smaller distribution for $1.00 < r_2 / r_1 < \sim 1.07$, and the decease from 40 to 87 ps is not so significant either. The comparison denotes that Peierls distortion continues to reinforce when Sb glass is aging, prominently for the more unstable LE model, whereas becoming quite marginally for deeply relaxed ME case.

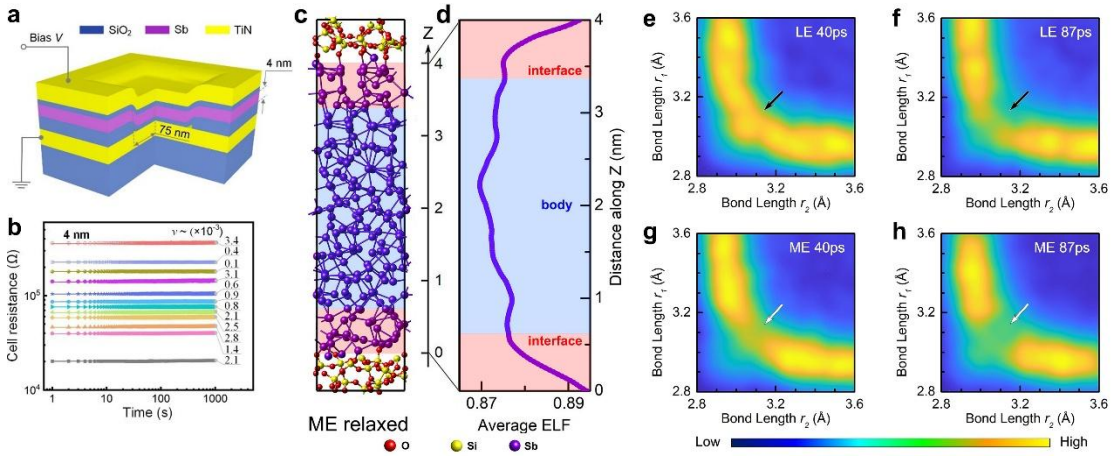

Figure 1. (a) Schematic of the 4 nm-thick Sb-based PCRAM device. (b) Temporal evolution of 12-level resistance states achieved by iterative RESET operations. (c) Amorphous ME model and (d) average ELF value along the thickness Z direction of Sb part. The degree of Peierls distortion evaluated by ALTBC analysis for the 300 K-annealed amorphous LE and ME Sb model at 40 ps (e and g) and 87ps (f and h), respectively.

4. CONCLUSIONS

In this work, by combining device characterizations with DFT MD simulations, we reveal that the ultralow resistance drift in the SiO_2-sandwiched ~4 nm-thick Sb films should originate from the slightly changed Peierls distortion in Sb across the Sb/SiO_2 interfaces. Our work sheds light on a new approach, i.e., interfacial regulation of nanoscale PCMs, to tailor ultralow resistance drift of PCRAM cells for the design of multibit memory and accurate computing chips. [3]

REFERENCES

1. J. Y. Raty, W. Zhang, J. Luckas, C. Chen, R. Mazzarello, C. Bichara, M. Wuttig, *Nat. Commun.* **6** (2015) 7467.
2. D. Adler, M. S. Shur, M. Silver, S. R. Ovshinsky, *J. Appl. Phys.* **51** (1980) 3289.
3. B. Chen, X. P. Wang, F. Jiao, L. Ning, J. Huang, J. Xie, S. Zhang, X. B. Li, F. Rao, *Adv. Sci.* **10** (2023) 2301043.

P-07

Mid-Infrared Reconfigurable Spatial Filtering via an Extraordinary Optical Transmission Phase-Change Metasurface

S. Kendall[1], J. Shields[1], C. Ruiz de Galarreta[1,2], J. Bertolotti[1], A. Alù[3], and C. D. Wright[1]*
[1]Centre for Metamaterials Research and Innovation, University of Exeter, Exeter, EX4 4QF, UK
[2]Institute of Materials Science of Barcelona, Campus de la UAB, Bellaterra, 09193, Spain
[3]Photonics Initiative, Advanced Science Research Center, City University of New York, New York, NY 10031, USA
*corresponding author: david.wright@exeter.ac.uk

ABSTRACT

Extraordinary optical transmission metasurfaces, with phase-change materials incorporated into their structure, are designed and fabricated to allow for dual-function switchable edge-detection and blurring imaging modes. This reconfigurable functionality is achieved with high-pass and low-pass filter designs via either amorphised or crystallised regions across the metasurface. **Key words**: Phase-change, metasurface, extraordinary optical transmission

1. INTRODUCTION

Recently, optical analogue optical computing has seen increased attention due to holding some inherent advantages over its digital counterpart; these advantages include spatial parallelism, ultra-high bandwidth and low-loss transmission [1]. Previous work in the field has explored both free-space and integrated photonic systems for uses including optical neural networks [2] and parallelized matrix-vector multiplication [3]. This work presents a design for a reconfigurable optical image processing metasurface within a free-space system: specifically, the metasurface performs dual-function high and low-pass filtering. This dual functionality is used here for edge detection and image blurring.

The reconfigurable metasurface design here is for use in a 4f system as a spatial filter. The dual functionality of the device is achieved via the integration of chalcogenide phase-change materials (PCMs) in the design of an extraordinary optical transmission (EOT) metasurface. The EOT effect results in massively enhanced light transmission, at a resonant wavelength, in a sub-wavelength array of holes in a metallic film. Here, a thin film of $Ge_2Sb_2Te_5$ (GST) is deposited on top of a gold film patterned with an array of sub-wavelength holes, all on a CaF_2 substrate (see Fig. 1a). GST is chosen due to having greatly differing optical properties (n and k) between its amorphous and crystalline phases [5]; switching between these phases allows for shifting of the EOT array's resonant wavelength. Switching the phase of the PCM is done via a heat stimulus, e.g. laser excitation or embedded microheaters. The metasurface design enable patterns to be written into the GST film in the form of either amorphised or crystallised regions. This in turn leads to a large change in optical transmission between the patterned regions, and therefore a form of reconfigurable optical spatial filtering can be achieved. COMSOL simulated transmission responses of our device are shown in Fig. 1b. An example of a high-pass spatial filter operation is shown in Fig. 1c.

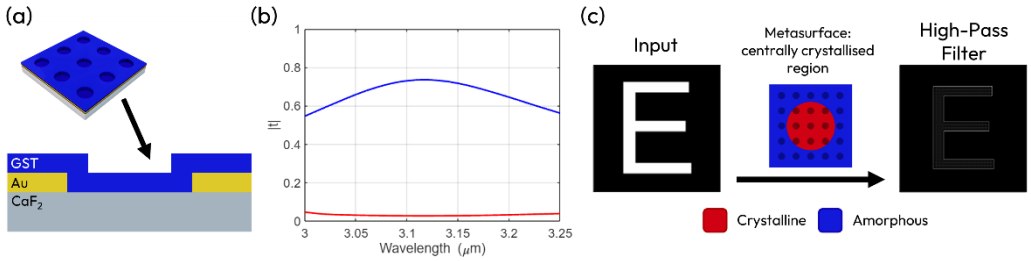

Fig. 1 (a) A schematic of the EOT device design. (b) Simulated transmission response of the device in the mid-infrared for the amorphous (blue line) and crystalline (red line) phases. (c) Simulated high-pass filter functionality of a device design functional in the mid-infrared.

2. EXPERIMENTAL

The presented devices were fabricated through processes of sputtering and electron beam lithography. Device functionality is targeted for the mid-infrared regime and so testing is carried out using FTIR spectroscopy. Figure. 2a shows initial experimental transmission results for the amorphous (blue line) transmission response and the near-zero crystalline (red line) response. Figure 2b shows the simulated functionality of the device for both low and high-pass examples for an input letter 'E'.

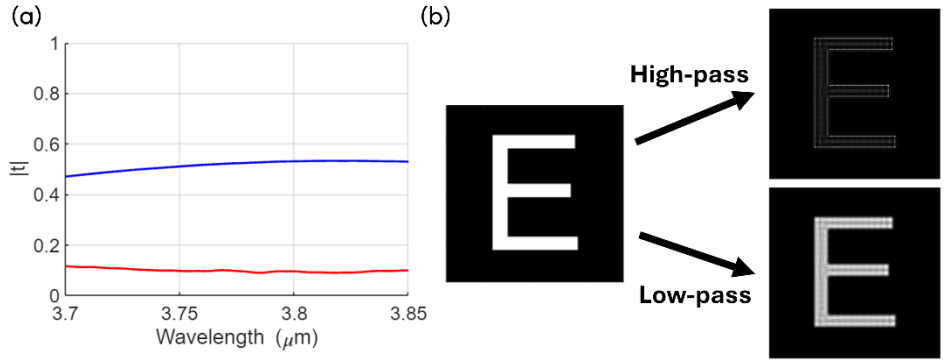

Fig. 2 (a) Experimental transmission results of the higher amorphous phase (blue line) and the near-zero crystalline phase (red line) around the crystalline minima (~3.8μm). (b) Functionality simulation results using the experimental results to show high-pass filtering (top) and low-pass filtering (bottom).

3. RESULTS & DISCUSSION

The initial experimental results demonstrate an ability to create reconfigurable low and high-pass spatial filters, operating in the mid-infrared waveband. The high-pass filter acts as an edge detection image processor with the edges of input image highlighted, while the low-pass filter performs image blurring with the edges becoming rounded.

4. CONCLUSIONS

We have presented a design for a phase-change reconfigurable metasurface for a spatial filter based optical image processing in the mid-infrared waveband. Simulations and preliminary experimental results are shown to validate the concept and applications of dual function edge detection and image blurring have been demonstrated.

Funding is acknowledged for part of this work from the EPSRC A-META project (EP/W003341/1), APT-NuCOM EPSRC project (EP/W022931/1) and the Marie Sklodowska-Curie Postdoctoral Fellowship 101068089 (METASCALE).

REFERENCES

1. McMahon, P. L. (2023). *The physics of optical computing*. Nature Reviews Physics, 1-18.
2. Lin, X. et al. (2018). *All-optical machine learning using diffractive deep neural networks*. Science 361, 1004-1008.
3. Feldmann, J. et al. (2021). *Parallel convolutional processing using an integrated photonic tensor core*. Nature 589, 52–58.
4. Ebberson, T. W. et al. (1998). *Extraordinary transmission through sub-wavelength hole arrays*. Nature 391, 667-669.
5. Ruiz de Galarreta C. et al. (2020). *Tunable optical metasurfaces enabled by chalcogenide phase-change materials: from the visible to the THz*. Journal of Optics 22, 114001.

P-09

Phase change materials combined with soft-NIL-prepared metasurfaces for large scale tunable photonic applications

Oumaima Meskini[1,2*], Mohammed Bouadellaoui[2], Maxime Bertoglio[1], Beniamino Sciacca[3], Badre Kerzabi[2], David Grosso[2,3] and Magali Putero[1]

[a] *Aix Marseille Univ, CNRS, IM2NP, Campus Scientifique de St. Jérôme, Marseille, France*
[b] *Solnil, Pépinière d'entreprises Luminy Biotech, Marseille, France*
[c] *Aix Marseille Univ, CNRS, CINaM, Marseille, France*
*corresponding author: oumaima.meskini@im2np.fr

ABSTRACT

We demonstrate the integration of GeTe phase change materials into large-area metasurfaces based on soft-nanoimprint lithography (soft-NIL) fabrication approach. Two integration strategies were explored using the soft-NIL patterns either as templates combined with solid-state dewetting, or as etch masks for reactive ion etching (RIE). Optical measurements, supported by numerical simulations confirmed dynamic modulations upon GeTe phase transition. Both high throughput methods yield high-quality metasurfaces with optical responses in reflection and transmission varying by factors of up to ×2.3 and ×3.7 in the NIR, respectively. Laser-induced switching of single meta-atoms was also demonstrated. This work paves the way towards scalable, cost-effective and tunable metasurfaces for programmable photonic devices.

Keywords: Metasurface, Photonics, Phase Change materials, GeTe, soft-Nanoimprint lithography (NIL), Reactive Ion Etching (RIE), laser switching.

1. INTRODUCTION

Controlling light propagation is a key challenge in the development of optical and photonic devices. Metasurfaces — ultra-thin devices made of sub-wavelength nanostructures — have emerged as powerful tools for manipulating light with high precision [1]. However, conventional metasurfaces are typically passive, with optical properties fixed at the design stage, during fabrication. This lack of tunability limits their versatility in applications such as multispectral filters, metalenses, and beam steerers. Incorporating phase-change materials (PCMs) into metasurfaces offers a route towards dynamic and reconfigurable photonic functionalities [2]. In this work, we explore the combination of GeTe with soft-NIL-patterned silica metasurfaces to produce large-scale, cost-effective and tunable photonic components.

2. EXPERIMENTAL

Dielectric metasurfaces were fabricated by soft-nanoimprint lithography (soft-NIL using elastomeric working stamps) of spin-coated sol–gel silica resins, followed by thermal annealing to stabilize the silica structure [3,4], to obtain the dielectric metasurface over 1×1 cm² areas.

Two approaches were investigated for integrating GeTe into these structures:

- Template strategy: imprinted dielectrics were used as structure directing templates onto which the GeTe layer was deposited by PVD before been reorganized by solid state thermal dewetting to redistribute the materials into structured PCM metasurface. In this first strategy, we selected a template of hexagonal array of square holes to yield a continuous grid-like PCM metasurface.
- Etching strategy: the nanoimprinted dielectric metasurface served as an etch mask atop a continuous PVD deposited GeTe layer to transfer the features into the PCM through reactive ion etching (RIE). In this second strategy, a square array of cylindrical pillars was selected to obtain discrete pillars meta-atoms with aspect ratio of around 0.5.

The optical constants of amorphous and crystalline GeTe were obtained by spectroscopic ellipsometry on the plain layer. Structural characterization was performed by X-ray diffraction and

by scanning electron microscopy (SEM), while optical properties were assessed via transmission and reflection UV-Vis-NIR spectrophotometry.

3. RESULTS & DISCUSSION

Figure 1 displays SEM images and photos of both systems, illustrating uniform faithfully transferred and directed PCM metasurface across the entire area (1 cm^2).

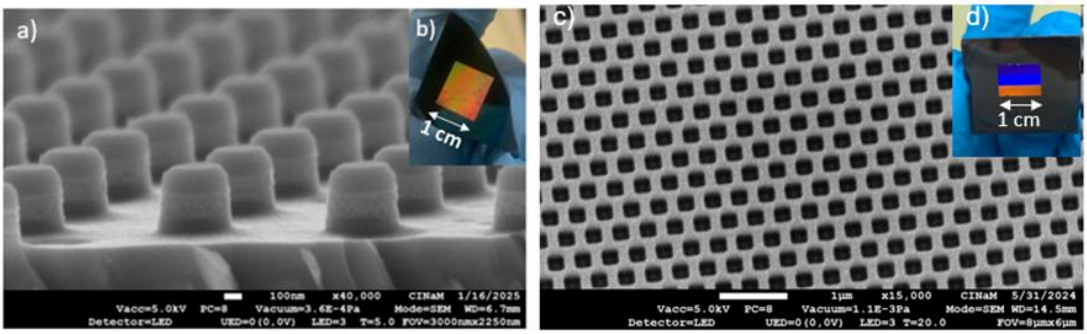

Fig. 1: (a) SEM images and (b) photos of GeTe metasurface fabricated via the etching strategy; (c) SEM images and (d) photos of GeTe metasurface produced by the template strategy. Both samples were produced on 1×1 cm^2.

The etching strategy approach was selected as the optimal method allowing faithful replica and significant modulation of optical responses, with reflection contrasts up to ~2.3 and transmission variations up to ~3.7 in the near-infrared (NIR) range. These metasurfaces were modeled using numerical simulations (planopsim). The impact of the phase transition on transmission and reflection was compared with simulations (see Fig. 2). Laser-induced switching of individual PCM meta-atoms was also investigated, confirming the potential for dynamic optical modulation. This comprehensive approach demonstrates the viability of PCM integration in advanced photonic architectures, supporting applications in polarization control, flat reconfigurable optics, and multispectral filtering.

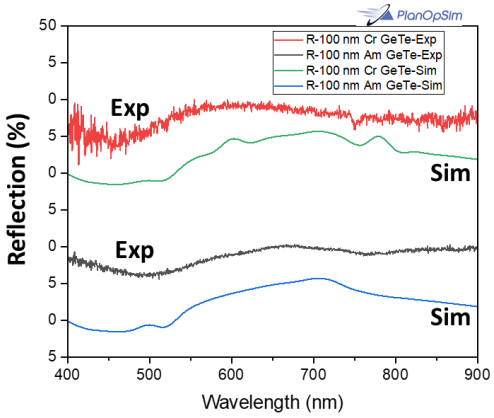

Fig.2: Experimental and simulated reflection of a combined silica-GeTe metasurface prepared by "NIL as a mask approach".

4. CONCLUSION

We have developed a scalable strategy for fabricating PCM-based tunable metasurfaces by combining soft-NIL and phase-change materials. This strategy is scalable, versatile and cost-effective. This work opens the pathways for next-generation metasurface-based devices featuring dynamic functionalities such as tunable metalenses, switchable polarizers, and multispectral optical filters.

REFERENCES

[1] N. Yu, P. Genevet, A.K. Mikhail, F. Aieta, J.-P. Tetienne, F. Capasso, Z. Gaburro. **Science** (2011), 334, 6054. https://doi.org/10.1126/science.1210713
[2] M. Wuttig, H. Bhaskaran, T. Taubner. **Nat. Photonics** (2017), 11 (8), 465–476. https://doi.org/10.1038/nphoton.2017.126
[3] T. Bottein, O. Dalstein, M. Putero, A. Cattoni, M. Faustini, M. Abbarchi, D. Grosso. **Nanoscale** (2018), 10, 1420–1431. https://doi.org/10.1039/C7NR07491C
[4] M. Modaresialam, Z. Chehadi, T. Bottein, M. Abbarchi, D. Grosso. **Chem. Mater.** 2021, 33, 5464–5482. https://doi.org/10.1021/acs.chemmater.1c00693

P-11

Nanostructures with low-loss phase-change materials: Towards large-scale reconfigurable nanophotonics

Fouad BENTATA[1,2,3], Mouad MRAOUNI[1,3], Celine CHEVALIER[1], Lotfi BERGUIGA[1], Xavier LETARTRE[1], Tam Trong NGUYEN[1], Capucine LAPRAIS[1], Nicolas BABOUX[1], Guillaume SAINT-GIRONS[1], Hai Son NGUYEN[1], Stephane MONFRAY[3], Patrice GENEVET[2,4], Sébastien CUEFF[1*]

[1]Université de Lyon, Institut des Nanotechnologies de Lyon–INL, CNRS UMR 5270 Ecole Centrale de Lyon, Ecully, 69134 France.
[2]Université Côte d'Azur, CNRS, CRHEA, Sophia Antipolis 06560 Valbonne, France.
[3]STMicroelectronics, 38920 Crolles, France.
[4]Physics department, Colorado School of Mines, Golden, CO-80401, USA.
*Corresponding author: sebastien.cueff@ec-lyon.fr

ABSTRACT

The direct patterning of Sb_2S_3 using standard lithography proves challenging due to its high chemical reactivity and low adhesion. Here, we present an alternative method for realizing tunable metasurfaces with Sb_2S_3 without damage. We successfully demonstrate photonic bandstructure tuning and present a reconfigurable structural color platform using Sb_2S_3.

Key words: Tunable metasurfaces, Phase change materials, Antimony trisulfide.

1. INTRODUCTION

Phase change materials (PCMs) have emerged as multifunctional materials for reconfigurable metasurface devices due to their reversible and non-volatile modulations of physical properties [1]. Among these materials, Sb_2S_3, originally used in solar cells, has been proposed as an emerging PCM for tunable optics in the visible and infrared range, thanks to its large bandgap and significant refractive index contrast ($\Delta n > 0.7$) between its amorphous and crystalline phases [2]. Despite the promising potential of Sb_2S_3, experimental demonstrations employing it in nanostructured reconfigurable devices are relatively scarce. The primary reason is its chemical instability, as it strongly reacts with most of the chemicals used in standard nanofabrication processes [3]. Here, we address the challenge of high-resolution patterning of Sb_2S_3 by eliminating direct exposure of the material to chemicals. Using this technique, we achieved high-resolution nanofabrication down to 80 nm. The optical tuning performance of the Sb_2S_3-based metasurfaces is evidenced by the experimental demonstration of tunable Dirac cone dispersion in the near-infrared and by the tuning of a metasurface structural color display.

2. EXPERIMENTAL

Sb_2S_3 is deposited in the amorphous state using e-beam evaporation. Subsequently, a protective layer of SiO_2 is deposited on top to prevent oxidation and sulfur loss during crystallization. The patterned metasurfaces are thermally crystallized at 280°C on a hot plate to demonstrate their

tunability. RCWA and FDTD simulations are employed to simulate photonic band structures and extract color palettes used for structural color.

3. RESULTS & DISCUSSION

We demonstrated the potential of Sb_2S_3 by designing a metasurface exhibiting Dirac cone dispersion in the wavelength range of 700–900 nm. The Dirac cone was tuned through crystallization of the metasurface, showcasing active control over its photonic properties.

To further highlight the low optical losses of Sb_2S_3 in the visible range, we designed a structural color metasurface capable of spanning the full RGB spectrum in its amorphous phase. Upon crystallization, the metasurface exhibited dramatic color changes, demonstrating its applicability for tunable structural color displays.

4. CONCLUSIONS

In conclusion, we have demonstrated capability to employ Sb_5S_3 in reconfigurable metasurfaces while avoiding all the complex challenges of classical lithography on the material, showing its potential. We proved this through active photonic band structure tuning and tunable structural color. Our work should thus enable faster development of Sb_2S_3-based metasurfaces.

REFERENCES

1. E. Mikheeva et al., *ACS photonics* **9** (2022).
2. M. Delaney et al., Adv. Funct. Mater. **30** (2020).
3. P. Moitra et al., Adv. Mat. **35** (2023).

P-13

Sol-gel-based Vanadium Dioxide Thin Film and Conformal Metasurface

Y. Ramanda[1], J. Remondina[2], M. Putero[2], V. Malgras[1] and D. Grosso[1,3*]
[1]Aix-Marseille Université, CNRS, CINaM, Marseille, 13009, France
[2]Aix-Marseille Université, CNRS, IM2NP, Marseille, 13013, France
[3]Solnil, Pépinière d'entreprises Luminy Biotech, 13009, Marseille FRANCE
*corresponding author: david.grosso@univ-amu.fr

ABSTRACT

Vanadium dioxide (VO_2) is a leading volatile phase-change material, demonstrating an insulator-to-metal transition near room temperature with abrupt switching properties. Despite its potential, scalable fabrication remains challenging. This study demonstrates the fabrication of VO_2 thin films and conformal metasurfaces using a sol-gel approach, achieving an exceptional performance with a refractive index contrast of 1.06, which advances scalable synthesis for photonic and electronic applications.

Key words: Sol-gel, Vanadium Dioxide.

1. INTRODUCTION

Vanadium dioxide (VO_2) demonstrates exceptional properties due to its rapid, reversible transition between insulating and metallic states.[1] This unique behavior enables practical applications including thermochromic smart windows, high-speed photonic devices, and neuromorphic computing systems.[2] The material undergoes a structural phase change from monoclinic to rutile crystal symmetry when heated through its transition temperature, accompanied by abrupt changes in electrical and optical properties.

Current manufacturing challenges limit the commercial implementation of VO_2 technologies. Vacuum deposition techniques yield excellent films but prove impractical for large-scale production. Solution processing methods offer a viable alternative, though traditional approaches based on vanadium pentoxide precursors require extended processing under controlled atmospheres.[3] This study develops an improved solution-based approach using optimized molecular precursors and thermal treatments. This method achieves thin films with switching characteristics comparable to vacuum-deposited counterparts while offering significantly superior scalability for industrial applications. These advances address critical barriers to the commercial adoption of VO_2-based devices.

2. EXPERIMENTAL

The VO_2 thin films were synthesized via a sol-gel approach using vanadium acetylacetonate ($VO(acac)_2$) as the precursor. Dip-coating followed by vacuum annealing at 600°C was used for thin film fabrication. The phase transition dynamics were characterized by *in situ* X-ray diffraction (XRD) combined with sheet resistance measurements (Rs), while the evolution of optical properties was analyzed via *in situ* spectroscopic ellipsometry. A conformal VO_2 metasurface was fabricated by dip-coating onto a soft-NIL SiO_2 substrate, followed by thermal treatment for optimum VO_2 thin film. The performance of the conformal metasurface was evaluated by spectrophotometry. The switching performances of each pixel of the conformal metasurface have been calculated considering the reflection contrast between the two states.

3. RESULTS & DISCUSSION

The study first optimized VO_2 thin film fabrication by testing vacuum thermal treatments at 600°C with varying heating rates. These experiments revealed that heating rate significantly affects film performance, with 2°C/s yielding optimal switching properties (Figure 1 showing the optical switching property). The second phase involved conformal metasurface fabrication, with Figure 2A showing the fabrication process and Figure 2B presenting the resulting SEM image. The reflection spectrum of the metasurface was recorded at 25°C and 90°C, as shown in Figure 2C. Spectral analysis revealed that increasing pillar diameters red-shifted the peak switching performance, demonstrating a structure-property relationship, as shown in Figure 2D.

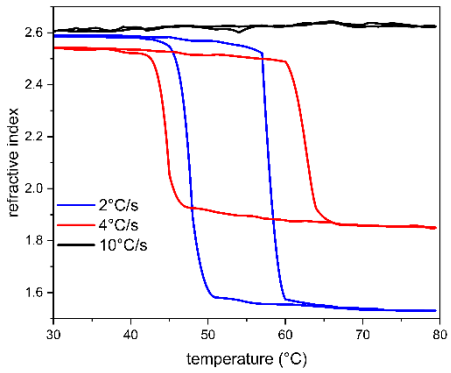

Figure 1. The refractive index evolution during the phase transition of VO_2 thin films prepared with different ramping rates.

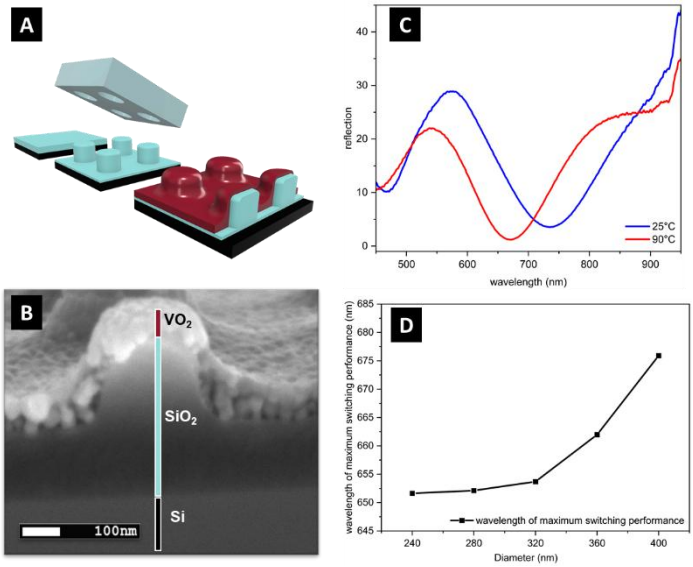

Figure 2. Characterization of the conformal metasurface. (A) fabrication schematic, (B) SEM image, (C) reflection spectra, and (D) relationship between pillar size and maximum switching wavelength.

4. CONCLUSIONS

The optimized sol-gel synthesis of VO_2 thin films using $VO(acac)_2$ eliminates reducing atmospheres while preserving phase purity. Controlled ramping at 2°C/s produced films with large crystallites, high optical contrast ($\Delta n = 1.06$), and sharp resistance switching (10^2 contrast). These films enabled tunable visible-light metasurfaces, demonstrating potential for dynamic photonic and optoelectronic applications.

REFERENCES

(1) Gutiérrez, Y.; Vázquez-Miranda, S.; Espinoza, S.; Khakurel, K.; Rebarz, M.; Zhang, Z.; Saiz, J. M.; Ramanathan, S.; Cueff, S. Subpicosecond Spectroscopic Ellipsometry of the Photoinduced Phase Transition in VO_2 Thin Films. *ACS Photonics* **2024**, *11* (11), 4883–4893. https://doi.org/10.1021/acsphotonics.4c01414.

(2) Ke, Y.; Wang, S.; Liu, G.; Li, M.; White, T. J.; Long, Y. Vanadium Dioxide: The Multistimuli Responsive Material and Its Applications. *Small* **2018**, *14* (39), 1802025. https://doi.org/10.1002/smll.201802025.

(3) Wang, S. Recent Progress in VO2 Smart Coatings: Strategies to Improve the Thermochromic Properties. *Prog. Mater. Sci.* **2016**.

P-15

VO_2 nanostructures with controlled hysteresis for multilevel nanoscale switchable devices

P. Kalousková[1], P. Kepič[2], M. Horák[2], T. Šikola[1,2], and F. Ligmajer[1,2*]

[1] Faculty of Mechanical Engineering, Brno University of Technology, Brno, Czechia
[2] Central European Institute of Technology, Brno University of Technology, Brno, Czechia
*corresponding author: filip.ligmajer@vutbr.cz

ABSTRACT

We present VO_2 nanostructure arrays with tunable hysteresis for multilevel nanoscale optical switchable devices. By controlling size and annealing conditions, we can tailor their phase-transition behavior and optical contrast. Electron beam lithography enables precise patterning, while thermal treatment induces the necessary crystallization and dewetting. These nanostructures offer scalable, energy-efficient switching elements for next-generation integrated nanophotonic and neuromorphic computing applications.

Key words: vanadium dioxide, insulator-metal transition, hysteresis control, dewetting

1. INTRODUCTION

Phase-change materials, with their solid–solid transition accompanied by a significant change of optical properties, play an important role in nanophotonics. The most utilized materials in this field are chalcogenide glasses, as they exhibit a nonvolatile amorphous–crystalline phase change accompanied by significant optical modulation [1]. Unfortunately, while energy consumption for retaining the data is zero, writing them requires an ultrafast melt-quench process at above 600°C and 10°C/ns [2]. In scenarios such as neuro-morphic computing [3] or random-access memories [4], a volatile phase-change material, vanadium dioxide (VO_2) can represent a more efficient solution: its insulator-metal transition requires only nanojoules of energy at microscale [5] and can be pushed down to room temperature by doping. In our recent work [6], we studied individual VO_2 nanoparticles (NPs) that exhibit metal-insulator transition at temperatures below 40°C, significantly decreasing the footprint and retention energy. Besides showing the transition temperatures' dependence on the NP's size, we proposed a concept of multi-level optical memory. However, to implement these nanostructures into an actual integrated device, the key aspect is to be able to fabricate them at specific positions with the desired hysteretic properties. Here, we show that one can create a versatile library of nanostructures with the specific optical contrast and transition temperature. Such a library is the crucial step towards implementing VO_2 nanostructures into tunable multilevel integrated nanophotonic devices.

2. EXPERIMENTAL

When amorphous 30 nm VO_2 film, deposited at room temperature by pulsed laser deposition (10 Hz, 2 J/cm^2, 5 mTorr of O_2, V target), is annealed (10 min, vacuum, 15 sccm O_2 flow), we can observe crystallization and dewetting of this film into individual NPs with increasing annealing temperature (see Fig. 1a). The increase of crystallization and NP separation with decreasing volume results in significant broadening of hysteresis [6] and reduction of memory-retention energy. However, the dewetting of the film is a stochastic process, and it is hard to control the NP's position, size, and hysteretic properties. To achieve this control, we fabricated arrays (spacing = 1.5 diameter) of amorphous (non-switching) VO_2 nanostructures with 30 nm height. We used positive resist electron beam lithography and the same deposition process and annealing conditions as for the films above.

3. RESULTS & DISCUSSION

Fig. 1c shows AFM micrographs of the annealed nanostructures with diameters listed in the graph. We can see that the crystallization and dewetting process occur at the same temperatures and with

almost the same effect as films. Even more interesting is that nanostructures (up to 400 nm) can be dewetted into individual NPs with up to 220 nm diameters. Moreover, there are always a few nanometers of ultrathin film beneath the dewetted NPs. In the upcoming period, we will study the hysteresis of these nanostructures using the infrared camera and 1550 nm light so we can obtain the library of building blocks for multilevel integrated photonic memory.

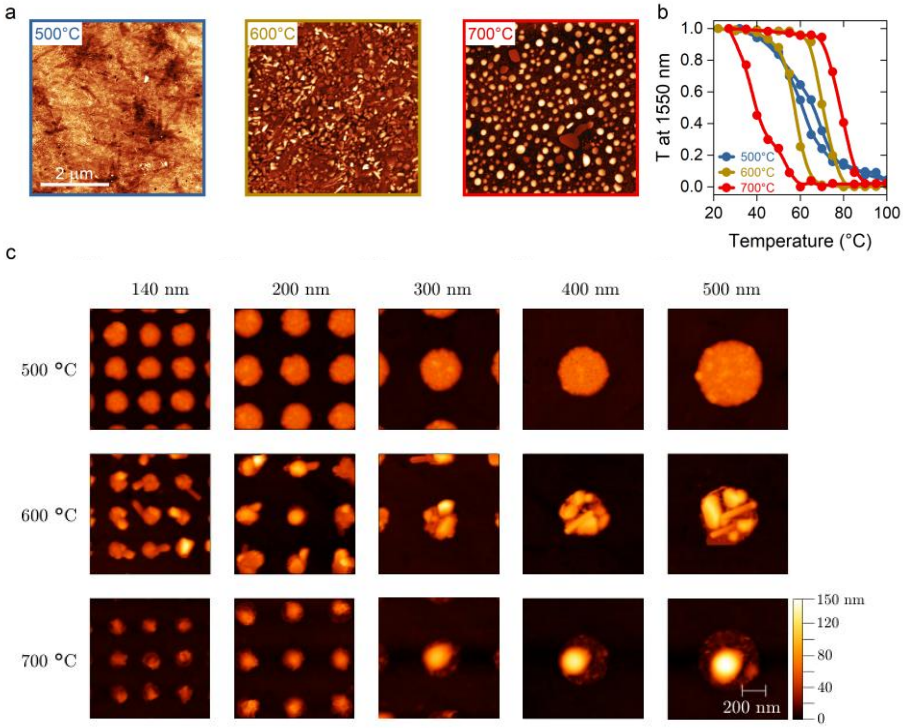

Fig. 6. a) AFM micrographs of 30 nm VO_2 films annealed for 10 minutes in a vacuum furnace with 15 sccm oxygen flow at listed temperatures. b) Transmission at 1550 nm wavelength as a function of temperature, showing hysteresis behavior of VO_2 films from (a) with hysteresis width significantly increasing when film dewetted into NPs at higher annealing temperature. c) AFM micrographs of lithographically patterned VO_2 nanostructures, with diameters listed in the graph, and annealed at listed temperatures

4. CONCLUSIONS

Here, we studied the hysteresis characteristics of the lithographically patterned VO_2 nanostructures annealed at various temperatures. By controlling their size and annealing temperature, we can create a library from which a desired combination of NPs can be chosen to create multilevel integrated photonic devices.

REFERENCES

1. M. Wuttig, H. Bhaskaran, T. Taubner: Phase-change materials for non-volatile photonic applications. Nat. Phot. **11** (2017) 465.
2. S. Abdollahramezani et al.: Electrically driven reprogrammable phase-change metasurface reaching 80% efficiency. Nat. Comm. **13** (2022) 1696.
3. P. Schofield et al..: Harnessing the Metal− Insulator Transition of VO_2 in Neuromorphic Computing. Adv. Mat. **35** (2023) 2205294.
4. Y. J. Lee et al.: Nanoelectronics Using Metal−Insulator Transition. Adv. Mat. **36** (2024) 2305353.
5. J. Parra et al.: Low-threshold power and tunable integrated optical limiter based on an ultracompact VO_2/Si waveguide. APL Phot. **6** (2021) 121301.
6. P. Kepič et al.: Coexisting Phases of Individual VO_2 Nanoparticles for Multilevel Nanoscale Memory. ACS Nano **19** (2025) 1167.

P-17

Fabrication-friendly Plasmonically-enhanced All-optical Integrated Photonic Phase-change Memory

J. Song[1], J. Pady[1], E. Gemo[2], N Farmakidis[3], H. Bhaskaran[3], I. Bente[4], W. H. P. Pernice[4,5] and C. D. Wright[1*]

[1] Centre for Metamaterial Research and Innovation, University of Exeter, UK
[2] Department of Electronics and Telecommunications, Politecnico di Torino, Torino, Italy
[3] Department of Materials, University of Oxford, Oxford OX1 3PH, UK
[4] Institute of Physics, University of Münster, Heisenberg. 11, 48149 Münster, Germany.
[5] Kirchhoff-Institute for Physics, Heidelberg University, Im Neuenheimer Feld 227, Germany.
*corresponding author: David.Wright@exeter.ac.uk

ABSTRACT

The device switching behaviour and optical properties of plasmonically-enhanced, all-optical, integrated photonic phase-change memory are determined by a combination of finite-element thermo-optic and bespoke phase-change computational models. Switching energies in the tens of pico-Joule range and switching speeds in the tens of nanosecond range are demonstrated for devices which offer a simple route for fabrication.

Key words: Integrated Photonics, Plasmonic Enhancement, In-memory Computation

1. INTRODUCTION

Rapid switching and energy-efficient integrated photonic phase-change memory and computing devices can be realised using the electric field enhancing properties of plasmonic resonant structures [1]. Previous designs, however, required the challenging (from a fabrication perspective) deposition of a nanoscale volume phase-change material (PCM) into the gap region of plasmonic dimer nanoantennas, themselves deposited on top of a Si_3N_4 waveguide [1]. Here, we develop a simpler structure consisting of a relatively large 'patch' of PCM (here $Ge_2Sb_2Te_5$ (GST)) deposited on top of the waveguide, with the dimer nanoantenna being fabricated directly onto this GST patch. This configuration can be seen in Fig. 1a and offers a simpler fabrication route. In spite of the PCM region not being directly in the gap region of the nanoantennas, but underneath it, finite element (FE) simulations reveal a very significant enhancement of the electric field in the PCM layer in the gap region when an optical pulse is applied to the waveguide (see Fig. 1b). This enhancement

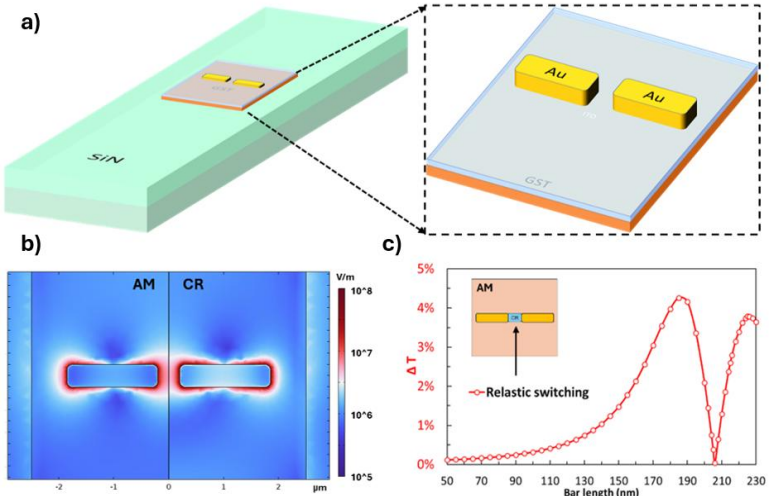

Fig. 1 a) The simplified all-optical plasmonically enhanced cell. A 500 x 500 nm GST patch 10 nm in thickness with a 5 nm thick ITO capping layer is deposited on top of a 1200 x 334 nm Si_3N_4 waveguide. On top of this are 40 nm wide, 30 nm thick Au bars. b) Normalised E-field distributions for the amorphous and crystalline phases. c) Optical contrast as a function of Au bar length, assuming realistic phase switching.

triggers a temperature increase sufficient for crystallising and amorphising the GST in the area between the nanoantennas. Figure 1c shows, for a range of Au antenna bar lengths, the optical contrast in device optical transmission achieved assuming a GST region of approximately 50x50 nm undergoes phase switching, with a maximum contrast seen at an antenna bar length of ~185 nm. To explore the phase switching in these devices, thermo-optic FE simulations are here coupled to a phase-change model based on a Gillespie-type cellular automata and classical nucleation and growth theory [2,3].

2. RESULTS & DISCUSSION

Using the previously described modelling techniques, the switching behaviour of the simplified plasmonic cell is demonstrated. Initially, the device starts in a fully amorphous configuration as this phase demonstrates lower insertion losses at a bar length 185 nm. A train of 1550 nm optical pulses with decreasing powers of 2.8, 1.3, 1.2, 0.95 mW is applied for 8 ns each; this crystallises the region between the antennas (see Fig. 2a). To re-amorphise, a single 2 mW, 8 ns pulse is used (see Fig. 2b). Figure 2c shows the resulting change in crystalline fraction within the central 50 x 50 nm region between the Au bars during crystallisation, as well as the optical contrast (which, at ~ 4.5% is in good agreement with that calculated in Fig. 1c). The switching energies for the crystallisation and re-amorphisation pulses are 50 and 16 pJ respectively. These energies are considerably smaller than what is typical for conventional phase-change photonic cells without plasmonic field enhancement [4] and similar to, although slightly larger than, previous more complex plasmonic cell designs [1].

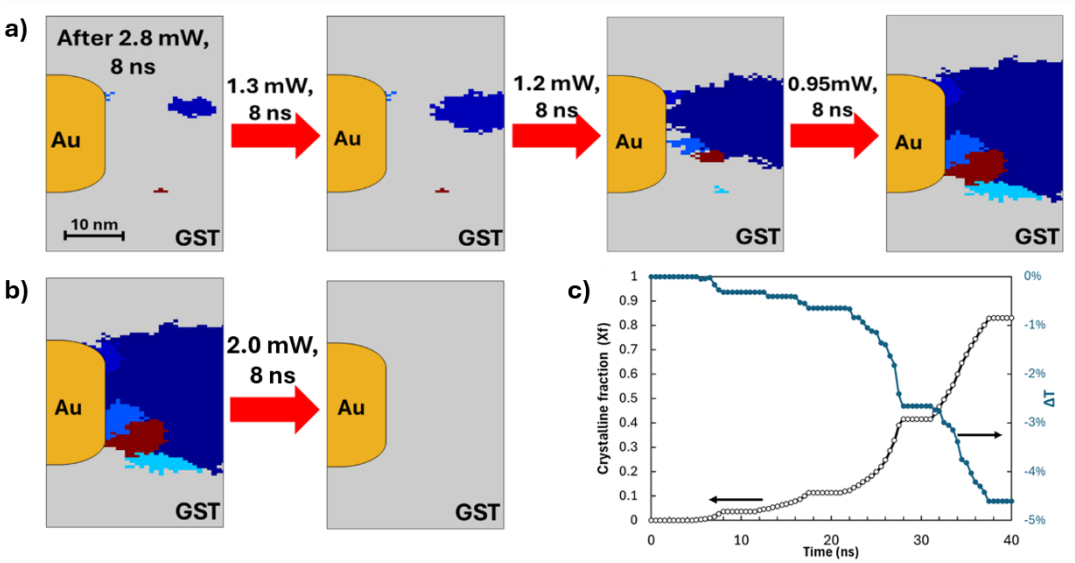

Fig. 2 a) Evolution of the GST phase distribution as a succession of crystallising optical pulses is applied. b) Change in GST phase distribution as a re-amorphising pulse is applied. Regions of colour represent crystallite grains of different orientations. c) Evolution of GST crystalline fraction in a 50 x 50 nm region centralised between the Au bars and the readout contrast both during the crystallisation shown in a).

3. CONCLUSIONS

Combined FE and phase-change simulations of a simple-to-fabricate, all-optical plasmonically enhanced phase-change cell have shown re-writable switching at lower energies and faster speeds than conventional configurations.

Funding is acknowledged from the EU Phoenics Project (101017237) and the EPSRC APT-NuCOM project (EP/W022931/1)

REFERENCES

1. E. Gemo, et al. *Opt. Express*, **27**, 17 (2019), 24724-24737.
2. P. Ashwin et al., *J. Appl. Phys.* **104** (2008) 084901.
3. Y. Wang et al., *npj Comput. Mater.* **7** (2021) 183.
4. C. Ríos et al., *Nat. Photonics* **9** (2015) 725-732.

P-19

Optical characterization of GeTe-Sb_2Te_3 heterostructures prepared by pulsed laser deposition

K. Shportko[1], S. Cremer[2], A. Lotnyk[2]
[1]V.E. Lashkaryov Institute of Semiconductor Physics of NAS of Ukraine, Nauki av. 41, 03028Kyiv, Ukraine, k.shportko@ukr.net,
[2]Leibniz Institute of Surface Engineering, Permoser str. 15, 04318 Leipzig, Germany, andriy.lotnyk@iom-leipzig.de

ABSTRACT

This work presents the fabrication and optical characterization of GeTe–Sb_2Te_3 heterostructures prepared by pulsed laser deposition. Spectroscopic ellipsometry has shown that the optical properties of these multilayers are governed by interfacial interdiffusion and layer thickness, leading to the formation of amorphous Ge–Sb–Te alloy regions in thinner films.

Key words: heterostructures, phase-change materials, optical properties.

1. INTRODUCTION

For several decades, germanium-based tellurides—widely recognized as phase-change materials—have attracted considerable attention due to their potential for use in non-volatile memory technologies and photonic applications. In recent years, the development of chalcogenide-based heterostructures has emerged as a promising approach to further enhance the functional performance of these materials. To support the advancement of next-generation devices, a thorough understanding of their optical properties is crucial.

2. EXPERIMENTAL

GeTe–Sb_2Te_3 heterostructures were deposited at room temperature by pulsed laser deposition using a 248 nm KrF excimer laser in an Ar-assisted UHV environment. Alternating ablation of GeTe and Sb_2Te_3 targets enabled the fabrication of periodic and non-periodic multilayers on SiO_2/Si(100) substrates. To prevent oxidation, the structures were capped with $LaAlO_x$ or SiO_2 layers [1].
The heterostructures were characterized at room temperature using spectroscopic ellipsometry in the 0.7–5 eV range. The experimental data was analyzed in the same way as in [2].

3. RESULTS

The effective dielectric function of heterostructures (Figure 1), as well as the dielectric functions of individual layers (Figure 2) within the studied heterostructures, were obtained from the fit of the spectroscopic ellipsometry data.

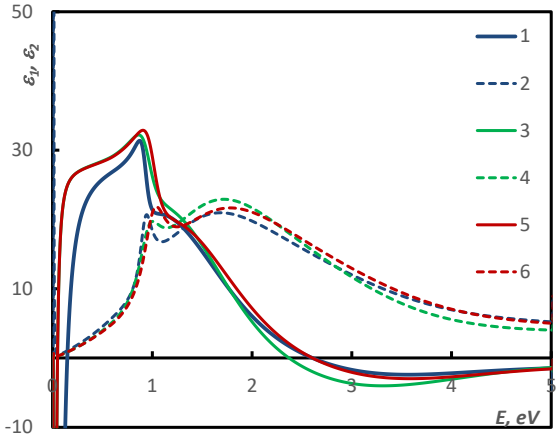

Figure 1. Effective dielectric function of heterostructures: 1, 2 – ML1, 3, 4 – ML2, 5, 6 – ML3.

Quantitative analysis of the dielectric functions displayed in the Fig. 2 has indicated that studied heterostructures are composed of an amorphous GeTe phase and a crystalline Sb_2Te_3 phase. Detailed analysis of optical data revealed interdiffusion of germanium into Sb_2Te_3 layers and antimony into GeTe layers, forming Ge–Sb–Te alloy (Fig. 2, curves 5 and 6) regions and indicating a notable degree of atomic intermixing at the interfaces [1].

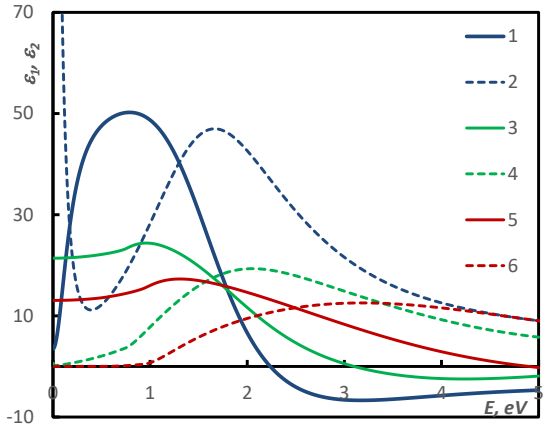

Figure 2. Real and imaginary part of the dielectric functions of individual layers:
1, 2 - Sb_2Te_3, 3, 4 - Ge-Sb-Te, 5, 6 – GeTe.

Further analysis of the optical data of several different heterostructures has shown that this interdiffusion is strongly influenced by the thickness of the layers: thinner layers exhibited more pronounced intermixing, leading to the formation of amorphous ternary Ge–Sb–Te alloy regions.

4. CONCLUSIONS

This study investigated the optical properties of GeTe–Sb_2Te_3 heterostructures. The findings demonstrate that these properties are predominantly governed by the interplay between interdiffusion processes and individual layer thicknesses. Specifically, the formation of ternary Ge–Sb–Te alloy regions was found to be strongly dependent on the thicknesses of the GeTe and Sb_2Te_3 layers.

These insights highlight the potential for tailoring heterostructure design to enhance the performance of phase-change materials, thereby broadening their scope of practical applications in optoelectronic and memory devices.

REFERENCES

1. S. Cremer, et. al., Applied Surface Science, **655** (2024), 159679.

2. K. Shportko, *Sci. Rep.* **9** (2019) 6030.

P-21

Optimisation of Device Readout Efficiency for Phase-Change Integrated Photonic Computing

J. Pady[1], J. Song[1], R. Xu[2], N. Farmakidis[3], H. Bhaskaran[3], W. H. P Pernice[2], C. D. Wright[1*]

[1]Centre for Metamaterial Research and Innovation, University of Exeter, UK.
[2] Kirchhoff-Institute for Physics, Heidelberg University, Im Neuenheimer Feld 227, Germany.
[3] Department of Materials, University of Oxford, Oxford, UK.
*corresponding author: David.Wright@exeter.ac.uk

ABSTRACT

The design of $Ge_2Sb_2Te_5$ (GST) cells commonly used in integrated phase-change photonic devices is investigated using coupled finite-element and phase switching modelling techniques, with a view to improving device readout efficiency. Results show that small cells not covering the entire width of the waveguide deliver significantly improved readout performance as compared to the conventional approach.

Key words: Integrated Photonics, Optical Memory, Optimisation.

1. INTRODUCTION

The phase-change material $Ge_2Sb_2Te_5$ (GST) can be used for the realisation of non-volatile optical memory and computing in integrated photonic systems [1]. Typically, these devices consist of a GST cell (along with a thin capping layer such as Al_2O_3) deposited onto a SiN (or Si) waveguide, as shown in Fig. 1a. Light propagating in the waveguide couples evanescently to the GST (see Fig. 1b), triggering heating and switching the state of the GST cell. The resulting alteration of device optical transmission provides memory [1] and computing [2] functionality. In this work, the GST cell geometry is investigated to optimise the device readout efficiency. These optimisations are carried out using finite-element thermo-optic simulations coupled to a bespoke phase-change model based on a Gillespie-type cellular automata and classical nucleation and growth theory [3,4].

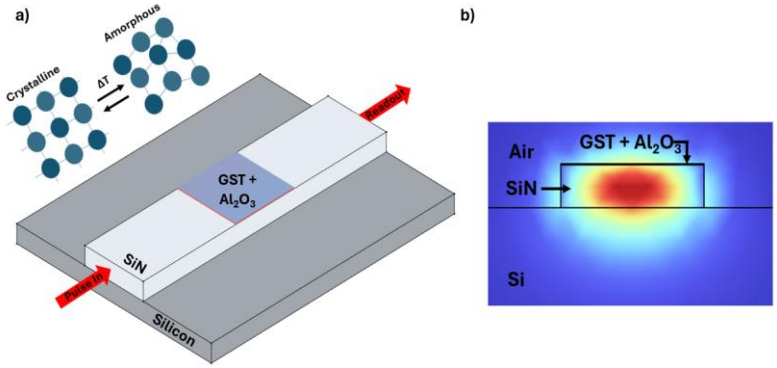

Fig. 1 a) Schematic of a 'conventional' integrated photonic phase-change memory device. A 10 nm GST layer with a 5 nm Al_2O_3 capping is fabricated on top of a Si_3N_4 waveguide 1.2 µm in width and 334 nm high. b) Simulated cross-section of the waveguide in operation showing the TE mode which couples evanescently to the GST cell.

2. RESULTS & DISCUSSION

Firstly, the effect of reducing the width of the GST cell across the waveguide is investigated. Figure 2a shows the GCA-simulated phase distribution obtained when writing an amorphous mark into a cell with a fully crystalline starting state and of various patch cell widths, using a 1550 nm, 10 mW, 25 ns *write* pulse. This clearly demonstrates that reducing cell width increases the fraction of GST that is amorphised, which in turn will affect the device readout efficiency. To quantify this change in readout efficiency and to determine a method to find optimised GST cell dimensions, a figure of merit (FOM) is defined using the device insertion loss (IL) and extinction ratio (ER) where FOM = ER/IL [5]. Fig. 2b shows the FOM values obtained for a range of GST cell widths, showing that

reducing GST width improves the readout efficiency. Next the effect of reducing GST cell length was investigated: a fixed cell width of 0.6 µm was selected for this, slightly larger than the width having the highest FOM in Fig. 2b, but a size that should be readily manufactured. Results are shown in Fig. 2c (blue line). We note that the FOM values in this work are smaller, but more realistic, than those that would be obtained by assuming, as in [5] for example, that the entirety of the GST undergoes amorphisation (red line Fig. 2c). Figure 2c suggests that the optimum GST length is 1.0 µm, with an FOM value of approximately 6.5. Therefore, for the waveguide used here, a cell dimension of around 1.0 x 0.6 µm positioned in the central region of the waveguide is suggested to be 'optimum', taking both readout optimisation and potential fabrication considerations into account. Figure 2d shows the change in crystalline fraction and optical transmission of this device as it undergoes the *write* process. Here, despite the reduced GST patch size, a transmission contrast easily sufficient for achieving multilevel switching is still achieved.

Experimental studies of the improvement in device readout efficiency that can be obtained by optimisation of the size and placement of the GST cell are now ongoing and results will be presented at the conference. Figure 2e shows an SEM image of one of the fabricated devices.

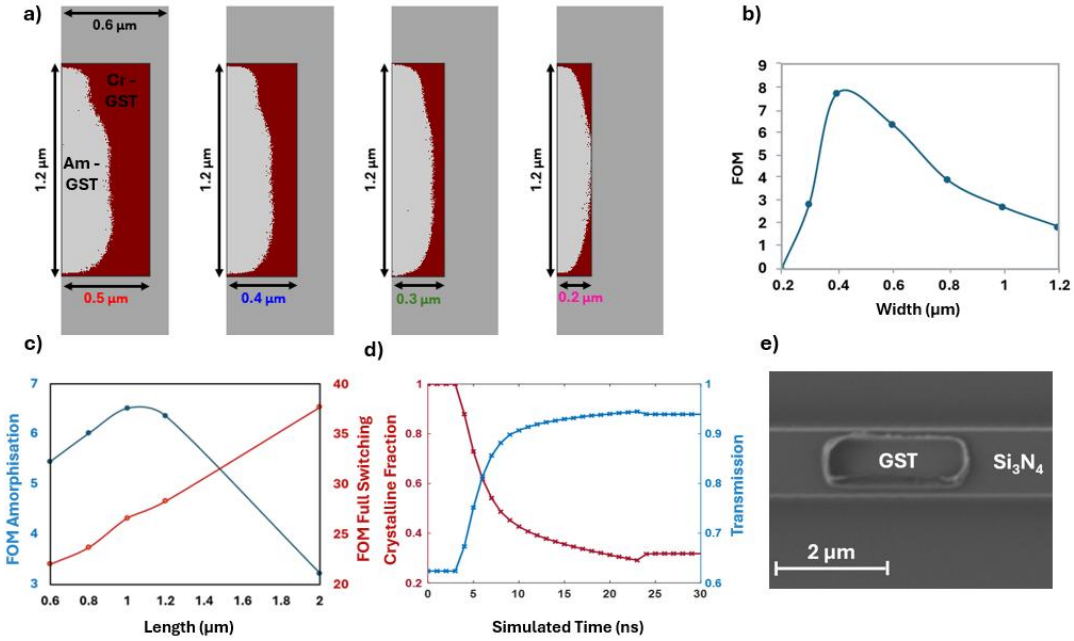

Fig. 2 a) GST phase distribution in devices with cells 1.2 µm in length and 1.0, 0.8, 0.6 and 0.4 µm in width after the *write* pulse is applied. b) The FOM values resulting from varying the GST cell width. c) FOM values resulting from varying the GST length in blue. In red - FOM if the entirety of the GST cell is assumed to be amorphised. d) Change in crystalline fraction and transmission as a function of time during the write pulse for the 1.0 x 0.6 µm 'optimum' cell size. e) SEM image of a fabricated GST photonic cell.

3. CONCLUSIONS

The optimisation of GST cell dimensions for phase-change integrated photonic memory and computing devices has been carried out. Reducing cell width and length to eliminate non-switching areas was shown to significantly improved readout efficiency.

Funding is acknowledged from the EU Phoenics Project (101017237) and the EPSRC APT-NuCOM project (EP/W022931/1).

REFERENCES

1. C. Ríos et al., *Nat. Photonics* **9** (2015) 725-732.
2. J. Feldmann et al., *Nature* **589** (2021) 52–58.
3. P. Ashwin et al., *J. Appl. Phys.* **104** (2008) 084901.
4. Y. Wang et al., *npj Comput. Mater.* **7** (2021) 183.
5. J. Parra et al., *Sci. Rep.* **12** (2022) 9774.

P-23

Pushing the limits of embedded phase-change memories with innovative Se-rich alloys

P. Meilleur[1,2,*], O. J. Mouawad[1], M. Tomelleri[1], J.-B. Dory[1], N. Bernier[1], Y. Brûlé[1], J. Lagrave[1], J.-Y. Raty[1,3], D. Benoit[2], F. Hippert[4] and P. Noé[1,*]

[1] Univ. Grenoble Alpes, CEA, LETI, F-38000, Grenoble, France.
[2] STMicroelectronics, F-38926 Crolles, France.
[3] FRS-FNRS, CESAM, Université de Liège, Sart-Tilman 4000, Belgium.
[4] Univ. Grenoble Alpes, CNRS, Grenoble INP, LMGP, F-38000 Grenoble, France.
*Corresponding authors: pierre.meilleur@cea.fr ; pierre.noe@cea.fr

ABSTRACT
$GeSe_{1-x}Te_x$ phase-change alloys are gaining traction as promising materials for embedded phase-change memory (ePCM) applications, offering a promising balance between device performance and application requirements. Recent prototype devices based on these alloys have demonstrated endurances exceeding 10^4 programming cycles. In this work, we analyze the phase-change mechanism involved in test vehicle devices in order to introduce novel strategies to mitigate undesirable effects induced by repeated programming pulses to significantly enhance device reliability. This study represents the first significant step toward enhancing the reliability, endurance, and scalability of Se-based phase-change devices, positioning them as strong contenders for next-generation embedded phase-change memory (ePCM) technologies.

Keywords: chalcogenide, GeSeTe, embedded phase-change memory, thermal stability

1. INTRODUCTION

Chalcogenide phase-change materials are particularly well-suited for phase-change data storage applications due to the high resistivity contrast between their amorphous and crystalline phases [1]. In ePCM, amorphous phase thermal stability against undesired crystallization is essential to ensure data retention under thermal stress [2]. This is commonly achieved by Ge enrichment of the canonical $Ge_2Sb_2Te_5$ alloy [3]. Recently, $GeSe_{1-x}Te_x$ alloys have emerged as promising alternatives [4]. Thin films of these materials exhibit a significant increase in crystallization temperature (T_x) with decreasing Te content, while preserving a strong resistivity contrast and showing minimal phase separation upon crystallization. As already demonstrated in GeTe [5], nitrogen "doping" (~10 at. %) of $GeSe_{1-x}Te_x$ alloys further improves their thermal stability and film morphology after crystallization [6]. Therefore, prototypical $GeSe_{1-x}Te_x$ alloy compositions were selected and integrated into CEA-Leti's Mad200 test vehicles for electrical characterization. Using Scanning Transmission Electron Microscopy (STEM), we analyze PCM devices programmed in SET and RESET states, with the aim of further improving devices performance through material optimization strategies.

2. EXPERIMENTAL

$Ge_{1+\delta}Se_{1-\delta-x}Te_x$ thin films of 25, 50, and 100 nm with $0 \leq x \leq 0.44$ and $-0.12 \leq \delta \leq 0.12$ were deposited on 300 mm Si wafers by magnetron co-sputtering of GeSe, GeTe, Ge and $GeSe_2$ targets in an Ar atmosphere. The sputtering powers were tuned to adjust the films composition. For nitrogen-doped samples, a controlled N_2 gas flow was introduced in Ar sputtering plasma during deposition. Resistivity measurements were carried out on additional films deposited on thermally oxidized bulk Si wafers. All films were capped after deposition with a 10 nm GeN_x layer to prevent surface oxidation. Film thicknesses were measured by X-ray reflectometry (XRR), and chemical compositions were evaluated by wavelength-dispersive X-ray fluorescence (WDXRF) and Rutherford Backscattering Spectroscopy (RBS). Mad200 memory test vehicles were fabricated in CEA-Leti's cleanrooms on 200 mm wafers.

3. RESULTS & DISCUSSION

$GeSe_{1-x}Te_x$ compositions—selected for integration in LETI's Mad200 devices—were chosen to balance phase-change performance and compatibility with back-end integration thermal budget, showing notable resistance to film delamination under thermal stress during high-temperature

processes. Four alloys were studied: $GeSe_{0.49}Te_{0.51}$ and $GeSe_{0.37}Te_{0.63}$, both with and without nitrogen doping. In order to crystallize films during the Mad200 integration flow, all films were annealed at 350 °C for 30 minutes. $GeSe_{1-x}Te_x$ films annealed in such conditions crystallize in the pseudo-metallic rhombohedral phase that exhibits a huge resistance contrast of several orders of magnitude lower than that of the amorphous phase of as-deposited films. In order to assess their functionality after integration in PCM, a staircase-up voltage pulse programming protocol was used (Fig. 1a). Among the tested materials, N-doped $GeSe_{0.49}Te_{0.51}$ achieved the best endurance, retaining a stable reading window over 10^4 cycles (Fig. 1b). However, data retention tests of the RESET state in devices revealed a notable drop of thermal stability compared to as-deposited films. Indeed, loss of the RESET state by recrystallization occurred after a few minutes at 220 °C that is a hundred of °C lower than the recrystallization temperature measured in the as-deposited thin films. The origin of this drop of thermal stability has been investigated by STEM analysis of devices in the SET and RESET states. STEM-EDX (Energy Dispersive X-ray) mapping of Ge, Se and Te elements in the devices revealed significant compositional changes after programming. In particular, a significant Se depletion with a local Te enrichment is observed in the active volume located above the bottom heater of the memory cell (Fig. 1c). As a result, since Te-rich $GeSe_{1-x}Te_x$ alloy crystallize at a significantly lower temperature than Se-rich ones, this explains the unexpected lower thermal stability of PCM devices. To overcome this issue, we explored new Te-poor $Ge_{1+\delta}Se_{1-\delta-x}Te_x$ films with $-0.12 \leq \delta \leq 0.12$ and $0 \leq x \leq 0.44$. Four-point probe measurements revealed that slight compositional shifts significantly impact both crystallization temperature and resistivity contrast. Notably for a fixed Te content, Se-rich films achieved unprecedented contrast, while Ge-rich alloys showed improved amorphous-phase stability. These findings underscore the potential of fine compositional tuning in the Ge–Se–Te system to improve $GeSe_{1-x}Te_x$ devices performance.

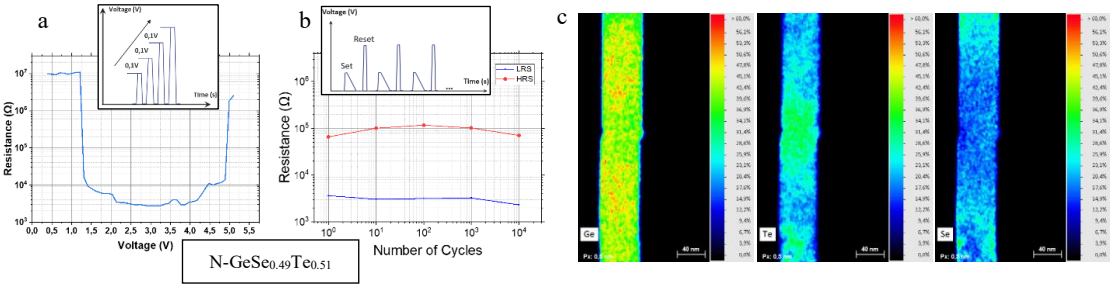

Fig. 1: (a) Resistance of the memory cell as a function of the applied voltage during the staircase-up procedure. SET and RESET operations occur at 1.3 V and 5 V in this device, respectively) (b) Resistance of the low-resistance state (LRS) and the high-resistance state (HRS) as a function of the number of programmation cycles. (c) STEM-EDX composition maps of Ge, Te and Se in a memory cell of a N-$GeSe_{0.37}Te_{0.63}$ device in the RESET state. The active material located above the heater is highly enriched in Te and depleted in Se.

4. CONCLUSIONS

This study highlights the strong potential of the Ge–Se–Te material system for ePCM applications. Integration of selected compositions into devices yielded promising results in terms of switching behavior and endurance. However, data retention remains a key challenge, primarily due to local compositional changes during cell programming. Through the investigation of Se-rich compositions near the GeSe–GeTe pseudo-binary line, we unexpectedly found that even small compositional variations can significantly impact phase-change properties. These findings provide a robust foundation for further material optimization and open new perspectives for the development of next-generation ePCM devices.

REFERENCES

[1] P. Noé *et al.*, *Semicond. Sci. Technol.* 33 (2018) 013002.
[2] P. Cappelletti *et al.*, *J. Phys. D: Appl. Phys.* 53 (2020) 193002.
[3] V. Sousa *et al.*, Symp. VLSI Tech. Dig. 2015, T98.
[4] a) M. Tomelleri *et al.*, *Phys. Status Solidi RRL*, **15** (2021) 2000451; b) K. Ren *et al.*, *Nanoscale* **11** (2019) 1595; c) E.-B. Lee *et al.*, *Microelectron. Eng.* **86** (2009) 1950.
[5] a) Y. Yin *et al.*, *J. Phys. D: Appl. Phys.* 46 (2013) 505311; b) A. Fantini *et al.*, Int. Electron devices meet. IEDM 104 (2010) 644; c) C. Peng *et al.*, *Scr. Mater.* 65 (2011) 327.
[6] A. Albanese *et al.*, *Phys. Status Solidi RRL*, (2025) 2400413.

P-25

Innovative Threshold-Changeable Memory (TCM) Based on Amorphous GeSbSeN

M. Kanaan[1,2,3], R. Antonelli[2,3], M. Borghi[4], J. Rottner[2], M. Bernard[2], Z. Saghi[2], T. Monniez[2], G. Bourgeois[2], S. Gout[2], A. Salvi[2], F. Andrieu[2], A. Souifi[3], S. Jeannot[1], G. Navarro[2]

[1] STMicroelectronics, 850 Rue Jean Monnet, 38920 Crolles, France.
[2] CEA-LETI, Univ. Grenoble Alpes, 38000 Grenoble, France.
[3] Univ. Grenoble Alpes, CNRS, LTM, 38054 Grenoble, France.
[4] STMicroelectronics, Via Olivetti 2, 20864 Agrate Brianza, Italy.
E-mail: gabriele.navarro@cea.fr

ABSTRACT

In this work, we present an innovative Threshold Changeable Memory (TCM) device based on amorphous GeSeSbN (GSSN). We developed and optimized a programming protocol to study the threshold voltage modulation effect and evaluated the impact of multiple readout techniques on the memory window (MW). Finally, preliminary results from a 16 kb 1T1R matrix demonstrate the potential of this technology for high-density memory applications.

Keywords: Amorphous Chalcogenides, Threshold changeable memory (TCM), Ovonic Threshold Switches (OTS), Selector only memory (SOM), Self-selective memory (SSM).

1. INTRODUCTION

Amorphous chalcogenides (AChs) are widely used as Ovonic Threshold Switching (OTS) selectors in emerging Non-Volatile Memory (eNVM) technologies due to their fast-switching speed, high ON-current density, and high non-linearity [1]. Recent research has revealed that certain ACh materials exhibit a memory effect characterized by a shift in threshold voltage when the polarity of the programming pulse is reversed [2, 3]. This phenomenon, referred to as Self-Selecting Memory (SSM) or Selector-Only Memory (SOM), enables a reduction in programming voltage and current [4], thereby offering the potential for increased memory density and reduced cost. In this study, we investigate the memory behavior of GeSbSeN (GSSN) [5], an amorphous chalcogenide (ACh) material that exhibits threshold voltage modulation, and is therefore referred to as Threshold-Changeable Memory (TCM). By tuning the polarity and parameters of the programming pulses, we successfully induced TCM behavior in GSSN using a novel programming protocol. The reliability of the memory effect was evaluated using various readout techniques, and promising preliminary results were obtained in a 16 kb 1T1R matrix.

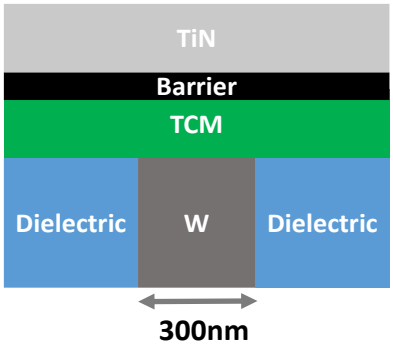

***Fig. 1**: Simplified schematic of the analytical TCM GSSN 1R device.*

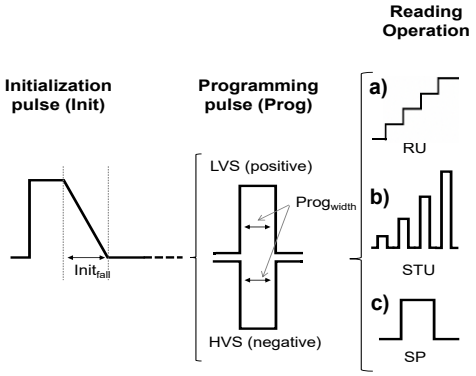

***Fig. 2**: Schematic of the programming protocol. High (HVS) and Low Voltage State (LVS) are obtained by applying negative and positive Prog pulses, respectively.*

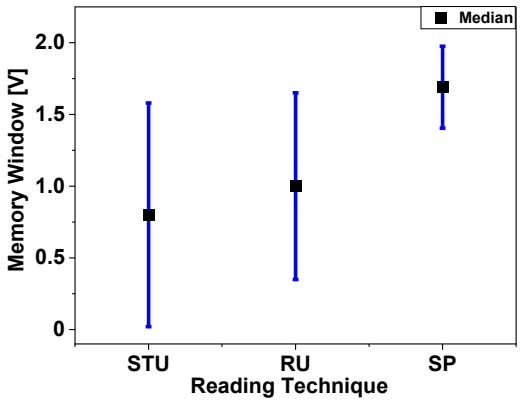

Fig. 3 Impact of readout technique on the memory window (MW). The SP method results in the widest MW along with reduced variability. Data points indicate the average MW, while the solid lines represent the corresponding standard deviation.

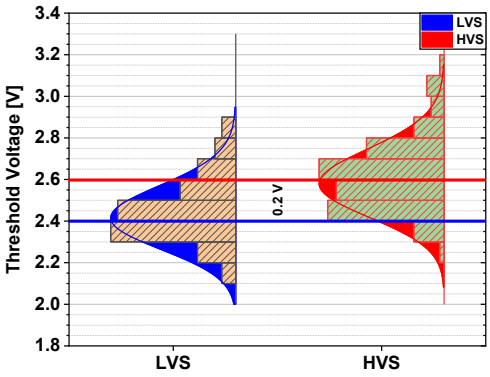

Fig. 4 Preliminary TCM behavior demonstrated in 16 kb array using a standard STU protocol. Further explorations are ongoing using new programming and reading approaches, compatible with what reported in Fig. 2.

2. EXPERIMENTAL

The analytical TCM devices investigated (1R) are based on a GeSeSbN (GSSN) chalcogenide material integrated over a tungsten bottom electrode with a 300 nm diameter (**Fig. 1**). GSSN was selected for its good endurance performance in our analytical devices featuring relaxed dimensions, suitable for preliminary investigations. GSSN was integrated as well in 16 kb 1T1R arrays, featuring Double-Patterned Self-Aligned (DPSA) architecture as described in [6].

3. RESULTS & DISCUSSION

We implemented a three-step testing protocol to systematically evaluate the Threshold-Changeable Memory (TCM) behavior: 1) Initialization (Init) step to establish a reference state; 2) Programming (Prog) step to modulate the threshold voltage by adjusting pulse polarity and parameters; 3) Readout step to measure the resulting threshold voltage. The readout can be performed using different techniques, including Staircase-Up (STU, consisting of successive square pulses), Ramp-Up (RU, based on a continuous voltage sweep), and Single-Pulse (SP, involving repeated sequences with progressively increasing read pulse amplitudes). **Fig. 2** displays a simplified schematic of the protocol. SP method exhibits the largest memory window (MW), defined as the difference between the threshold voltages of the high and low voltage states ($MW = V_{HVS} - V_{LVS}$), along with the lowest variability compared to the other readout protocols (**Fig. 3**), which are likely affected by sub-threshold induced threshold shift phenomenon [7]. Finally, we present TCM results obtained from 16 kb arrays (**Fig. 4**) based on DPSA architecture.

4. CONCLUSIONS

We provided for the first time the demonstration of TCM behavior in GSSN AChs, integrated in both analytical cells and 16 kb arrays. Thanks to our programming protocol, we demonstrate the relevance of SP reading to enhance the device MW.

ACKNOWLEDGMENTS

This work has been partially supported by the French Public Authorities within the frame of France 2030 as part of the IPCEI Microelectronics and Connectivity.

REFERENCES

[1] Huai-Yu Cheng et al 2019 J. Phys. D: Appl. Phys. 52 473002.
[2] T. Ravsher et al., IEEE IEDM 2021, pp. 28.4.1–28.4.4.
[3] J. Lee et al., TED vol. 71, no. 4, pp. 1–7, 2024.
[4] S. Hong et al., IEEE IEDM 2022, pp. 18.6.1-18.6.4.
[5] A. Verdy et al., IEEE IEDM 2018, pp. 37.4.1-37.4.4.
[6] G. Bourgeois et al., 2023 7th IEEE EDTM 2023, pp. 1–3.
[7] S. Ban et al., EDL vol. 45, no. 1, pp. 128-131, Jan. 2024.

P-27

Thermal metrology for phase change materials

T. Chakrabarty[1,2], A. Patil[2], E. Blandre[1], P.-Y. Cresson[1], Y. Le-Friec[2], S. Jeannot[2], E. Dubois[1], and J. F. Robillard[1]*

[1]Univ. Lille, CNRS, Centrale Lille, Junia, Univ. Polytechnique Hauts-de-France, UMR 8520 - IEMN – Institut d'Electronique de Microélectronique et de Nanotechnologie, F-59000 Lille, France

[2]STMicroelectronics, 850 rue jean Monnet 38920 Crolles, France

*Corresponding author: jean-francois.robillard@iemn.fr

ABSTRACT

The thermal characteristics of the phase change materials as well as the nearby dielectric materials affect the phase change memory's performance. In this study, we report on the thermal conductivity of the dielectric SiN and the nitrogen doped GeSbTe using 3ω method and show that the value is consistent with earlier measurements using Raman thermometry.

Key words: Phase change materials, Thermal Conductivity, Thermal Boundary Resistance, 3ω method, Raman thermometry.

1. INTRODUCTION

Phase change memory (PCM) for automotive applications necessitates higher crystallization temperatures which have been demonstrated by increasing the Ge content and by doping the material with Nitrogen. Nitrogen doping causes a reduction of the GST thermal conductivity compared to its undoped version [1] which reduces the reset current of the PCM cell. Moreover, the thermal properties of the dielectric SiN layer surrounding the GST material will also impact on the temperature distribution inside the GST cell. A higher thermal boundary resistance (TBR) between the GST and the surrounding SiN layer will confine the heat inside the GST cell, further reducing the reset current. The effect of this boundary resistance on the reset current reduction has been observed through simulation [2]. So, it is important to measure these thermal properties to optimize the PCM technology. In this work, we use a 3ω approach with 2D analytical multilayer modeling to measure the thermal properties of the dielectric SiN and then we utilize this to extract the thermal properties of the amorphous nitrogen doped GeSbTe (GGSTN). Raman thermometry is also used to characterize the amorphous GGSTN samples, and a comparison of the two values is provided.

2. EXPERIMENTAL

Five SiN samples having SiN thickness of 54 nm, 81 nm, 107 nm, 180 nm and 272 nm were prepared by PECVD on Si wafers. Thicknesses were confirmed by the ellipsometry measurements. For the GGSTN sample, 200 nm GGSTN thin films were deposited by physical vapor deposition on Si wafers and later 45 nm SiN layers were deposited on top to avoid oxidation.

To perform the 3ω measurements, gold heaters were fabricated on top of all samples and the temperature coefficient of resistance (TCR), α of these heaters was measured. As the Au heaters were fabricated on different batches, a small variation between the TCR was observed (mean $\alpha = 3.5\times10^{-3}$ K^{-1}). An AC signal of several frequencies ($\omega=2\pi f$) was applied across the heater and corresponding first ($V_{1\omega}$) and third harmonic ($V_{3\omega}$) voltages were recorded. Raman measurements were performed on a Horiba Labram HR using a 473 nm laser with an 1800 grooves/mm grating. During Raman measurements, amorphous GGSTN samples were kept under vacuum using a LINKAM HFS350-PB4 temperature-controlled stage. SbTe vibrations peak shift are considered as thermometer and thermal conductance are calculated. Later, FEM model is used to convert this thermal conductance into GGSTN thermal conductivity.

3. RESULTS & DISCUSSION

We start the 3ω measurements with the SiN samples and record the corresponding third harmonic voltages and convert them to temperature oscillations using TCR value. As the thickness of SiN layer is small compared to the width of the Au heaters; the SiN layer, TBR between Au and SiN ($TBR_{Au\text{-}SiN}$) and TBR between SiN and Si ($TBR_{SiN\text{-}Si}$) can be considered as a 1D resistance connected to the Si wafer and the expression of the temperature oscillations can be analytically obtained. Details about the model can be found in [3]. Fitting this model with experimental data, the 1D thermal resistance, R_{th} are extracted. and it can be expressed by:

$$R_{th} = \frac{d}{K_{SiN}} S + TBR_{Au-SiN} + TBR_{SiN-Si} \quad (1)$$

Here, d is the thickness of SiN layer, K_{SiN} is the SiN thermal conductivity and S is the correction factor to be accounted for heat spreading inside the SiN film. A total of 75 measurements are performed at room temperature and the extracted values are plotted in Fig. 1 against multiplication of films thickness and correction factor or the effective film thickness (d×S). The points are fitted using Eq. 1 and the inverse value of the slope provides the intrinsic thermal conductivity of the SiN (K_{SiN}) which is found to be 1.65±0.01 $Wm^{-1}K^{-1}$. Moreover, the extrapolation to zero thickness provides the sum of 2 TBR value which is determined to be 8.42±0.55 m^2K/GW.

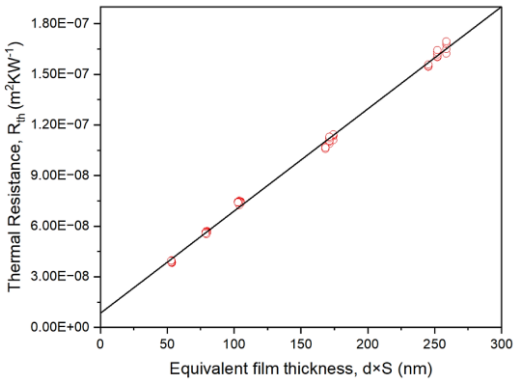

Fig. 1 Measured thermal resistance, R_{TH} as a function of multiplication of films thickness and correction factor.

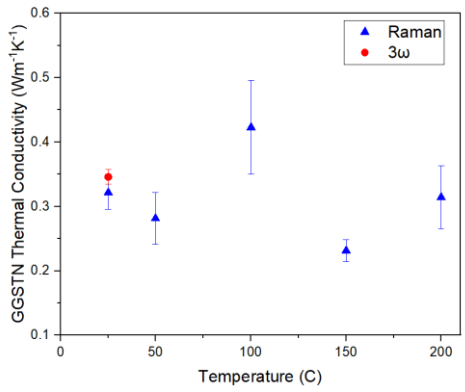

Fig. 2 Amorphous GGSTN thermal conductivity using Raman thermometry and 3ω method.

After that, this K_{SiN} value is considered and 3ω measurements are done to the GGSTN samples. The GGSTN thermal conductivity (K_{GGSTN}) is then extracted using the multilayer model for 3ω proposed by Borca [4]. Raman thermometry was also performed in the same sample and the thermal conductivity was extracted as a function of temperature. The values obtained by both 3ω and Raman methods are shown in Fig. 2. It is observed that the amorphous phase thermal conductivity (K_{GGSTN}) doesn't exhibit temperature dependence. Additionally, a higher degree of agreement between the two measurement methods is noted.

4. CONCLUSIONS

In this study, the thermal conductivity of SiN and GGSTN are measured by 3w method, yielding values to be 1.65±0.01 $Wm^{-1}K^{-1}$ and 0.346±0.01 $Wm^{-1}K^{-1}$ respectively. Besides, the Raman approach shows similar thermal conductivity values for the GGSTN. Measuring various GGSTN thickness samples, TBR can also be extracted in GGSTN samples which would provide us with another crucial parameters for PCM performance optimization.

REFERENCES

[1] A. Patil et al., J. Appl. Phys. 136, 175102 (2024).
[2] S. Durai et al., IEEE Transactions on Computer-Aided Design of Integrated Circuits and Systems 39, 1834–1840 (2020).
[3] J. Paterson et al., J. Appl. Phys. 127, 245105 (2020).
[4] T. Borca-Tasciuc et al., Review of Scientific Instruments 72, 2139–2147 (2001).

P-29

Driving the Segregation and Crystallization in Ge-rich GeSbTe by Dopant Introduction

V. Bogenschutz[1,2], E. Nolot[2], O. Daoudi[2], F. Fillot[2], K. Guy[2], M. Bernard[2], L. Fellouh[2], J.-B. Dory[2], J. Rottner[2], Q. K. Nguyen[2], G. Bourgeois[2], S. Gout[2], A. Salvi[2], S. Jeannot[1], H. Renevier[3] and G. Navarro[2,*]

[1] STMicroelectronics, 850 Rue Jean Monnet, 38920 Crolles, France

[2] CEA- Leti, Univ. Grenoble Alpes, F-38000 Grenoble, France

[3] Univ. Grenoble Alpes, CNRS, Grenoble-INP, LMGP, 38000 Grenoble, France

*Corresponding author: gabriele.navarro@cea.fr

ABSTRACT

In this work, we demonstrated the possibility to control the stoichiometry of the segregated GeSbTe phase in Ge-rich GeSbTe system by innovative doping. We combined results from Resistivity vs Temperature, Raman spectroscopy and X-ray Diffraction analyses. We assessed the increase in Sb/Te ratio in the segregated GeSbTe phase with dopant introduction, leading to direct crystallization into a hexagonal GeSbTe phase.

Key words: Phase-Change Material, Crystallization, Thin Films, Doping, Ge-rich GeSbTe

1. INTRODUCTION

Among the phase-change materials, $Ge_2Sb_2Te_5$ is considered the reference material for phase change memories [1]. However, it has a low crystallization temperature close to 150°C, which makes it unsuitable for applications where high thermal stability is required. To meet more stringent requirements of dedicated applications such as automotive ones, solutions to increase the crystallization temperature have been explored, such as Ge enrichment (Ge-rich GeSbTe system) [2], light element doping or exploration of new compounds. O. Daoudi et al. [3] showed that the crystallization of GeSbTe phase in Ge-rich GeSbTe system is driven by the Sb/Te ratio. Indeed, compositions with low Sb/Te ratios first crystallize into a metastable cubic GeSbTe phase followed by a phase transition toward a stable hexagonal phase at higher temperatures. On the contrary, alloys with high Sb/Te ratio demonstrate a direct crystallization into a stable hexagonal phase, providing better uniformity of the crystalline phase (higher degree of order and larger grains). In this work, we investigate the effect of an innovative doping solution to tune the crystallization kinetics of known Ge-rich GeSbTe system, towards the appearing of a GeSbTe phase with high Sb/Te ratio featuring a fast crystallization towards a stable hexagonal phase.

2. EXPERIMENTAL

We analyzed three compositions with different dopant contents (from D1 i.e., the lowest content to D3 i.e., the highest content) and compared them with the reference sample (i.e. without dopant). As-deposited Sb and Te contents were the same for each sample (doped and undoped) to maintain a constant starting low Sb/Te ratio.
We combined results from different characterization techniques such as Resistivity vs Temperature (R vs T) measurements, Raman spectroscopy and X-Ray Diffraction (XRD) analyses. Both Raman and XRD analyses were performed *ex situ* on samples heated up at different annealing temperatures with a 10°C/min heating rate. Complementary In-Lab *in situ* XRD analyses were conducted on selected compositions to confirm the *ex situ* results.

3. RESULTS & DISCUSSION

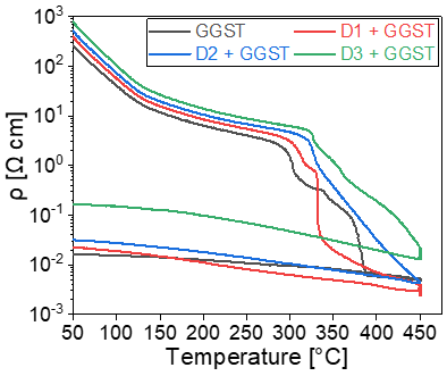

Fig. 1: *Resistivity as a function of Temperature (R vs T) for the reference (GGST) and for the doped samples measured at a 10°C/min heating rate.*

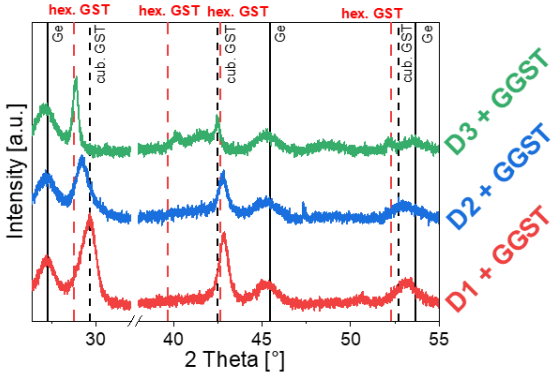

Fig. 2: *XRD patterns obtained on doped samples annealed at 375°C.*

RvsT measurements (**Fig. 1**) show the increase in amorphous resistivity and in crystallization temperature of the layers with increasing dopant content. For the undoped Ge-rich GeSbTe (black curve) the double step transition confirms the known crystallization kinetics for this alloy as previously reported in [4] The modification of the shape of the curves with increasing dopant content suggests different crystallization kinetics.

XRD patterns obtained on doped samples annealed at 375°C (**Fig. 2**), reveals the segregation of a cubic Ge phase accompanied by the crystallization of a "Ge-poor" GeSbTe phase. We observe the progressive shift of the main Bragg's peak of GeSbTe at about 29.5° toward lower angles (wrt cubic $Ge_2Sb_2Te_5$ phase) with increasing dopant content. This shift is attributed to two correlated phenomena: (i) a modification of the stoichiometry of the crystallized phase toward Sb-rich GeSbTe phase, with the consequent (ii) preferred crystallization of a hexagonal GeSbTe phase rather than a cubic one. This is supported by the apparition of the Bragg's peak at around 40° belonging to the hexagonal class in the highest doped system (D3 + GGST), confirming the formation of hexagonal phase at high dopant content. The results are then confirmed by complementary XRD and Raman analyses.

4. CONCLUSIONS

The higher amorphous resistivity and the likely formation of an Sb-rich GeSbTe phase make doped Ge-rich GeSbTe alloys a valuable option for next-generation of Phase-Change Memory devices with both increased resistivity window and improved crystallization kinetics.

REFERENCES

[1] P. Cappelletti et al., "Phase change memory for automotive grade embedded NVM applications," J. Phys. D. Appl. Phys., vol. 53, nº 19, p. 193002, 2020.
[2] P. Zuliani et al., "Overcoming Temperature Limitations in Phase Change Memories With Optimized $Ge_xSb_yTe_z$," IEEE Trans. Electron Devices, vol. 60, nº 12, p. 4020-4026, 2013.
[3] O. Daoudi et al., "The effects of Sb/Te ratio on crystallization kinetics in Ge-rich GeSbTe phase-change materials," Journal of Applied Physics, vol. 136, nº 15, p. 155105, 2024.
[4] L. Prazakova, et al., "Temperature driven structural evolution of Ge-rich GeSbTe alloys and role of N-doping," J. Appl. Phys. 7 December 2020; 128 (21): 215102.

P-31

Time-resolved X-Ray Diffraction from laser-irradiated Ge-rich GST thin films

Thomas Fernandes[1,2], Michael Texier[1], Philipp Hans[1], Solène Comby-Dassonneville[1], Florent Mignerot[1], Simon Jeannot[2], Celine Mariette[3], Yannick le Friec[2], Olivier Thomas[1].

1- Aix Marseille Univ, Université de Toulon, CNRS, IM2NP, Marseille, France

2- STMicroelectronics, Crolles, France

3-European Synchrotron Radiation Facility, Grenoble F-38034, France

ABSTRACT

Crystallized Ge-rich Ge-Sb-Te thin films for memory applications were investigated using laser irradiation experiments combined with *in situ* X-ray diffraction (XRD) measurements. The samples were irradiated with 800 nm, 100 ps laser pulses at fluences ranging from 14 to 219 mJ·cm^{-2}. Time-resolved measurements were performed with a temporal resolution of 100 ps. At low fluence (18 mJ/cm^2) the evolution of Bragg peak positions indicates a reversible sub-ns strain evolution both in Ge and in $Ge_2Sb_2Te_5$.

Key words: Phase change materials, X-Ray diffraction, Synchrotron radiation, laser, time-resolved, Non-volatile memories, GST.

INTRODUCTION

Phase Change Materials (PCM) are very promising candidates for future non-volatile memory applications [1]. The large differences in the physical properties (resistivity, optical reflectivity …) between the amorphous and crystalline phases allows modifying and reading the state of the memory. The most studied PCM is $Ge_2Sb_2Te_5$ (GST), with a crystallization temperature within the 150-170°C range. This temperature is too low for data retention for automotive applications but Ge-rich GST (GGST) alloys with crystallization temperature of 350°C [2] are fully suitable for this purpose. While *in situ* furnace-annealing of GGST have been performed at low heating rates (few °C/min) evidencing a sequential crystallization of the Ge and GST phases [3], real memories are switched at the ns timescale. Since at such short timescales one may expect different phase formation mechanisms to occur we have studied the influence of short laser pulses on GGST thin films. Time-resolved experiments, in a pump (laser) – probe (X-ray) scheme, of the phase transformations in GGST were performed *in situ* on ID09 beamline at ESRF in order to understand the behaviour of Ge and GST at sub-ns up to ns timescales.

EXPERIMENTAL

The pump-probe experiments have been performed on ID09 beamline at ESRF (France)[4]. Samples were irradiated in situ using a laser operating at an 800 nm wavelength and a pulse duration of approximately 100 ps, in order to match the minimal pulse length of the X-ray beam, which operated within a frequency range of 10–1000 Hz. Laser fluence was varied from 14 to 219 mJ/cm² and a focused pink (18 keV, ΔE/E ~ 1.5 %, size ~ 25 µm (V) x 49 µm (H)) X-ray beam has been used for probing the sample response at an incidence of 1° with high enough flux (~10^8 photons/100ps pulse). The laser had an angle of incidence of 15° with respect to the normal to the sample surface. A charge coupled device (CCD) detector was used with a total active area of 170×170mm². A piezoelectric stage allowed moving the sample under the laser and X-ray beams (resolution 4µm, total range 100mm). The investigated samples are 50nm thick GGST thin films with the following stacking: Si(001) substrate // 15nm SiN// 50nm GGST// 15nm SiN. GGST layers are deposited by physical vapor deposition (PVD). SiN capping is then deposited by chemical vapor deposition. This capping allows protecting the phase change material from oxidation. In addition, samples were kept under nitrogen flow during the experiments. The samples were cut from 300 mm wafers in large coupons of size 150×50 mm² to allow testing different areas on the same sample. As deposited samples are amorphous. In the following we discuss the behavior of a sample crystallized *via* furnace annealing at 455°C for 30 minutes.

RESULTS & DISCUSSION

The 1D diffraction patterns, extracted from the 2D patterns [5], exhibit Ge **111** and Ge **220** as well as GST **200** and GST **220** diffraction peaks (both cubic phases). Fitting these peaks using a double pseudo-Voigt function for both Ge **111** and GST **200**, along with a linear background, allows the

integrated intensity, integral breadth, and peak position to be extracted. The strain can be calculated from the peak position. Figure 1 presents the strain evolution of Ge **111** (a) and GST **200** (b) for three different sample conditions: (i) an initially annealed sample, (ii) two amorphized samples obtained at fluences of 42 mJ/cm² and 54 mJ/cm², and (iii) the same amorphized samples after re-crystallization at 30 mJ/cm². The GST has not been completely amorphized, the germanium likewise. Each measurement was made at 18mJ/cm² (a low fluence to ensure that the sample state is not modified during the measurement) always at the same position.

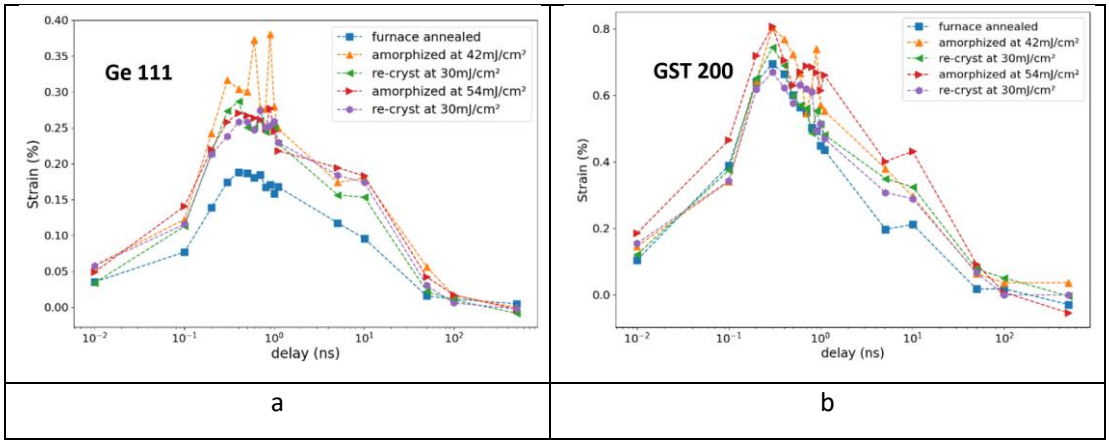

Fig. 1: *Strain evolution for Ge **111** (a) and GST **200 (b)** at various time delays between laser pump and X-ray probe and for 5 different samples. These time-resolved experiments were performed at a fluence of 18 mJ/cm² on an initially 50 nm-thick oven-crystallized GGST thin film.*

Irrespective of the state of the sample (fully crystalline or laser-irradiated in different states) all the strain plots in Figure 1 show the same behavior for Ge **111** and GST **200**. Strain vs time delay reaches a maximum at about 300 ps and then decreases slowly over about 50 ns. The maximum strain values are positive in both cases: 0.38% for Ge **111** and 0.8% for GST **200**. Whereas the furnace annealed sample exhibit a significantly reduced strain for Ge **111**, all other plots are within 10% strain values. This tensile strain evolution together with the difference in strain for Ge 111 and GST 200 points to a thermal behavior. The maximum strain is probably related to the maximum temperature reached via thermoelastic deformation (free thermal expansion coefficients for Ge and cubic GST are reported respectively as: 5.8×10^{-6} K^{-1} and 17.4×10^{-6} K^{-1}). In the same way the slow strain relaxation (over about 50 ns) is interpreted as a consequence of heat diffusion in the thick silicon substrate, which acts as a sink. Detailed modelling is underway to support these interpretations.

CONCLUSIONS

Time-resolved X-ray diffraction was conducted on laser-irradiated crystallized Ge-rich GST thin films at the ESRF ID09 beamline. The samples were prepared under varying laser conditions to investigate the influence of these parameters on structural dynamics. X-ray diffraction allows recording the elastic strain evolution in Ge and GST as a function of time delay in the 100 ps – 500 ns range. A large difference in strain for Ge and GST nanocrystals is observed and is attributed to thermoelastic deformation. The slow relaxation of strain (10s of ns) is attributed to the slow cooling of the film via thermal diffusion in the thick silicon substrate.

REFERENCES

1. H.S.P. Wong *et al., Proc. IEEE 98* (2010) 2201.
2. P. Zuliani *et al., Solid State Electron. 111* (2015) 27.
3. O. Thomas *et al., Microelectronic Engineering 244-246* (2021) 111573.
4. M. Cammarata *et al., Rev. Sci. Instrum. 80 (*2009).
5. T. Fernandes *et al., Phys. Status Solidi RRL 2400392* (2024).

P-33

The effects of V doping in CrN based ultra-low energy consumption phase change material

Wei-Chiao CHANG[1*], Yi SHUANG[1,2], Daisuke ANDO[1] and Yuji SUTOU[1,2]
[1] Department of Materials Science, Graduate School of Engineering, Tohoku University, Sendai 980-8579, Japan
[2] Advanced Institute for Materials Research, Tohoku University, Sendai 980-8577, Japan
[*] chang.weichiao.s1@dc.tohoku.ac.jp

ABSTRACT

CrN as a novel PCM, achieves a reduction in low power consumption[1]. Despite this improvement in energy saving, programming energy is still high when compared with novel memory devices such as ReRAM[2]. In this study, V-doped CrN PCRAM shows a 50% reduction of energy consumption. In addition, the mechanism is discussed based on XPS results.

Key words: phase-change materials, phase-change random access memory, AlCrN, transition metal nitride, radio frequency magnetron sputtering

1. INTRODUCTION

Recently, the application of 5G, AI, and IoT has drawn attention from all over the world. These technologies lead to a new style of work and life. According to the information explosion, the need for memory devices has increased sharply. Phase-change random access memory (PCRAM) is a type of non-volatile memories (NVMs) that has been studied. Ge-Sb-Te (GST) is an example of a phase-change material (PCM) that performs amorphous-crystalline phase changes. The stability of this phase change provides excellent cycling properties as a memory device. However, the reset process (amorphization) requires a significant amount of energy, which is a bottleneck in the large-scale adoption of PCRAM. Therefore, our group has been developing CrN as a PCM and has found a crystalline-crystalline phase change. This type of melting-free phase change has resulted in a 90% reduction in reset energy. Consequently, the nitride of transition metals has potential for development in PCM. In this study, we investigated thin films of V-doped CrN (VCrN) to achieve much lower energy consumption.

2. EXPERIMENTAL

The VCrN thin films were deposited using RF sputtering. The composition of the thin films was controlled by adjusting the power applied to V (99.9%) and Cr (99.99%) targets in an atmosphere of Ar and N_2 at 0.22 Pa. To form contact holes and top/bottom W electrodes for PCRAM, we used a focused ion beam (FIB) and RF sputtering. The annealing process up to 500°C was carried out by placing the samples on a hot plate set in a chamber that was evacuated and then filled with Ar at 2.2×10^5 Pa. The crystal structures were identified using XRD (Ultima IV, Rigaku). The switching of PCRAM was driven by electrical pulses generated by a pulse generator (Keysight B1525A), and the electrical properties were measured simultaneously using a semiconductor parameter analyzer (Keysight B1500A).

3. RESULTS & DISCUSSION

The electrical properties show that VCrN-PCRAM exhibits a resistance change of 10^3 Ω after applying a 50 ns, 2V electrical pulse. VCrN-PCRAM compared to CrN-PCRAM shows lower reset voltage leading to a 50% reduction of programming energy. Therefore, we consider VCrN to have significant potential as a next-generation PCM for achieving low-power operation in memory devices. Based on XPS results, the covalent bond between Cr and N in CrN tends to become weaker because the introduction of V decreases the binding energy of Cr 2p. As a result, the energy consumption of the transformation from CrN to CrN_2 decreases.

4. CONCLUSIONS

An investigation of the relationship between the composition of V and the binding energy of the VCrN system has been completed. Furthermore, the reduction of programming energy of the VCrN-PCRAM is induced by binding energy change of each element.

REFERENCES

1. Yi Shuang et al., ACS Nano, 18, 32, 21135-21143 (2024).

2. Lanza, M., et al., ACS Nano, 2021. 15(11): p. 17214-17231.

P-35

Crystallization investigations of Ge-rich GST cells using *in situ* thermal pulses coupled with STEM-EDX and HR-TEM analyses

F. Mignerot[1]*, M. Texier[1], I. Florea[2], T. Fernandes[1], S. Comby-Dassonneville[1], S. Jeannot[3], Y. le Friec[3] and O. Thomas[1]
[1]Aix-Marseille University, University of Toulon, CNRS, IM2NP, Marseille, France
[2] Université Côte d'Azur, CRHEA, CNRS, Sophia-Antipolis, France
[3]STMicroelectronics, Crolles, France
*corresponding author: florent.MIGNEROT@univ-amu.fr

ABSTRACT

The crystallization of initially amorphous Ge-rich Ge-Sb-Te nanostructures was investigated using thermal pulses heating coupled with *in situ* STEM-EDX and HR-TEM analyses. The onset of crystallization was found to start at 350°C with pure cubic Ge grains first, followed by cubic GST at 390°C. Initially localized at the interfaces, the crystallization of both phases spreads heterogeneously in the cell. The spatial distribution of grains is compared with the variations in chemical compositional the nanometric scale.

Key words: Phase change materials, in situ heating, STEM-EDX, HR-TEM, GST.

1. INTRODUCTION

Phase Change Materials (PCM) composed of ternary alloys, commonly $Ge_2Sb_2Te_5$ (GST) are considered to replace classical non-volatile memories in various applications and domains [1]. The growing interest in this technology is related to the significant difference in physical properties between the amorphous and crystalline phases, which allows for easy modification and reading of the memory state, coupled with a fast-switching capacity of the order of ns. Typical crystallization temperature for GST is in the range of 150-170°C, a temperature too low for data retention in automotive applications. To address this limitation, Ge-rich GST (GGST) alloy with a crystallization temperature of 350°C was developed. While this material is non-stochiometric, recent studies show the presence of the Ge, GeTe, Sb and GST phases during and after crystallization of GGST layers produced by thermal heating at low heating rates [2-4]. In order to investigate the phase separation in conditions closer to the working conditions of memories (i.e. ns timescale), rapid heating experiments are performed by applying brief thermal pulses to GGST amorphous confined nanostructures, *in situ* in TEM/STEM microscopes. Crystallographic and chemical analyses of the GGST alloy are compared to elucidate the interplay between local composition fluctuations, the influence of interfaces and the microstructure evolution during rapid crystallization of this material.

2. EXPERIMENTAL

Nanostructures composed of embedded GGST lines were supplied by STMicroelectronics. The GGST alloy, which is initially amorphous, is deposited on an underlayer (UL) with a different composition and covered by a top electrode made of ceramic material (figure 1.A). Transmission electron microscopy (TEM) thin foils were lifted-out by means of focused ion beam (FIB) micromachining. Thin foils were glued on a microelectromechanical system (MEMS) designed for *in situ* TEM heating and thinned-down to approximately 50nm in thickness. Scanning-TEM (STEM) combined with energy dispersive X-ray spectroscopy (EDX), and high resolution TEM (HRTEM) were performed using aberration corrected microscopes. Sample heating was achieved every 10°C *via* thermal pulses, ranging from 250°C to 400°C. Pulses had a duration of 10 ms, followed by a holding time of 300 ms to ensure that the target temperature is reached. Elemental maps and HRTEM images were taken at room temperature after each pulse to characterize the crystallization state and the local chemical composition.

3. RESULTS & DISCUSSION

The STEM-EDX analyses have been performed after each thermal pulse to follow the evolution of the spatial distribution of the Ge, Sb and Te elements as a function of the temperature, within the cell and the UL. While the Sb concentration remains quite homogeneous regardless of temperature, inhomogeneities in Ge and Te compositions are evidenced from 320°C (figure 1.B). A local increase in Te content is observed in the peripheral area of the cell, close to the interface with the surrounding capping layer and in the underlayer. A Ge enrichment of the UL occurs as the temperature increases, accompanied by a Te depletion in the same area. This depletion goes with a Te enrichment right above the UL, in the bottom part of the GGST cell, as illustrated on the elemental map after the thermal pulse at 380°C (see figure 1.B). The quantification of Te-rich regions exhibits a Te/Sb ratio of 2.7, very close to the theoretical ratio of 2.5 expected for the GST phase. The first crystallization events are observed at 350°C during *in situ* HRTEM experiments. HRTEM analysis after heating at 400°C reveals a complete crystallization of the various investigated cells. The Fast Fourier transforms (FFT) calculated from HRTEM images were generated and combined with radial integration profiles to identify the different phases in presence (figure 1.D). Ge 111, Ge 220 and Ge 113 reflections are clearly identified, revealing the presence of the Ge cubic phase. These reflections start appearing around 350°C, indicating that the crystallization temperature of the material starts with the formation of Ge grains. Other reflections with a d-spacing of 3.48 Å and 3.01 Å are identified as the 111 and 002 reflections of the GST metastable cubic phase. GST reflections appears at 390°C, highlighting two crystallization temperatures: 350°C for Ge, and 390°C for GST. By selecting all the reflections of each phase in the Fourier spectra of the experimental HRTEM images, numerical dark field images are produced, which allow mapping the various crystallized phases (see figure 1.C), and disclose the crystallization of the Ge and GST nanograins mainly in the bottom part of the cell.

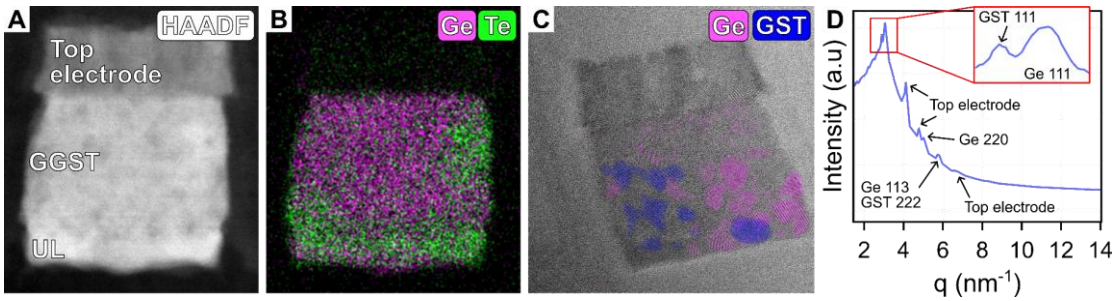

Fig. 1 *(A) STEM-HAADF image of a representative GGST cell with (B) its elemental map showing Ge, Sb and Te after a thermal pulse at 380°C. (C) HRTEM image of another GGST cell heated at 400°C, showing evidence of Ge and GST cubic phases inside the cell. (D) Radial integration profile of the corresponding FFT of (C) used to identify the different phases.*

4. CONCLUSIONS

In situ heating inside TEM using thermal pulses of 320ms has been performed to characterize the crystallization and chemical segregation of GGST phase change material in confined nanostructures. The sequential crystallization of the Ge and GST phases revealed in earlier studies is confirmed for this rapid heating condition: the formation of Ge grains occurs at 350°C, followed by the crystallization of the metastable GST phase at 390°C. STEM-EDX analyses suggest an opposite diffusion flow of the Ge and Te species at the interface between the GGST cell and the underlayer as the temperature increases.

REFERENCES

1. P. Zuliani *et al.*, *Solid-State-Electronics.* **111** (2015) 27.
2. P. Hans *et al.*, *J. Appl. Phys.* **134** (2023) 105102.
3. E. Rahier *et al.*, *Phys. Status Solidi RRL*. **17** (2023) 2200450.
4. S. Ran *et al.*, *Sci. Rep.* **15** (2025) 11357.

P-37

High-quality synthesis of $Ge_2Sb_2Te_5/TiTe_2$ thin films

Jiangjing Wang[1], Chao Nie[1]
1 Center for Alloy Innovation and Design, State Key Laboratory for Mechanical Behavior of Materials, Xi'an Jiaotong University, Xi'an 710049, China
*corresponding author: j.wang@xjtu.edu.cn

ABSTRACT

Phase-change heterostructure (PCH) devices with alternately stacked layers of phase change materials (PCM) and confinement material (CM) have been proposed to suppress the resistance noise and drift of PCM during device operation, which holds great promise for high-performance neuro-inspired computing [1]. Upon SET and RESET operations, the PCM slabs undergo crystallization and amorphization, while the CM crystalline slabs remained unchanged. To guarantee excellent device performances, it is important to obtain sharp atomic interfaces between CM and PCM sublayers. In previous work, we synthesized high quality $Sb_2Te_3/TiTe_2$ PCH films [2]. However, the temperature of chip service environment usually reaches ~85°C. To meet the requirements of the chip operating temperature, we managed to use $Ge_2Sb_2Te_5$ instead of Sb_2Te_3 as the PCM layer. In this work, we optimized the in-situ heating conditions and synthesized the GST-PCH films at the wafer-scale via magnetron sputtering. The X-ray diffraction (XRD) experiments demonstrated the consistency of the layered crystal orientation at the wafer-scale. The Atomic force microscopy (AFM) and high angle annular dark field scanning transmission electron microscopy (HAADF-STEM) experiments confirmed the atomically flat surfaces and interfaces between CM and PCM layers. We further built a light-controlled electrical test platform to measure the resistance drift of thin films by coupling laser with source meter. We used lasers to trigger the amorphization, and then used source meter to measure the resistance drift coefficient of the GST-PCH thin films. The synthesis of high quality $Ge_2Sb_2Te_5/TiTe_2$ thin film paves the way for the design and development of future phase change memory devices.

Key words: phase change heterostructure, thin film, sputtering, $Ge_2Sb_2Te_5$, $TiTe_2$.

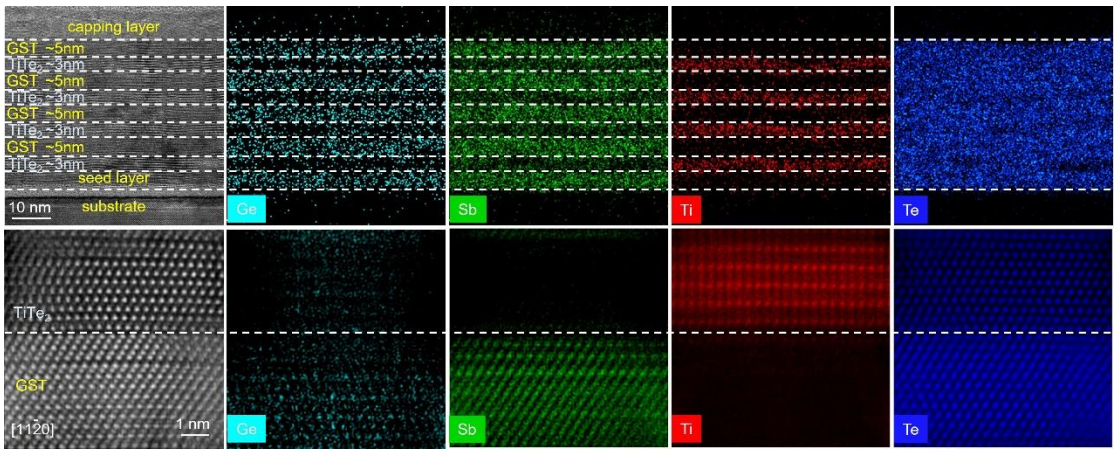

REFERENCES

1. K. Ding, J. Wang, W. Zhang, et al. Phase-change heterostructure enables ultralow noise and drift for memory operation. Science **366**, (2019) 210-215.

2. C. Nie, W. Zhang, J. Wang, et al. Role of seed layer in growing atomically flat $TiTe_2/Sb_2Te_3$ heterostructure thin films at the wafer scale. (2025) arXiv:2503.00459.

P-39

Influence of Sputtering Parameters on the Stoichiometry and Crystallization Behavior of Germanium Telluride (GeTe) Films Grown by Confocal Magnetron Sputtering

Shan Song[1,3*], Wahyu Diyatmika[2], Günther Ruhl[4], Seppe van Dyck[5], René Heller[6], Alexander Busch[2], Sven Zimmermann[1,3], Jörg Heß[2]

[1]Center for Micro and Nano Technologies (ZfM), Chemnitz University of Technology, Reichenhainer Str. 70, 09126 Chemnitz, Germany
[2]VON ARDENNE GmbH, Am Hahnweg 8, 01328 Dresden, Germany
[3] Fraunhofer Institute for Electronic Nano Systems (ENAS), Technologie-Campus 3, 09126 Chemnitz, Germany
[4] Technology Campus Teisnach Sensors, Deggendorf Institute of Technology, Technologiecampus 3, 94244 Teisnach, Germany
[5]Dept. of Solid-State Sciences, Ghent University, Krijgslaan 281, 9000 Gent, Belgium
[6]Helmholtz Zentrum Dresden Rossendorf e.V., Bautzner Landstr. 400, 01328 Dresden, Germany
*shan.song@zfm.tu-chemnitz.de

ABSTRACT

In this work, we investigate the influence of sputtering parameters on the chemical composition and crystallization behavior of germanium telluride films deposited on 200-mm silicon wafers. Depth-profiling X-ray photoelectron spectroscopy and in-situ X-ray diffractometry are employed to characterize the films. Optical and electrical measurements reveal a significant contrast in refractive index and a five-order-of-magnitude decrease in sheet resistance upon crystallization.

Key words: Germanium telluride, sputtering, XPS depth profile, in situ XRD.

1. INTRODUCTION

Germanium Telluride (GeTe) has attracted great attention in recent years due to its excellent reversible phase-switching behavior and the pronounced contrast in its electrical and optical properties between the amorphous and crystalline states. These characteristics make GeTe a promising candidate for a wide range of applications including phase-change random access memory (PCRAM), photonics, and optoelectronic devices. To further enhance the contrast in properties between the amorphous and crystalline states, numerous studies have explored superlattice structures and modifications to the chemical composition through co-sputtering and doping. In this work, we employ confocal magnetron sputtering with varying sputtering parameters to deposit GeTe thin films with different stoichiometries on 200-mm silicon wafers. Our objective is to investigate the effects of deposition parameters and capping layers on the chemical composition, crystallinity, and overall material properties of the GeTe thin films.

2. EXPERIMENTAL

GeTe films were deposited on 200-mm silicon wafers coated with a 1-µm-thick SiO_2 layer using a CS400SR sputtering cluster (VON ARDENNE GmbH). The deposition was performed from a nominally stoichiometric GeTe target, with variations in sputtering power and working pressure. Detailed deposition parameters are summarized in Table 1.

To prevent surface oxidation, a 15-nm-thick SiN layer was directly deposited onto the GeTe layer without breaking vacuum. The chemical composition of the deposited films was analyzed using Rutherford Backscattering Spectroscopy (RBS), while elemental distributions within the layer stacks were further examined through X-ray Photoelectron Spectroscopy (XPS) depth profiling. Phase transition and crystallization behavior were characterized by in-situ X-ray diffraction (XRD) during thermal annealing. Additionally, electrical properties were evaluated by measuring sheet

resistance using a four-point probe (4PP), and optical properties were assessed by determining the refractive index via spectroscopic ellipsometry.

Table 1. Deposition parameters of the GeTe thin film samples

Parameter	Value
Sputter Target	GeTe (50/50 compound target)
Sputter Power	DC: 100–200 W; RF: 100–200 W
Deposition Pressure	1–20 µbar
Film Thickness (GeTe)	20 nm, 50 nm, and 150 nm
Capping layer	SiNx

3. RESULTS & DISCUSSION

The XPS depth profile reveals the chemical composition across the layer stacks. At higher working pressures, a significant decrease in germanium concentration is observed, while the tellurium content remains relatively stable. When the working pressure exceeds 5 µbar, the presence of oxygen during deposition leads to the formation of germanium and tellurium oxides within the film. In contrast, variations in sputtering power and the choice between DC and RF sputtering modes have no significant effect on the chemical composition.

The impact of annealing conditions on the chemical composition was also examined. For SiNx-capped GeTe layers, no significant change in Ge, Te, or O content were observed between the as-deposited state and samples annealed either in air or under vacuum, demonstrating the effectiveness of the 15 nm-thick SiN_x capping layer in preventing oxidation. In contrast, uncapped GeTe films developed a native oxide layer, which appears to act as a partial barrier to further oxidation. However, Ge depletion and Te enrichment were detected at the interface between the GeTe film and the oxidized surface layer.

The stoichiometry of the grown layer was analyzed through RBS measurements. It can be speculated that the deviation from stoichiometry affects phase stability and structure: Ge-rich or Te-rich compositions can lead to the formation of secondary phases or structural disorder, which in turn alters the crystallization temperature. From the in-situ X-ray diffraction patterns, we could then determine whether the stoichiometric GeTe compositions tend to crystallize more rapidly than off-stoichiometric counterparts.

Interestingly, the sheet resistance of annealed GeTe layers deposited under varying power and pressure conditions remains relatively consistent, likely due to similar film thicknesses and compositions. However, films deposited using RF power at the lowest deposition pressure of 1 µbar exhibit reduced uniformity in sheet resistance, suggesting the choice of deposition power is crucial.

4. CONCLUSIONS

Our findings indicate that working pressure plays a critical role in the confocal sputtering of GeTe. This is primarily due to its direct influence on the sputtering yield disparity between Ge and Te atoms, as well as on oxygen incorporation during deposition. Sputtering with DC power results in more homogeneous phase-change material thin films, offering better suitability for commercial-scale production. Additionally, stoichiometric GeTe compositions exhibit faster crystallization compared to off-stoichiometric variants, which is particularly beneficial for applications such as optical data storage, where rapid switching is essential. These insights provide valuable experimental guidance for the development of potential applications, including phase-change random access memory and photonic devices.

P-02

Threshold Switching in Solid-State Amorphous Tellurium Accessed via On-Device Electrothermal Melt-Quenching

Namwook Hur[1], Seunghwan Kim[2], Yu Bin Park[3], Changhwan Kim[1], Sohui Yoon[1], Youngseok Cho[2], Tae Hoon Lee[3], and Joonki Suh[1,2,*]

[1]Department of Materials Science and Engineering, Ulsan National Institute of Science and Technology, Ulsan 44919, Republic of Korea
[2]Graduate School of Semiconductor Materials and Devices Engineering, Ulsan National Institute of Science and Technology, Ulsan 44919, Republic of Korea
[3]School of Materials Science and Engineering, Kyungpook National University, Daegu 41566, Republic of Korea
*Corresponding author: jsuh@unist.ac.kr

ABSTRACT

Chalcogenide glasses have been renowned for Ovonic threshold switching (OTS); the fundamental role of amorphous chalcogen remains to be discovered. Here, disordered tellurium is demonstrated within a nanoscale device via electrothermal quenching, and its switching characteristics, trap properties, and oscillations are analyzed during the order-to-disorder transition. This work provides insights into the key role of the chalcogen element for OTS.

Key words: *Ovonic Threshold Switching, Joule heating, Tellurium, Phase-Transition, Oscillation*

1. INTRODUCTION

Amorphous chalcogenide alloys exhibit a distinctive form of volatile electronic switching, known as ovonic threshold switching (OTS). This phenomenon is characterized by an abrupt increase in current, often spanning several orders of magnitude, at the threshold voltage (V_{th}), occurring on a nanosecond timescale. Specifically, since the constituent chalcogen species strictly govern the switching behavior—prior pulse polarity effect and self-regulating oscillation—characterizing disordered monatomic chalcogens are essential for uncovering their material-dependent properties. In parallel, elemental Te alone has been intensively investigated across a wide range of fields, from materials science to practical device applications. Nevertheless, integrating amorphous chalcogens, particularly monatomic tellurium (Te), into electronic devices remains challenging due to Te's intrinsically low crystallization temperature. For this purpose, we demonstrate an electrothermally reconfigured amorphous Te phase stabilized under cryogenic conditions. The order-to-disorder transitions yield V_{th} shift, sub-threshold current contrast, and self-regulatory behavior, which will be discussed in the Results and Discussion section.

2. EXPERIMENTAL

For the device fabrication, the W (100 nm)/Si_3N_4 (30 nm) layers were sequentially deposited on the bare substrate. Nanoscale holes were then patterned via dry etching. Next, a Te layer and a capping layer were deposited inside the hole. W metallization was done for both bottom and top electrodes. Electrical measurements were performed using a Keithley 4200A-SCS semiconductor analyzer. The cryogenic environment was constructed using liquid nitrogen (LN2) gas. The dark-field scanning transmission electron microscope (HAADF-STEM) with corresponding energy dispersive spectrometry (EDS) image was analyzed using a high-resolution TEM (JEOL, JEM-ARM300F).

3. RESULTS & DISCUSSION

Fig. 1a represents the experimental design for demonstrating the ordered and disordered Te solid states from a two-terminal Te device. To regulate the atomic arrangement within the programming region, we adopted melt-quenching processes wherein an ultrafast quenching speed on the nanosecond timescale leads to amorphization, while slower cooling promotes crystallization. The HRS was programmed with a 5 V pulse (rise/width/fall times of 20 ns/100 ns/20 ns), while the LRS was achieved using a 3 V pulse (1 μs/100 ns/1 μs). Based on quenching-rate-guided phase

regulation, we obtained *I-V* curves corresponding to two distinct Te phases—high resistance state (HRS) and low resistance state (LRS)—across 50 devices (**Fig. 1b**). During the order-to-disorder transition, a V_{th} increased by ~0.81 V, and a sub-threshold current measured at 0.5 V (I_{DC}) decreased by approximately three orders of magnitude. Meanwhile, both solid states were thermally unstable at the ambient room temperature (RT). Therefore, the specific trap characteristics were examined under cryogenic conditions. **Fig. 1c** presents sustainable phase retentions for over 10^3 seconds in the ordered and disordered phases at 80 K, emphasizing the necessity of cryogenic stabilization for preserving chalcogen phases. Distinct trap properties were extracted using a thermally assisted hopping (TAH) model. **Fig. 1d** showcases DC *I-V* curves in the sub-threshold voltage region at 80 K. The extracted trap property of the HRS exhibited a ~0.93 nm reduced trap distance (Δz) and 0.06 eV larger activation energy (E_a) than the LRS, indicating denser deep-level trap formations during amorphization. Concerning its trap nature, self-oscillation performance emerged in the elemental chalcogen device at 80 K (**Fig. 1e**). The reliable oscillations were represented in the HRS, driven by self-modulation of the applied bias in response to a 100-μs square pulse. Meanwhile, the LRS exhibited a constant current without any oscillatory behaviors, representing a lack of physical factors to establish self-regulated properties. To support experimental outcomes, various Te phases were analyzed using *ab initio* molecular-dynamics (AIMD) simulations. The mobility gap (E_g) and mid-gap state (MGS) were calculated by the total density of states (TDOS) and corresponding normalized inverse participation ratios (IPR). As a result, disordered Te presented a 0.7126 eV of E_g with a distinct MGS inside the mobility gap (**Fig. 1f**). Finally, the maximally localized Wannier function (MLWF) spread in the various Te phases indicated a reinforcement of electron delocalization toward disorder-to-liquid phases.

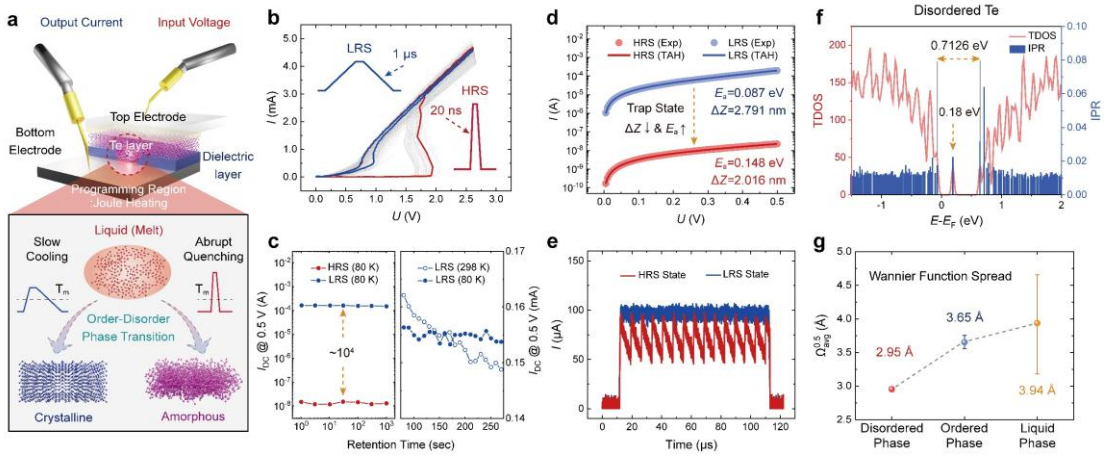

Fig. 1. (**a**) The conceptual design of the ordered-disordered solid states from a liquid Te inside a Joule heating device. (**b**) AC *I-V* curves of both the HRS and LRS at 50 individual Te-devices. (**c**) Time-dependent retentions of HRS and LRS states at 80 K and comparison of LRS states at RT. (**d**) DC *I-V* curves in the sub-threshold region of HRS and LRS at 80 K with thermally assisted hopping (TAH) conduction model fitting. (**e**) Self-oscillation phenomenon in the monatomic Te at 80 K. (**f**) Total density of states (TDOS) and their normalized inverse participation ratio (IPR) of disordered Te. (**g**) Maximally localized Wannier function spread of disordered, ordered, and liquid phases.

4. CONCLUSIONS

In conclusion, we have selectively demonstrated the electrothermally controlled crystallographic arrangement of monatomic Te by utilizing Joule heating within a nanoscale device. The two solid states of ordered and disordered Te phases were successfully established and stabilized by tuning the melt-quenching rate under a cryogenic environment. Reversible order-to-disorder phase transitions exhibited a significant difference in the V_{th}, sub-threshold current, and further reliable oscillations through a high degree of deep-level traps. Our investigation offers a meaningful perspective on the critical role of the chalcogen element in the basis of OTS behavior in amorphous chalcogenide glasses.

REFERENCES

P-04

Viscosity and the breakdown of Stokes-Einstein relation in supercooled liquid $Ge_2Sb_2Te_5$ from simulations with a neural network potential

S. Marcorini,* R. Pomodoro, O. Abou El Kheir and M. Bernasconi
Department of Materials Science, University of Milano-Bicocca, Milan, Italy
*corresponding author: s.marcorini@campus.unimib.it

ABSTRACT

Phase change materials (PCMs) are exploited in non-volatile electronic memories and photonic devices that rely on a fast and reversible transformation between the amorphous and crystalline phase upon heating. The recrystallization of the amorphous phase at the operation conditions of the memories occurs in the supercooled liquid phase above the glass transition temperature T_g. The dynamics of the supercooled liquid is thus of great relevance for the operation of the devices and, close to T_g, also for the structural relaxations of the glass that affect the performances of the memories. Information on the atomic dynamics is provided by the diffusion coefficient (D) and by the viscosity (η) which are, however, both difficult to be measured experimentally at the operation conditions of the devices due to the fast crystallization.

In this work, we leverage a machine learning interatomic potential [1] for the flagship PCM compound $Ge_2Sb_2Te_5$ to compute η, D and the α-relaxation time in a wide temperature range from 1200 K to about 100 K above T_g. Large scale molecular dynamics simulations allowed quantifying the fragility of the liquid, the validity of the Maxwell relation and the breakdown of the Stokes-Einstein relation between η and D in the supercooled liquid phase.

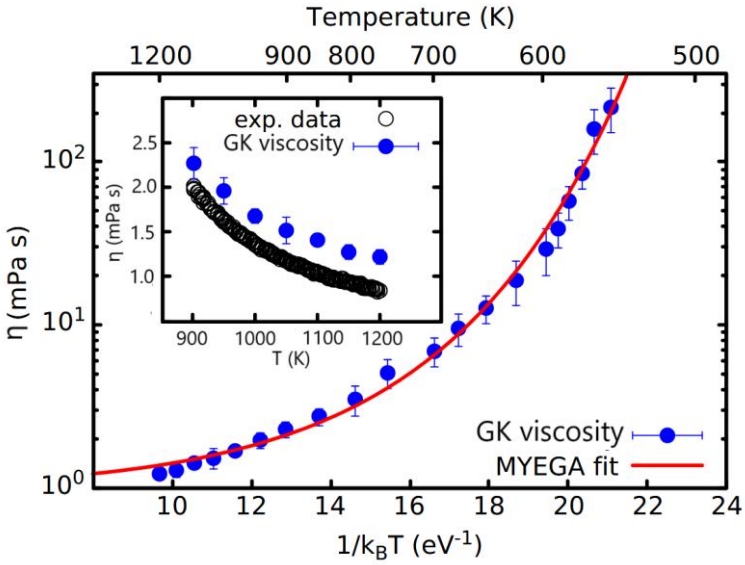

Figure 1: Angell plot for the viscosity η as a function of inverse temperature. The blue dots refer to the viscosity obtained from Green-Kubo integration of the stress tensor extracted from simulations. The continuous line is the fitting with a MYEGA function, from which it is possible to obtain an estimate of T_g and the fragility. In the inset, we present a comparison of the viscosity above the melting temperature from our simulations and from the experimental measurements of Ref. [2].

REFERENCES

1. O. Abou El Kheir, L. Bonati, M. Parrinello, and M. Bernasconi, npj Comput. Mater. 10, 33 (2024)
2. M. Schumacher, H. Weber, P. Jóvári, Y. Tsuchiya, T. G. Youngs, I. Kaban, and R. Mazzarello, Sci. Rep. 6, 27434 (2016).

P-06

Towards cryogenic phase change materials for neuromorphic image recognition

Piotr K. Popek, Bart J. Kooi
Zernike Institute for Advanced Materials, University of Groningen, The Netherlands,
p.k.popek@rug.nl

ABSTRACT

Phase change materials (PCM) in a cryogenic environment remain a relatively unexplored, yet increasingly promising topic. RESPITE, an EIC Pathfinder project, focusing on cryogenic neuromorphic computing for on-chip vision and cognition solutions, aims to combine superconductor-based detectors and neurons with novel PCM-based memory cells acting as synaptic weights. Due to expected higher resistance contrast, faster switching and reduced resistance drift, low temperatures may prove beneficial for such applications. Because of relatively high threshold voltage and switching energy of conventional $Ge_2Sb_2Te_5$ cells, focus was set on Sb-rich PCMs, which were considered to be more promising candidates [1].

In the present work, Sb_8Te_3 thin films were grown by pulsed lased deposition (PLD) from a home-made target. Deposition parameters were optimized, especially for reduction of particulate formation. Grown thin films were then characterized, including their morphology and composition, in particular their uniformity over a wider deposition area. Cryogenic sheet resistance and ellipsometry measurements were conducted and their contrasts between amorphous (as deposited) and crystallized phases were determined – Figure 1. Finally, a prototype PCM-based memory chip was developed and its performance has been tested.

Key words: cryogenic, neuromorphic computing, Sb-rich, PLD.

REFERENCES

J.L.M. Oosthoek, K. Attenborough, G.A.M. Hurkx, F.J. Jedema, D.J. Gravesteijn, B.J. Kooi, J. Appl. Phys. 110, (2011) 024505.

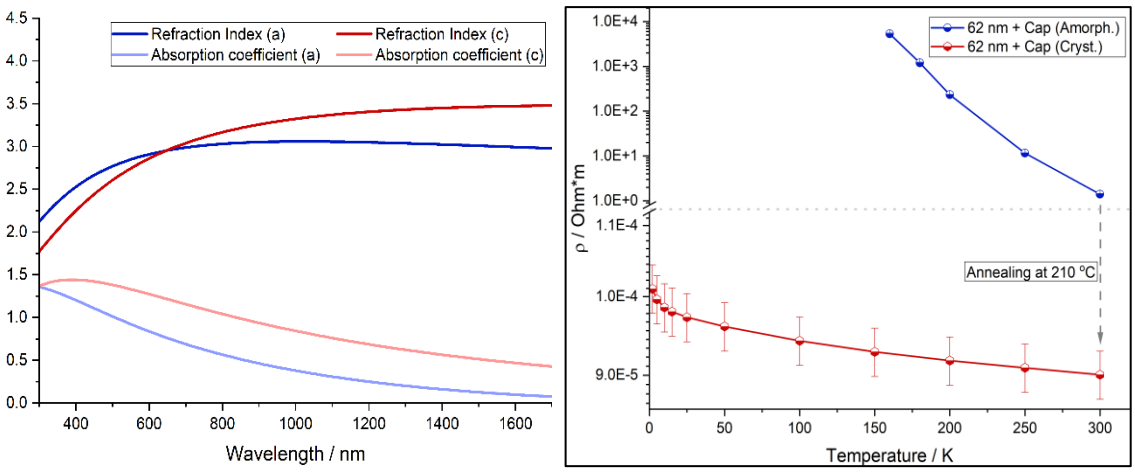

Figure 1 (Left) Refraction index and absorption coefficient of Sb_8Te_3 film as a function of wavelength calculated using the Tauc-Lorentz model for both amorphous (a) and crystalline (c) phases. The optical absorption contrast between both phases is large for most wavelengths. The absorption coefficient of the amorphous phase gets low for the higher wavelengths, which is of significance for the 1550 nm telecom wavelength. (Right) A comparison between resistivities of the amorphous as-deposited and the crystallized film as a function of temperature. In case of the amorphous film, the measurements were discontinued below 160 K due to long settling times. The resistivity contrast between the two phases is very large (notice the axis break and the scale difference between the two regions separated by the dotted line).

P-08

Ab-initio study of electromigration in liquid GeAsSe alloys for selector device

M. Cobelli[1], D. Baratella[1], P. Fantini[2] and M. Bernasconi[1] *
[1]Department of Materials Science, University of Milano-Bicocca, Milan, Italy
[2]Micron Technology Inc., Vimercate, Italy
*corresponding author: marco.bernasconi@unimib.it

ABSTRACT

Selenide amorphous alloys are of interest for applications in selector devices that exploit a sort of reversible dielectric breakdown named ovonic threshold switching. In the on-state of the device the system is typically brought in the supercooled liquid phase above the glass transition temperature where the atomic mobility is sufficiently high to cause demixing driven by the electric field. The electromigration force F responsible for ionic migration is proportional to the electric field E, via the effective charge Z^* ($F = Z^* E$), which is thus of great relevance for the electrothermal modeling of the devices. In this work, we have computed Z^* for a prototypical GeAsSe (GAS) selector alloy by leveraging a non-equilibrium Green's function (NEGF) method [1] based on density functional theory. The effective charges in the metallic liquid are obtained from the calculation of the atomic forces, including the wind force, in the presence of both an electric field and an electronic current.

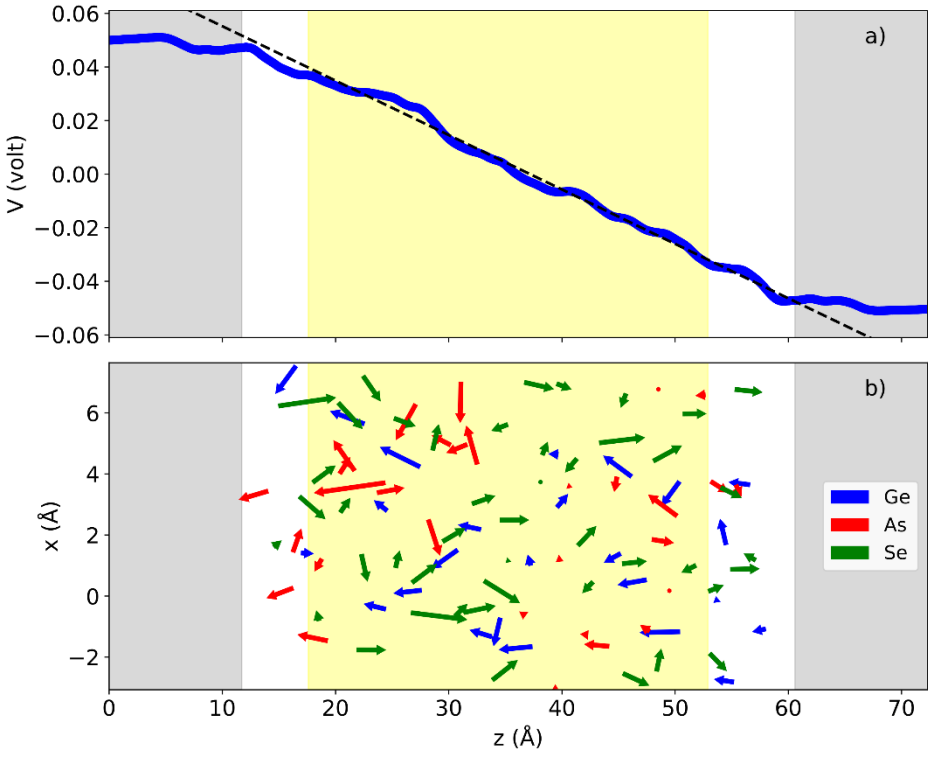

Figure 1: (a) Profile of the planar average of the electrostatic potential as a function of the position along the z direction in a Al/GAS/Al model. The shaded area at the edges correspond to two Al electrodes, while at a center a nearly constant planar averaged electric field is found. (b) Map of the electromigration forces taken as the difference of the forces computed at zero and finite bias on individual atoms. The projection of the forces on the xz plane is shown for a representative Al/GAS/Al model at 0.1V. Only atoms in the central region (shaded area), where the plane-averaged electric field is approximately uniform, are considered in the calculation of Z^*

	Ge	As	Se	charge/atom
Z^*	4.48 ± 0.134	0.691 ± 0.420	-3.087 ± 0.369	-0.0062 ± 0.570

Table 1: Effective charges for liquid GAS ($Ge_{25}As_{30}Se_{45}$) at 1100 K. The total charge per formula unit is given in the last column and it is obtained by summing the atomic charges weighted by the stoichiometry of the elements in the alloy.

REFERENCES

1. I. Rungger and S. Sanvito, *Phys. Rev. B* **78** (2008) 035407.

P-10

Self-aligned Atomically Thin Thermal Barrier for Highly Energy-Efficient Phase-Change Memory

Beomsung Park[1], Sang-woo Park[2], Sohui Yoon[1], Namwook Hur[1], Hongsik Jeong[1,2], and Joonki Suh[1,2,*]

[1]Department of Materials Science and Engineering, Ulsan National Institute of Science and Technology, Ulsan 44919, Republic of Korea
[2]Graduate School of Semiconductor Materials and Devices Engineering, Ulsan National Institute of Science and Technology, Ulsan 44919, Republic of Korea
*Corresponding author: jsuh@unist.ac.kr

ABSTRACT

Phase-change memory (PCM) is a promising nonvolatile memory with fast operational speed, but high energy consumption remains a challenge. This study enhances energy efficiency by adding a WSe_2 layer at the PCM interface, reducing SET energy by 16% and RESET current by 48%. The WSe_2 layer improves Joule heating through excellent thermal boundary resistance. This transfer-free method offers a potential solution for ultra-low energy, high-performance memory.

Key words: *Phase Change Memory (PCM), Thermal Boundary Resistance (TBR), Transition Metal Dichalcogenides (TMD)*

1. INTRODUCTION

Phase-change memory (PCM) has garnered significant attention as a high-speed, nonvolatile memory solution for storage-class applications. Despite its promising performance, the energy consumption associated with electro-thermal programming remains a key challenge. One of the primary factors contributing to high energy consumption in PCM is the inefficient thermal management during the programming process. In this study, optimizing thermal design to minimize energy usage is critical. Transition metal dichalcogenides (TMDs) have emerged as promising materials due to their excellent thermal boundary resistance (TBR) properties. TBR plays a crucial role in controlling the flow of heat between the phase-change material ($Ge_2Sb_2Te_5$) and the underlying electrode heater, influencing the overall energy efficiency of PCM devices. The integration of TMD layers, such as WSe_2, at the interface between the phase-change material and the heater can enhance the thermal management by boosting the Joule heating effect in the out-of-plane direction. This approach can significantly reduce the energy required for phase-change switching and improve the thermal stability of PCM devices. By leveraging the superior TBR characteristics of TMDs, a more energy-efficient and thermally optimized PCM device architecture can be achieved, paving the way for the development of next-generation memory technologies with ultra-low energy consumption.

2. EXPERIMENTAL

The fabrication process begins with the deposition of a 50 nm thick W layer using DC sputtering. Next, a 30 nm Si_3N_4 layer is deposited via plasma-enhanced chemical vapor deposition (PECVD). Following this, hole etching is performed using electron beam lithography to define specific patterns. Subsequently, a WSe_2 layer is formed through a selenization process using chemical vapor deposition (CVD). After that, GST ($Ge_2Sb_2Te_5$) patterning is carried out via photolithography, followed by the deposition of a 180 nm thick GST layer using RF sputtering. Then, a 20 nm TiN layer is deposited using high-step coverage (HSC sputter), and a lift-off process is used to remove excess materials. The wafer is then annealed at 180°C for 2 minutes using a rapid thermal process (RTP). Lastly, W metallization was done for both bottom and top electrodes. Electrical measurements were performed using a Keithley 4200A-SCS semiconductor analyzer.

3. RESULTS & DISCUSSION

Fig. 1a shows the structural layout of a phase-change memory (PCM) device. The scale bar in the image is 500 nm, giving an idea of the nanometer-scale thickness of these materials. **Fig. 1b** shows the XPS spectra of W and Se after the W selenization process. The peaks for W 4f and Se 3d are presented, where W 4f refers to the tungsten 4f binding energy and Se 3d represents the selenium 3d binding energy. The XPS analysis reveals how the chemical composition of the tungsten layer changes after the selenization process, showing the formation of WSe_2. The GIWAXS images show the as-deposited W layer on the left and the WSe_2 layer after selenization on the right. These X-ray diffraction patterns demonstrate the crystalline structure of the materials before and after the selenization process. The selenized W layer shows a well-formed crystalline structure, characteristic of WSe_2, in comparison to the as-deposited W layer (**Fig. 1c**). The graph displays the resistance-current characteristics for both conventional PCM (black line) and the WSe_2-PCM (red line). The graph shows that the WSe_2-PCM device exhibits different resistance switching behavior, such as lower operating currents compared to conventional PCM, highlighting its potential advantages in terms of energy efficiency and performance (**Fig. 1d**). **Fig. 1e** compares the SET and RESET energies of conventional PCM and WSe_2-PCM devices, specifically in the case of a 400 nm hole diameter. The WSe_2-PCM device demonstrates lower energy consumption during the switching operations, making it more efficient than conventional PCM. The bar chart compares the current densities in conventional PCM (400 nm, 200 nm hole diameter) and WSe_2-PCM (400 nm hole diameter). The WSe_2-PCM device shows higher current density, indicating improved performance and better scalability compared to conventional PCM (**Fig. 1f**). This graph plots the endurance of the WSe_2-PCM device in terms of operation cycles. The data shows that the WSe_2-PCM device has a significantly higher endurance, with stable SET/RESET switching after many cycles. This suggests that the WSe_2-PCM device has enhanced reliability over time compared to conventional PCM (**Fig. 1g**).

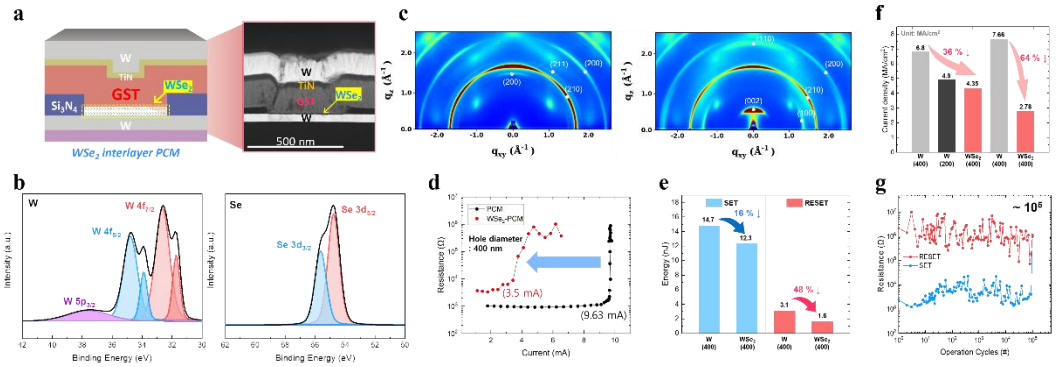

Fig. 1. (**a**) The conceptual design of cross-sectional WSe_2-PCM device. The scale bar is 500 nm. (**b**) X-ray Photoelectron Spectroscope (XPS) after W Selenization. (**c**) Grazing-Incidence Wide-Angle X-ray Scattering (GIWAXS) image of as-deposited W (left) and after W Selenization sample (right). (**d**) R-I curve of conventional PCM (black line) and WSe_2-PCM (Red line) (**e**) SET and RESET energy of conventional PCM and WSe_2-PCM in 400 nm hole diameter. (**f**) Current density of conventional PCM (400 nm, 200 nm hole diameter) and WSe_2-PCM (400 nm hole diameter). (**g**) Endurance of WSe_2-PCM.

4. CONCLUSIONS

In conclusion, we presented the enhancement of PCM energy efficiency by introducing a WSe_2 layer at the interface between GST and the bottom electrode heater. The WSe_2-PCM devices show 16% lower SET energy, and 48% lower RESET current compared to devices without WSe_2. This improvement is attributed to the superior TBR of WSe_2, which boosts the Joule heating effect. The transfer-free selenization method ensures the perfect formation of the WSe_2 layer, making it a promising solution for next-generation ultra-low energy PCM devices.

REFERENCE

P-12

Phase-change heterostructures based on $MoSe_2$ intercalated with $Ge_2Sb_2Te_5$

S. De Simone[1]*, A. Foglietti[1,2], S. Calvi[1,3], A. Díaz Fattorini[1,3], C. Petrucci[1,3], F. Arciprete[1,3], M. Longo[3,1] and R. Calarco[1]

[1]Institute for Microelectronics and Microsystems (IMM), Consiglio Nazionale delle Ricerche (CNR), Via del Fosso del Cavaliere 100, 00133 Rome, Italy;
[2] Department of Chemistry University of Rome Tor Vergata, Via della Ricerca Scientifica 1, 00133 Rome, Italy;
[3] Department of Physics, University of "Tor Vergata", Via della Ricerca Scientifica 1, 00133 Rome, Italy.

*corresponding author: sara.desimone@cnr.it

ABSTRACT

We report an experimental study of $MoSe_2$ thin films grown by RF-sputtering at room temperature and their integration into $MoSe_2/Ge_2Sb_2Te_5$ phase-change heterostructures. Structural and morphological properties were analyzed via temperature-dependent X-Ray diffraction (XRD), Atomic force microscopy (AFM), and Scanning electron microscopy (SEM).

Key words: $MoSe_2$, heterostructures, sputtering.

1. INTRODUCTION

In recent years, the advancement of non-volatile memory technologies has become crucial to meet the demand for faster, more reliable, and energy-efficient data storage. Heterostructures incorporating chalcogenide thin films offer key advantages: enhanced switching speed, resistance, and scalability. The realization of heterostructures combining phase-change materials (PCMs) and transition metal dichalcogenides (TMDCs) offers a promising future path. These layered systems leverage the fast-switching and high-contrast properties of PCMs with the unique electronic and thermal characteristics of TMDCs, thus enabling several functionalities such as multi-level data storage and unlocking new capabilities in memory and logic applications.

2. EXPERIMENTAL

Sample deposition

Amorphous $MoSe_2$ and $MoSe_2$/GST225 heterostructures were deposited in Ar atmosphere using radio frequency sputtering in a custom-built high-vacuum chamber system (IONVAC PROCESS). $MoSe_2$ monolayers with thicknesses of approximately 20, 80, and 160 nm were grown at room temperature (RT) on various substrates to study the influence of deposition parameters on the growth of individual layers. Heterostructures consisting of alternating layers of GST225 and ultrathin $MoSe_2$ as confining layers were also deposited at RT. The elemental composition of the as-deposited layers was evaluated using energy dispersive X-Ray fluorescence.

Morphological, structural and electrical characterization

The deposited samples were characterized to evaluate the morphological, structural properties of single and alternating layers as a function of the deposition parameters, aiming to identify the deposition conditions that ensure thermal stability, low surface roughness, and flat morphology. Crystallization temperature experiments were conducted using a D8 Discover diffractometer equipped with a Cu-Kα_1 X-ray source. Grazing incidence diffraction (GID) (ω - 2θ) scans were recorded during sample annealing over a temperature range of (30 – 350) °C. In particular, SEM and AFM images of MoS_2 samples deposited on different substrates were recorded to gain insights into the possible interactions between the TMDCs and the substrate

3. RESULTS & DISCUSSION

Figure 1 presents several key characterizations of the $MoSe_2$ films. The XRD spectra in a) reveal that the (002) diffraction peak of $MoSe_2$ appears around 250 °C during annealing from 30 °C to 350 °C, marking the onset of crystallization. In b) the SEM image of an as-deposited $MoSe_2$ film, approximately 80 nm thick, shows a fine-grained surface morphology with uniformly distributed nanostructures. The film surface is free of large agglomerates or cracks, indicating good film coverage and uniformity. These observations are further supported by the AFM image c) of the same film, which confirms homogeneous surface features seen in the SEM analysis.

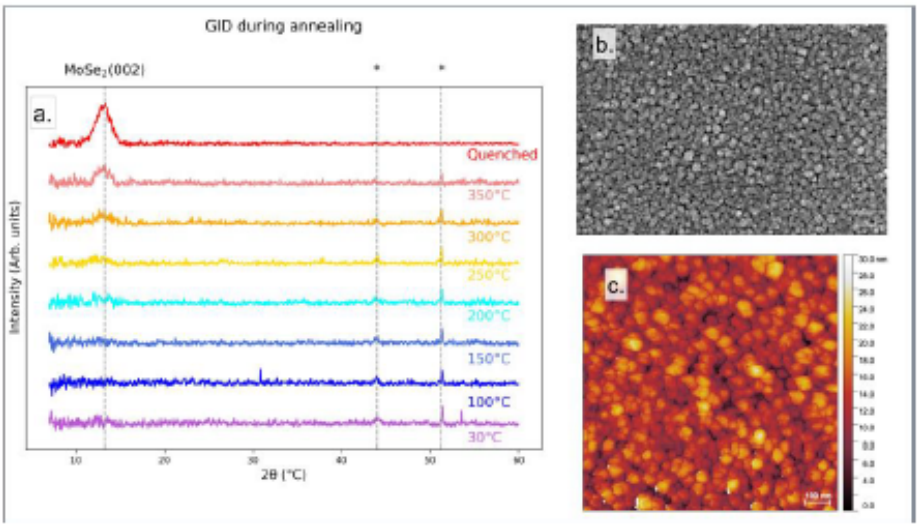

Fig. 1 *Characterization of $MoSe_2$ thin films: (a) GID scans collected during annealing, showing the emergence of the (002) diffraction peak around 250 °C, indicating the onset of crystallization; (b) SEM image of an as-deposited ~80 nm thick film, revealing a fine-grained, uniform surface morphology without visible defects or cracks; (c) AFM image of the same as-deposited film, confirming homogeneous surface coverage and consistent nanoscale features observed by SEM.*

As a final step, alternating 20 nm layers of GST225 and 7 nm layers of $MoSe_2$ were deposited to investigate the thermal confinement effect achieved by inserting thin TMDC layers between active PCM films. The resulting heterostructure was annealed up to the crystallization temperature of $MoSe_2$, higher than that of GST225, and its structural response was compared to that of the individual thin films. Diffraction peaks corresponding to the cubic and trigonal phases of GST225 were observed. It could be derived that the cubic-phase features persist alongside the emerging (013) peak of trigonal GST, indicating phase coexistence. This incomplete transition could be attributed to the $MoSe_2$ layers, which likely act as thermoelectric confinement barriers that locally alter the kinetics of phase transformation.

4. CONCLUSIONS

The XRD, SEM and AFM analysis of the single-layer $MoSe_2$ films revealed that crystallization begins between 250 °C and 300 °C. Moreover, the film surface exhibited a uniformly smooth yet intricate texture, with nanoscale features dispersed evenly across the layer, indicating excellent morphological uniformity.
The $MoSe_2$/GST225 heterostructure showed a peculiar crystallization behavior, evidencing the role of $MoSe_2$ as a thermal confinement layer, and the potential of such a heterostructure for phase change memory devices.

REFERENCES

1. T. S. et al.,Nano Letters, (2013).13(12), 6078-6083;
2. B. M., *et al.* Stable chalcogenide *Sci Rep* 14, (2024). 15713

P-14

Structural and electronic characterization of Ti-doped GST films: preliminary results

C. Petrucci[1,2], S. Prili[1,2], S. Calvi[1,2], E. Placidi[2], S. De Simone[2], M. Longo[2,4] R. Calarco[2] and F. Arciprete[1,2]

[1]Department of Physics, University of Rome "Tor Vergata", Via della Ricerca Scientifica 1, Rome 00133, Italy

[2]Institute for Microelectronics and Microsystems (CNR–IMM), Via del Fosso del Cavaliere 100, Rome 00133, Italy

[3]Department of Physics, University of Rome "La Sapienza", Piazzale Aldo Moro 5, 00185 Rome, Italy

[4]Department of Chemistry, University of Rome "Tor Vergata", Via della Ricerca Scientifica 1, 00133 Rome, Italy

corresponding author: christian.petrucci@roma2.infn.eu

ABSTRACT

In this work, we have studied the effect of the incorporation of Titanium in Ge-Sb-Te (GST) alloys, in samples grown via Molecular Beam Epitaxy (MBE), focusing on the possible modification of crystalline structure, investigated via X-Ray Diffraction (XRD), and electronic structure, studied by X-Ray Photoemission Spectroscopy (XPS)

Key words: Ti-doped GST, vacancy ordering, XPS.

1. INTRODUCTION

Among phase change materials (PCMs), GST has established itself as one of the most widespread alloys suitable for data storage applications. Nevertheless, a series of operating limitations affect the efficiency of GST-based alloys, such as low crystallization temperature, resulting in poor state retention, and a high RESET current, which leads to high power consumption. A tentative improvement in these performances is given by doping GST with foreign elements. Titanium-doped GST systems have shown a higher crystallization temperature and an improved data retention ability [1]. In our work, increasing amounts of Ti were used to dope epitaxial GST thin films. XPS has been carried out to investigate the influence of Ti on the electronic properties of the alloys, while XRD has been carried out for a structural characterization of the sample to investigate the effect of Ti incorporation on GST block stacking. Particular attention is paid to understanding the condition for a substitutional incorporation and site occupation of Ti in the GST matrix. Latter analysis is also helpful for the interpretation of the mechanisms that compromise the structural stability upon thermal treatments of $TiTe_2$/GST heterostructures [2][3].

2. EXPERIMENTAL

A series of GST samples with an increasing Ti concentration has been grown via MBE, by means of Knudsen Cells for Ge, Sb and Te evaporation, while an electron beam evaporator was used for Ti. Mica (Muscovite) was chosen as substrate to exploit its natural surface passivation obtained after mechanical exfoliation, allowing van der Waals epitaxy. The electronic properties were studied by analyzing both valence bands and Ge, Sb and Te core levels. All the samples have been annealed in UHV before XPS analysis. Symmetric ω–2θ diffractograms have been collected for XRD characterization.

3. RESULTS & DISCUSSION

In Figure 1, we report diffraction curves for both as-grown and UHV-annealed samples for increasing Ti concentrations, from 0 (pure GST) to the ~6%. For all the samples, *ω–2θ* XRD curves show 2 main reflections at ≈ 26° and 53° (black asterisk) corresponding to GST(111) and GST(222) reflections, respectively (substrate peaks are marked by orange triangles). This indicates that, regardless of Ti concentration, GST epitaxy is always achieved, leading to textured films with (111) out of plane orientation. Interestingly, in the case pure GST (0% Ti), we also observe two broad bumps at ≈ 19° and 46° indicative of the formation of vacancy layers (VLs) along the (111) direction [4]. Surprisingly, VLs completely disappear upon Ti doping, indicating the influence of Ti in the GST vacancy ordering process. Regarding the electronic properties, the valence band of Ti-doped GST (not shown) exhibits clear changes in lineshape as a function of Ti concentration. These variations will be further investigated in conjunction with the analysis core-levels and Ti-induced bonding configurations within the GST matrix.

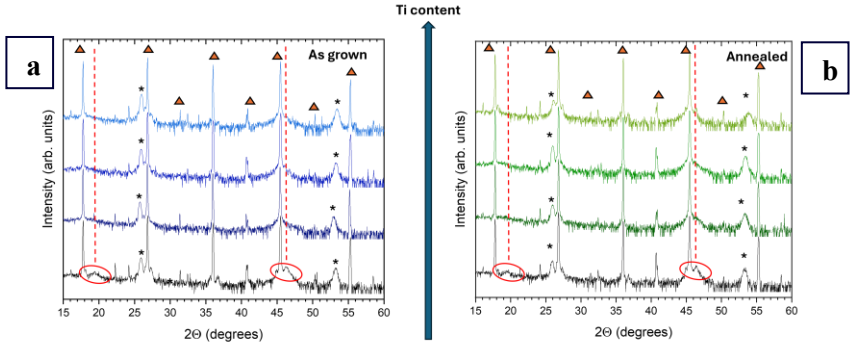

Figure 1: a,b) Diffraction curves of Ti-doped GST samples. Peaks marked with orange triangles are related to Mica substrate. Reflections marked with black asterisks refer to cubic GST phase. The vacancy layers peaks (red circles) disappears when Ti is added.

4. CONCLUSIONS

The evolution of structural and electronic properties of Ti-GST alloys have been studied as a function of Ti concentration. We have shown that the addition of Ti in GST matrix influences vacancy ordering, as evidenced by the disappearance of vacancy layers diffraction peaks. The electronic structure is also affected by the incorporation of Ti, The Ti-induced bonding configurations within the GST matrix is discussed.

REFERENCES

1. Cao, Liangliang, et al. "Advantage of Ti-doped Ge2Sb2Te5 material for phase change memory applications." *ECS Solid State Letters* 4.12 (2015): P102.

2. Ding, Keyuan, et al. "Phase-change heterostructure enables ultralow noise and drift for memory operation." *Science* 366.6462 (2019): 210-215.

3. Cohen, Guy M., et al. "Low RESET Current Mushroom-Cell Phase-Change Memory Using Fiber-Textured Homostructure GeSbTe on Highly Oriented Seed Layer." *physica status solidi (RRL)–Rapid Research Letters* 18.10 (2024): 2300426.

4. Bragaglia, Valeria, et al. "Metal-insulator transition driven by vacancy ordering in GeSbTe phase change materials." *Scientific reports* 6.1 (2016): 23843.

P-16

Exploring ZnSb Phase Change Material Alloys for Nonvolatile Embedded-Memory Applications

H. Neggaz*, J. Remondina, M. Bertoglio, M. Putero, and A. Portavoce
Aix-Marseille Univ., CNRS IM2NP Campus Scientifique de St. Jérôme 13013 Marseille, France

*Corresponding author: hamid.neggaz@im2np.fr

ABSTRACT

We investigated the Zn-Sb system for phase change memory (PCM) applications, focusing on ZnSb and Zn_4Sb_3 thin films. Using *in situ* XRD, XRR and atom probe tomography, we analyzed phase formation, density changes, and atomic redistribution during crystallization. Zn_4Sb_3 crystallizes at 145°C with low activation energies, while ZnSb crystallizes at 270°C via a two-step sequence involving high formation energy and low growth activation energy. These contrasting behaviors highlight how compositional tuning in the Zn-Sb system can tailor phase-change properties for memory device integration.

Key words: Phase Change Memory (PCM), ZnSb compound, Phase Sequence, Crystallization, Density Changes, Atom Probe Tomography (ATP).

1. INTRODUCTION

Phase-change materials (PCMs) are pivotal in the development of emerging memory technologies, particularly in phase-change memory (PCRAM) devices. Among the most extensively studied PCMs are $Ge_xSb_yTe_z$ (GST) and Ge-rich GST [1], GaSb [2], and SbTe [3], owing to their favorable switching characteristics and reliability. In this context, our study explores Zn-Sb alloys, promising intermetallic semiconductors, traditionally investigated for their thermoelectric properties [4]. Recent research has revealed their potential as phase-change material, demonstrating both reversible switching behavior and significant electrical contrast between amorphous and crystalline states [5]. Yimin et al. [6] reported a crystallization temperature of 257°C with an activation energy of 5.63 eV, leading to a 10-years thermal stability at 201°C, and a notable resistivity contrast of approximately 10^{-4} Ω/sq for ZnSb. The aim of this work is to gain deeper insight into atomic redistribution mechanisms and physico-chemical processes involved in ZnSb crystallization, with a focus on its potential use in non-volatile embedded memory applications.

2. EXPERIMENTAL

Various magnetron sputtering approaches were employed to synthesize Zn-Sb thin films: direct deposition from a pre-alloyed ZnSb (50:50) target, co-sputtering from individual Zn and Sb targets with controlled composition variations, and bilayer deposition to investigate reactive diffusion mechanisms. *In situ* X-ray diffraction (XRD) was used to monitor phase sequences and determine crystallization temperatures, while X-ray reflectivity (XRR) provided insights into thickness and density changes upon crystallization. Furthermore, atom probe tomography was used to probe the local atomic composition, offering valuable insights into the mechanisms of phase formation and elemental redistribution during crystallization.

3. RESULTS & DISCUSSION

Our results reveal markedly different crystallization behaviors between ZnSb (50:50) and Zn_4Sb_3 (57:43) compositions (see Figs. 1 and 2). Zn_4Sb_3 forms at significantly lower temperature (145°C) compared to ZnSb, which crystallizes at 270°C. These compounds also display distinct activation energy profiles during phase formation. For Zn_4Sb_3, the nucleation energy (E_n) and the growth activation energy (E_g) are found to be ~1.6 eV and 1.7 eV, respectively, which are both lower than

those reported for GST225 (E_n = 2.3 eV), indicating easier crystallization. In contrast, ZnSb exhibits a two-step crystallization process characterized by sequential formation of two intermediate phases with a temperature offset of approximately 10 °C. This process involves high formation energy of ~ 5.3 eV and remarkably low growth activation energy ~ 0.6 eV, suggesting significant nucleation energy barrier, but rapid crystal growth once initiated.

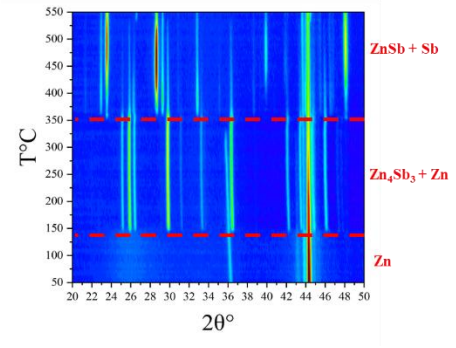

Fig. 1: *in situ* XRD recorded during ramp annealing (5°C/min) on a ZnSb co-sputtered thin film. The horizontal dotted red lines delimitate temperature domains of each phase.

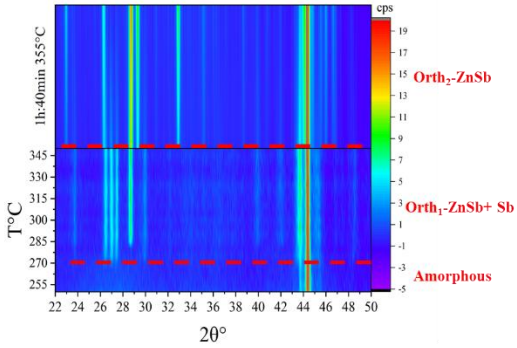

Fig. 2: *in situ* XRD recorded during ramp annealing (5°C/min) from 50 to 350°C followed by an isotherm (1h:40min) on a Zn_4Sb_3 co-sputtered thin film. The horizontal dotted red lines delimitate temperature domains of each phase.

4. CONCLUSIONS

This study highlights the significant difference in phase sequence and activation energies between the two compounds, namely ZnSb and Zn_4Sb_3. **ZnSb** crystallization exhibits high activation energy, which leads to good thermal stability and long retention time at elevated temperature, properties that are highly desirable for embedded memory applications. In contrast, Zn_4Sb_3 crystallization shows much lower activation energy, enabling fast crystallization, making it a promising candidate for optical and photonic applications where rapid phase transitions are beneficial.

REFERENCES

[1] J. Remondina, E. Rahier, M. A. Luong, N. Ratel-Ramond, S. Ran, D. Grosso, C. Mocuta, A. Portavoce, Y. Le Friec, D. Benoit, E. Petroni, A. Claverie and Putero, Phys. status solidi – Rapid Res. Lett., 2025, 2500035. doi:10.1002/pssr.202500035.

[2] R. Ume, H. Gong, V. Tokranov, M. Yakimov, K. Brew, G. Cohen, C. Lavoie, S. Schujman, J. Liu, A. I. Frenkel, K. Beckmann, N. Cady and S. Oktyabrsky, J. Appl. Phys., 2022, 132, 35103. doi:10.1063/5.0096022.

[3] M. Zhu, L. Wu, F. Rao, Z. Song, K. Ren, X. Ji, S. Song, D. Yao and S. Feng, Appl. Phys. Lett., 2014, 104, 53119. doi:10.1063/1.4863430

[4] A. Ostovari Moghaddam, E. Trofimov, T. Zhang, J. Arbiol and A. Cabot, Trans. Nonferrous Met. Soc. China (English Ed.), 2021, 31, 753–763. doi:10.1016/S1003-6326(21)65536-X.

[5] L. Song, M. Roelsgaard, A. B. Blichfeld, A.-C. Dippel, K. M. Ø. Jensen, J. Zhang and B. B. Iversen, IUCrJ, 2021, 8, 444–454. doi:10.1107/S2052252521002852.

[6] Y. Chen, G. Wang, X. Shen, T. Xu, R. P. Wang, L. Wu, Y. Lu, J. Li, S. Dai and Q. Nie, CrystEngComm, 2014, 16, 757–762. doi:10.1039/C3CE42024H.

P-18

Nanoscale investigation of electrically-induced transformations in Ge-rich GST for advanced phase change memory applications

C. Boujrouf[1*], A. Portavoce[1], M. Bocquet[1], L. Patout[1], Y. Le Friec[2], A. Charaï[1]

[1] Aix-Marseille University, IM2NP Laboratory, France
[2]STMicroelectronics, 850 Rue Jean Monnet, 38920 Crolles, France
*chaymaa.boujrouf@im2np.fr

ABSTRACT

This work investigates the impact of local electrical stimulation on Ge-rich GST thin films using Conductive AFM and HR-TEM. Structural and chemical analyses reveal early-stage phase transformations at the nanoscale, offering insights to improve reliability and scalability of phase change memory technologies.

Key words: Ge-rich GST, phase change materials, conductive AFM, crystallization, electrical switching

1. INTRODUCTION

Phase change materials (PCMs) are at the core of emerging non-volatile memory technologies, offering high speed, scalability, and thermal stability. Among these, Germanium-Antimony-Tellurium (GST) alloys stand out due to their ability to undergo rapid and reversible transitions between amorphous (high-resistance) and crystalline (low-resistance) phases, enabling efficient SET and RESET operations. These unique properties make GST-based materials strong candidates for demanding environments, including automotive and embedded applications [1-2]. The majority of studies on GST thin films focus on thermal annealing under vacuum or laser irradiation, probing only the Joule-effect mediated thermal component of the electrical pulse. Investigations involving electrical stimulation remain limited, despite their relevance compared to operating conditions in actual memory cells, combining Joule heating, electric field and current density effects [3]. In contrast, this work aims at investigating electrical component effect on the first stage of GST thin film crystallization.

2. EXPERIMENTAL

We focus on Ge-rich GST compositions, engineered to enhance thermal stability [4]. We apply localized electrical stimulation using Conductive Atomic Force Microscopy (C-AFM) to induce phase transitions at the nanoscale. Subsequent high-resolution Transmission Electron Microscopy (HR-TEM) allows us to precisely characterize the microstructural and compositional changes in the electrically stressed regions.

3. RESULTS & DISCUSSION

TEM analysis reveals that electrical stimulation leads to partial or complete crystallization in localized regions of the Ge-rich GST layer. Elemental mapping confirms the redistribution of Ge, Sb, and Te atoms, depending on the intensity and duration of the electrical pulse. The data indicate that crystallization can be initiated through combined thermal and electrical mechanisms, with the electric field playing a non-negligible role in structural transformation. These observations highlight the sensitivity of GST microstructure to electrical parameters, emphasizing the need to account for electric field effects in device modeling and material optimization.

4. CONCLUSIONS

Our findings reveal critical correlations between electrical stress, local phase transitions, and the evolution of crystallinity and elemental distribution. These insights contribute to a deeper understanding of the structure-property relationships that govern the behavior of GST-based materials under operational conditions. This work provides valuable guidance for the design and optimization of next-generation phase change memory devices with enhanced endurance and performance.

REFERENCES

[1] S. Raoux, F. Xiong, M. [ig, and E. Pop, "Phase change materials and phase change memory," *MRS Bull*, vol. 39, no. 8, pp. 703–710, Aug. 2014, doi: 10.1557/mrs.2014.139.
[2] D. Ielmini, "Threshold switching mechanism by high-field energy gain in the hopping transport of chalcogenide glasses," *Phys Rev B Condens Matter Mater Phys*, vol. 78, no. 3, Jul. 2008, doi: 10.1103/PhysRevB.78.035308.
[3] L. Zhang *et al.*, "Operando electrical biasing TEM experiments of Ge-rich GST thin films with FIB sample preparation," *J Alloys Compd*, vol. 1003, Oct. 2024, doi: 10.1016/j.jallcom.2024.175626.
[4] L. Prazakova *et al.*, "The effect of Ge content on structural evolution of Ge-rich GeSbTe alloys at increasing temperature," *Materialia (Oxf)*, vol. 21, Mar. 2022, doi: 10.1016/j.mtla.2022.101345.

P-20

Thermal melting induced band-gap closing and electronic delocalization in Ovonic threshold switching material GeSe

Nian-Ke Chen and Xian-Bin Li
State Key Laboratory of Integrated Optoelectronics, College of Electronic Science and Engineering, Jilin University, Changchun 130012, China.
*corresponding author: chennianke@jlu.edu.cn or lixianbin@jlu.edu.cn

ABSTRACT

First-principles calculations reveal that thermal-induced structural transition of the Ovonic threshold switching (OTS) material (amorphous GeSe), not only reduces its band gap but also causes the originally localized band-edge states to become delocalized. As a result, the conductivity of the OTS material can be enhanced. Therefore, thermal-induced structural transitions may play an important role in the OTS holding-on state of OTS+PCM devices in 3D-crossbar memory chips.

Key words: Ovonic threshold switching, atomic and electronic structures, first-principles calculations.

1. INTRODUCTION

Ovonic threshold switching (OTS) devices play a critical role in suppressing sneak-path currents in phase-change memory (PCM) chips based on 3D-Xpoint architecture. OTS materials are primarily amorphous chalcogenides that act as insulators under low electric voltage but become good conductors when the applied voltage exceeds a threshold value. After switching, the device will work for a period of time, named the holding-ON stage, to operate the PCM cell. Although the mechanism of OTS is still in debate, it is generally believed to be electronically initiated.[1] As a result, changes in atomic structures and their influences are often overlooked. However, for the RESET operation of the 1S1R (OTS+PCM) devices, the operation voltage is often large enough to ensure that the electrical current density can melt the PCM materials [9]. Considering that the melting points of PCM materials are higher than the glass-transition temperatures of OTS materials, the atomic structures of OTS materials should also be changed by the significant Joule heating effect during the holding-ON stage. Therefore, thermally-induced structural transitions of OTS materials and their corresponding effects on the electronic properties of OTS materials must be reconsidered for the OTS+PCM devices. In this presentation, we will introduce the Joule-heating effect induced electronic structure transitions in typical OTS material GeSe investigated by first-principles calculations.[2] A mechanism of thermal-induced band-gap closing and electronic delocalization is revealed, which can enhance the electrical conductivity of OTS materials. Therefore, we suggest that the structural transition or even melting of OTS materials be carefully considered in OTS+PCM devices.

2. EXPERIMENTAL

Density-functional theory (DFT) calculations are performed using the Vienna ab initio simulation package (VASP). Projector augmented-wave (PAW) pseudopotentials with generalized gradient approximation (GGA) exchange-correlation functional developed by Perdew, Burke and Ernzerhof (PBE) are used. The k-point grids for integration of the Brillouin zone are Monkhorst–Pack grids of 2 × 2 × 2 for DOS and IPR calculations. The models of GeSe contain 108 Ge and 108 Se atoms. The liquid and amorphous models of GeSe were obtained by the melt-quench method via molecular dynamic simulations.

3. RESULTS & DISCUSSION

Figure 1a shows the finite-element analysis (FEA) model of the OTS+PCM nanodevice that was built based on a previously reported pillar OTS+PCM device.[3] The properties of typical OTS and PCM materials, specifically GeSe and $Ge_2Sb_2Te_5$, are used as parameters for the FEA simulations.

Note that, the purpose of the simulation is to compare the temperatures of OTS and PCM cells in the nanodevice when the electrical current is large enough to RESET the PCM cell. To simplify, we only simulate the Joule heating and thermal diffusion effects of the two cells under a rectangle electrical pulse without considering the switching process. Figure 1b shows the temperature distribution in the nanodevice when the temperature of the PCM cell reaches 1000 K which is higher than the melting point of crystalline $Ge_2Sb_2Te_5$ (~900 K). At this time, the temperature of the OTS cell can reach 1260 K. Therefore, thermal-induced structural transitions of OTS materials can be significant in such devices. Next, the changes in the atomic and electronic structures of amorphous GeSe after melting are investigated using DFT calculations. Figure 1c shows the density of states (DOS) of amorphous GeSe at 300 K, where a band gap is clearly visible, despite the presence of a localized in-gap state. Then, the band gap gradually decreases as the temperature increases. After melting, the band gap of liquid GeSe at 1100 K is completely closed, indicating a transition to a metallic state (Fig. 1d). As a result, the carrier concentrations in liquid GeSe will significantly increase. Moreover, the localization of the band edge states will also be changed by thermal-induced structural transitions. For example, the IPR in Fig. 1e indicates that the band edge states are all localized. However, the IPR of the band edge states is dramatically reduced after melting (Fig. 1f). As such, carrier mobility should be enhanced. Therefore, we suggest that the structural/electronic transitions induced by Joule heating during the holding-on stage be considered in OTS+PCM devices.

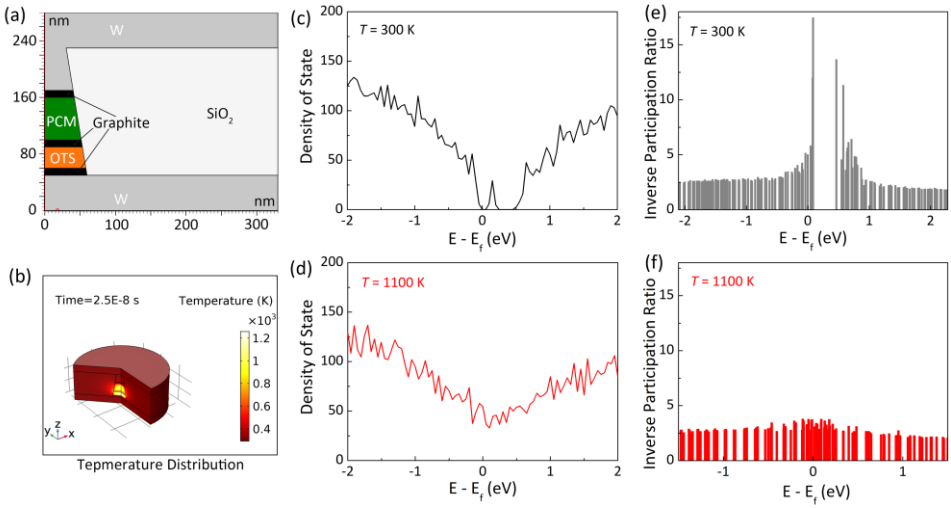

Fig. 1. (a) Model of the OTS+PCM nanodevice used for finite element analysis. (b) Transient temperature distribution in the device during the holding-on stage. Electronic properties of amorphous and liquid GeSe calculated by HSE06 functionals. (c-d) DOS and IPR of amorphous GeSe, respectively. (e-f) DOS and IPR of liquid GeSe, respectively.

4. CONCLUSIONS

In brief, first-principles calculations reveal the thermal-induced electronic structure transitions in typical OTS material GeSe. DFT calculations reveal that thermal-induced structure transition of GeSe will reduce its band gap and then increase the concentration of carriers. Unexpectedly, the transition also results in a delocalization of band-tail states of GeSe which enhances its carrier mobilities. The present work offers a detailed atomic/electronic picture of OTS materials when the materials are heated in the OTS+PCM devices.

REFERENCES

1. M. Le Gallo *et al.*, *J. Appl. Phys.* **119** (2016) 025704.
2. N. K. Chen *et al.*, *Adv. Funct. Mater.* **34** (2024) 2410622.
3. W.-C. Chien *et al.*, *IEEE T. Electron Dev.* **65** (2018) 5172.

P-22

Atomistic simulations of Ge–Sb–Te devices for memory applications and neuromorphic computing tasks

Yuxing Zhou[1], Daniel F. Thomas du Toit[1], Xueqi Xing[2], Jiangjing Wang[2], Stephen R. Elliott[3], Wei Zhang[2,*], and Volker L. Deringer[1,*]
[1]Department of Chemistry, Inorganic Chemistry Laboratory, University of Oxford, Oxford OX1 3QR, United Kingdom
[2]Center for Alloy Innovation and Design (CAID), State Key Laboratory for Mechanical Behavior of Materials, Xi'an Jiaotong University, Xi'an 710049, China
[3]Department of Chemistry, Inorganic Chemistry Laboratory, University of Oxford, Oxford OX1 3QR, United Kingdom
Presenting author. E-mail: yuxing.zhou@chem.ox.ac.uk

ABSTRACT

Atomistic simulations play an important role in understand fundamental properties and working mechanisms of PCM devices. Our recent work has shown that machine-learning (ML)-driven molecular dynamics simulations enable accurate description of Ge–Sb–Te alloys, particularly for compounds on the $GeTe–Sb_2Te_3$ tie-line (GST)[1]. Using an ML potential based on the Gaussian approximation potential (GAP) framework, we demonstrate a device-scale RESET ("1→0") simulation over 50 ps in a device-scale model of 532,980 atoms (corresponding to a real device size of 40 × 20 × 20 nm^3). However, realistic switching operations in GST devices usually take tens of nanoseconds. More importantly, non-isothermal conditions are prominent in GST devices, which can lead to distinct SET or RESET states as compared to isothermal conditions, thus complicating accurate modelling of phase transitions in real devices.

In this talk, we demonstrate device-scale simulations of GST devices under realistic programming conditions. We first introduce a new ML potential based on the Atomic Cluster Expansion (ACE) framework[2]. We show that the new ACE potential is more than 400 times faster than the GAP potential, which enables full-loop simulations (multiple RESET to SET operations) of cross-point and mushroom-type devices at extensive length scales (involving sub-million atoms) and time scales (tens of nanoseconds). Next, we present a new simulation protocol that describes non-isothermal conditions and temperature gradients of any desired level of spatiotemporal complexity[3]. Based on these ML-driven MD simulations, we show temperature-dependent crystallisation behaviours of GST, elucidating the interplay between nucleation and growth under non-isothermal crystallisation in GST memory devices. We also showcase an in-silico study of neuromorphic computing operations of GST mushroom-type devices, which provides atomic insights into the spike-timing dependent plasticity achieved with GST. This talk presents a platform for the predictive modelling of PCM-based memory and neuromorphic devices, and more widely, it highlights the power of highly scalable atomistic machine-learning models for modern materials science and engineering.

REFERENCES

1 Y. Zhou, E. Ma, W. Zhang, V. L. Deringer, *Nat. Electron.* **6**, 746–754 (2023).
2 Y. Zhou, D. F. Thomas du Toit, S. R. Elliott, W. Zhang, V. L. Deringer, preprint at arXiv:2502.08393 (2025).
3 Y. Zhou, X. Xing, J. Wang, D. F. Thomas du Toit, S. R. Elliott, W. Zhang, V. L. Deringer, *in preparation.*

P-24

Multiscale Design of Doped Antimony-Based Phase-Change Materials

Qundao Xu[1], Meng Xu[2], and Ming Xu[1]*
[1] Huazhong University of Science and Technology, China
[2] the University of Hong Kong, China
*corresponding author: mxu@hust.edu.cn (M.X.)

ABSTRACT

This study utilizes multiscale molecular dynamics simulations to systematically investigate the effects of doping in antimony-based phase-change materials (PCMs). Three distinct dopant categories—tetrahedral, octahedral, and compact polyhedral configurations—are found to exhibit markedly different influences on crystallization kinetics and thermal stability. Through this analysis, four optimized PCM candidates are identified, offering a pathway for performance-tailored material design.

Key words: PCM, dopant, molecular dynamics, crystallization kinetics, stability.

1. INTRODUCTION

Recent advances in artificial intelligence (AI) have driven demand for high-performance memory hardware[1]. Phase-change memory is a promising candidate, offering rapid switching and in-memory computing[2], but its performance heavily depends on the optimization of phase-change materials (PCMs). Antimony (Sb), known for its ultrafast crystallization but limited amorphous-phase stability[3,4]. Doping has emerged as a key strategy for improving Sb-based phase-change memory. For example, Al and Zn enhance thermal stability, Sn and In accelerate crystallization, and Ti increases electrical resistance. However, the mechanisms behind these effects remain poorly understood, often requiring trial and error. To address this, we systematically investigated the impact of various dopants using *ab-initio* molecular dynamics (AIMD) simulations. Our results reveal three distinct dopant categories based on their local coordination environments: tetrahedral (Al, Zn, Ga), octahedral (Cd, In, Sn), and polyhedral (Sc, Ti, Y, Zr). Each group has a unique influence on material properties, with tetrahedral dopants balancing speed and stability, octahedral dopants enhancing crystallization, and polyhedral dopants significantly improving thermal stability. This work provides a structure-property framework for rational PCM design, supporting next-generation memory devices[5].

2. EXPERIMENTAL

First-principles calculations were performed using the Vienna *ab* initio Simulation Package (VASP), employing the generalized gradient approximation with the Perdew-Burke-Ernzerhof (GGA-PBE) exchange-correlation functional and the projector augmented-wave (PAW) method. The amorphous structures were generated via melt-quenching MD simulations with a cooling rate of 30 K/ps. For large-scale MD simulations, the LAMMPS code was utilized, where the interatomic interactions were described using a potential energy surface constructed via DeepMD-kit.

3. RESULTS & DISCUSSION

As shown in Fig. 1a, we first constructed amorphous models for ten different doped materials using high-throughput calculations. The atomic environments were then characterized using the Smooth Overlap of Atomic Positions (SOAP) descriptor. Dimensionality reduction and clustering analyses of these SOAP features, coupled with similarity assessments, revealed a systematic classification of the dopant elements into three distinct groups. Building on this initial classification, we performed comprehensive studies of the local atomic structures and electronic properties of these amorphous systems (Fig. 1b). Our computational results indicate that metallic-like dopants in a-Sb exhibit clear local structural preferences: Al, Zn, and Ga predominantly form tetrahedral motifs, Cd, In, and Sn favor octahedral configurations, while Sc, Ti, Y, and Zr tend to form unique polyhedral structures.

Based on our calculations of dynamical properties and electronic structures, combined with experimental performance data for selected materials, we identified three key trends: (1) tetrahedral dopants provide a balance between crystallization speed and thermal stability; (2) octahedral dopants exhibit strong potential for ultrafast phase-change memory applications; and (3) polyhedral dopants significantly enhance the thermal stability of a-Sb (Fig. 1c). To verify these predictions, we conducted large-scale molecular dynamics simulations to assess the crystallization dynamics of these doped systems. The observed behaviors closely matched our theoretical forecasts, providing strong support for this structure-property classification.

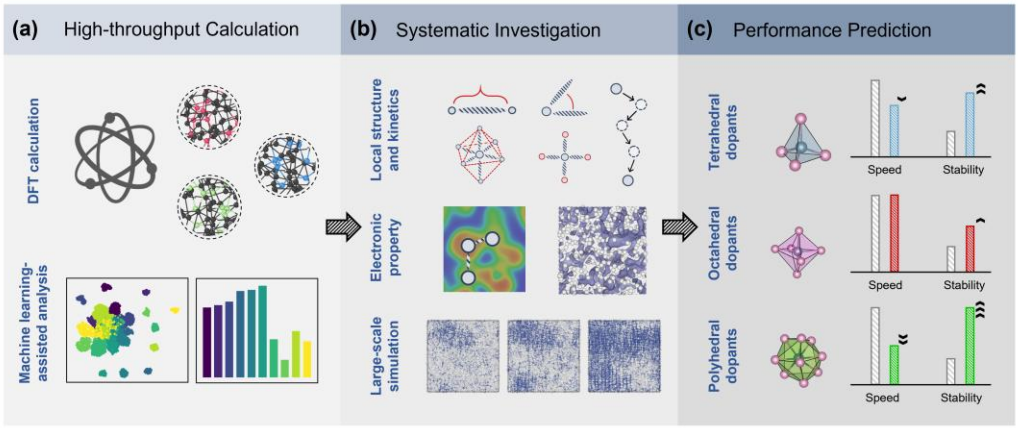

Fig. 1 Schematic representation of the workflow in this study, highlighting the three interconnected components of our methodology: (a) Machine learning-assisted analysis based on DFT calculations, (b) Systematic investigation of doped PCMs, spanning from DFT calculations to large-scale MD simulations, and (c) Performance prediction for tetrahedral, octahedral, and polyhedral dopants.

4. CONCLUSIONS

In this work, we investigated the local structures and properties of ten doped amorphous Sb materials (a-XSb, X = Al, Zn, Ga, In, Sn, Ti, Cd, Sc, Y, Zr) using multi-scale simulations. Experimental validation for six systems (a-AlSb to a-TiSb) allowed us to predict the properties of four novel dopants (a-CdSb, a-ScSb, a-YSb, a-ZrSb). Machine learning-assisted MD simulations revealed that a-CdSb adopts octahedral coordination, which enhances thermal stability while preserving fast crystallization kinetics. In contrast, a-ScSb, a-YSb, and a-ZrSb exhibit compact polyhedral coordination, leading to superior thermal stability due to stronger heteropolar bonds. These findings provide insights into the structure-property relationships of Sb-based glasses for advanced memory design.

REFERENCES

1 Wang, H. *et al.* Scientific discovery in the age of artificial intelligence. *Nature* **620**, 47-60 (2023).
2 Ambrogio, S. *et al.* An analog-AI chip for energy-efficient speech recognition and transcription. *Nature* **620**, 768-775 (2023).
3 Salinga, M. *et al.* Monatomic phase change memory. *Nat. Mater.* **17**, 681-685 (2018).
4 Shen, J. *et al.* Toward the Speed Limit of Phase-Change Memory. *Adv. Mater.* **35**, e2208065 (2023).
5 Xu, Q. *et al.* Enhancing elemental phase-change chalcogenide glass through tailored alloying. *Acta Mater.* **289**, 120896 (2025).

P-26

Structural ordering of amorphous motifs under electric field in threshold switching chalcogenides

Wen-Xiong Song[1]*
[1]Shanghai Institute of Microsystem and Information Technology, China
*corresponding author: songwx@mail.sim.ac.cn

ABSTRACT

Threshold switching, the ensuing abrupt conductivity increase at a critical threshold voltage (V_{th}), makes amorphous chalcogenides appealing for crossbar memory applications, particularly for the recently developed selector-only memory. However, the unknown mechanism behind threshold switching hinders effective development of memories based on amorphous chalcogenides. Here, by combining device measurements and first-principles simulations, we identify an atomic-scale conductive filament (CF) region induced by electric polarization. The CF formation occurs as the polarization increases the material's dipole moments through the formation of preferred bond orientations under the electric field, resulting in significant structural changes in the CF region. The CF exhibits size-dependent characteristics and appears in various sub-10nm devices. The abrupt conductivity increase after switching on is contributed by delocalized electronic states confined to the CF, and the CF formation is responsible for the polarity-induced V_{th} shift in selector-only memory. These findings provide a conceptual foundation for maximising the potential of amorphous chalcogenides in novel crossbar memory technologies.

Key words: threshold switching, amorphous chalcogenides, conductive filament.

P-28

Complex charge density waves and phases transitions in two-dimensional III_2–VI_3 materials for low-power consumption memory

Yu-Ting Huang, Nian-Ke Chen*, and Xian-Bin Li*
State Key Laboratory of Integrated Optoelectronics, College of Electronic Science and Engineering, Jilin University, 130012 Changchun, China
*Corresponding author: chennianke@jlu.edu.cn or lixianbin@jlu.edu.cn

ABSTRACT

First-principles calculations reveal multiple charge density wave (CDW) orders, including chiral Star-of-David configurations, in 2D III_2–VI_3 materials. Large, flat imaginary optical phonon frequencies across the Brillouin zone enable diverse CDW phases in this simple electronic structure system. The CDW phase transitions in III_2–VI_3 materials involve metal-to-insulator and insulator-to-insulator transitions, which offer new platform for the low-power-consumption data memory.

Key words: charge density wave; 2D III_2–VI_3 materials; phase transitions; first-principles calculations

1. INTRODUCTION

Charge density wave (CDW) is the phenomenon of a material that undergoes a spontaneous periodic modulation of solid lattice and charge density[1]. The origin of CDW can be attributed to Fermi surface nesting or electron-phonon coupling, where the CDW vector (Q_{CDW}) corresponds to localized extreme points of electronic susceptibility or imaginary phonon frequencies. Although the possible presence of FSN or EPC in these materials, there is no clear evidence indicating that these factors explicitly determine the formation of specific CDW configurations, whereas the strong electron correlation effect may play a role. Since the origin of CDW remains controversial as its properties are highly material-dependent, exploring unique CDW is of significant importance for understanding their property, origin and novel applications.

In this talk, we propose a new family of multiple CDW orders, including chiral Star-of-David configuration (c-SoD) in nine 2D III_2–VI_3 ferroelectric data-storage van der Waals materials, backed by first-principles calculations. The distinct feature of this system is the presence of large and flat imaginary frequencies in the optical phonon branch across the Brillouin zone, which facilitates the formation of the diverse CDW phases. The electronic structure of 2D III_2–VI_3 is relatively simple, with only III-*s,p* and VI-*p* orbitals contributing to the formation of the CDW order. Despite that, the CDW transitions involve both metal-to-insulator and insulator-to-insulator transitions, accompanied by a significant increase in the bandgap caused by an enhanced electronic localization, which offer a platform for the design of low-power-consumption memory. Our study not only reveals a new dimension in the family of 2D CDWs, but is also expected to offer deeper insights into the origins of the CDWs[2].

2. EXPERIMENTAL

In this work, the Vienna ab initio simulation package was used for DFT calculations[3]. The projector augmented wave (PAW) pseudopotential and the Perdew–Burke–Ernzerhof (PBE) exchange-correlation functional were employed. The 4d, 5s, and 5p orbitals of In atoms, and the 4s and 4p orbitals of Se atoms are considered, the energy cutoff was set to 311 eV. The Heyd-Scuseria-Ernzerhof hybrid functional (HSE06) with a mixing parameter of 25% was used for band structure calculations. A vacuum region with thickness of 20 Å is constructed in the vertical direction of all cells to reduce the influence of periodic boundaries. The simulated STM patterns were obtained using the VASP package and the VASPKIT processing program[4].

3. RESULTS & DISCUSSION

DFT calculations have demonstrated the energetic instability of the centrosymmetric phase of 2D β-In_2Se_3 shown in Figure 1a, leading to an in-plane ferroelectric polarization. Intriguingly, we

observe that the charge density wave (CDW) phase adopts a structural reorganization characterized by the lattice vectors $\boldsymbol{a}_{CDW}=4\boldsymbol{a}+\boldsymbol{b}$ and $\boldsymbol{b}_{CDW}=\boldsymbol{a}+3\boldsymbol{b}$, where $\boldsymbol{a}$ and $\boldsymbol{b}$ are the lattice vectors of pristine centrosymmetric phase marked by black arrows in Figure 1(b). This reconstruction breaks the spatial translational invariance of the Se(*m*) displacements. Figure 1c illustrates the atomic distortions during CDW formation. A central Se(*m1*) atom anchors the CDW structure, surrounded by six nearest-neighbor Se(*m2*) atoms that rotate either clockwise (left-handed, LH) or counterclockwise (right-handed, RH). Concurrently, six Se(*m3*) atoms displace radially inward toward the Se(*m1*) center. The collective distortions result in a $\sqrt{13}\times\sqrt{13}$ c-SoD configuration. The fast Fourier transform (FFT) patterns of atomic structures and DFT-simulated scanning tunneling microscopy (STM) images of the c-SoD CDW phase (Figures. 1g-k) reveal lattice reconstruction signatures in both reciprocal space and real space. Finally, through structural relaxation, we identified eight additional c-SoD CDW configurations in 2D III_2–VI_3 compounds. And the HSE06 band structure calculations reveal that the CDW transitions in 2D III_2–VI_3 contains both metal-to-insulator and insulator-to-insulator CDW transitions accompanied by large openings in the bandgap, which position them independently at the top of the CDW electronic-property map and expands the territory of the 2D CDW family.

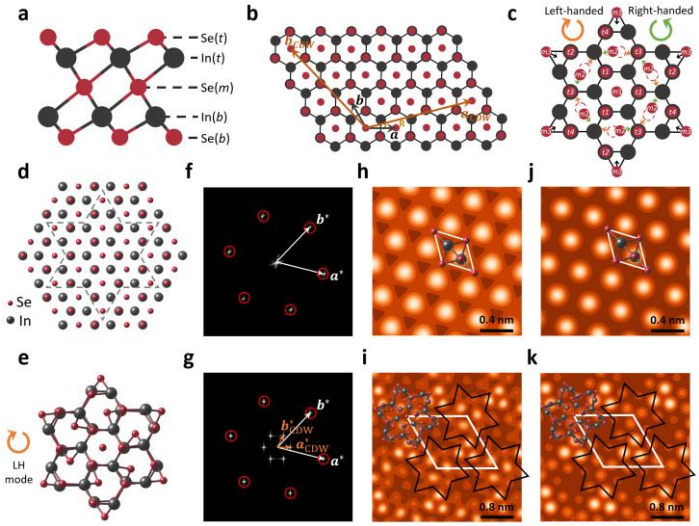

Figure 1. Atomic structures and simulated STM patterns of the pristine high-symmetry phase and c-SoD CDW phase of monolayer β-In_2Se_3.

4. CONCLUSIONS

Through first-principles calculations and STM simulations, the c-SoD CDW phase is first discovered in 2D β-In_2Se_3 and the entire family of 2D β-III_2–VI_3. Different from traditional SoD CDW materials such as $NbSe_2$ or TaS_2, which exhibits strong correlation characteristics, the electronic structures of 2D III_2–VI_3 materials are rather simple with only *s*- and *p*-orbitals observed near the Fermi-level. However, due to the flat and extensive imaginary phonon frequencies and the Mexican-hat PES of the Se(*m*) atoms, the CDW orders of 2D β- In_2Se_3 are complex. Simultaneously, the CDW transition is accompanied by an increase in electron localization, which results in significantly wider bandgaps in 2D III_2–VI_3 materials compared to traditional 2D CDW materials. Our work provides a new branch of CDW materials and expands its electronic property map, which may bring new insights and platforms for future data-storage devices.

REFERENCES

1. D. E. Moncton, et al. *Phys. Rev. Lett.* (1975) 34,734–737.
2. Yu-Ting Huang et al. *Nat. Commun.* (2024) 15, 9983.
3. Kresse, G. & Furthmüller, J. *Phys.Rev.B* (1996) 54, 11169–11186.
4. Vei Wang et al. *Comput.Phys.Commun.* (2021) 267,108033.

P-30

On the origin and growth of voids in N-doped Ge-rich GeSbTe alloys subjected to thermal annealing

M. A. Luong *, S. Ran, S. Sabyasachi, A. Claverie and N. Cherkashin *

CEMES-CNRS and University of Toulouse, 29 Rue Jeanne Marvig, 31055 Toulouse, France
*corresponding author: minhanhapc@gmail.com, nikolay.cherkashin@cemes.fr

ABSTRACT

When N-doped Ge-rich GeSbTe films are heated, voids are formed. We study using "corrected" TEM images how their size and density, as well as the film thickness change over time. Phase separation in viscous liquid NGGST and densification-induced tensile stress are identified as the origin for voids appearance. Following nucleation, they grow by Ostwald ripening. The growth law is established.

Key words: phase change memories, Ge-rich GeSbTe, densification, stress, viscous liquid, voids

1. INTRODUCTION

Non-volatile phase change memories (PCMs) based on Ge-rich GeSbTe alloys (GGST) are being investigated for data storage and embedded components in automotive applications, owing to their high thermal stability and data retention capabilities [1]. Among several dopants, N doped Ge-rich GeSbTe alloys (NGGST) receives highly interest for boosting the thermal stability of GGST films [2-3]. While considerable focus has been placed on understanding the structural and chemical evolution during the reversible amorphous-to-crystalline phase transition, less attention has been given to material densification, thickness evolution and formation of voids in NGGST thin film. In fact, the origin of void formation in crystalline GST-225 is barely discussed in literature, mostly referencing to the precipitation of vacancies during densification/volume shrinkage of the as-deposited amorphous material upon crystallization [4]. However, some of authors claim no void formation during such a process [5].
To explore this phenomenon, we have studied in detail void formation and evolution in NGGST thin-films by means of transmission electron microscopy (TEM) techniques. Herein, with a direct visualization of the structures by TEM, we address the thickness/volume changes in NGGST films in relation to the changes in the voids characteristics.

2. EXPERIMENTAL

A 100 nm-thick N doped Ge rich GST layer was deposited by physical vapor deposition (PVD) onto a naturally oxidized 300 mm Si (100) wafer and covered by a 20 nm-thick TiN or a 10nm SiN cap layer. The samples were diced into 2cm x 2cm pieces and isochronally and isothermally annealed in a conventional furnace under nitrogen flux. Cross-sectional specimens were prepared by focus ion beam (FIB) technique operating with a 30 keV Ga ion beam and finally polished and cleaned at 2 keV–3 pA. JEOL 2100Plus TEM microscope (200kV) was used for imaging voids in bright-field defocused conditions. High-angle annular dark-field (HAADF)-STEM and dualEELS data were acquired on a probe corrected ARM JEM JEOL 200F microscope, operated at 200 kV. For a reliable distance measurement over moderate magnification TEM images, we developed a method for their correction for distortions and calibration errors [6], which allowed to reduce the error from the typical 5%-10% down to 0.1%.

3. RESULTS & DISCUSSION

Figure 1 show bright-field defocused TEM images of voids in the as-deposited and annealed NGGST films subjected to different thermal annealing conditions. Chemical analysis using STEM-EELS revealed that the voids are not empty but filled with argon, the vector gas used for depositing the layers by sputtering. Voids are found to be nucleated in the amorphous NGGST layer during phase separation and prior to crystallization (Fig. 1b). We evidenced that voids do not migrate

during in-situ isothermal annealing experiment. Their nucleation and growth are basically induced by discrete and sudden events of exfoliation and coalescence phenomena at internal boundaries formed following phase separation. At the same time, the layer shrinks by approximately 2% as measured on ex-situ annealed samples. When increasing the annealing time, the layer expands and reaches a thickness 5%-6% larger than that of the as-deposited layer, then stabilizes (Fig. 1c-f). At this stage, the layer is fully crystallized. Before the layer thickness has stabilized, voids grow in size, their density decreases and their volume fraction increases as well. The layer thickness is found to decrease due to densification and increase due to formation of voids. The average relative change in the material atomic density from as-deposited to annealed state i.e., densification, has been related analytically to the void volume fraction and the change in the layer thickness and is found of about 3%. The void volume fraction does not necessarily compensate for the densification effect or, on the contrary, can provide an increase in the layer thickness above its as-deposited value. All together, these data indicate that material densification induces tensile stress which provokes either exfoliation (dewetting) at domain boundaries or generation of vacancies followed by their precipitation, resulting in the formation of voids occupying some layer's volume.
Once the thickness has been stabilized, voids continue to grow in size, their density decreases and its volume fraction of about 4-5% remains constant. As the voids have reached such a maturate, likely stress-free state, their thermal evolution well corresponds to the characteristics of the Ostwald ripening regime, i.e., when precipitates evolve by exchanging the constituents they are composed of (here, vacancies and Ar) leading to the growth of the larger voids at the expense of the smaller ones. By applying isothermal and isochronal annealing, we determined the parameters of their growth laws described by the Lifshitz-Slezov theory (Fig. 1g). In particular, the activation energy for the void growth is found to be of about 1.32 eV.

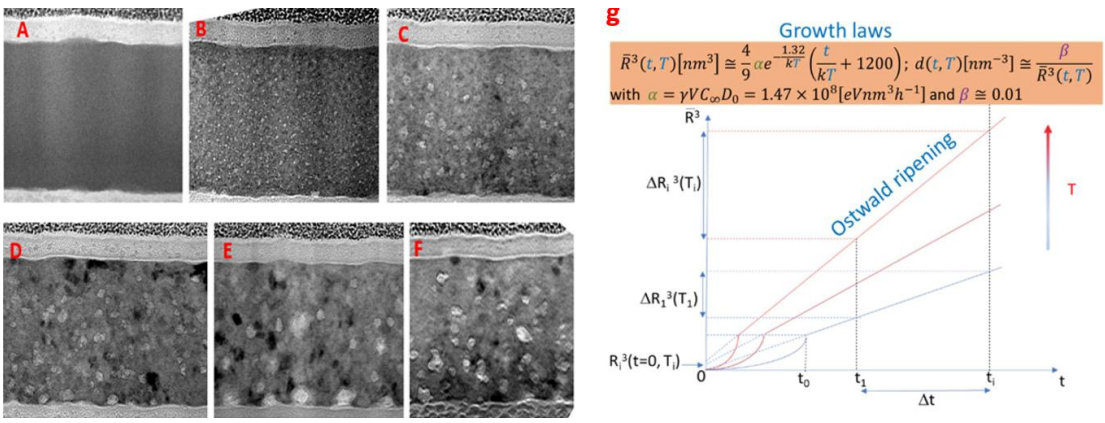

Figure 1: (A-F) Corrected for distortions, bright field defocused cross-sectional TEM images of voids in Si/NGGST/SiN samples annealed at various temperatures and durations; (g) The growth law derived from the mature-state voids characteristics measured after isothermal and isochronal annealing, illustrating the dependence of void size (volume) and density on time and temperature.

4. CONCLUSIONS

This study provides valuable insights into the thermally activated nucleation and growth of voids in NGGST materials, including the densification induced initial shrinking followed by surprising expansion of the NGGST layer upon crystallization, identification of the degree of the material densification, and the statistical analysis of void's size/density and volume fraction allowing to deduce the parameters governing their growth laws.

REFERENCES

1. E. Rahier et al., *ACS Applied Electronic Materials* (2022) 4(6).
2. M.A. Luong et al., *Physica Status Solidi (RRL) - Rapid Research Letters* (2020).
3. M.A. Luong et al., *Physica Rapid Research Ltrs* (2024) 2300421.
4. L. Krusin-Elbaum et al., *APL* **90** (2007) 141902.
5. W. K. Njoroge et al., *J. Vac. Sci. Technol.* **20** (2002) 230.
6. N. Cherkashin et al., *Ultramicroscopy* **253** (2023) 113778 ; *Sci. Rep.* **7(1)** (2017) 12394.

P-32

Impedance Spectroscopy of intermediate states in Ge-rich GeSbTe PCM cells

Adrien Delpoux[1], Sijia Ran[2], Laura Pecourt[4], Roberto Simola[4], Alain Claverie[2], Simon Jeannot[3], Jérémie Grisolia[1*]

[1]*Laboratoire de Physique & Chimie des Nano-Objets (LPCNO),* Toulouse, France
[2]*Centre d'Elaboration de matériaux & d'Etudes Structurales (CEMES-CNRS),* Toulouse, France
[3]*STMicroelectronics,* Crolles, France
[4]*STMicroelectronics,* Rousset, France
*jeremie.grisolia@insa-toulouse.fr

ABSTRACT

We investigate the electrical characteristics of intermediate states of Ge-rich GST (GGST) PCMs by impedance spectroscopy. We highlight that all these states present resistive and capacitive components. When programming the memory between the SET and the RESET states, the resistance can be increased continuously. This increase is accompanied by a continuous decrease of the capacitance.

Key words: GeSbTe alloys, Electrical characterization, Impedance spectroscopy, Phase change memory, Intermediate resistance state.

1. INTRODUCTION

Phase change memory (PCM) is one of the main emerging memory technologies whose properties can be tailored by material and cell engineering. These memories use the phase transition of chalcogenide materials (GST), from a high resistance amorphous state (RESET) to a low resistance crystalline state (SET), to store binary data. Up to now, most of the electrical characterizations were carried out through DC bias measurements. However, as the characteristics of PCM devices based on Germanium-rich GeSbTe alloys (GGST) result from contributions of different chemical phases and heterogeneities [1], AC bias measurements would be preferable to investigate their electrical properties in detail, eventually identifying the capacitance and resistance contributions. For this reason, we investigate here RESET, SET and Intermediate Resistance States (IRS) GGST PCM using impedance spectroscopy.

2. EXPERIMENTAL

PCM cells made of GGST (wall architecture) were tested via two metallic pads connected to the cells. Electrical currents were measured using a cryogenic probe station (Janis ST-500-1, $0.5\mu m$ Tungsten probes) operating at room temperature. Prior testing, a forming procedure was applied using a 4200A-SCS Parameter Analyzer. Samples were then programmed in RESET, SET and five different IRSs. They were characterized by impedance spectroscopy using a Keysight Impedance Analyzer E4990A with a 400 mV DC voltage and 50mV AC voltage. The measurements are probed from 20 Hz to 1 MHz. After forming, we perform 5-10 cycles to ensure the proper functioning of the PCM.

3. RESULTS & DISCUSSION

The results obtained are shown in Fig.1a-b. The Nyquist plot from Fig.1a corresponds to the measure of the RESET state and has a shape of a perfect semi-circle. A Nyquist plot with a perfect semi-circle corresponds to an equivalent electrical circuit composed of a resistance R in parallel to a capacitance C, this is illustrated in Fig.1c. We add a resistance in serie R_s to mimic any stray resistance (e.g. heater, wafer circuitry) and also the interface heater/GGST resistance. Parameters R and C correspond directly to the electronic properties of the active GGST layer. The SET Nyquist plot is not identical than the RESET one due to a resistance a thousand time lower than in RESET. Thus, the characteristic frequency $f_c = 1/2\pi RC$ is then shifted to higher frequency, out of measurement range. Actually, we only see the beginning of the semi-circle in the SET state. To avoid any loss of accuracy in the fit in low resistance states, we add a known capacitance in parallel C_p as shown in Fig.2a. It enables us to shift in lower frequencies the Nyquist plot of those states and then increase the fit accuracy.

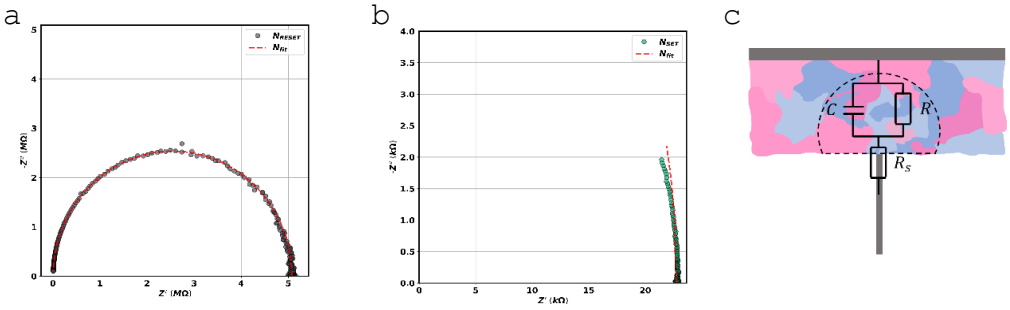

Figure 1 – a) Nyquist plot of the RESET state. b) Nyquist plot of the SET state. c) Schematic drawing of the equivalent circuit.

The theoretical impedance of this new equivalent circuit is computed to fit the values by considering C_p. IRSs are programmed such as IRS1 correspond to the lowest IRS and IRS5 to the highest IRS. On each state, we extract the resistance R_s, R and the capacitance C with the equivalent circuit depicted in Fig.2a. We use different value of C_p ranging from $0 - 30pF$. The relative resistance and capacitance change through different state are shown in Fig.2b. The R-C curve reveals a decrease of capacitance as the resistance of the cell increases. The capacitance decreases

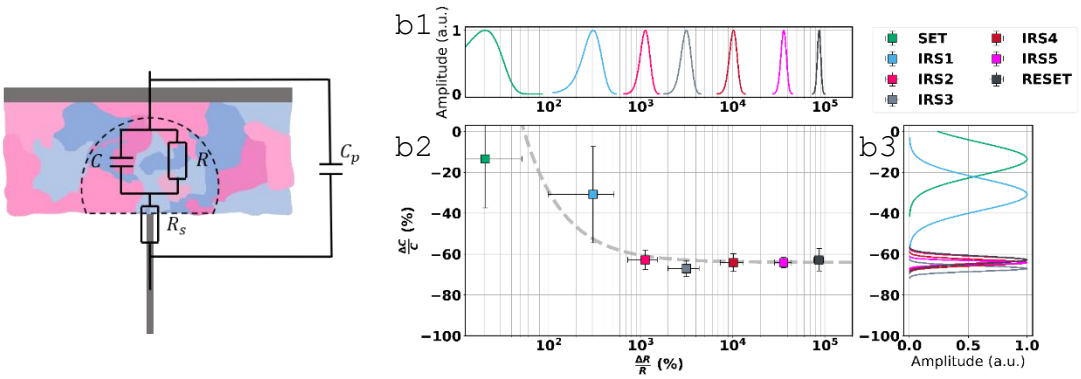

Figure 2 – a) Schematic drawing of the equivalent circuit with a parallel capacitance C_p. b1) Resistance distribution of programmed states. b2) Extracted value of R and C for SET, RESET and IRCS1-5. Each point is obtained by averaging 75 measurements. "Error bars" correspond to 3 times the standard deviation. The capacitance change is computed relative to the maximum capacitance attainable as a reference. The resistance relative change is computed relative to the lowest value attainable by the resistance as a reference. b3) Capacitance distribution of programmed states.

significantly from the polycrystalline SET state to IRS2, whereas it decreases less significantly from IRS2 to RESET to reach a value about -63%. IRS are states with mixed polycrystal and amorphous GGST regions as shown in [2] & [3]. This mixture in various proportions is probably at the origin of the increase of resistance, as well as of the change in capacitance. This will be discussed in the poster.

4. CONCLUSIONS

We have investigated, using impedance spectroscopy, the electrical characteristics of various intermediate states which can be programmed on Ge-rich GST (GGST) PCMs. We highlight an important variation of resistance but also capacitance between the SET and RESET states. Moreover, we found a monotonous variation of R and C through SET, IRSs and RESET, that confirm the importance to describe the states using both (R, C) and not only R.

REFERENCES

[1] ***Bourgine A. et al. Solid-State Electronics, 172, 2020.***
[2] ***L. Laurin et al., IEEE International Reliability Physics Symposium (IRPS), 2023.***
[3] ***Ran et al, Scientific Reports , Vol. 15, No. 1 Springer Science and Business Media LLC, 2025.***

P-34

Design of All-dielectric Ge-rich Ge-Sb-Te based optical modulator with high modulation efficiency

Atchyut Phalgun M[1], Aastik Agnihotri[1], Srinivasan krishnamurthy[2,3] and Anbarasu Manivannan[1*]
[1]Department of Electrical Engineering, Indian Institute of Technology Madras, Chennai, India,
[2]Department of Physics, Indian Institute of Technology Madras, Chennai, India 600036
[3]Sivananthan Laboratories, Bolingbrook, IL 60440, USA
*email: anbarasu@ee.iitm.ac.in

ABSTRACT

Reflective optical modulator with dynamic amplitude modulation of light at 1550 nm wavelength with high modulation efficiency is most critical component for free space optical communication. Here we present metal and meta-structure free optical modulator using Ge rich Ge-Sb-Te phase change material with a modulation efficiency of 91% at 1550 nm with nearly independent of angle of incidence.

Key words: optical modulator, 1550 nm, Ge-Sb-Te

1. INTRODUCTION

Free-space optical (FSO) communication offers higher data rates and lower beam divergence compared to traditional radio frequency (RF) systems. A key component in FSO systems is the reflective optical modulator, which enables bidirectional communication by modulating and reflecting incoming optical signals. Phase change materials have been explored as a potential candidate for optical modulators at 1550 nm because of their reversible transition, while several optical modulator designs based on phase change materials (PCMs) have been reported for operation at 1550 nm, most of which rely on metal heaters for actuation in reflection mode[1-4]. However, the use of metal introduces significant optical losses, leading to reduced modulation depth and overall efficiency. In this work, we demonstrate a metal-free reflective optical modulator based on a Ge-Sb-Te material and Si–SiO_2 distributed Bragg reflector (DBR) stack. Here, doped silicon is employed as the heater element, effectively eliminating the losses associated with metal reflectors and heaters. This approach enables enhanced modulation efficiency and depth, making it a promising candidate for high-performance FSO communication systems.

2. Design and Experimental:

The device stack, shown in Figure 1(a), was optimized using a custom transfer matrix method (TMM) code and verified through COMSOL Multiphysics simulations. The design is based on a distributed Bragg reflector (DBR) with alternating high- and low-index layers to achieve high reflectivity at the target wavelength. To ensure constructive interference, the optical thickness of each layer follows the quarter-wavelength condition: $d = \frac{\lambda}{4n}$, where d is the physical thickness of the layer, λ is the design wavelength in free space, and n is the refractive index of the material. From the above, the thickness of Si and SiO2 is chosen to be 110 nm and 270 nm, respectively. SiNx capping layer was added on top of PCM to minimise the unwanted surface reflections and also provide index matching with the underlying PCM layer. Here we have selected Ge rich Ge-Sb-Te mainly because of higher Δn ($\Delta n = n_{crystalline} - n_{amorphous}$) and Δk ($\Delta k = k_{crystalline} - k_{amorphous}$) contrast compared to GST225, where Δn ~ 3.2 and Δk ~ 1.3 at 1550 nm. The film was deposited on a glass substrate via DC sputtering using a stoichiometric target of 99.99% purity (ACI alloys). The sputtering process operated at a base pressure of $2*10^{-6}$ mbar with an argon flow rate of 10 SCCM, maintaining a constant current mode of 34 mA. The thickness and refractive index of the PCM layer were measured using a J.A. Woollam spectroscopic ellipsometer, scanning at angles of 70°, 72°, and 74°. The ellipsometric data were fitted using Tauc-Lorentz and Cody-Lorentz general oscillator models. The elemental composition of the as-deposited Ge-Sb-Te thin film was verified using an energy dispersive x-ray analysis tool (EDAX) where stoichiometry was within 2% variation.

3. RESULTS & DISCUSSION

Figure 1 presents the proposed design, which is entirely free of metals, meta-structure, and plasmonic components. Figure 1(b) shows the complex permittivity of the Ge-rich Ge-Sb-Te material used in the structure. Figures 1(c)–1(f) illustrate the TE and TM reflectance as functions of wavelength and incident angle for both amorphous and crystalline phases. The design achieves a high modulation contrast ($R_{amorphous} - R_{crystalline}$) of approximately ~91% at a wavelength of 1550 nm and demonstrates near angle-independence across a broad range of incident angles (0°–40°). Figure 1(g) shows the electro-thermal switching behavior of the structure, which utilizes a 20 µm × 20 µm doped silicon heater finger. For phase transitions, a 400 ns, 8 V pulse is used for amorphization, while a 2 µs, 3.5 V pulse is applied for crystallization.

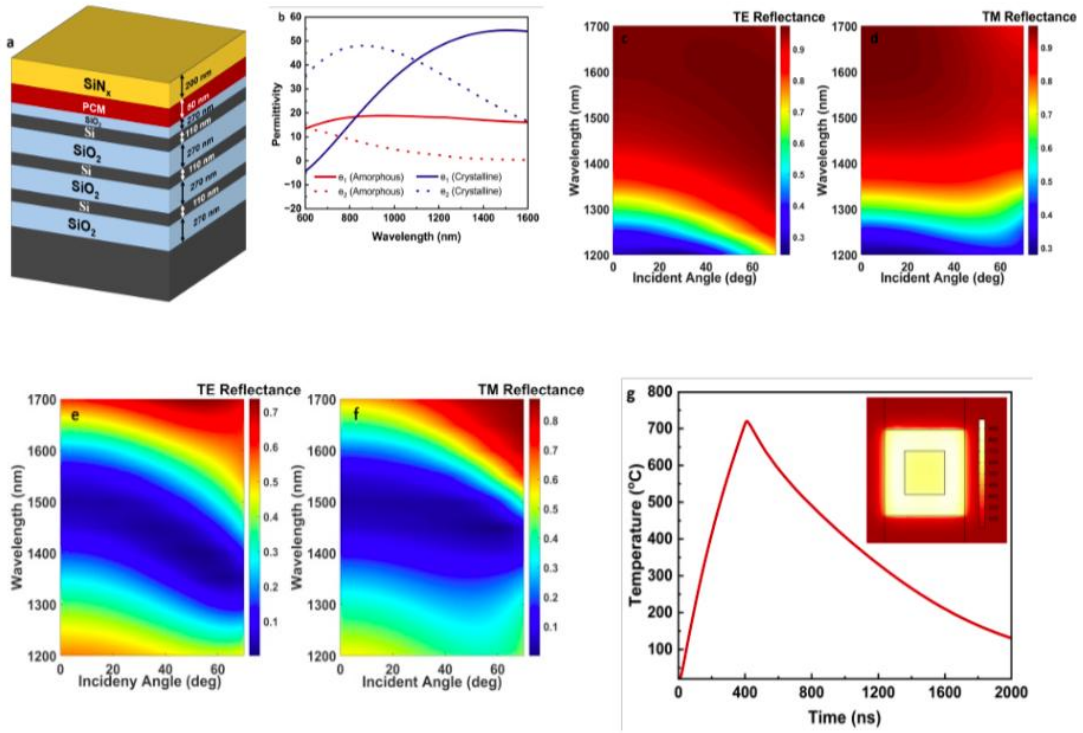

Fig1: (a) The optical modulator design, (b) measured dielectric permittivity of the Ge-rich Ge-Sb-Te phase change material, (c) & (d) amorphous phase reflectance over various incident angles and wavelength for TE and TM polarisations,(e) & (f) crystalline phase reflectance over various incident angles and wavelength for TE and TM polarisations, (g) electro-thermal simulations for amorphization.

4. CONCLUSIONS

In this study, we have designed a metal- and metasurface-free reflective optical modulator operating at 1550 nm, utilising a Si/SiO_2 distributed Bragg reflector and Ge-rich Ge-Sb-Te as the active material. The design achieves a high modulation efficiency of ~91% and maintains consistent modulation depth across a broad wavelength range (1500–1600 nm) and wide incident angles. Electro-thermal simulations further confirm efficient switching using a doped-silicon heater element.

REFERENCES

1. Zhang, Y., *16*(6), 661-666.
2. Zhang, Y., *Nature communications*, *10*(1), 4279
3. Abdollahramezani, *Nature communications*, *13*(1), 1696
4. F Popescu, C. C., *Advanced Materials*, *36*(36), 2400627.

P-36

Improving Insertion Loss and Isolation in GeTe-based RF Switch using Coplanar Waveguide Layout Optimization

Aastik Agnihotri[1], Atchyut Phalgun M[1], and Anbarasu Manivannan*[1]
[1]Dept. of Electrical Engineering, Indian Institute of Technology Madras, India
*email: anbarasu@ee.iitm.ac.in

ABSTRACT

Phase-change material (PCM) based radio-frequency (RF) switches offer exceptional performance for RF and mmWave applications. However, both ON and OFF-state performance start to degrade at higher frequencies. To improve insertion loss and isolation, design strategies like substrate-embedded micro-heater, variable barrier thickness, and an optimized coplanar waveguide (CPW) layout in germanium telluride (GeTe) based RF switch are incorporated, achieving <0.38 dB insertion loss and >35.5 dB isolation over DC-60 GHz.

Key words: Phase-change material (PCM), Germanium Telluride (GeTe), RF switch, SPST, Coplanar waveguide (CPW), E-Field, Ansys HFSS.

1. INTRODUCTION

The shift towards higher RF and mmWave spectrum exposes undesirable parasitics in microelectronic devices, limiting their use at lower bands—RF switches being a key example. Current RFSOI CMOS and GaN SLCFET-based RF switches (SPDT) offer insertion loss of 1.3 dB and 0.3 dB, and isolation of 43 dB and 30 dB, respectively, at 18 GHz[1, 2]. In contrast, PCM-based switches (SP4T) have achieved 0.4 dB insertion loss and 36 dB isolation[3] at the same frequency, challenging both technologies. Phase-change materials like GeTe exhibit high amorphous and low crystalline resistivity, with a contrast of 10^8 Ω-m[4]. Switching is driven by Joule-heated pulses via micro-heaters: a fast (~ns) pulse induces amorphization ($T_{PCM} > T_{melting}$), and a moderate (~µs) pulse crystallizes ($T_{crystallisation} < T_{PCM} < T_{melting}$), both nonvolatile, as no continuous supply is needed. This study shows how material and layout choices impact the RF traces-heater overlap capacitances, and the E-field distribution, which can be tuned to improve isolation while keeping insertion loss low.

2. SIMULATIONS

The GeTe-based RF switch utilized Ansys HFSS for design and simulations. The cross-section of the RF switch with different layers is shown in Fig. 1(a). Tungsten-based micro-heater (2 µm wide) is embedded into the sapphire (tan δ = $1x10^{-4}$) substrate, ensuring a flat surface for the subsequent layers. Relevant material properties are taken from published data[4], remaining from the Ansys HFSS material library. The frequency sweep from DC-60GHz extracted the S-parameters to quantify RF performance.

3. RESULTS & DISCUSSION

Embedding the micro-heater into the substrate and increasing the low dielectric constant insulator layer thickness from 100 nm to 300 nm improves isolation by less than 1.75 dB while worsening insertion loss only by 0.06 dB at 60 GHz, indicating minimal contribution of overlap capacitance from the 10 µm long micro-heater. Maintaining SiO_2 barrier thickness at 300 nm, further design optimization in the CPW structure of the RF switch highlights the significance of RF signal trace width and the gap separating the adjacent ground planes. At high frequencies, the gap width becomes comparable to the wavelength (λ) of a signal passing through it. Thus, shrinking the gap draws the return-current loop closer to the signal trace, confining the E-Field lines and preventing their bulging into the air/substrate that otherwise leaks across the amorphous GeTe, degrading the isolation. Maintaining the characteristic impedance at 50 Ω required reducing trace width as well, finally settling with 10 µm wide and 5.2 µm gap size. Lastly, two ground-plane layout designs, interrupted (no adjacent ground to PCM region) (Fig. 1(c)), and continuous (with adjacent ground) (Fig. 1(f)), highlight transverse E-field plots (Fig. 1(d) and Fig. 1(g)) with better confinement in the

latter, boosting isolation by ~8 dB (Fig. 1(b)). The interrupted layout suffers from impedance mismatch (Fig. 1(b)). increasing insertion loss from 0.38 dB to 1.27 dB as seen in Fig. 1(e). A 1 µm-thick copper layer has been used to demonstrate a gold alternative.

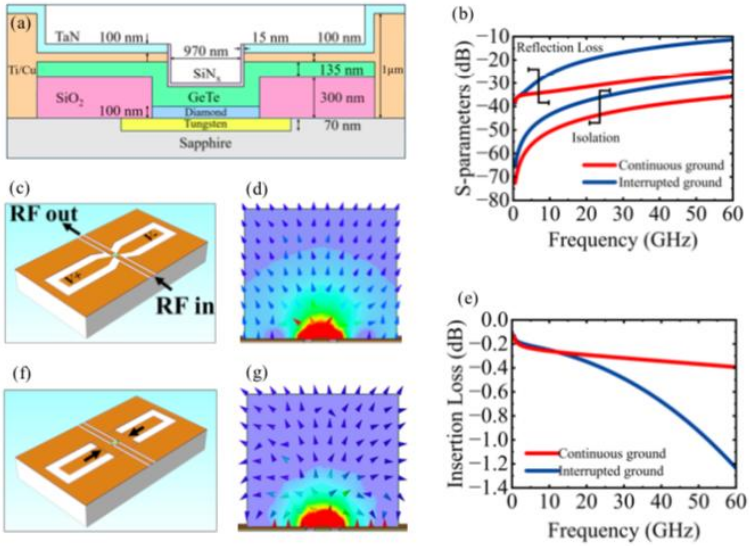

Fig. 1: (a) RF switch cross-section (dimensions not to scale). (b) Reflection Loss & Isolation plot. (c) Interrupted ground plane layout (substrate thickness not to scale) producing (d) bulged E-Field (Transverse to the RF signal propagation). (e) Insertion loss plot. (f) Continuous ground plane (additional ground plane segments shown by the arrows) layout with (g) confined E-Field.

From the insertion loss plot, when $\lambda \gg$ device size, the switch behaves as a lumped RC network. The interrupted ground layout avoids the traces' side-ground shunt capacitance near the PCM region, reducing the insertion loss. As λ approaches the device dimensions, distributed CPW behaviour dominates, with continuous ground layout ensuring a better return path for the current.

4. CONCLUSIONS

This study highlights the importance of maintaining a standard CPW layout in a four-terminal SPST PCM-based RF switch using a substrate-embedded micro-heater, variable thickness dielectric barriers, and ground–signal gap tuning, which boosts both ON and OFF-state performance, achieving <0.38 dB insertion loss and >35.5 dB isolation from DC-60 GHz.

REFERENCES

1. pSemi, “PE42525 product specification,” (2023).
2. R. S. Howell et al., Proc. IEEE MTT-S Int. Microw. Symp. (IMS) (2016) 1–3.
3. F. Amin et al., Proc. IEEE MTT-S Int. Microw. Symp. (IMS) (2021) 431–434.
4. T. Singh, R.R. Mansour, IEEE Trans. Electron Devices 67 (2020) 5717–5727.

P-38

Ferroelectric domain structure and growth of GeTe thin films on silicon substrates: the key role of atomic steps

B. Croes[1,2], L. Meynier[1], A. Llopez[1], S. Curiotto[1], P. Müller[1], F. Cheynis[1], M. Texier[3], S. Cherifi[2], and F. Leroy[1]*
[1]CINaM, Aix Marseille Univ, CNRS, AMUTECH, Marseille, France
[2]IPCMS, Université de Strasbourg, CNRS, Strasbourg, France
[3]IM2NP, Aix Marseille Univ, Univ Toulon, CNRS, AMUTECH, Marseille, France

*corresponding author: frederic.leroy.3@univ-amu.fr

ABSTRACT

A significant progress toward next-generation electronic devices could involve the manipulation of charge carrier spin textures in semiconductors. In this context, GeTe has recently emerged as a promising ferroelectric Rashba semiconductor. Here we address the growth, morphology and control of the domain structure of GeTe thin films grown by molecular beam epitaxy on (miscut) silicon substrates.

Key words: GeTe, ferroelectrics, domain structure, stress

1. INTRODUCTION

Due to their remarkable functional properties, the control of the domain structure in ferroelectric thin films and heterostructures is the subject of extensive research[1-3]. It has been demonstrated that unconventional polar textures result from the combined effects of mechanical stress as well as electrostatic/mechanic compatibility conditions at ferroelectric domain walls[4]. Among ferroelectrics, GeTe has experienced a remarkable surge of interest. As a thermoelectric material, it has achieved a record-breaking power factor in its ferroelectric phase[5]. In the same way, significant progress has been made in exploring spintronic properties in ferroelectric GeTe thin films, taking advantage of the Rashba effect[6]. Notably, studies have demonstrated the reversal of ferroelectric polarization under an electric field[7], accompanied by a corresponding switch in the spin chirality of the band structure[8,9]. Such attributes could pave the way for next-generation devices, provided local ferroelectric polarization can be precisely manipulated. In that perspective the synthesis of high crystalline quality thin films as well as strain engineering methods to enable the control of ferroelectricity using the ferroelastic properties of this material are highly demanded.

2. EXPERIMENTAL

The ferroelectric/ferroelastic (ferroic) α-GeTe films are epitaxially grown on Si substrates by molecular beam epitaxy. After growth, the GeTe films are characterized by low-energy electron microscopy (LEEM), and scanning tunneling microscopy (STM[10]). To study the GeTe/Si interface and the internal structure of GeTe thin films we have used High Resolution-Transmission Electron Microscopy (HR-TEM) combined with 3D-reciprocal space maps based on x-ray diffraction at BM32 beamline (ESRF synchrotron). The ferroelectric domain structure is characterized by second harmonic generation microscopy (SHG).

3. RESULTS & DISCUSSION

In this presentation, I will discuss the organization of ferroelectric nanodomains in GeTe thin films grown on Si(111)[11], the type of domain wall and the structure of the interface with the substrate. Quasi-monocrystalline GeTe thin films can be produced on Si(111) by molecular beam epitaxy, by first depositing an atomic monolayer of Sb[12-14]. This substrate enables ferroelectric domains to be studied and controlled, as they are not limited by grain boundaries. Ferroelectric nanodomain volume fraction and domain size were measured by x-ray diffraction and LEEM over a wide range of film thicknesses (10-1800 nm). SHG microscopy combined with polarimetric analysis provides

the local symmetry of these domains. Using HR-TEM we show that the domain walls are at 71° and that the GeTe/Si interface is stabilized by interfacial dislocations. The reversible appearance↔disappearance of ferroelectric nanodomains by thermal cycling is attributed to thermal stress induced by the substrate[15]. We also demonstrate that using miscut Si substrates we can induce anisotropic stress relaxation mechanisms to drive the ferroelectric domain structure[16].

4. CONCLUSIONS

In conclusion α-GeTe thin films epitaxially grown on Si substrates have been investigated. We have quantified the influence of the substrate on the morphology, crystallography and domain structure of GeTe films. In addition we put in evidence that stress engineering on GeTe thin films can be addressed selecting suitable miscut silicon substrates. This shows that atomic steps at the GeTe/Si interface play a crucial role in stress relief mechanisms and can be used to modify the ferroelectric domain structure. We believe this approach dedicated to GeTe thin films will motivate new strategies to further optimize the thermoelectric and spintronic properties of this material.

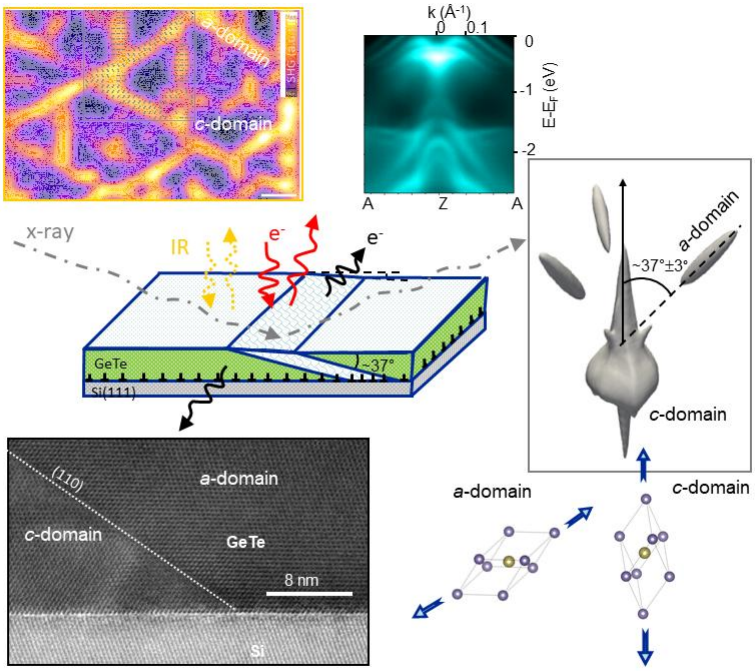

REFERENCES

1. A. K. Yadav et al., *Nature* **530** (2016) 7589.
2. P. Shafer et al., *P. Natl. Acad. Sci. USA* **115** (2018) 915–920
3. S. Das et al., *Nature* **568** (2019) 368–372
4. A. Tagantsev et al., *Domains in Ferroic crystals and thin films* (2010), pp. 1–821
5. Q. Xiang et al., *ACS Applied Materials & Interfaces* **17** (2025) 18781–18789
6. B. Croes et al., *Nano Letters* **24** (2024) 13 224–13 231
7. A. V. Kolobov et al., *APL Mater* **2** (2014) 066101
8. C. Rinaldi et al., *Nano Letters* **18** (2018) 2751–2758
9. J. Krempasky et al., *Phys. Rev. X*, **8** (2018) 021067
10. F. Cheynis et al., *Review of Scientific Instruments* **85**, (2014) 043705
11. B. Croes et al., *Phys. Rev. Materials* **5** (2021) 124415
12. R. Wang et al., *J. Phys. Chem. C*, **118** (2014) 29724
13. B. Croes et al., *Phys. Rev. Materials* **6** (2022) 064407
14. B. Croes et al., *Phys. Rev. Materials* **7** (2023) 014409
15. B. Croes et al., *J. Appl. Phys.* **134** (2023) 204103
16. L. Meynier et al., *J. Appl. Phys.* Submitted (2025)

P-40

Evolution of structural disorder and energy landscape in amorphous $Ge_2Sb_2Te_5$ under non-equilibrium conditions

F. C. Mocanu[1], S. R. Elliott[2], and K. Konstantinou[3]*
[1]Materials Modelling Laboratory, University of Oxford, United Kingdom
[2]Physical and Theoretical Chemistry Laboratory, University of Oxford, United Kingdom
[3]Department of Mechanical and Materials Engineering, University of Turku, Finland
*konstantinos.konstantinou@utu.fi

Primary knock-on atom simulations result in an enhanced chemical disorder within the amorphous network of $Ge_2Sb_2Te_5$. Local atomic environments with homopolar bonds are formed inside the structure. The system can access liquid-like states in the energy landscape during the simulation, lowering the energy barriers for local relaxation. This facilitates structural recovery of the glass network by enabling fast atomic rearrangements.

Key words: non-equilibrium simulations, primary knock-on atom, chemical disorder, liquid states, amorphous materials, phase-change memory.

1. INTRODUCTION

As an innovative idea, chalcogenide phase-change materials have been proposed for spaceborne solid-state memory modules because of their non-volatile, reconfigurable, fast-switching, and space-radiation-tolerant capabilities [1]. Therefore, the ability to predict and characterize the structural transformations of phase-change memory materials exposed to non-equilibrium conditions is crucial for tailoring their properties for such applications. In our previous work, non-equilibrium cascades in amorphous $Ge_2Sb_2Te_5$ have been investigated by means of first-principles molecular-dynamics simulations [2]. The final equilibrated models showed a notable degree of healing and reversibility, as both the atomic and electronic structures recovered from the damage imposed during the simulations [2]. In this study, chemical estimations of disorder are employed to gain insights into the structural evolution and the overall response of the amorphous material to the non-equilibrium events, exploring the impact of the cascades on the local atomic structure of the glass. The intricate energy landscape of an amorphous structure can have profound effects on the properties of the material and its response to irradiation [3]. Here, the evolution of the potential energy landscape of the simulated system during the non-equilibrium events is presented in a configurational map to illustrate how its nature can facilitate intrinsically the reorganization of the atomic structure and the subsequent recovery of the glassy network.

2. EXPERIMENTAL

Non-equilibrium events were modelled by carrying out thermal-spike simulations in a 315-atom model of amorphous $Ge_2Sb_2Te_5$. The collision effects were caused by primary knock-on Te atoms with initial kinetic energies ranging from 25 to 200 eV [2]. A stochastic-boundary-conditions approach was implemented to model the non-equilibrium dynamics of the cascade-damage events [4]. Ab initio molecular-dynamics simulations were carried out using the CP2K code. In order to capture the time evolution of the chemical order of the amorphous structure during the simulations, the binary order parameter of Cargill and Spaepen has been calculated [5], from the perspective of the quasi-binary (A/B) classification. In addition, simple order parameters, based on the different local atomic environments inside the glassy network, have been constructed to investigate the chemical disorder in the amorphous models after the damage events. The data from the molecular-dynamics trajectories were utilized to construct 2D maps, by employing a smooth-overlap-of-atomic-positions (SOAP) descriptor to represent the configuration of each snapshot [6], while multi-dimensional scaling (MDS) has been adopted as the embedding technique [7].

3. RESULTS & DISCUSSION

The temporal evolution of the chemical order of the amorphous structure during the 200 eV primary knock-on atom simulation is shown in **Fig. 1a** [8]. On the timescale of 1-2 ps after the beginning of the simulation, the non-equilibrium cascade causes a significant reduction in the chemical order of

the simulated structure (by as much as 50%), highlighting the impact of the cascade event on the amorphous network. Also, this is indicative of the destruction and formation of bonds inside the glass model. Thereafter, and during the thermal quench of the event, the chemical order of the simulated structure partially recovers toward its initial value. The degree of disorder in the final equilibrated structure, at the end of the molecular-dynamics simulation, is increased for the whole model and per atomic species, compared to the initial glass model (at t=0). In addition, the modifications in the local order within the amorphous network of the final model have been evaluated by calculating local-order parameters for all the atoms (**Fig. 1b**) [8]. The ordered A–B alternation, visible in yellow, is disrupted by random and disordered atoms in the geometry of the model structure, that are shown in green, blue, and indigo. These configurations are typically correlated to local atomic environments with homopolar, A–A and B–B, bonds. The evolution of the potential energy landscape along the entire molecular-dynamics trajectory for the 200 eV primary knock-on atom event is explored via the configurational map shown in **Fig. 1c** [8]. During the simulation, the trajectory of the modelled system was able to cover the entire distance between the liquid and amorphous regions, highlighting clearly that, during this non-equilibrium event, liquid-like configurations are being accessed by the simulated structure. From the high-energy liquid states, structural relaxation can occur quickly during the remaining thermal quench of the model structure [8]. Such fast relaxation and structural reorganization can assist the recovery of the glassy network of the $Ge_2Sb_2Te_5$ simulated structure [2,8].

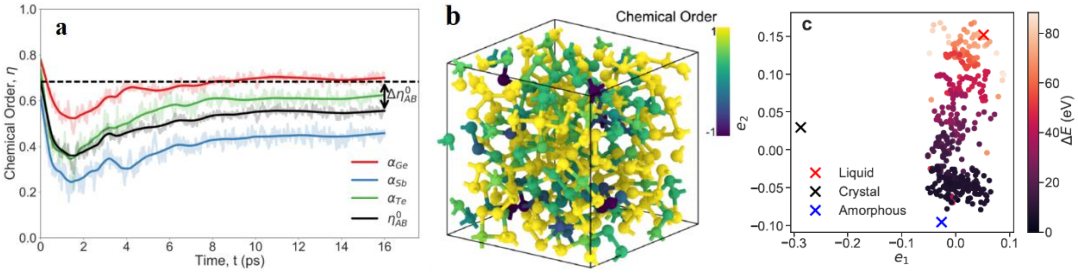

Fig. 1. 200 eV primary knock-on Te atom simulation: **a** Time evolution of the chemical order within the glassy network of the amorphous $Ge_2Sb_2Te_5$ model. **b** Local quasi-binary chemical order in the glassy structure after the event. **c** 2D SOAP-based similarity map visualizing the entire molecular-dynamics trajectory, plotted as a function of the calculated potential energy of the modelled system, at each point.

4. CONCLUSIONS

Starting with a 200 eV primary knock-on atom energy, the simulated $Ge_2Sb_2Te_5$ system is able to access liquid-like states in the energy landscape, as revealed from a configurational map constructed from suitable structural descriptors. Consequently, from these high-energy states, the configuration can relax, due to lower energy barriers for structural reorganization. This provides a thermodynamic insight into the radiation tolerance of the amorphous material, which, combined with the pronounced flexibility of the chemical bonding and the available free volume within the glassy $Ge_2Sb_2Te_5$ structure, accounts for the essential attributes leading to the fast recovery of this material after the non-equilibrium damage events. The results demonstrate that the degree of chemical disorder is increased within the recovered amorphous network of $Ge_2Sb_2Te_5$, while local atomic environments with homopolar bonds are formed in the geometry of the model structures.

REFERENCES

1. S. R. Ovshinsky et al., *IEEE Trans. Nucl. Sci.* **15** (1968) 311; H. J. Kim et al., *npj Microgravity* **10** (2024) 20.
2. K. Konstantinou, T. H. Lee, F. C. Mocanu, and S. R. Elliott, *Proc. Natl. Acad. Sci. USA* **115** (2018) 5353; *J. Phys.: Condens. Matter* **30** (2018) 455401.
3. P. K. Gupta and W. Kob, *J. Non-Cryst. Solids X* **3** (2019) 100031.
4. L. Kantorovich and N. Rompotis, *Phys. Rev. B* **78** (2008) 094305.
5. G. S. Cargill and F. Spaepen, *J. Non-Cryst. Solids* **43** (1981) 91.
6. A. P. Bartók et al., *Phys. Rev. B* **87** (2013) 219902.
7. J. B. Kruskal, *Psychometrica* **29** (1964) 1.
8. F. C. Mocanu, S. R. Elliott, and K. Konstantinou, *Phys. Stat. Solidi RRL* (2025) 2500037.